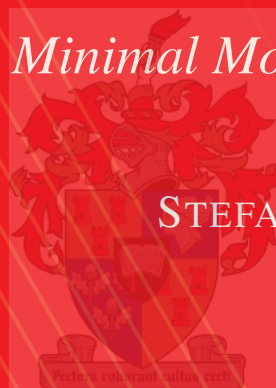# Quantifying Insulin Signaling

in Mouse C2C12 Skeletal Muscle:

A Minimal Modelling Approach

STEFAN KÜHN

2021

Quantifying the Insulin Response in Mouse C2C12 Skeletal Muscle: A Minimal Modelling Approach

by

Stefan Kühn

Dissertation presented for the degree of Doctor of Philosophy in the Faculty of Science at Stellenbosch University. This dissertation has also been presented at the Vrije Universiteit Amsterdam in terms of a joint-degree agreement.

VRIJE UNIVERSITEIT

Quantifying the Insulin Response in Mouse C2C12 Skeletal Muscle:

A Minimal Modelling Approach

ACADEMISCH PROEFSCHRIFT

ter verkrijging van de graad Doctor of Philosophy
aan de Vrije Universiteit Amsterdam,
op gezag van de rector magnificus
prof.dr. V. Subramaniam,
in het openbaar te verdedigen
ten overstaan van de promotiecommissie
van de Faculteit der Bètawetenschappen
op woensdag 7 juli 2021 om 9.45 uur
in het auditorium van de universiteit,
De Boelelaan 1105

door

Stefan Kühn

geboren te Bellville, Zuid-Afrika

promotoren: prof.dr. J.L. Snoep
                  prof.dr. H.V. Westerhoff

Declaration

By submitting this dissertation electronically, I declare that the entirety of the work contained therein is my own, original work, that I am the sole author thereof (save to the extent explicitly otherwise stated), that reproduction and publication thereof by Stellenbosch University will not infringe any third party rights and that I have not previously in its entirety or in part submitted it for obtaining any qualification. This dissertation has also been presented at the Vrije Universiteit Amsterdam in terms of a joint-degree agreement.

June 2021
Date: ....

i

This work has, at times, been a labour of love, anguish, hope, and despair. However now, at its end; I am left with nothing except overwhelming gratitude to all who lent me their strength, wisdom, and inspiration in those moments where mine failed.

To those giants upon whose shoulders I've stood: Jacky Snoep, Dawie Van Niekerk, Hans Westerhoff, Frank Bruggeman, and Jannie Hofmeyr - thank you.

To my colleagues who kept the faith when I could not: Johan Eicher, Theresa Kouril, Arrie Arends, Cobus Van Dyk, Klarissa Shaw, and the entirety of the MSB Laboratory - thank you.

To those without whose love and support I would be lost: Doreen, Johann, Robert, Amalsha, Reuben, Muneera, and Charles - thank you.

"It is a strange fancy to suppose that science can bring reason to an irrational world, when all it can ever do is give another twist to a normal madness."

— John Gray

Dieses Werk gehört nicht nur mir, es gehört meiner Familie: Mutter, Vater, Sabine, und Oma. Ohne euch, ohne eure Liebe und Unterstützung währe alles sinnlos.

Contents

Contents

Contents

List of Figures

List of Figures

List of Tables

Summary

The insulin signalling cascade is one of the most important regulatory and signalling pathways in humans. Dysregulation or dysfunction of the insulin signalling pathways often underlies the molecular ætiology of diseases such as diabetes, obesity, and Alzheimer's. In turn, these diseases are the harbingers of various co-morbidities such as cardio-vascular disease, chronic inflammation, and dementia. The healthcare, economic, personal, and mortality burden of these diseases cannot be overstated.

Mathematical modelling of insulin signalling is indispensable in the effort to understand the dynamics of the insulin signalling cascade and how malfunctions therein lead to disease. However, despite the availability and complexity of existing models, few have explicitly connected the signalling cascade, glucose transporter activity, and metabolism with one another. In order to study these interactions, a 'three-module' approach was adopted that defined the signalling cascade, glucose transporter activity, and metabolism as core, 'input-output' modules. The present work is limited to the signalling cascade and glucose transporter activity modules whereas work by Dr. Cobus van Dyk is concerned with the metabolic module.

With this in mind, this thesis sets forth three aims. Firstly, to establish standardised culturing conditions which can be used to determine the *basal* state of insulin signalling and glucose transporter activity. Secondly, to develop a core, mathematical model based on Western blotting and radio-labelled glucose -assay data which is able to describe the concentration- and time-dependence of the signalling cascade and glucose transporter activity in response to insulin. Thirdly, to determine the clustering behaviour of GFP-tagged GLUT4 molecules in response to insulin.

The first goal was to standardise culturing conditions. Herein, the ability of high

(25mM), medium (15mM), and low (5mM) glucose culturing conditions were evaluated with regards to their ability to sensitise or desensitise the insulin signalling cascade as well as the degree to which they are able to induce the differentiation of C2C12 myoblasts into myocytes. The glucose and lactate concentrations in the external media were used to determine the glucose-lactate flux of the C2C12 cells. This served as a proxy for the induction of insulin-dependent glucose transport and metabolism. A modified Ladd staining protocol was used to assess the degree to which C2C12 cells could differentiate under the culturing protocols.

The second goal was to construct a core, mathematical model of insulin signalling and glucose transporter activity. The time-dependent phosphorylation and dephosphorylation of the insulin receptor and the serine 473 and threonine 308 sites of Akt in response to varying insulin concentrations was investigated using Western blotting techniques. The glucose transporter (GLUT4) activity was assayed using radio-carbon glucose. The data were used to optimise parameters for a core, ODE-based model of the signalling and glucose transporter modules.

The third goal, to investigate the clustering behaviour of GLUT4 in response to insulin, was investigated by using confocal microscopy to image GFP-tagged GLUT4 molecules before and after being stimulated with insulin. A hierarchical clustering algorithm as well as further geometric and statistical analyses were used to determine the number, size, density, and distribution of GLUT4 clusters pre and post insulin exposure.

Of the remaining chapters, Chapter 1 discusses the background, context, scope, and aims of this study as well as further elaborating on the 'three module' approach. The literature review in Chapter 2 provides an overview of the relevant literature as delineated by the scope and aims of this study. The materials and methods are provided in Chapter 3, with specific alterations or methodologies being further discussed in the relevant experimental chapters. The final chapter, Chapter 7, provides the reader with general discussions, limitations, and final thoughts concerning this work.

Opsomming

Die insulien seinkaskade is een van die belangrikste regulerings- en sein padweë in mense. Disregulering of disfunksie van die insulien sinweë is dikwels onderliggend aan die molekulêre etiologie van siektes soos diabetes, vetsug en Alzheimers. Verder is hierdie siektes die draers van verskillende ko-morbiditeite soos hartvatsiektes, chroniese ontsteking, demensie en ander. Die gesondheids, ekonomiese, persoonlike en sterfteslas van hierdie siektes kan nie oorskat word nie.

Wiskundige modellering van insulien seinweë is onontbeerlik in die poging om die dinamika van die insulien seinkaskade te verstaan en hoe wanfunksies daarin tot siektes lei. Ondanks die beskikbaarheid en ingewikkeldheid van die bestaande modelle, het min die seinkaskade, glukose-vervoerderaktiwiteit en metabolisme egter eksplisiet met mekaar verbind. Ten einde hierdie interaksies te bestudeer, is 'n 'drie-module'-benadering aangewend wat die seinkaskade, glukose-vervoerderaktiwiteit en metabolisme as kernmodules as 'n 'inset-uitset' model gedefinieer het. Die huidige werk is beperk tot die seinkaskade en glukose-vervoerdersaktiwiteitsmodules, terwyl werk deur dr. Cobus van Dyk gemoeid is met die metaboliese module.

Met die oog hierop stel hierdie proefskrif drie doelstellings. Eerstens, om gestandaardiseerde kweektoestande vas te stel wat gebruik kan word om die *basale* toestand van insulien seine en glukose-vervoerderaktiwiteit te bepaal. Tweedens, om 'nkern, wiskundige model te ontwikkel gebaseer op Westerse klad-tegnieke en radio-toetsdata, wat die konsentrasie en tydafhanklikheid van die seinkaskade en glukosever-voerder kan beskryf as 'n gevolg van insulien blootstelling. Derdens, om die groeperingsgedrag van GFP-gemerkte GLUT4-molekules in reaksie op insulien te bepaal.

Die eerste doelwit, met betrekking tot gestandaardiseerde kweektoestande, word

aangebied in hoofstuk 4. Hierin is die vermoë van hoë (25mM), medium (15mM) en lae (5mM) kweektoestande geëvalueer met betrekking tot hul kapasiteit om die insulien seinkaskade te sensitiseer of te desensitiseer, asook die mate waarin hulle die differensiasie van C2C12-myoblaste in miosiete kan veroorsaak. Die skynbare glukose-laktaatvloei in die eksterne media dien as 'n gevolmagtigde maatstaf vir die induksie van insulienafhanklike glukosevervoer en metabolisme. 'n Gemodifiseerde LADD-kleuringprotokol is gebruik om die mate waarin C2C12-selle kan onderskei te bepaal.

Die tweede doelwit, om 'n kern, wiskundige model van insulien seinweë en die glukosevervoerder aktiwiteit te konstrueer, word in hoofstuk 5 nagestreef. Die fosforilering en ontfosforylering van die insulienreseptor en die serien 473 en treonien 308-posisies van die intermediêre seinmolekule (Akt) in reaksie op wisselende insulienkonsentrasies, sowel as tyd, is met behulp van Westerse klad-tegnieke ondersoek. Die glukose-vervoerder (GLUT4) -aktiwiteit is met behulp van radio-koolstof glukose ondersoek. Die data is gebruik om parameters te optimaliseer vir 'n kern-GDV-gebaseerde model van die sein en glukose-vervoermodules.

Die derde doelwit, wat die groeperingsgedrag van GLUT4 in reaksie op insulien ondersoek het, word in hoofstuk 6 aangebied. Konfokale mikroskopie is gebruik om GFP-gemerkte GLUT4-molekules wat sonder en met insulien gestimuleer is te analiseer. 'n Hiërargiese groeperingsalgoritme sowel as verdere meetkundige en statistiese ontledings is gebruik om die aantal, grootte, digtheid en verspreiding van GLUT4-groepe voor en na insulienblootstelling te bepaal.

Van die hoofstukke wat nog nie hier bespreek is nie, bied hoofstuk 1 die agtergrond, konteks, omvang en doelstellings van hierdie studie, asook die uitwerking van die 'drie module'-benadering. Terwyl die literatuuroorsig in hoofstuk 2 bied 'n ondersoek van die relevante literatuur soos uiteengesit in die omvang en doelstellings van hierdie studie. Die materiaale en metodes word in hoofstuk 3 verskaf, met spesifieke wysigings of metodologieë wat in die betrokke eksperimentele hoofstukke verder bespreek word. Die finale hoofstuk, hoofstuk 7, sal die leser voorsien met algemene besprekings, beperkings en afsluitende gedagtes rakende hierdie werk.

Terminology

Akt: AKR Mouse thymoma / Protein Kinase B

A: Ampere

ATP: Adenosine Triphosphate

BSA: Bovine Serum Albumin

Ci: Curie

DMEM: Dulbecco's Modified Eagle Medium

DMSO: Dimethyl Sulfoxide

DNA: Deoxyribonucleic Acid

DTT: 1 4 Dithiothreitol

EDTA: Ethylenediaminetetraacetic acid

ES: Equine Serum

FBA: Flux Balance Analysis

FBS: Foetal Bovine Serum

g: gram

G6PDH: Glucose-6-Phosphate Dehydrogenase

GSV: Glucose Storage Vesicles

GTT: Glucose Tolerance Test

HXK: Hexokinase (EC 2.7.1.1)

IR: Insulin Receptor

IRS: Insulin Receptor Substrate

L: Liter

LDH: L-Lactate Dehydrogenase (EC 1.1.1.27)

LG: Low Glucose

LN$_2$:   Liquid Nitrogen

m: milli: 10^{-3}

MCA: Metabolic Control Analysis

mTORC1:   Mammalian Target of Rapamycin Complex 1

NAD$^+$: β-Nicotinamide Dinucleotide (oxidised)

NADP$^+$: β-Nicotinamide Dinucleotide Phosphate (oxidised)

PBS: Phosphate Buffered Saline

PET: Polyethylene

RIPA: Radio-immunoprecipitation Assay

RNA: Ribonucleic Acid

RT: Room Temperature (25°C)

RTK: Receptor Tyrosine Kinase

SDS: Sodium Dodecyl Sulfate

SkMC: skeletal muscle cell

T2D: Type 2 Diabetes

TCE: Trichloroethylene

μ: micro: 10^{-6}

V: Volt

Chapter 1

Introduction

Conditions resembling diabetes are described at various points in history - spanning almost 3000 years [1]. Serious academic study of these conditions began in the 16th century when the Swiss physician Paracelsus first discovered crystalline glucose residue upon evaporating the urine of patients with 'irritated kidneys' [2]. The distinction between Type 1 and Type 2 diabetes was formally clarified in the latter half of the 1700s by Matthew Dobson [2]. Type 1 diabetes is an auto-immune disease that destroys the insulin producing β-cells in the pancreas [3]. Type 2 diabetes (T2D) is a lifestyle disease. Persistent exposure to insulin steadily desensitises the cellular response to insulin until the organism becomes insulin resistant [4, 5]. Insulin was discovered in the first quarter of the 20th century and first used to treat type 1 diabetes in the early 1920s [6]. The successful treatment of comatose diabetics by insulin formally cemented its role as one of the crucial elements in the ætiology of type 1 and 2 diabetes [7].

Despite centuries of study, diabetes - specifically type 2 diabetes - remains one of the fastest growing lifestyle diseases globally [8]. It is estimated that nearly 10% of the global population will be affected by type 2 diabetes by 2045 [9]. However, since the burden of this disease is increasingly shifting to lower- and middle-income regions of the world, the true number may be greater as nearly half of the diabetics in these countries remain undiagnosed [10].

The most-common preventatives or curatives for type 2 diabetes (henceforth T2D) involve changes in lifestyle. However, three of the greatest risk-factors for T2D -

1

excessive sugar consumption [11], sedentary lifestyles [12], and stress [13, 14] - have become ingrained in a plurality of modern lifestyles. Changing them is often a task that many are unwilling or unable to tackle. Moreover, the rate at which these factors are affecting people, predominantly in modernising economies, is on the rise [8]. These data, combined with a near-global inertia to change, are especially concerning in the light of the healthcare [15], economic [16], and mortality [17, 18] burdens imposed by the increasing prevalence of T2D.

The failures of 'top-down' interventions which focus on better nutrition, more exercise, and less stress have increased interest in 'bottom-up' solutions that rely on a keen understanding of the molecular mechanisms that lead to T2D. Skeletal musculature accounts for 70 - 90% of mammalian post-prandial glucose clearance [19]. Further, skeletal muscle is predominant in regulating glucose homeostasis [20]. It therefore seemed a prudent point of initiation for this study.

1.1 Insulin Signalling: A Three-Module Approach

The canonical insulin signalling cascade is initiated when insulin binds the insulin receptor (IRS) [21]. This instantiates a phosphorylation cascade among multiple intermediate proteins which reaches Akt (previously known as protein kinase B) [22]. Once Akt has been phosphorylated, along with AS160, it sets in motion the transport and eventual fusion of the GLUT4 glucose transporter to the plasma membrane [23, 24]. Consequently, exposure to insulin increases the concentration of GLUT4 at the plasma membrane which in turn increases the glucose influx into the cell [25, 26].

The insulin signalling pathway consists of several dozen proteins [21], each of which interacts with various downstream and upstream proteins. Additional complexity is layered onto this by one of the primary regulatory mechanisms of this pathway - differential phosphorylation on specific amino acids (primarily serine, threonine, or tyrosine) of several proteins within the cascade [21]. Lastly, certain proteins - such as the insulin receptor - can be phosphorylated at multiple amino acid residues simultaneously [27].

The present work shall attempt to model insulin signalling, glucose transporter (GLUT4) activity, and glucose metabolism pathways as three distinct modules in an effort to manage the complexity of these pathways. The goal is not to create a highly-detailed model or one which can explain the specific dynamics of all the individual elements in the insulin signalling pathway. Rather, the minimal modelling approach in this work seeks to link three modules in the insulin signalling cascade; an insulin signalling module, a glucose transporter module, and a glucose metabolism module. These modules will be simplified into an 'input-output' ODE-based model which links the main components - the insulin receptor, Akt, and GLUT4 - at the subcellular level. Smaller, albeit more limited, models such as this one can be more easily parameterised with a limited data set. Consequently, this model will be parameterised using direct experimental evidence. This focus on a smaller model and experimental scope significantly simplifies experimental and modelling considerations. This work would provide a platform which future models could expand on a similar basis as one could develop purpose-built minimal models for each module that could conceivably be integrated into a single, larger model.

Consequently, the decision was made to focus on 'nodes' (components) in insulin signalling which represent the signalling pathway, the glucose transporter, and glucose metabolism. A representation of the components that are involved in transmitting the insulinic signal from the insulin receptor to GLUT4 can be seen in Fig. 1.1. Here, the insulin signalling cascade has been carved into five distinct clusters centred around the insulin receptor (IR, green), insulin receptor substrate (IRS, yellow), phosphoinositide 3-kinase (PI3K, purple), protein kinase B (Akt, red), and the glucose transporter (GLUT4, orange). This was further pared down to include only the IR and Akt proteins since these represent the input and output nodes of the 'insulin signalling' module and were therefore considered sufficient for the construction of a minimal model. Similarly, GLUT4 was isolated to represent the 'glucose transporter' module. In other words, the diagram in Fig. 1.1 was simplified into three modules - insulin signalling, glucose transport, and glucose metabolism (Fig. 1.2). Each of these modules could be assessed by measuring their input and output components. In the case of the insulin
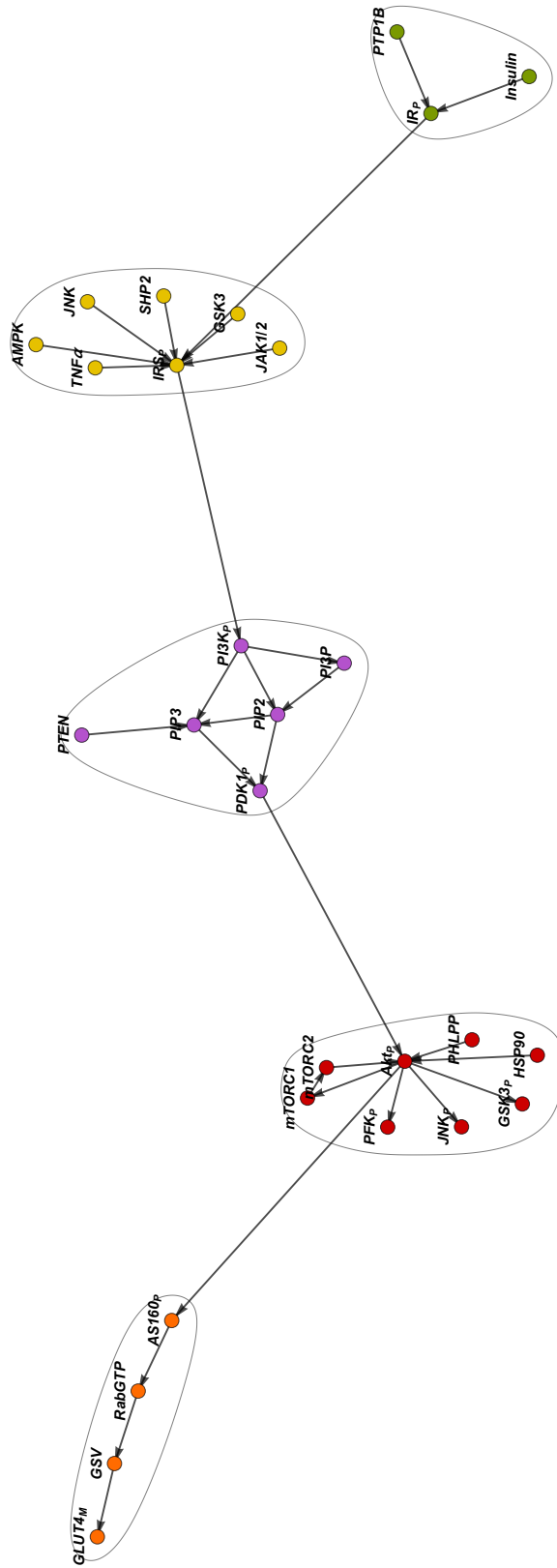
Figure 1.1: This community graph identifies closely-related clusters of interactions within the insulin signalling pathway. The IRS and its interactions are highlighted in red, and form a densely populated hub. Similarly, the hubs centred around PI3K (purple), Akt (yellow), and AS160 (orange) are all highly regulated control points in the insulin signalling pathway (please see Chapter 2). Due to the number of signals which originate and terminate at these nodes, it is conceivable that regulation or dysregulation of the insulinic pathway would occur here. The nodes for this graph are retrieved from the literature review presented in Chapter 2 and fed into the Mathematica 'CommunityGraphPlot' function which assigns nodes to communities based on the number of edges which join them.
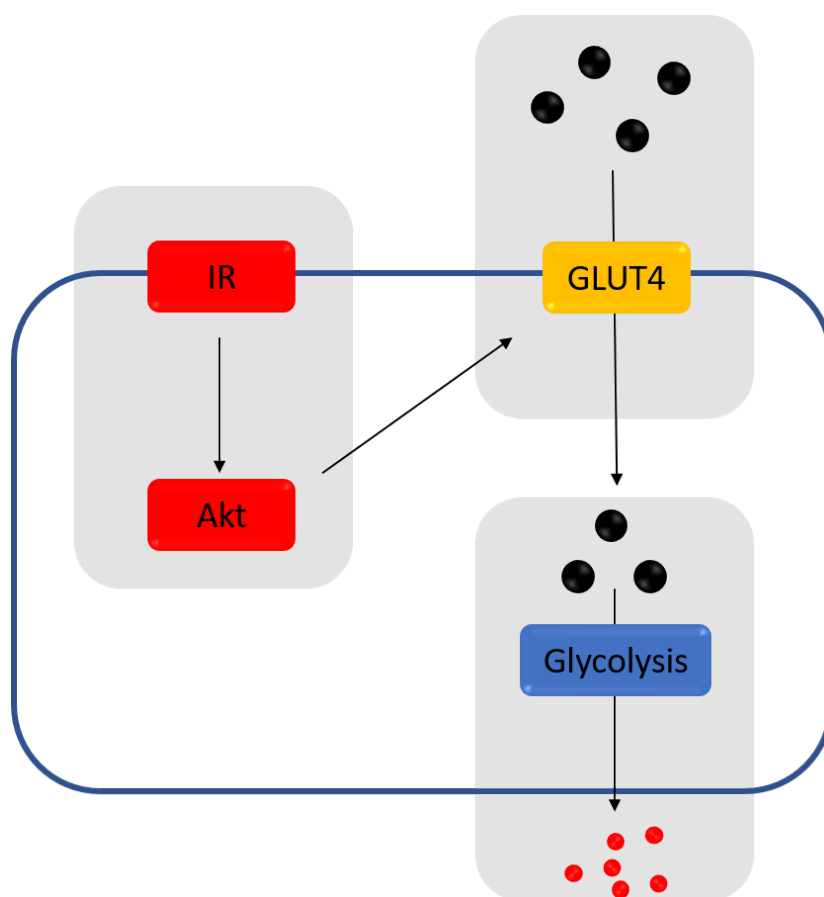
Figure 1.2: The simplified three module representation of insulin signalling. The signalling module encompasses the insulin receptor (IR) and Akt as inputs and outputs respectively. External and internal glucose (black spheres) are the respective inputs and outputs for the glucose transporter module. This module is assessed by measuring the activity of the GLUT4 transporter. The metabolism module uses glucose as input and yields lactate (red spheres) as output.

.

signalling module this would be the degree to which the insulin receptor and Akt are phosphorylated. The glucose transporter module would be assayed according to how much glucose is imported from the external media and the glucose metabolism module would be assessed by measuring glucose and lactate as input and output respectively.

The insulin signalling module represents the transduction of the signal from insulin through to GLUT4. This means that one can build a representative model of the dynamics of the signalling cascade without needing to take glucose transport into account. While a large part of the insulin signalling pathway is already known, the precise interactions between the components is not fully konwn. Additionally, the in-

sulin signalling pathway interacts with components from other metabolic or signalling pathways. This significant complexity meant that the modelling approach explored in this thesis would not attempt to incorporate every known quantity in the insulin signalling pathway. The goal was not to create the most-detailed model, rather to determine whether a minimal model which focused on a smaller selection of well-studied components could generate novel insights into insulin signalling.

The GLUT4 cluster was relegated to the glucose transport module. Unlike the insulin signalling cluster which was investigated using Western blotting, the glucose transport module was investigated by using radiolabelled glucose transporter assays. Using these assays, one can gain an accurate picture of the fraction of GLUT4 in the plasma membrane under basal conditions, insulin stimulated conditions, and dysregulated conditions. Therefore, should dysfunction occur at any point throughout insulin signalling, it will immediately be apparent in the behaviour of the glucose transporter. This can indicate dysregulation upstream - with Akt or the IR - or in the absence of such dysregulation, the transporter itself could be at fault.

Finally, the metabolic module is composed of two studies. Firstly, the study contained in this thesis which provides a bird's eye view of metabolism by tying the *overall* glucose consumption and lactate production rates to increases in insulin stimulation. Should the insulin signalling or glucose transport modules fall prey to dysfunction, this should be immediately apparent in the initial rates at which glucose is metabolised to lactate. The second study is a sister-project to the present work which was completed by Dr. Cobus van Dyk and focuses on the *internal* glucose metabolism of C2C12 cells.

1.2 Motivation

While a variety of studies exist that independently investigate the behaviour of the signalling cascade [28, 29], the behaviour of the glucose transporters [30, 31], or the effects of insulin exposure on metabolism [32, 33], few models link each of these 'modules' together in a single kinetic model. The present study will attempt to resolve this shortcoming, as will the work by Van Dyk et al [34].

Deepening the understanding of how the various modules within a cell act with and upon each other may lead to benefits beyond the purely academic. If a disease state is caused by dysregulation of the insulin cascade, knowing whether this lies with the signalling network, the GLUT4 protein, or with glycolysis may yield insights into which pharmaceutical or therapeutic interventions could alleviate the disease state. Further, such an understanding may assist with the development or targeting of treatments.

1.3 Problem Statement

The 'Three-Module' approach outlined in Section 1.1 can be approached, analytically, from a mathematical, modelling perspective. Such a construct, albeit simplified, can compare the 'normal' state of insulin signalling with a dysregulated state across all three modules: signalling, glucose transport, and glucose flux. The current lack of such a model therefore is the overall problem the present work shall address.

1.4 Aims and Objectives

The overall aim of this study was as follows: to characterise and determine, by way of a simplified, mathematical model, which of the modules outlined in Section 1.1 are dysfunctional in a hyperglycaemic, hyperinsulinemic insulin-resistant state. In order to achieve these aims, the following objectives were developed:

Firstly, to establish the correct physiological conditions wherein the cells are to be grown. This stems from the hypothesis that 'standard' culturing protocols, which often contain up to five times the glucose content (25 mM)than what is physiological (5.5 - 7 mM in humans), might be inducing *pseudo* insulin-resistant states. Therefore, as a proxy-measure of insulin functioning, the glucose-lactate flux will be measured across a variety of culturing and experimental conditions until an insulin induction of glucose-lactate flux is determined. Similarly, the degree to which cells under these 'new' culturing conditions differentiate will be quantified since the phenotype of myoblasts and myotubes differs substantially, a factor which could influence any experimental results.

Secondly, the 'normal' or *basal* kinetic state of insulin signalling will be investigated with respect to the IR and Akt protein phosphorylation as well as the glucose transport activity. Western Blot analysis will be used to determine the insulin dose and time dependent phosphorylation and dephosphorylation of the IR and Akt proteins. The glucose transport will be characterised in terms of the increase or decrease of its transport capacity (assayed via C^{14} uptake) in response to the time- and dose-dependent addition or removal of insulin. The Western blotting and glucose transport data shall be included in a minimal, ODE-based kinetic model of the insulin signalling cascade.

Thirdly, the behaviour of GFP-tagged GLUT4 proteins in response to insulin will be determined with regards to their propensity to cluster as well as their distribution throughout the cell. This investigation necessitates the replicable transfection of myoblasts with the GFP-tagged GLUT4 plasmid as well as a method to visualise the GLUT4 distribution via confocal microscopy. Thereafter a computational workflow with which to eliminate background noise, deconvolve the images, and isolate the relevant pixel positions will be developed. Lastly, this will lead to the development of a clustering algorithm that uses the pixel positions as input, divides them into clusters, has some exclusion criteria, and is able to output the size and density of each cluster. This will provide insight into the distribution and movement of the GLUT4 module in a post-insulinic state.

1.5 Scope and Focus

The data gathered during this study apply exclusively to *in vitro* observations in cultured mouse skeletal muscle (C2C12) cells. The adoption of a core modelling approach which characterises the insulin signalling cascade as an 'input-output' relation is sufficiently broad to encourage similar approaches for insulin resistant states or additional cell lines. However, such a model is limited with regards to the level of mechanistic detail it contains. Therefore, while it cannot point to the precise molecular mechanism which causes insulin insensitivity, it can point to the module chiefly responsible therefor. This should allow future studies to direct their efforts towards the modules most

relevant for their aims.

Chapter 2

On Insulin Signalling, Metabolism, and Modelling

2.1 Insulin Signalling

The insulin signalling pathway is an important regulator of cellular homeostasis [35]. It regulates many processes such as: glucose metabolism [36], protein synthesis [37], lipid synthesis [38], exercise metabolism [39], and stress responses [40]. Primarily, the insulin responsive tissues are skeletal and cardiac muscle as well as adipose tissues [41]. However, without insulin mediated metabolic and stress responses, cells, tissues, and organisms would quickly suffer from a host of dysfunctions - not the least of which are the diabetic conditions.

When pancreatic β-cells detect an increase in blood glucose, they release insulin into the bloodstream [42]. Circulating insulin will then bind to free insulin receptors on any of the target tissues (Fig. 2.1). Subsequently, this will trigger the activation of the insulin signalling cascade (Fig. 2.2) which results in the upregulation of glycogen synthesis, glycolysis, and fatty acid and lipid synthesis [37, 38, 43]. Similarly, this will *also* trigger the downregulation of various catabolic processes such as proteolysis, fatty-acid breakdown, and glycogenolysis. Since nearly 70% of post-prandial, insulin-mediated glucose consumption occurs in the skeletal muscle, the present review and study shall focus thereon.
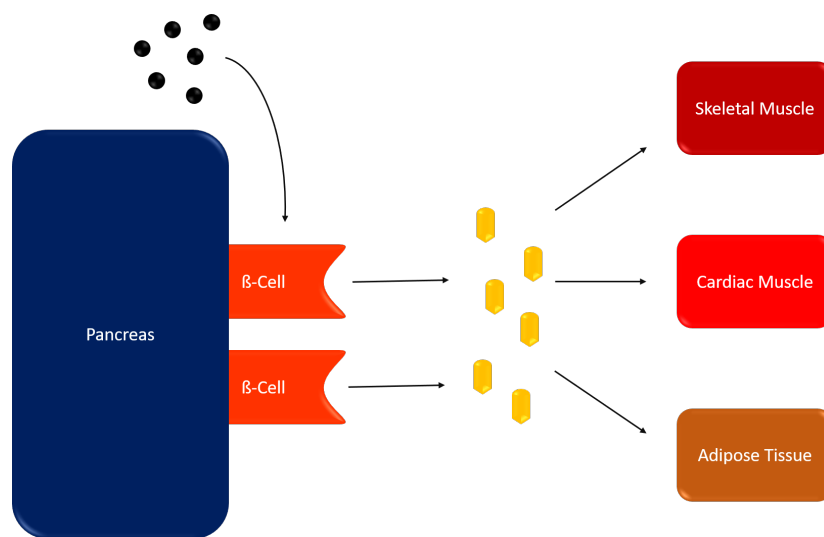
Figure 2.1: Glucose (black spheres) is sensed by β-cells on the pancreas which then release insulin. Increases in insulin concentrations are primarily sensed by skeletal muscle, cardiac muscle, and adipose tissue. In return, these tissues respond by either up- or down-regulating anabolic and catabolic processes as necessary.
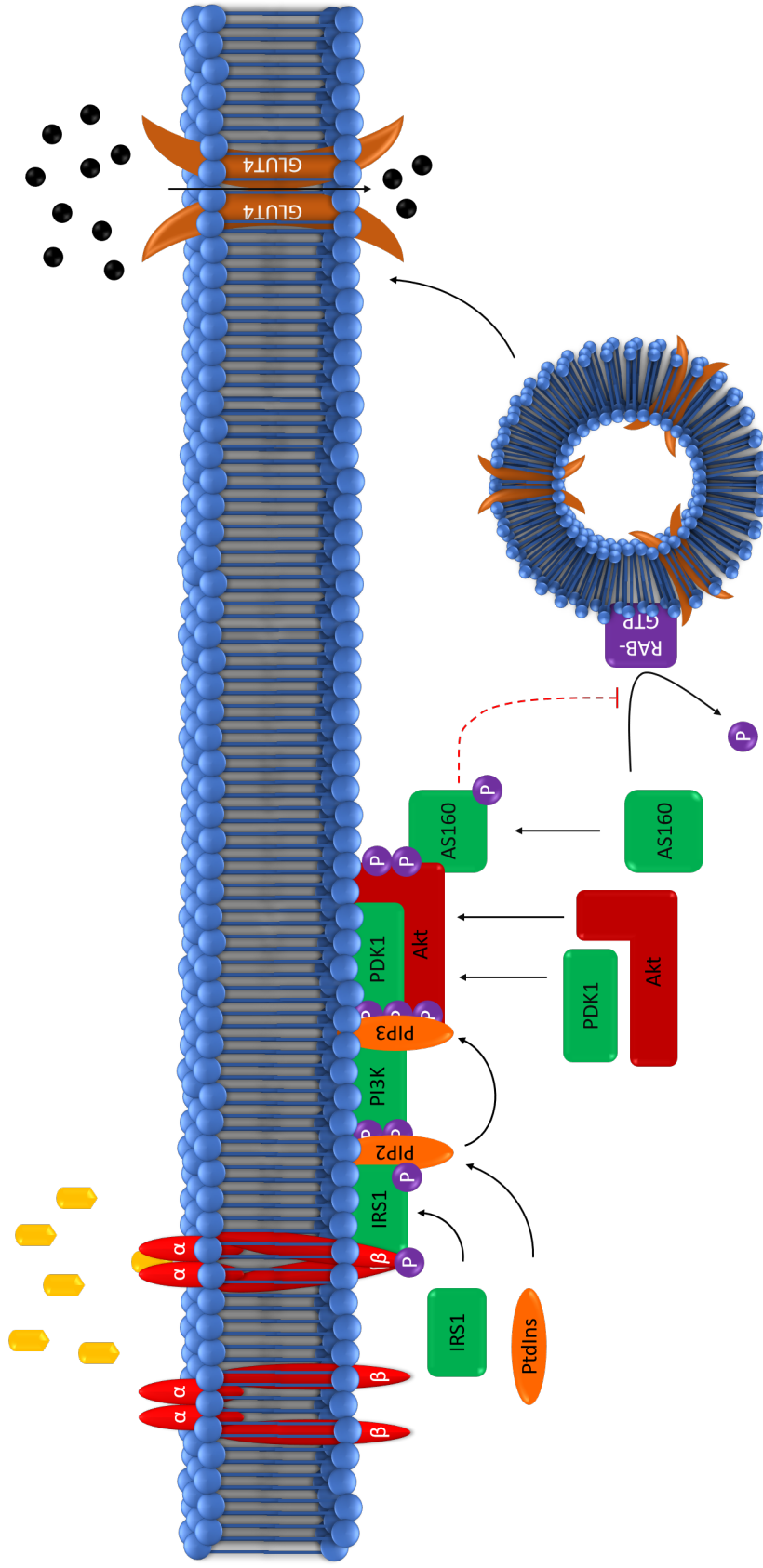
Figure 2.2: The classical view of insulin signalling. The (yellow) insulin binds to the α subunits of the IR. This leads to the dimerisation of the β subunits and thereby initiates the autophosphorylation of the $beta$ subunit Tyr residues. This alters the affinity of the IR for the IRS. This concentrates the IRS near the PM and the IR. As a result, IRS binds to the IR and is phosphorylated. Subsequently, PI3K and its substrate are concentrated near the membrane, bind, and generate PIP3. This allows PDK1 and thereby Akt to bind to the PM - the latter being phosphorylated by PDK1 and mTOR Complex 2 (not shown). The phosphorylation of AS160 by Akt initiates the translocation and fusion of GSVs to the PM. This final step enables GLUT4 to increase glucose (black spheres) uptake from the extracellular environment.

2.1.1 Insulin

Insulin initiates and regulates a signalling cascade that is responsible for a host of metabolic activities: glucose, lipid, and protein metabolism [38, 44–46], cell growth and differentiation [47, 48], inflammation and the immune response [49, 50], and neural signalling [51]. Insulin is a small, 5.8 kDa peptide hormone. Its 51 amino acid structure is strongly conserved and insulin derived from disparate species is often cross-reactive [52].

The average circulating concentration of insulin in humans is between 10 and 100pM [53]. This is maintained by the release of insulin from the β-cells every 3 to 15 minutes [54, 55]. Once the blood glucose levels rise above resting physiological levels, greater quantities of glucose diffuse into the β-cells via the GLUT2 transporter [56]. Consequently, insulin is released more frequently [57] insulin levels can rise to between 6 nM and 42 nM [58, 59].

2.1.2 Insulin Receptor

The insulin receptor (IR) is embedded in the plasma membrane of a cell. The number of IR proteins found on a cell can range from a few hundred (for example, in erythrocytes), to a few hundred thousand in target cells such as adipose or muscle cells [60–62]. There are two isoforms of the IR: IR-A and IR-B. IR-A appears to primarily regulate growth, development, and IGF signalling whereas IR-B is responsible for metabolic regulation [63]. After binding to insulin, the IR-A isoform is phosphorylated at its intracellular tyrosine sites and internalises [64, 65]. In addition to mediating mitogensis, this results in the degradation of the IR-A and the subsequent attenuation of the Akt-dependent signalling cascade [66]. IR-B, however, remains at the cell membrane after insulin exposure, conducting the insulinic signal into the Akt-dependent pathway [67]. It is therefore conceivable that myoblasts primarily express IR-A whereas myocytes would express IR-B. The IR-A:IR-B ratio is a predictor of dysregulation in the insulin signalling pathway. Diabetic patients were found to have elevated IR-A:IR-B ratios [63]. Considering the mitogenic activity associated with IR-A [65], this could also be a predictor for dysregulation in the cell cycle, if not tumorigenesis.
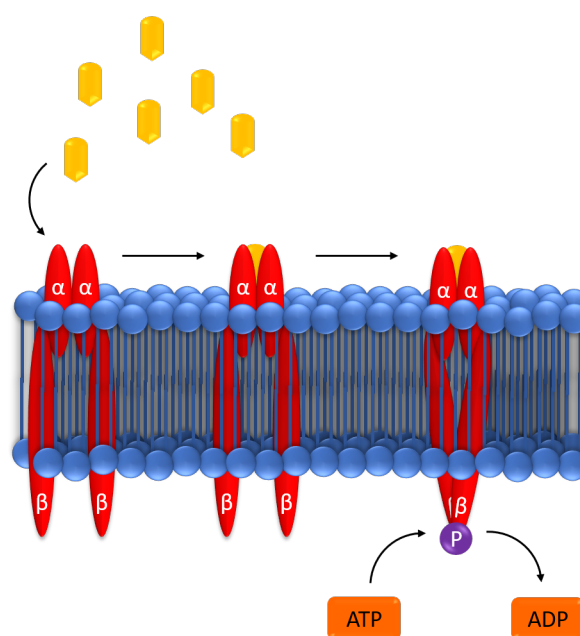
Figure 2.3: Insulin (yellow), binds to the α-subunit of the (red) IR. This initiates the dimerisation of the β-subunits which activates the IR tyrosine kinase domain. The activated IR tyrosine kinase uses ATP as a substrate to autophosphorylate each β-subunit which thereby becomes active.

Structurally, the IR isoforms consist of two homodimers: an α_2 juxtamembrane homodimer and a β_2 transmembrane homodimer [68]. An α subunit binds insulin. The β homodimer anchors the IR in the membrane and transmits the signal by phosphorylation of its Receptor Tyrosine Kinase (RTK) domains which are located in the cytoplasmic compartment [69].

After insulin binds to the IR (Fig. 2.3), the two α subunits crosslink with one another [21]. This leads to conformational changes in the IR which induces further crosslinking along the β subunits [70]. Consequently, the RTK domain of the IR is activated. The RTK domain sequesters ATP from the intracellular environment and begins autophosphorylating. There are seven, key tyrosine residues on the IR that can be autophosphorylated [71], all of them along the β domain. Phosphorylation of tyrosine residues 1158, 1162, and 1163 in the active loop leads to the stabilisation of the active site. This allows ATP and IRS1/2 to bind and undergo phosphorylation by the IR. Phosphorylation of the remaining residues: 965 and 972 in the juxtamembrane domain and of 1328 and 1334 in the C-terminus are thought to assist with the conformational changes necessary to open the active site of the IR [71].

2.1.3 Insulin Receptor Substrates

Immediately downstream from the IR is a family of four Insulin Receptor Substrate Proteins (IRS-1 to IRS-4) [72]. IRS-1 through IRS-4 are important for the transmission of signals from not only insulin, but also from immune, inflammation, and stress responses as well as growth and metabolism [73]. More specifically, IRS-1 and IRS-2 have been shown to be the important mediators in insulin and growth signalling. Knockouts of either gene resulted in insulin resistance and growth retardation in mice whereas knockouts of IRS-3 and IRS-4 appear to, at most, have mild defects in growth and neural development [38, 74]. Therefore, for the duration of this review, the use of IRS will be limited to mean IRS-1/2.

The IRS is a 1242 amino acid protein with a mass of 131 kDa [75]. IRS contains a Pleckstrin Homology (PH) domain and a Phospho-Tyrosine Binding (PTB) domain [76]. The PTB domain facilitates binding between the IRS-1 and the tyrosine-phosphorylated IR therefore bringing IRS proteins into near contact with the PM [73]. The PH domain recruits various molecules such as PIP2 to the IRS and consequently the PM [77]. The IRS-1 is unique in that the PH and PTB domains are arranged 'back to back' which could indicate that the successful binding of the PTB may lead to the activation of the PH domain [78]. Phosphorylation of C-terminal tyrosine sites recruits Src 2 Homology (SH2) domain proteins such as PI3K to the IRS and, consequently, to the PM [38]. IRS functions as a mediator of cell-signalling rather than an instigator thereof. This review will be limited to the interactions between IR, IRS, PI3K, and PIP2/3.

Once the IR has autophosphorylated and its active site has opened to IRS and ATP (Fig. 2.4), the IRS protein will bind and undergo rapid phosphorylation of various serine, threonine, and tyrosine residues [79, 80]. Canon has it that phosphorylation of tyrosine residues is associated with an increase in insulin-related metabolic activity [81] whereas Ser/Thr phosphorylation results in attenuation of the insulinic signal [82]. Evidence for the latter stems from studies which showed the following: constitutively high levels of serine phosphorylation under *basal* conditions [83]; most likely due to GSK-3 activity [84], elevated levels of serine phosphorylation in insulin resistant pa-

15
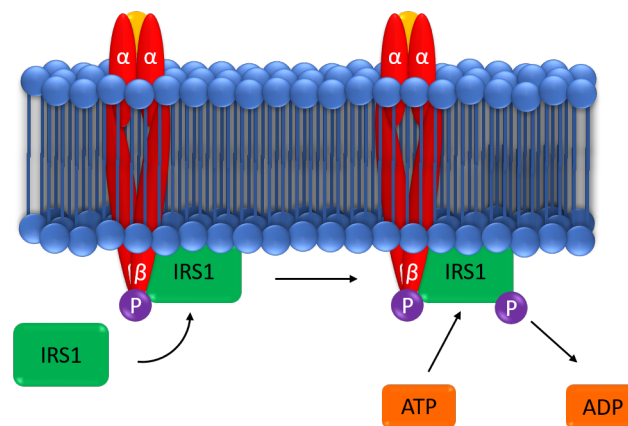
Figure 2.4: The active IR recruits the insulin receptor substrate (IRS) to the PM. The membrane-associated IRS is now a target for the IR kinase domain which uses ATP as a substrate in order to phosphorylate IRS which in turn is activated thereby.

tients [85], and the degradation of IRS in response to greater Ser/Thr phosphorylation [86].

This 'on/off' dichotomy between tyrosine and serine/threonine phosphorylation does not reflect the entirety of signalling through IRS. However, the broader interplay of phosphorylation states and phosphorylation sites is beyond the scope of this review.

2.1.4 PI3K

Phosphoinositide 3-kinases (PI3Ks) are a family of inositol phosphorylases that primarily act on phosphatidylinositol (PtdIns) in response to upstream signalling [87]. There are currently, four classes (I - IV) of PI3Ks [87, 88]. Each class of PI3K has differing specificities for PtdIns substrates and, consequently, is involved in separate cell functions (see Table 2.1). Class IV PI3Ks consist of a group of kinases that are mechanistically related to PI3Ks such as mTOR or DNAPK [89, 90]. However, their recognition as *bona fide* PI3Ks remains controversial. Class I PI3Ks are the most thoroughly studied molecules due to their direct involvement in or implication for the PI3K/Akt-dependent pathway of insulin signalling [91].

Class I PI3Ks - hereafter referred to as PI3K - are heterodimeric proteins that consist of an 85kDa regulatory subunit (p85) and a 110kDa catalytic subunit (p110) [92].

The unphosphorylated p85 subunit inhibits the p110 subunit [96]. Upon insulin

Table 2.1: An overview of the substrates and consequent metabolic processes that are affected by activation of each class of PI3K

Class of PI3K	Substrate	Function	Reference
I	PtdIns, PIP, PIP2	Signal propagation in the IRS-PI3K-AKt pathway	[92]
II	PtdIns	Angiogenesis, cilium function	[93, 94]
III	PtdIns	Initiator/Regulator of autophagy	[95]
IV	PtdIns	Oxygen sensing, DNA repair, nutrient homeostasis	[89, 90]

stimulation, the C-terminal tail of IRS becomes tyrosine phosphorylated. This provides a binding site for proteins with SH2 domains such as PI3K [97]. The binding between IRS and PI3K occurs at the p85 subunit of PI3K. This brings PI3K into close proximity with the tyrosine kinase domain of the IR [98]. Thereafter, PI3K undergoes phosphorylation on tyrosine 688 [99]. Consequently the inhibition of PI3Kp110 by the p85 subunit is relieved. This implies that under basal, unstimulated conditions, the ratio of active to inactive PI3K skews towards the latter.

The activation of the catalytic p110 subunit of PI3K opens the kinase domain to binding by $PI(4,5)P2$ and ATP [100]. This facilitates the phosphorylation of $PI(4,5)P2$ into $PI(3,4,5)P3$ [101]. This is a crucial step in furthering the insulin signal from the IR/IRS complex to downstream actors such as PDK1 and Akt [91, 102]. The PIP molecules, PDK1, and Akt will be discussed in detail in the following sections.

2.1.5 The Phosphatidyl Inositide Phosphates (PIPs)

Phosphatidylinositides are membrane-associated phospholipid molecules implicated in a variety of cellular processes necessary for growth, division, and survival [103]. The production of PtdIns and their phosphorylated forms is upregulated during insulin stimulation - owing in part to the increased activity of PI3K [104, 105]. Phosphatidylinositol can be phosphorylated on the D3, D4, or D5 positions of its inositol ring. This
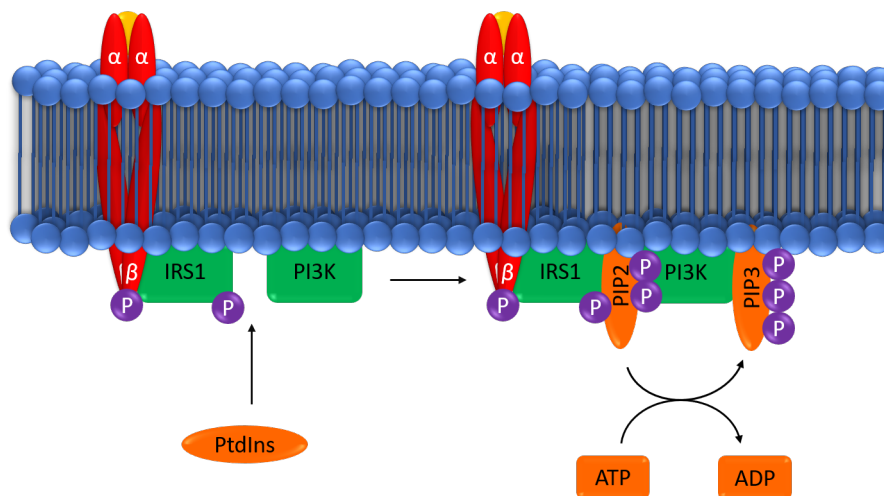
Figure 2.5: The binding of PtdIns to the PH domains of active IRS and PI3K results in the conversion of PtdIns to PI3P, PI3P to PI(4,5)P2, or PI(4,5)P2 PI(3,4,5)P3. In each case the phosphate donor is ATP. The PIPs act as 'targeting' molecules in this instance whereby they are essential in recruiting other proteins (e.g. PDK1, Akt) to the PM.

generates a phosphatidylinositol mono-, di-, or tri-phosphate (PI3P, PIP2, or PIP3 respectively) [106]. While these PIPs are implicated in several signalling pathways, of present interest remains their interactions with PDK-1 and Akt. Crucially, PIPs provide the link between the IR-PI3K (Fig. 2.5) and the PDK1-Akt (Fig. 2.6) arms of the signalling cascade. Activating PI3K in the absence of the PtdIns substrate does not induce increase in glucose transport [107, 108]

The PtdIns molecules mediate the induction of glucose transport by binding to PH domains on phosphoinositide-dependent kinase and Akt proteins [109, 110]. After the phosphorylation of PtdIns into a PIP by PI3K, the PIP acts as 'anchor' proteins to which PDK1 and Akt proteins bind. These anchor-points for allow for free-floating, cytosolic PDK1 and Akt to attach to via their PH domain [111]. This process is accelerated during insulin stimulation [112]. However, as will be discussed further, the functions of PDK1 and Akt are different in nature. While both attach to the PM-PIP complex, PDK1 is a necessary regulator of Akt function whereas the binding of PIP3 to Akt induces the recruitment of GSV-bound AS160 to the PM. All three molecules - PIP3, PDK1, and Akt - are essential in GLUT4 translocation and eventual fusion [112]. Finally, the presence of a phospholipid binding site on AS160 which preferentially binds PI3P implicates a PI3P-AS160 interaction in the activation of GLUT4

[105]. However, the precise mechanism by which this occurs is still unknown.

2.1.6 PDK1

Phosphoinositide-dependent kinase 1 (PDK1) is the downstream effector of PI3K and the PIPs. It is a 63 kDa, membrane-associating serine/threonine kinase protein and it consists of an N-terminal kinase domain and a C-terminal PH domain [102]. While PDK1 retains greater binding affinity for PI(3,4)P2 and PI(3,4,5)P3, it is nonetheless able to bind all forms of PIPs [113]. Further, PDK1 interacts with a host of downstream signalling molecules such as S6-kinase 1 (S6K), protein kinase C (PKC), and protein kinase A (PKA). Amongst these is Akt - the next direct link to GLUT4 translocation [113–115].

Upon stimulation by insulin, the PI3K will rapidly convert PIP and PIP2 to PIP3. These phospholipids remain membrane-associated until they are recognised by the PH domain of PDK1 [116, 117]. Since PDK1 is constitutively active - only being recruited to the PM in greater numbers on insulin stimulation - it needs no further modulation until it binds with Akt, which has been recruited to the PM via a PH-PIP3 interaction [118, 119]. The close proximity of Akt and PDK1 will result in Akt being phosphorylated at serine 473 and threonine 308 [102]. This makes PDK1 a necessary intermediate in proper insulin signalling.

The necessity of PDK1 is further underscored by studies that seek to disrupt the normal functioning of PDK1. Bayascas et al (2008) disrupted the PH domain on PDK1 in mice, eliminating the interaction between PDK1 and PIP3 [120]. The mice grew to be insulin resistant, underweight, and stunted. Similarly, the disruption of PDK1 functioning by inhibiting PI3K - therefore starving PDK1 of substrate - lead to dysregulation of the insulin signalling cascade [121]. In this study, the β cells, being unable to upregulate glucose transport in the presence of glucose and insulin, steadily released ever-increasing levels of insulin to compensate. Further studies have shown that disrupting PDK1 will lead to liver failure [122] or a diabetic state due to β-cell death [123].
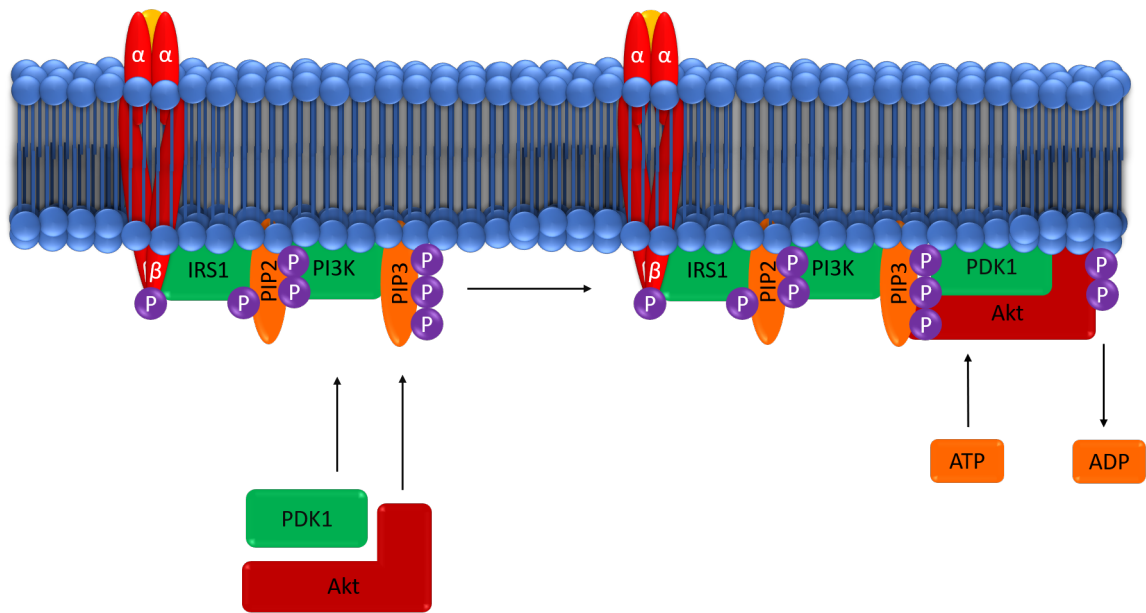
Figure 2.6: PI(3,4,5)P3 is a target molecule for PDK1 which consequently translocates to the membrane. Similarly, PI(3,4,5)P3 and PDK1 now act as recruiters for Akt. Once Akt has translocated to the membrane, it is phosphorylated by PDK1 on several residues, but most notably Ser473. This, in addition to Thr308 phosphorylation by mTORC2, results in the 'active' form of Akt.

2.1.7 Akt

The family of Akt kinase proteins consists of three isoforms - Akt1, Akt2, and Akt3 (previously Protein Kinase Bα, β, and γ) [124]. All Akt isoforms share a similar domain structure: an N-terminal PH domain, a central kinase domain, and a C-terminal, hydrophobic regulatory domain [125]. The PH domain binds PIPs (specifically PI(3,4)P2 and PI(3,4,5)P3) associated with the membrane-bound PDK1 protein (Fig. 2.6) [116, 126, 127]. The kinase domain contains a conserved threonine residue (Thr308) which is responsible for the activation thereof [128]. Similarly, the hydrophobic motif contains a conserved serine (Ser473) which acts as a regulatory site for Akt activity [129].

The functionality of Akt is defined by dual phosphorylation on Thr308 and Ser473 [98]. It has been suggested that phosphorylation of the Thr308 residue by itself is necessary and sufficient for the induction of Akt kinase activity [91]. However, full induction of Akt activity appears to require the phosphorylation of Ser473 as well [98, 120].
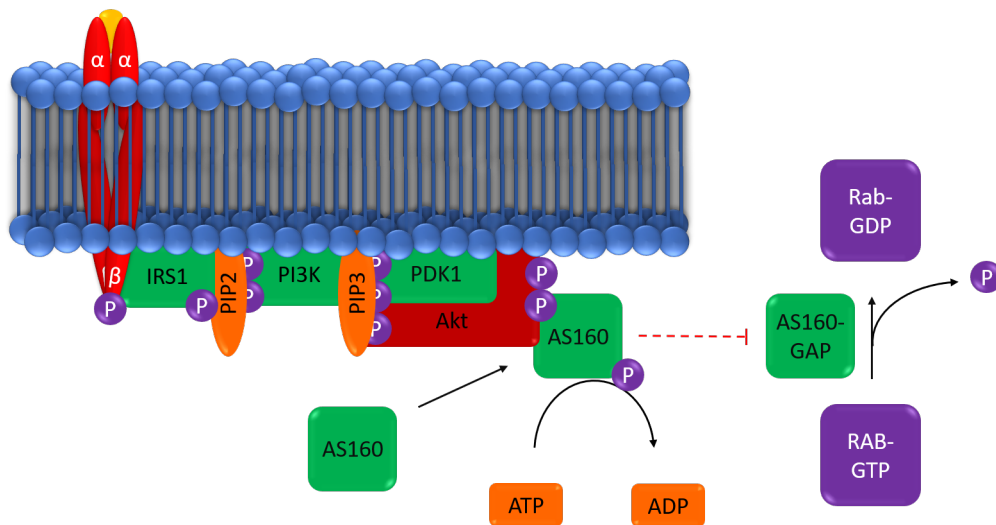
Figure 2.7: Phosphorylated Akt targets AS160 which contains a GTP-ase activating domain (GAP). The AS160-GAP constitutively hydrolyses the GTP on the Rab-GTP complex - an action which prevents the translocation of GLUT4 storage vesicles to the PM. The phosphorylation of AS160 by active Akt inhibits the AS160-GAP activity, preventing the hydrolysis of Rab-GTP, and ultimately encouraging the translocation of GLUT4 to the PM.

Upon insulin induction and the subsequent generation of PI(3,4)P2 and PI(3,4,5)P3, Akt co-localises to the PM with PDK1 [77, 130]. Both proteins attach to PIPs by their PH domains. In Akt this is thought to engender a conformational change that exposes the central, active site of the kinase domain [91]. This gives PDK1 access to Thr308 which is subsequently phosphorylated, leading to the recruitment and activation of downstream effectors [91, 129, 131].

The Ser473 residue of Akt is phosphorylated by mTORC2 which is activated when binding with PI3P [132, 133]. While less able to induce GLUT4 translocation by itself, the Ser473 residue nonetheless appears responsible for the modulation of Akt kinase activity [134]. More specifically, it has been suggested that phosphorylation of Ser473 'stabilises' the phospho-Thr308 site by preventing dephosphorylation and thereby extending its half-life [127].

The next - and final - downstream target of Akt is AS160 (Fig. 2.7) [135]. The Ser/Thr kinase domain of Akt targets as many as six potential phosphorylation sites on AS160 [136]. However, most commonly the AS160 residues Ser588 and Thr642 are targeted [137, 138]. AS160 phosphorylation responds strongly to increases in insulin

concentration and has been shown to be significantly reduced in diabetic patients [135]. AS160 is considered to be a crucial component of the insulin signalling cascade as it links the IRS-PI3K-Akt axis to the induction of glucose transport [139, 140].

The 160kDa AS160 protein contains a constitutively active Rab-GAP (GTP-ase Activating Protein) domain [141]. The Rab-GAP domain activates innate GTP-ase domains on small G-proteins known as Rabs [142]. In the context of insulin signalling, Rabs are often found on the surface of GLUT4-storage vesicles (GSVs) [143, 144]. Evidence points to Rab4, Rab8, Rab10, Rab11, and Rab14 mediating functions such as GLUT4 recycling, internalisation, trafficking, and membrane fusion [143, 145, 146]. This suggests that the Rab-GTP complex is the 'active' form of Rab which is responsible for GLUT4 regulation. Unphosphorylated AS160 would therefore perpetually result in active GAP domains which hydrolyze GTP, thereby inactivating Rab-mediated GLUT4 activity [147]. Phosphorylation of AS160 by Akt inhibits the activity of the Rab-GAPs which, in turn, preserves the Rab-GTP complex [30, 148]. Therefore, Akt relieves the persistent inhibition of Rab-mediated GLUT4 trafficking by downregulating AS160-Rab-GAP activity.

Lastly, owing to the variety of signals that impinge on Akt, it can be viewed as a molecular 'switchboard' which directs incoming signals to their appropriate termini. On closer analysis, two broad categories of Akt pathways emerge: first, a set of reactive, stress-related pathways that activate based on factors such as oxidative stress [149], inflammation [150], psychological stress [151, 152], nutrient stress [153], or temperature stress [154]. Secondly, and more germane to the present study, a set of pathways which maintain homeostatic features such as the cell-cycle [155], cellular energetics [156], and protein synthesis [157]. A non-exhaustive summary of these pathways can be found in Table 2.2.

2.1.8 Glucose Transporters: Focus on GLUT4

The dynamics of glucose transport, glycolysis, as well as the induction thereof differs from tissue to tissue. However, there is one common thread - glucose must be imported into the cell. Glucose import is accomplished by a family of 14 *Solute Carrier* proteins

Table 2.2: A brief summary of Akt and its downstream effectors.

Pathway	Mediator	Function	Reference
Reactive	Hsp90	Protein folding, cell signalling, regulation of apoptosis	[158–160]
	IKK	Modulates anti-tumorigenic behaviour of NF-κB	[161, 162]
	JNK	Pro-apoptotic signal	[163]
	PP2A	Tumor-suppressor, cell-cycle regulation	[164]
	PHLPP	Tumor-suppressor, abrogates aberrant Akt activity	[165]
	TBK1	Induces pro-survival Akt pathways in response to immune signalling	[166, 167]
Homeostatic	GSK3	Activates synthesis of glycogen	[168, 169]
	AS160	Regulates GLUT4 trafficking to PM	[141, 170]
	mTORC1	Regulates protein synthesis and mRNA transcription	[171]
	mTORC2	Activation and feedback regulation of Akt	[172, 173]
	FOXO	Cell-cycle regulation and DNA repair	[174]
	PFK	Regulation of glycolysis and glycogenolysis	[175, 176]

(SLC2), more commonly known as glucose transporters or the GLUT family [177]. These proteins facilitate the unidirectional diffusion of (primarily) glucose across the plasma membrane and into the cell. However, they are also responsible for the import of polyols, small carbon compounds, and other monosaccharides into the cell.

The GLUTs are divided into three classes (I,II, and III) depending on their sequence homology [178]. However, the structure and sequence of the glucose transporters remain highly conserved among species [179]. Generally, a glucose transporter is $\pm$ 500

amino acids large, has 12 trans-membrane domains, and conserved N and C termini. A brief summary of all 14 glucose transporters is provided in Table 2.3.

Table 2.3: A short overview of the 14 GLUT proteins (including HMIT) as well as their predominant functions.

Class	Name	Function	Reference
I	GLUT1	Basal glucose uptake in various tissues	[180]
	GLUT2	Import of glucose into β cells	[56]
	GLUT3	Low-affinity, inducible transporter in neurons	[181]
	GLUT4	Insulin stimulated glucose uptake in muscle and adipose tissue	[182]
	GLUT14	GLUT3 duplicate, primarily active in testes	[183]
II	GLUT5	Fructose transporter in the intestine	[184]
	GLUT7	Intestinal hexose transporter with low affinity for glucose and fructose	[185]
	GLUT9	Urate transporter in kidneys and liver with low glucose affinity	[186]
	GLUT11	High affinity fructose transporter in muscle and heart	[187]
III	GLUT6	Inflammation-responsive lysosomal monosaccharide transporter	[188]
	GLUT8	Intracellular hexose transporter found on endosomes and lysosomes	[189]
	GLUT10	Low activity, non specific transporter found in almost all tissues	[177]
	GLUT12	Insulin insensitive glucose transporter found mainly in the heart	[190]
	HMIT	H$^+$/myo-inonsitol symporter found in the brain	[191]

GLUT4   The GLUT4 glucose transporter is crucial for glucose homeostasis and is in fact the canonically 'main' glucose transporter in insulin sensitive tissues [182, 192]. Under basal conditions, GLUT4 is distributed among the plasma membrane and the perinuclear space with the balance favouring the latter [193]. Nearly 75% of GLUT4

is thought to reside in the perinuclear space under basal conditions [194]. At the perinuclear space, GLUT4s are stored in specialised 'storage veiscles' - GLUT4 Storage Vesicles or GSVs [31]. GLUT4 storage vesicles are between 50 and 100 nm in diameter and can contain up to 25 GLUT4 molecules [195]. The formation of GSVs is most-likely preceded by the budding off from an as yet unidentified donor membrane [196]. Li et al (2009) suggested that the membrane donor for the GSVs may be found near the perinuclear compartment which suggests that it may be another vesicle or endosome [197].

The GSVs are clustered around a structure known as the 'Mictrotubule Organisational Center' or MTOC [198]. This structure, located close to the nucleus, is responsible for the tethering of the microtubules (MTs) as well as various endosomes and smaller organelles that rely on the network of MTs to travel throughout the cell. Once the insulin signal terminates with the GSVs, these dissociate from the MTOC and, aided by MyoVa and KIF5B kinesin motor proteins, travel along the MTs to reach the peri-membrane space [196, 199].

Stimulation by insulin initiates several events simultaneously. The rate at which GLUT4 undergoes endocytosis is reduced significantly [200]. Under basal conditions, GLUT4 experiences a steady 'recycling' to and from the PM. The insulin signal tilts the balance of this cycling in favour of the non-excretory exocytotic mechanisms that deposit GLUT4 in the PM [201]. Simultaneously, the reservoir of GLUT4 present in GSVs near the MTOC attach to MTs and begin their journey towards the PM. The reliance on MTs for translocation results in the GSVs translocating, tethering, and fusing in distinct clusters. This results in 'punctate' clusters of GLUT4 near the membrane termini of MTs [202].

Once the GSVs have reached the PM, GLUT4 is activated in three distinct stages: tethering, fusion, and GLUT4 activation [192, 203]. Tethering, the first of these stages, occurs once the GSV has reached the PM and halted. Here, Myo1c, a membrane-associated motor protein and the exocyst subunits Exo6 and Exo84 tether the GSVs to the plasma membrane. The precise mechanism by which this occurs is not yet known, however considering that the exocyst contains a GAP domain, it is likely that

it interacts with the Rab-GTPs on the surface of the GSV membrane.

The second step, fusion, requires a large assembly of membrane associated proteins: SNARE, Syntaxin-4, Sec1/Munc18-like (SM) proteins, VAMP2, VAMP3, and VAMP8 as well as SNAP23 [201, 204–208]. While the precise nature of their interactions would go beyond the scope of this thesis, one can briefly summarise it as follows (Fig. 2.8). The SNARE proteins are a family of receptor proteins which associate with Soluble NSF Attachment Proteins (SNAPs). The SNAPs are directly involved in the tethering and fusion of vesicle with the PM. Once the GSV and associated SNARE complexes are between 4 and 8 nm from each other and the PM, what follows is a progressive 'unzipping' of the GSV and the PM. Once sufficiently unzipped, the SNARE complexes will join the loose ends of the GSVs with those of the PM, completing this cycle of non-excretory exocytosis [209, 210].

Now that GLUT4 is located within the PM, all that remains is for it to be activated. The precise nature of GLUT4 activation is yet to be uncovered, however it is certain that membrane-associated products of PI3K (PI3P and PI(4,5)P2) are involved [108, 203]. Specifically, it appears as if both PI3P and PI(4,5)P2 assist with the unmasking of the C-terminus of GLUT4. While both products play a role in the insulin-mediated translocation and activation of GLUT4, it seems as if PI3P alone has the power to induce GLUT4 into an active conformation. It has been suggested that this is due to F-actin remodelling of the PM in response to PI3P [211, 212].
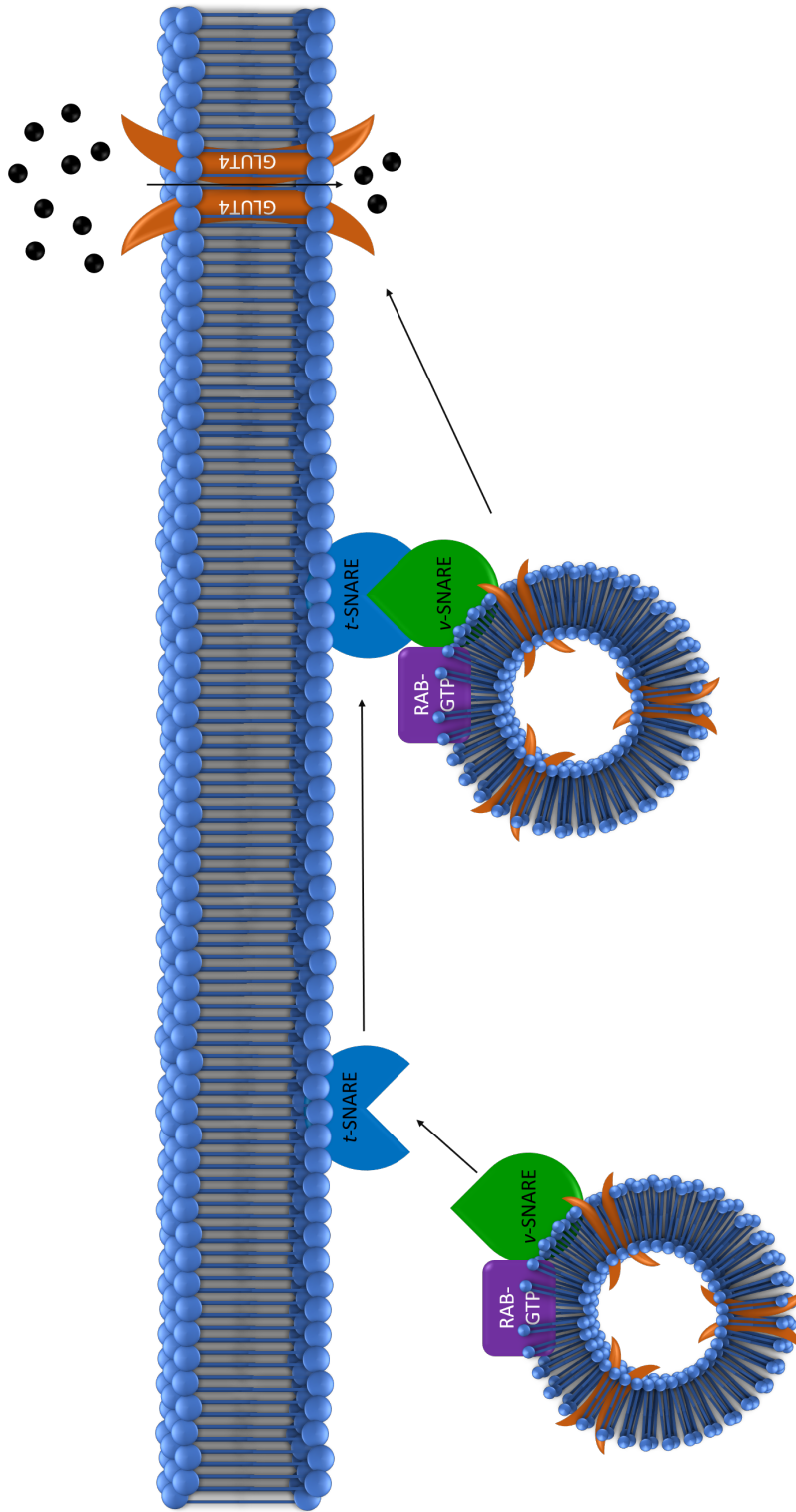
Figure 2.8: The targeting complex v-SNARE likely binds with Rab-GTP which is on the surface of the GSV. Its complement, the t-SNARE complex remains bound with the PM. As more GSVs are transported to the plasma membrane, the perimembrane space - about 8 nM from the internal membrane surface - becomes crowded with v-SNARE molecules which are attached to the GSVs. The v-SNARE and t-SNARE molecules will sooner or later bind one to one another as the GSVs collide with one another and the membrane. The SNARE complexes begin 'unzipping' the PM as well as the GSV. Munc18c on the v-SNARE complex has been implicated in joining the ends of the two membranes. Once a single, cohesive membrane has been formed and the GLUT4 is at the cell surface, it is activated and begins transporting glucose (black spheres) into the cell.

2.1.9   Insulin Signalling: Summary

This signalling cascade is subject to regulation by feedback mechanisms that depend on the activity of various phosphatase proteins [213]. As to not exceed the scope of this review, focus is directed on the following three phosphatases by way of illustration: SHIP2, PTEN, and PHLPP. The Src2 Homology Inositol polyphosphate 5-Phosphatase (SHIP2), is an important regulator of PI(3,4,5)P3 availability [214]. When it is activated by PI(3,4)P2, it hydrolyses the 5-phosphate of PI(3,4,5)P3 [215]. This has important downstream implications as it prevents the recruitment of Akt to the PM. This abrogates insulin signalling through Akt and results in fewer GLUT4 molecules translocating to the PM.

Similarly, PTEN (Phosphatase and TENsin homologue) is a PI(3,4,5)P3 phosphatase [216]. However, unlike SHIP2, this enzyme hydrolyses the 3-phosphate of its target substrate. This inhibits the ability of PDK1 to recruit Akt to the PM and results in the downregulation of insulin-stimulated glucose update.

Lastly, PH domain Leucine-rich Protein Phosphatase (PHLPP) directly inactivates Akt by hydrolysing the phosphate on serine 473 [165]. This severely impacts (although not completely abolishes) the ability of Akt to phosphorylate the AS160-GAP domain. Consequently, this prevents GLUT4 from being translocated to and integrated with the PM.

This process is broadly summarised in Fig. 2.9. This presentation shows the insulin signalling cascade as an 'input-output' mechanism which represents only the direct interactions between the signalling molecules. Herein, the 'main' insulin signalling is highlighted in green while other, secondary pathways that activate (or are activated by) the insulin signalling cascade are highlighted as blue, dashed lines. Similarly, pathways which attenuate the Akt-dependent GLUT4 activation are indicated by the red, dashed lines.
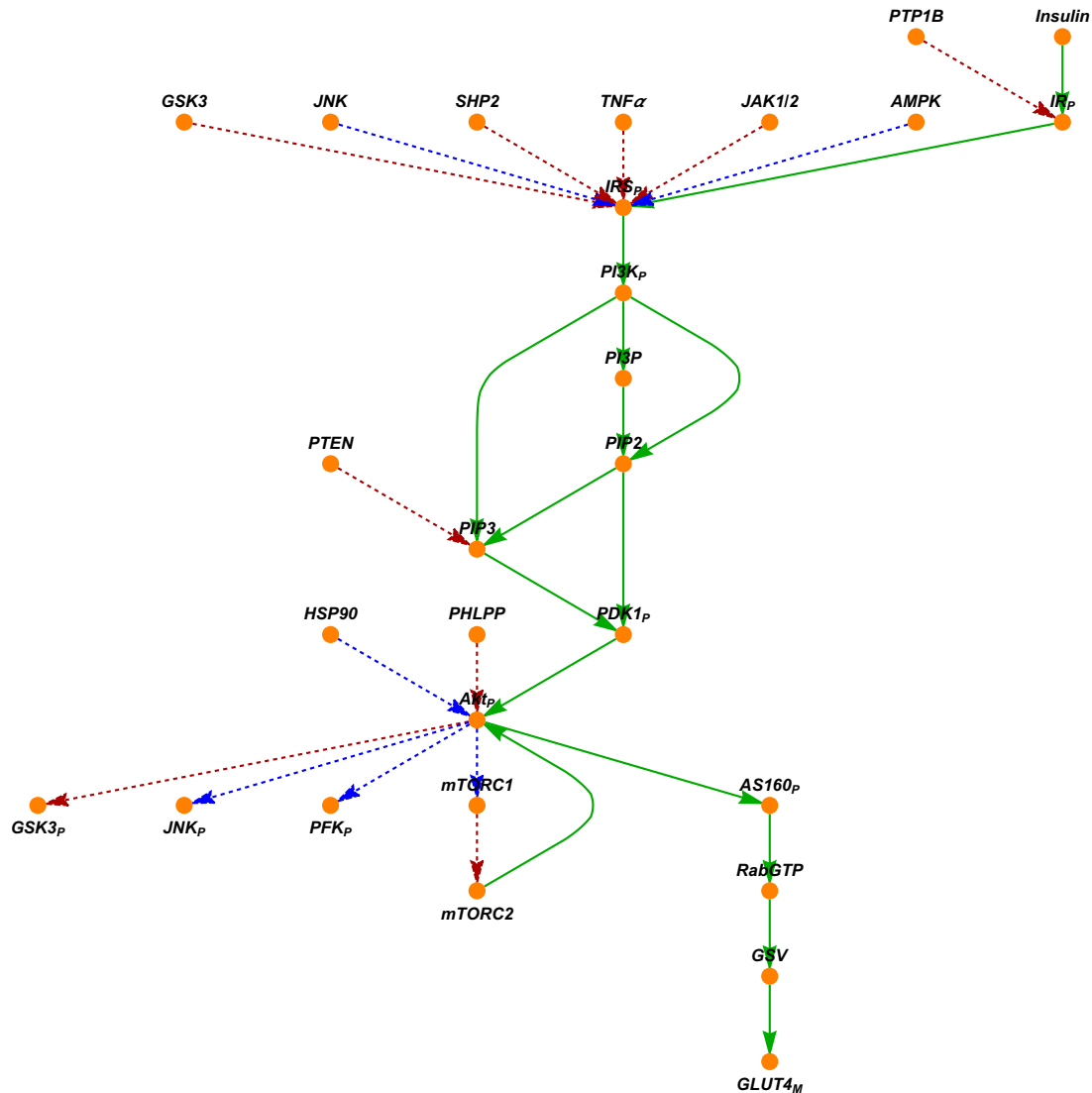
Figure 2.9: A more simplified schematic of the insulin signalling pathway(s). This graph highlights the interactions between the activated and inactivated agents in the signalling cascade. The main, IR-IRS-PI3K-Akt pathway is highlighted with the solid, green lines. Whereas secondary interactions are indicated with dashed lines. The blue dashed lines indicate pathways which are not directly activated by or related to the insulinic state of the organism. The red dashed lines indicate pathways which either inhibit or downregulate signalling intermediates and therefore attenuate the activation of GLUT4 via the Akt-dependent pathway.

2.2   Metabolism and Physiology

Type 2 diabetes manifests on a tissue, organ, and whole-body level. In moving away from the cellular level, the question arises: how does the human organism respond to an induction of insulin signalling?

The brain contains insulin, IGF1, and IGF2 receptors [217]. How insulin reaches the brain is still a matter of debate, however the leading theories include transport via the cerebrospinal fluid or through the vascular system, or via the hypothalamus which lacks a selective barrier. In addition to mediating increased glucose uptake through GLUT1 and GLUT3, it appears as if insulin directly affects neural signalling and brain chemistry [218].

In the liver, the effects of insulin signalling are far more significant to metabolic homeostasis than in the brain. Specifically, the activity of the insulin signalling cascade has profound implications for the metabolism of lipids, proteins, and glucose. Lipogenesis is stimulated when Akt activates mTORC1 [219]. Protein synthesis in the liver is stimulated by insulin through the Akt-GSK3 and Akt-mTORC1 pathways [220].

Upon insulin stimulation, the liver regulates glucose metabolism as follows: inhibiting glycogenolysis, stimulating glycogenesis, stimulating glycolysis, and inhibiting gluconeogenesis. Insulin mediates the activation of protein phosphatase 1 (PP1) via Akt [221]. This results in the dephosphorylation and subsequent inactivation of glycogen phosphorylase - thus inhibiting glycogenolysis [222]. Simultaneously, insulin mediates the deactivation of glycogen synthase kinase 3 (GSK3) by Akt. As a result, glycogen synthase remains active and able to further polymerise glycogen molecules. Further, by effecting the Akt-mediated phosphorylation and inhibition of FoxO, insulin relieves the inhibition of glucokinase by FoxO [223]. Simultaneously, this prevents the stimulation of Phosphoenolpyruvate carboxykinase 1 (Pck1) and glucose 6-phosphatase (G6PC) - two regulation points for gluconeogenesis [224]. Consequently, in the insulinic liver, net glycolysis to pyruvate is upregulated while gluconeogenesis is downregulated.

2.2.1   Muscle Physiology

Skeletal muscle primarily subsists on fatty acids at rest, it can account for between 70 and 90% of glucose consumption in the postprandial and exercising states [225]. This is further reflected by skeletal muscle being the primary reservoir for insulin-responsive GLUT4 transporters [31, 182]. The translocation of GLUT4 can be achieved either through dietary means, which result in the release of insulin, or through exercise.

Exercise induces insulin-independent translocation of GLUT4 to the PM [226]. These effects can persist as long as 16 hours after the bout of exercise [227]. Wojtaszewski et al (2000) showed that exercise reduced the half-activation time ($t_{0.5}$) of glucose uptake from $\pm$ 34 minutes to $\pm$ 11 minutes [228].

This ligand-independent activation of insulin signalling appears to be mediated primarily through AMPK. It appears as though this molecule is responsible at turns for the *direct* activation of insulin signalling through IR, IRS, and AS160-GAP phosphorylation as well as *indirect* activation by 'priming' skeletal muscle for insulin signalling. This latter mechanism likely plays a role in the anti-inflammatory effects of exercise and AMPK signalling.

Insulin and AMPK signalling are important for the proper growth and development of skeletal muscle tissues [229]. Both *ir-* and *igfr*-knockout mice experience extremely low birthweight, developmental retardation, and ultimately death within days of being born [230]. Similarly, $\text{AMPK}\alpha 1^{-/-}$ mice are unable to regain insulin sensitivity, whereas knocking out both forms of AMPK is lethal for the embryo [231].

Further, the differentiation of myoblasts to myotubes is associated with a five to ten-fold increase in surface IR [232]. This is accompanied by an increase in GLUT4 expression [233]. Myoblasts which have been induced to exhibit the diabetic phenotype (abrogated insulin signalling) by using excess (25mM) glucose in the growth medium differentiate into adipose tissue instead of myotubes [234].

In addition to mediating glucose uptake, skeletal muscle is also known for its flexibility in selection. The ability of skeletal muscle to subsist on glucose, fatty acids, or the products of proteolysis allows the muscle, along with the liver, to regulate the availability and utilisation of fuel by the organism [235]. Consequently, the skeletal

muscle tissue is an appropriate target for studies wishing to further examine the role of insulin or the insulin signalling network in metabolism or disease.

2.2.2 Obesity, Inflammation, and Type 2 Diabetes

One of the metabolic states most-closely associated with dysfunctional insulin signalling is obesity [236]. Obesity is primarily caused by the interplay of sedentary lifestyles and overfeeding [237]. However, the contribution of genetic or inflammatory factors should not be dismissed [238, 239]. Obesity is a physiological state characterised by severe overweight, inflammation, and excess fatty tissue [238, 240, 241]. People who are diagnosed with obesity tend to have a Body Mass Index (BMI) greater than 30 as well as more than 25 - 33% body fat. Of particular interest is the excess body fat as it likely contributes to the necessary dysregulation of whole-body metabolism, inflammation responses, and insulin signalling that lead to type 2 diabetes [242, 243].

A primary symptom of obesity is dyslipidemia; elevated levels of free fatty-acids (FFAs) and triglycerides (TGs) [244]. Dyslipidemia and the associated FFAs and TGs eventually lead to inflammation [245]. The swelling of the adipocytes constricts the capillaries and blood flow into adipose tissue [243, 246]. The restriction of blood flow likely creates hypoxic conditions in the fatty tissue. Hypoxia alters the redox balance and raises the oxidative stress in affected tissues [247]. The greater oxidative stress likely leads to the production of free radicals [248, 249]. This rise in free radical levels induces pro-inflammatory mechanisms [250]. This is the first point of inflammatory burden.

The second pro-inflammatory mechanism is associated with the increased burden of free fatty-acids. Fatty acids are well-known inducers of pro-inflammatory signals [244, 251, 252]. It is likely that this mechanism involves FFAs binding to G protein-coupled receptors (GPCRs) which then activate the release pro-inflammatory cytokines TNFα and IL-6 [253]. Additionally, FFAs induce the release of IKKβ, IL-1, and JNK [252]. This places an immense burden of inflammation on any physiology and has been implicated in various diseases such as: hypertension [254], depression [255], cardiovascular disease [256], and arthritis [257].

Triglycerides present the third arm of the pro-inflammatory cascade. While the effects of elevated levels of triglycerides are seemingly less severe than elevated levels of FFAs, their effects nonetheless remain contributory to the overall inflammatory response in obese individuals [258]. Triglycerides activate the NF-κB and VCAM-1 pro-inflammatory signalling pathways - most likely through GPCR signalling [258]. Additionally, TGs have been associated with vascular inflammation [259] and increased FFA release [260].

The effects of obesity however do not remain limited to adipose tissue. The release of pro-inflammatory cytokines from the adipose tissue profoundly affects skeletal muscle cells. Prolonged sedentary periods decrease the mitochondrial content of skeletal muscle [261, 262]. This in turn depletes the capacity of skeletal muscle to oxidise FFAs effectively [263]. Under resting conditions, FFAs satisfy the majority of the Gibbs energy demand in skeletal muscle. A reduction of this capacity, especially in already obese individuals is likely to further accumulate inflammatory damage. A further effect on skeletal muscle is found in the consequences of elevated pro-inflammatory cytokine levels. Inflammatory markers such as TNFα, IL-1, or IKKβ are able to induce insulin resistance [264–266]. The persistent, supranormal concentrations of pro-inflammatory cytokines, the depletion of skeletal muscle FFA-oxidative capacity, and the abrogation of insulin signalling should ultimately result in the development of type 2 diabetes.

2.2.3   Mouse Skeletal Muscle (C2C12) Cells

The C2C12 mouse SkMC, like most SkMCs begin their lifecycle as precursor myoblasts. When given sufficient nutrients, time, and growth factors whether *in vivo* or *in vitro* these cells begin aligning parallel to one another [267]. Thereafter, they begin fusing into multi-nucleated fibres - undergoing further *differentiation* - until they achieve morphological parity with muscle fibres or myotubes [268]. The differentiation of muscle cells is aided by factors such as HsP90 [269], Vitamin D [270], calcium [271], and insulin [272, 273]. Considering the importance of skeletal muscle in metabolic homeostasis and its dependence on insulin signalling the choice of an SkMC line for this study was *von selbstsprechend*.

Indeed, the documented use of C2C12 as a model cell line for insulin signalling [268, 269, 274, 275] as well as the ease with which these cells differentiate [268] cemented their use for the present study. However, despite the widespread use of C2C12 cells as a model for insulin signalling and glucose uptake, there remained the issue of C2C12 cells *not* having an insulin responsive GLUT4 mechanism [276, 277]. It is likely for this reason that studies choose to use transgenic cell lines [274], glucose analogues [278, 279], or non-insulinic inducers of the signalling pathway instead [269, 280]. Glucose analogues such as 2-Deoxy Glucose, 2-NBDG, or Fluorodeoxyglucose accumulate in the cytosol, and inhibit hexokinase, and inhibit glucose transport due to the accumulation of intracellular glucose [281, 282]. Consequently, these metabolites are unlikely to provide a *bona fide* account of glucose transporter activity.

A final aspect to consider is the glucose concentration at which C2C12 cells are cultured. Work by Luo et al (2019) which suggests that high glucose concentrations down-regulate Akt signalling [279]. Further, considering that the observed expression ratio of GLUT1:GLUT4 shifts towards the latter as the cells differentiate [283], a greater degree of differentiation is desirable when investigating GLUT4. However, considering negative effects of high glucose concentrations on C2C12 differentiation [279] as well as the scarcity of reports which mention the *degree* of SkMC differentiation, it is difficult to draw *exact* conclusions regarding the functioning of glucose uptake in these cells. Therefore, determining the *basal* state of insulin signalling under conditions that are as physiologically relevant as possible is a priority.

2.3 Systems Biology and Mathematical Modelling

Biological data are being collected at ever more rapid paces, aided by high throughput methods from fields such as proteomics [284], NMR [285], and bioinformatics [286]. The need for tools which consolidate the available knowledge while providing interactive, predictive mechanisms one can use to generate knowledge and meaning from a dataset is therefore paramount. Systems biology relies on the development of computational representations - models - of *das Ding an sich*. While there are innumerable

models in existence, broadly, there are two approaches: 'top down' or 'bottom up' models [287]. The modelling approach depends on the available dataset as well as the research questions one wishes to answer.

The top down approach attempts to find models from large (such as whole genome or organismal) datasets rather than uncovering it by studying lower-level interactions [288]. These models often rely on data generated by -omics fields and seek to provide 'macro-level' explanations that may ignore details on lower rungs of the hierarchy - especially if they do not contribute meaningfully to larger scale phenomena [288, 289]. Top down models develop hypotheses based on higher order phenomena which then seek to be validated through experimentation [290]. For example, the top down approach may predict protein expression levels or enzyme kinetics based on transcriptomic or metabolomic data respectively. These predictions would then require validation by directed experimentation. The top down approach therefore seeks to steadily reduce the data until the most parsimonious explanation of a phenomenon is reached.

Bottom up modelling by contrast attempts to successively integrate low complexity phenomena into more complex systems [291]. Bottom up models rely on detailed information regarding the parts of a system. The behaviour of the system is then deduced based on the functional characteristics and interactions of an artificial subset of constitutive factors. Whereas top down relies on directed experimentation for hypothesis testing, bottom up models require exploratory experimentation for hypothesis formulation.

Bottom up modelling often begins with a known molecular mechanism and then attempts to computationally predict how the system to which the mechanism belongs might behave. These preliminary predictions would then be used to develop hypotheses which may be tested experimentally or through further computation. Due to the smaller scale of bottom up modelling, hypotheses can be tested by perturbing the factors within a system in order to observe how the system reacts. This, fundamentally, makes bottom up models mechanistic in nature [290].

Top down and bottom up modelling have both been successfully used to decode the fundamental, functional machinery of cells and organisms. This includes signal

transduction networks such as insulin signalling [292] and metabolic pathways such as glycolysis [293]. While the more applied outcomes of systems biology include drug development [294] or process optimisation [295], fundamentally systems biology is a tool which is used to uncover and explain natural phenomena from metabolic pathways to global economies and pandemics [296].

Constructing a model of biological processes is not a trivial task and several approaches can be considered, each of which depend on the nature of the data, experimental design, and questions the researcher wishes to answer. One such approach is FBA of large, genome-scale metabolic models. This approach relies on reconstructions of metabolic networks from genomic data. Based on the stoichiometries of these metabolic networks, the FBA approach will calculate the fluxes of metabolites through each reaction and often seeks to answer questions of optimisation; i.e. how to optimise growth rate or metabolite production [297]. Such an approach was used to tease apart the metabolism of glucose and glutamine in cancer cells which exhibit the Warburg effect [298].

Another paradigm is MCA which is based on ODEs much like the approach used in this thesis. Metabolic control analysis uses a step-wise reconstruction of metabolic pathways in order to determine how the control of flux is distributed in the network [299]. This approach is smaller in scale than those which rely on -omics data (such as FBA), but is probably able to answer more directed questions regarding which enzymes or steps in a pathway can be inhibited or activated in order to modulate the flux of metabolites. Such an approach can be used for signal transduction networks [300]. Other approaches such as domino systems biology [301], supply and demand analysis [302], and a method by which models are determined from inaccurate or incomplete data [303] also exist. However, the examination of these and other approaches is beyond the scope of this review.

2.3.1 Models of the Insulin Response: An Overview

Possibly the earliest computational model of insulin action dates to the work by Sherwin et al in 1974 [304]. This work sought to determine the delivery and clearance

kinetics of insulin in humans. The model divides the insulin delivery and clearance mechanisms into three distinct compartments: the blood plasma, a small, rapidly equilibrating compartment, and a larger, more slowly equilibrating compartment. It is likely that the latter two compartments refer to the peripheral and hepatic vascular systems respectively [305]. The use of radioionidated insulin, as a tracer molecule, and an early iteration of Simulation, Analysis, And Modelling software (SAAM), to derive the deliver and clearance parameters, presented a novel approach to understanding insulin signalling [304].

In the intervening years, the modelling of insulin has advanced significantly and followed the usual divide between top-down and bottom-up models. An example of the top-down approach is the model by Dalla-Man et al [33]. Unlike earlier models which administered GTTs (GTTs), this model used stable isotope tracers in subjects' meals to gather data regarding the insulin and glucose fluxes in an individual. Herein, the molecular mechanisms which govern insulin signalling or glucose metabolism are shunted into so-called 'black boxes' as they are neither investigated, simulated, nor germane to the objectives of the study. The authors set out to measure the glucose and insulin fluxes in humans in response to a meal [33]. Using these data, the authors constructed a limited model which was able to simulate the appearance and disappearance of glucose and insulin from plasma samples [33, 306]. Similar top-down approaches are used to simulate insulin and glucose fluxes in response to GTTs where glucose is administered orally or intravenously and the subjects' blood plasma is analysed periodically for insulin or glucose levels [307, 308].

In 2002, Sedaghat, Sherman, and Quon published one of the most-comprehensive bottom-up accounts of the insulin signalling cascade [292]. This model includes nearly all known effectors downstream of the IR, as well as a preliminary investigation into the induction of glucose transport. Additionally, the 'Sedaghat' model includes various feedback mechanisms through phosphorylases such as PTEN or SHIP1 [292]. Much like the work of Sherwin et al in 1974, the Sedaghat model presents an important milestone in the application of systems biology to insulin signalling. However, it is necessary to note that their over-reliance on second-hand data as well as paucity of pa-

rameter analysis and lack of rigour when deciding on parameter values compromised the strength of the model in the prediction of details. Nonetheless, it provided a good mechanistic overview of the signalling cascade and in the intervening years, certain predicted behaviours such as the 'overshoot' behaviour of autophosphorylation [309], cell-surface mobilisation of GLUT4 [310], as well as the general mechanism underlying this model have been validated [311, 312]. The pioneering work by Sedaghat, Sherman, and Quon was further used as a baseline in the development of several other mathematical models of insulin signalling [149, 311, 313, 314].

The molecular models continued being developed, leading to the inclusion of glycogen breakdown and glucose transporter dynamics [310]. The model developed by Liu et al built on previous work by Sedaghat et al [292]. The novel inclusion of glycogen phosphorylase, glucose transporters, and insulin secretion enabled the model to accurately reproduce experimental data. However, it too lacked direct validation through experimental data. Additionally, the underlying assumption that the behaviour of the signalling cascade was independent of tissue type is not reflected by the physiologies of skeletal muscle or adipose tissue.

The work of Brännmark et al in 2013 presents the first detailed modelling account of insulin signalling in the diabetic state [315]. Herein adipose tissue from diabetic and non-diabetic people are subjected to immunoblotting as well as glucose (2-deoxy) uptake assays. The results were used to build a mechanistic model of normal and diabetic-state insulin signalling in human adipocytes. In order to simulate the diabetic state, the authors artificially reduced the IR concentration to 55% [315]. Absent any salient feedback mechanism this was sufficient to explain the altered phosphorylation profile of IRS1. However, available evidence does not support a reduction of IR concentrations in diabetic individuals [316–318]. This suggests, in line with the conclusions of Brännmark et al, that some as yet unknown mechanism might regulate IRS phosphorylation. Similarly, the authors reduced the available concentration of GLUT4 by 50%. However, it is not clear from their modelling whether this reflects a reduction of *cytosolic* GLUT4, GLUT4 at the PM, or *inducible* GLUT4. Lastly, the authors attenuated the positive feedback from mTORC1 on to IRS1 by 85%. While this was

sufficient to account for the majority of defects seen in the diabetic state, it is unknown whether the model incorporated feedback inhibition of Akt by mTORC1.

Other models sought to reduce the complexity of the *entire* cascade by instead focussing on sub-compartments. An example of such an approach which ignores some of the complexity in favour of a more focussed scientific question and research design can be found in the work of Sonntag et al [319]. This model sought to describe the regulation of AMPK by IRS in response to insulin. AMPK was found to be sensitive to nutrient levels *and* insulin in HeLa cells and C2C12 myocytes. The latter being an important distinction from certain studies which establish findings in immature myoblasts. Similarly the work by Dalle Pezze et al [320] in the same group explored the regulation of mTORC2, another sub-compartment of the insulin signalling pathway. These models are both notable for their combination of specific research questions, models, and experimental data with which the model predictions are tested and the questions answered.

Work by Kubota et al [321] explored the impact of the insulin-Akt pathway in response to differences in pulsatile or sustained insulin addition. Sustained, pulsatile, or combined secretion of insulin contributed to distinct signalling outcomes (in terms of glucose transport or the phosphorylation of signalling intermediates) in the Akt-dependent insulin signalling pathway. The authors define these outcomes as 'temporal codes' which feature differences in network structure, EC_{50} values, and time constants. These temporal codes were present in various regulatory aspects such as feedforward or feedback behaviour and they allowed Akt greater flexibility with regards to which signalling intermediates it interacts with and when [321].

Temporal coding and a reduced-complexity insulin signalling model and a glycolytic model were used by Noguchi et al [322]. The authors used metabolomic and immunoblotting techniques as well as a unique approach of stimulating rat hepatoma cells with insulin in a pulsatile manner. With these approaches, the authors assessed the glycolytic, gluconeogenic, and glycogenic activity of cells in response to changes in Akt phosphorylation. However, the use of hepatoma cells may provide results that are not typically seen in healthy cells.

The modelling strategy employed in this thesis is that of a 'minimal model' (see Chapter 5). This approach is similar to the 'domino' approach discussed in [301] in that the model consists of several 'input-output' modules which describe certain aspects of the network. However, in contrast to the domino strategy, the modules used in the minimal strategy are determined *a priori* by aligning the research questions, experimental strategy, and available data with one another. Further, the domino strategy allows for the model to be expanded if necessary - 'adding more dominoes' - to account for shortcomings or blindspots.

A minimal model, was used by Bergman [323] to simulate insulin and glucose fluxes based on data gathered through a GTT. It relied on creating several metabolic 'black boxes' or compartments of each of the organs involved in insulin-glucose metabolism. Similarly, the minimal model will recreate an ODE-based description of the modules in Section 1.1. The goal is not to create the best-possible model or the model which described the insulin signalling cascade in the most detail. The goal is to determine whether: a) a minimal description of the insulin signalling pathway is possible, b) such a strategy can provide insights into the normal functioning of the insulin signalling pathway, and c) if such a model can be used to trace dysregulation to a single module which would then require more detailed investigation.

Chapter 3

Materials and Methods

3.1   Media and Buffer Formulations

Growth Media   Standard C2C12 growth media primarily consisted of LG DMEM (Sigma: D6046) which contained the following: 1 g/L glucose, 4 mM L-Glutamine, phenol red, and a variety of vitamins, amino acids, and inorganic salts. The precise composition may be found on the manufacturer's website. The DMEM was supplemented with a further 1 % v/v 200 g/L glucose solution (Gibco: A2494001) to yield $\pm$ 15 mM of glucose. The media was also supplemented with 10 % v/v of undialysed FBS (Gibco: 10493106). The final pH of the growth media was pH 7.4 ($\pm$ 0.2).

Differentiation Media   Standard C2C12 differentiation media consisted of LG DMEM (Sigma: D6046) supplemented with 1 % v/v 200g/L glucose solution (Gibco A2494001) and 2 % ES (Sigma: H1270). The final pH of the differentiation media was pH 7.4 ($\pm$ 0.2).

Cryo-Storage Media   Storage media consisted of LG DMEM supplemented with 20 % FBS and 5 % DMSO (Sigma: D2650). The final pH of the storage media was pH 7.4 ($\pm$ 0.2).

Phosphate Buffered Saline   Two PBS tablets (Gibco : 18912014) were added to 1 L MilliQ water, pH-adjusted to $\pm$7.4, and then autoclaved. This yielded a 1$\times$ PBS

buffer.

Tris-Buffered Saline   A 10× stock is prepared which contains 200 mM Tris and 1.5 M NaCl in MilliQ water. The pH is adjusted to 7.6 with HCl.

Lysis Buffer   This modified version of a RIPA buffer consisted of 50 mM Tris-HCl, 150 mM NaCl, 1 % v/v Triton X-100, in MilliQ and pH-adjusted to ±7.4.

RIPA Buffer   Every 10 mL of RIPA buffer contained the following: 25 mM Tris-HCl, 150 mM NaCl, 0.1 % m/v SDS, 1 % v/v Triton X-100, 0.5 % m/v Na.Deoxycholate, 1 cOmplete™ EDTA-Free Protease Inibitor Cocktail tablet (Sigma: 4693132001), and 1 PhosSTOP™ tablet (Sigma: 4906845001) in MilliQ and pH-adjusted to ±7.4.

Quenching Buffer   This buffer consisted of 1× PBS buffer and 500 mM D-Glucose at a pH of 7.6.

Sample Buffer   Sample buffer refers to an 8:2 mixture of 4× Laemmli concentrate which contains: 0.25 M Tris base, 0.28 M SDS, 40 % v/v glycerol, and 20 % v/v 2-mercapto-ethanol. This was then supplemented with 500 mM DTT.

Stacking Buffer   Stacking buffer is a 0.5 M Tris-HCl and 4 % v/v from a 10 % m/v SDS solution made up in MilliQ water. Thereafter, pH is adjusted to 6.8.

Resolving Buffer   Resolving buffer is a 1.5 M Tris-HCl and 4 % v/v from a 10 % m/v SDS solution made up in MilliQ water. Thereafter, pH is adjusted to 8.8.

Running Buffer   The composition of the running buffer is as follows: 190 mM glycine, 25 mM Tris-HCl, and 1 % m/v SDS, in MilliQ water.

Transfer Buffer   The transfer buffer consists of 50 mM Tris-HCl, 380 mM glycine, 0.1 % m/v SDS, and 20 % v/v methanol in MilliQ water.

Resolving Gel   The 8% resolving gels were created by mixing 3.2 mL of acrylamide with 3 mL resolving buffer and 5.8 mL dH$_2$O. A further 90 μL trichloroethylene (TCE), 84 μL 10% APS, and 6 μL Temed were added for a total volume of 12 mL. The resolving gel was poured and allowed to polymerise for 40 minutes with 1 mL of pure isopropanol to cover the top.

Stacking Gel   The stacking gel (4%) consisted of 400 μL acrylamide, 750 μL stacking buffer, 1.85 mL dH$_2$O, 14 μL TCE, and 3 μL Temed. Once mixed, the isopropanol was poured off the resolving gel and the stacking gel was poured on top. The comb was inserted and the gel was allowed to polymerise for another 40 minutes.

3.2   Methodologies

3.2.1   Replicates and Statistical Analyses

Unless otherwise mentioned, all experiments were performed as biological triplicates. In other words, three independent cell culture flasks or dishes were grown and subjected to the same experimental protocols for each data point. Similarly, unless otherwise stated, these samples were also evaluated as technical duplicates. This meant that, for example, a single ^{14}C glucose uptake assay data point would have three independent samples each of which would be evaluated twice in the scintillation counter. The average the technical repeats would be viewed as the result of a single biological sample. The biological samples would then be averaged and used to calculate the SEM values and n would be set as $n = 3$.

All data were gathered and transferred into Microsoft Excel spreadsheets which would be imported into Wolfram™ Mathematica™ for further analyses. Where data were non-normal (i.e. Chapter 6), Mann-Whitney U tests were performed to compare the means of the data. Further, in Chapter 6, Spearman's Rank correlation testing was used for these data since they were non-parametric. When comparing two sample populations (e.g. Chapter 4), a Student's T-test was performed.

3.2.2 Cell Culturing

The materials, reagents, and media necessary for the cell culturing in this study may be found in Tables 3.6, 3.1, and 3.2.

Cell Thawing, Growth, Maintenance, and Differentiation

Mouse skeletal myoblasts (C2C12) were thawed from LN_2-stored cryovials and seeded in T75 (NEST: 708003) vented flasks which contained 10 mL growth medium. The incubation parameters were: $37^\circ C$, 5% CO_2, and >85% relative humidity (Nuaire: NU-5800). Medium was replaced every second day until a confluence between 70% and 80% was obtained. Cells were then sub-cultured in ratios of 1:6 or 1:10 depending on the needs of the experiment or size of the dish or flask (100 mm or T175; NEST:704001 and 709003). Thereafter the cells were allowed to reach 80% confluence whereupon the growth media was replaced with differentiation media. The cells were allowed to differentiate for five days and the media was replaced every second day. On the fifth day, the cells were prepared for the coming experiments by (unless otherwise stated) an overnight starvation in serum-free LG DMEM. On the day of the experiment, the cells were between 80% and 90% differentiated and had covered nearly 100 % of the surface of the culture flask.

Sub-Culturing and Storage of Cells

Cells were subcultured at 70% confluence by aspirating the growth medium and washing with 1 mL (100 mm dish, T75) or 2 mL (T175) Trypsin-EDTA (0.025%: 0.01%; Gibco: R001100) which were subsequently discarded. After washing, a further 4 mL (100 mm dish, T75) or 8 mL (T175) of trypsin solution were added to the dishes and incubated at $37^\circ C$ and 5% CO_2 for 5 - 8 min and periodically examined under a microscope. Once sufficient (approx. 90%) numbers of cells had detached, the trypsin solution was quenched with twice the corresponding volume of growth medium. Subsequently, cells were either sub-cultured as mentioned above or prepared for storage at $-80^\circ C$. Cells to be frozen were centrifuged at $750 \times g$ for 5 min. The remaining media was aspirated and the pellet was dissolved in 3 mL cryo-storage media. From

this solution, 100 μL were aliquoted for cell counting. Using a haemocytometer, cells were counted and appropriately diluted (with growth media) or concentrated (via centrifugation) until a final concentration of 3×10^5 cells/mL was achieved. Thereafter, 1 mL was added to each cryovial and these were immediately stored in liquid nitrogen (LN$_2$).

3.2.3 Glycolytic Flux and Spectrophotometry

The equipment, reagents, media, and materials for these experiments may be found in Tables 3.6, 3.1, 3.2, and 3.3. For these and subsequent sections, 'room temperature' is approximately 25 °C.

Sample Collection

Cells were sub-cultured into T175 flasks as per Section 3.2.2. Each flask was seeded with roughly 400,000 cells. On the morning of the experiment, cells were starved of serum and glucose in 37°C PBS which was supplemented to 1 mM MgCl$_2$ and 1 mM CaCl$_2$ for four hours. The cells were then exposed to various concentrations of insulin; these ranged from 10 pM to 1 μM. Cells were returned to the incubator and allowed to incubate for 30 minutes. The PBS was removed and each triplicate of flasks was then given 20 mL of 37°C LG DMEM which was supplemented to the respective concentration of insulin. Samples were extracted at 100 μL volumes at various timepoints thereafter (see chapter Chapter 5) and frozen at -20°C for further use in glucose and lactate determination assays. Once all of the necessary samples had been collected, the DMEM was removed and the cells were thrice-washed with 37°C PBS. Thereafter, excess PBS was removed and each flask was given 1 mL of lysis buffer and scraped until the growth surface was clear. Finally, 1 mL of the scraped cells was removed and stored at -20 °C for protein determination.

Protein Determination

Relative protein concentrations were determined via the linearised Bradford protocol as described by [324]. Each sample was diluted 100-, 40-, and 20-fold whereupon 20

μL of sample were added, in triplicate, to a 96-well Greiner F-bottom microtiter plate and Bradford solution was added for a 300 μL final volume. Standards were performed for each instance of protein determination and ranged from 0.5 mg/mL BSA to approx. 0.0039 mg/mL over a series of seven two-fold dilutions with dH$_2$O. The ratio of OD$_{590}$ to OD$_{450}$ yielded, upon blanking, a linear standard curve in the form of $y = mx + c$. Sample protein concentrations were calculated at each dilution and averaged.

Glucose Determination

End-point glucose determination assays were prepared as follows: for each 96-well plate, 10 mL of 0.1 M Tris-HCl buffer (pH $\pm$8): 2 mM Mg.ATP (Sigma: A9187), 4 mM NADP$^+$ (Sigma: N3139), 4 mM MgCl$_2$, 100 U hexokinase (HXK) (Sigma: H6380), and 40 U glucose-6-phosphate dehydrogenase G6PDH (*S. cerevisiae*; Sigma: G7877) were prepared. A series of glucose dilutions which ranged from 1 g/L to 0.0078 g/L was established using LG DMEM and MilliQ water. Respectively, 10 μL sample (or standard) and 90 μL of the assay cocktail were added (in triplicate) to a Greiner F-bottom 96-well plate and reactions were allowed to proceed at room temperature for 30 minutes. Plates were then read in a spectrophotometer at 340 nm (BMG Labtech SPECTROstar Nano).

Lactate Determination

End-point lactate determination assays were prepared as follows: for each 96-well plate, 10 mL of 1x PBS buffer (pH $\pm$7.4): 5 mM NAD$^+$ (Sigma: N7004), 2.5 % v/v Hydrazine, and 40 U LDH (Sigma: L2625) were prepared. A series of lactate dilutions ranging from 0.0039 g/L to 0.5 g/L was established using pure L-Lactate (Sigma: L7022) and MilliQ water. Respectively, 10 μL sample (or standard) and 90 μL of the assay cocktail were added (in triplicate) to a Greiner F-bottom 96-well plate and allowed to react at room temperature for 30 minutes. The samples were then read in a spectrophotometer at OD$_{340}$ (BMG Labtech SPECTROstar Nano).

3.2.4 Radiolabelled Glucose Uptake Determination

These experiments were conducted in order to determine the basal and induced activities of the GLUT1 and GLUT4 glucose transporters. The premise is that, when starved of glucose and serum, these cells will exhibit a pronounced increase in glucose uptake in response to insulin stimulation. Exposure to radiolabeled - ^{14}C - glucose as an admixture of unlabeled glucose in serum-free DMEM should result in a proportional uptake of either. Further, washing the cells with ice-cold quenching buffer (containing 500 mM unlabeled glucose), would wash any remaining labeled glucose from the cell surface and transporters by outcompeting the labeled glucose. Comparing the scintillation counts of each sample to its respective reference sample will therefore yield the proportion of labeled glucose that entered the cells. Lastly, comparing the samples from each time, or concentration series would provide information about the time-, and concentration-dependent activity of the GLUT1 and GLUT4 transporters. Since GLUT1 does not respond to insulin with an increased transport activity, GLUT4 is assumed to be transporter responsible for the any increase in glucose transport activity. The relevant materials may be found in Tables 3.6, 3.1, 3.2, and 3.3.

Preparation

Cells were cultured in 100 mm dishes as described in Section 3.2.2. One the day of the experiment, cells were glucose- and serum-starved for four hours in 37 °C PBS which had been supplemented to 1 mM $MgCl_2$ and 1 mM $CaCl_2$. While the cells were starving, the glucose solution was prepared by adding 10 μCi of radiolabeled glucose to 9.99 mL of LG DMEM. This yielded a final concentration of 1 μCi/mL which was then heated to 37 °C. The quenching buffer was aliquoted into an appropriate number of 15 mL tubes which were promptly placed on ice until needed. Once the four-hour starving period had expired, the cells were either exposed to a constant concentration of insulin over a set of timepoints *or* they were incubated with a range of insulin concentrations over 30 minutes, at 37 °C. It must be noted that each concentration or time-point represents an independent, biological triplicate.

Methodology

Once the respective incubation period was over, the PBS-insulin buffer was quickly and as completely as possible removed. The radiolabeled glucose-DMEM mixture was added to the cells for two seconds before being quenched with the ice-cold quenching buffer. The cells were washed by swirling the quenching buffer in each dish and then disposing of it as completely as possible. Thereafter, the cells were harvested by adding 500 μL of lysis buffer to each dish and scraping until the growth area was clear. The cells were then either immediately prepared for scintillation counting or frozen overnight at -20 °C.

Scintillation counting occurred within 24 hours of each sampling by removing 100 μL of the cell mixture and depositing them into a PET scintillation vial – the remainder would be used for protein determination or repeat scintillations. The cell mixture was then further supplemented with five mL of scintillation fluid. Scintillation vials were then placed in a Perkin Elmer Tri-Carb 2810TR scintillation counter. Each sample was analysed for 10 minutes and returned an average total count which was representative of the total amount of radiolabeled glucose present. Lastly, included in each cycle of the scintillation counter was a blank sample which contained only 5 mL scintillation fluid and one reference vial for each sample that contained 100 μL of the radiolabeled glucose-DMEM mixture *before* it was added to the cells.

3.2.5 Western Blotting

Western blotting was kindly performed by Dr. T. Kouril of Stellenbosch University, South Africa. The relevant materials may be found in Tables 3.6, 3.2, 3.4, 3.5, and 3.7.

Sample Collection

Cells were cultured in 100 mm culture dishes as per section Section 3.2.2. On the day of the assay, cells were serum and glucose starved for four hours in 37 °C PBS which had been supplemented to 1 mM $CaCl_2$ and 1 mM $MgCl_2$. Thereafter, the cells were either exposed to varying insulin concentrations for 30 minutes, or exposed to a constant insulin concentration for a set of time points. After each time point,

the PBS was removed, 500 μL of RIPA buffer was added to each dish, and the cells were harvested by scraping until the growth area was clear. Finally, 500 μL of the cell suspension was collected, deposited in a sterile Eppendorf tube, and immediately submersed in LN_2 before transfer to long-term storage at -80 °C.

Method

Samples were thawed at room temperature, briefly agitated in a vortex mixer, and then centrifuged for $5000 \times g$ for 15 minutes. Then, 100 μL of the supernatant is removed and mixed with 20 μL sample buffer. From this, 50 μL was removed and diluted with a further 40 μL of sample buffer and the requisite volume of TBS until the desired dilution was achieved. The rest was stored at -20 °C.

Each well was loaded with 10 μg of sample. Further, each gel contained marker proteins as well as a control sample (cells exposed to 100 nM insulin for 30 minutes concurrent to the experiment). The outer chamber was filled with with $1\times$ running buffer and electrophoresis ocurred at 25 mA per gel. A Gel Doc was used to evaluate the success and quality of electrophoresis.

After electrophoresis, gels were equilibrated in transfer buffer for 15 minutes. During this time, the PVDF membrane was activated in absolute methanol for five minutes after which it was equilibrated in transfer buffer until use. The *sandwich* was prepared as follows: sponge - blotting paper - PVDF membrane - gel - blotting paper - sponge, oriented from anode to cathode respectively. This sandwich was then placed in the chamber of the transfer system and underwent overnight electrophoresis at 15 - 20 V and 4 °C.

Once the proteins had transferred onto the membrane, the latter was washed in $1\times$ TBS buffer supplemented with 0.1 % v/v Tween®20 (TBS-T), for one, five, and 15 minutes respectively - the spent TBS-T was discarded and new TBS-T was added after each wash. Gels and membranes were visualised using a Gel-Doc imaging system to ensure the majority of protein had indeed transferred onto the membrane. Once confirmed, the membrane was blocked using 5 % v/v skim milk in TBS-T. The specific regions of interest on each membrane were excised and placed into their corresponding

antibody solutions overnight at 4 °C. The following day, each membrane strip was individually washed in TBS-T as previously described. Subsequently, each strip was incubated in its respective secondary antibody for one hour at RT and washed in TBS-T as previously described. Lastly, each membrane was incubated with Clarity Western ECL Substrate (Bio-Rad: 170-5061) for five minutes and then visualised using the MyECL imager.

The data were then analysed in the ImageLab software suite to determine the normalisation factors for each band. Similarly, ImageJ was used to generate intensity profiles for each band. The peaks were then manually selected for each band and the area under each peak was determined. These values were normalised with the factors determined from the ImageLab software.

3.2.6 GLUT4-GFP Transfections

pB-GLUT4-7myc-GFP was a gift from Jonathan Bogan (Addgene plasmid # 52872) [325]. The relevant materials may be found in Tables 3.6, 3.1, and 3.2.

Plasmid Amplification

Transformed *E.coli* (DH5α) cells were purchased from Addgene (52872), innoculated to: 50 mL LB medium supplemented to 2 μg/mL Ampicillin (Sigma: A9518), and incubated overnight at 37°C and 180 rpm. Bacterial cultures were then prepared either for expansion or storage in -80°C as 1:1 glycerol stocks.

Plasmid Isolation

Plasmid DNA was isolated using the GeneJET™Plasmid Midiprep Kit (ThermoFisher: K0481) according to the manufacturer's instructions. Briefly: overnight *E.coli* cultures were transferred to sterile 50 mL Falcon tubes and centrifuged for at 4°C and $4500 \times g$ for 10 min. The supernatant was discarded and the pellet was resuspended in 2 mL proprietary resuspension buffer (containing 4% v/v RNAse) by vortexing. A further 2 mL of proprietary lysis buffer was added and the cells were left to incubate at RT for 3 min before inverting 6 times. This mixture was neutralised with 2 mL of the provided

neutralisation buffer by inverting 6 times. In order to neutralise endotoxins, 0.5 mL of endotoxin binding buffer was added, inverted a further six times, and left to incubate at RT for 5 min. The mixture was washed with 3 mL EtOH (absolute) and centrifuged for 40 min at $4500 \times g$. The supernatant was transferred to a fresh 15 mL Falcon tube, washed with 3 mL EtOH (absolute), and inverted 6 times. The resulting mixture was transferred to a provided filtration column and centrifuged for 3 min at $3000 \times g$. After the flow-through had been discarded, the column was re-filled with 4 mL of Wash Solution 1 and centrifuged for 2 min at $3000 \times g$. Once again the flow-through was discarded and the column was re-filled with Wash Solution 2 and centrifuged for 2 min at $3000 \times g$. This step was once. Thereafter, the column was dry-centrifuged for 5 min at $3000 \times g$. Finally, the filter was aseptically removed and placed into a fresh, sterile 15 mL Falcon tube. To this, 0.35 mL of Elution buffer were added, incubated for 2 min at RT, and centrifuged for 5 min at $3000 \times g$. The filter was discarded and the remaining dsDNA was aliquoted for quantification or storage at -20°C.

DNA Quantification

Double-stranded DNA was diluted 1:9 in 200 μL sterile MilliQ water before being transferred to a quartz cuvette (Hellma: 105-201-15-40). After blanking with MilliQ water, the sample was read in a spectrophotometer (Agilent: Cary 60), and the A_{260}/A_{280} was determined. Values lower than 1.8 or greater than 2.0 indicated RNA or phenol contamination respectively. Samples within the acceptable range had their dsDNA concentration calculated by multiplying the A_{260} value by 50 μg/mL and the dilution factor.

Transfection

Cells (C2C12) were seeded into a 100 mm dish and given 24 hours to acclimate in complete growth media. The following day, the spent culturing media was aspirated and replaced with 1 mL of unsupplemented, 37°C Opti-MEM (Gibco: 31985070). Thereafter, 1mL of unsupplemented, 37°C Opti-MEM, 10 μg plasmid, and 15 μL X-tremeGENE™ transfection reagent (Sigma: 6366236001) were added to a sterile,

RNAse-free Eppendorf tube and briefly agitated in a vortex mixer. The plasmid mixture was then allowed to incubate for 15 min at room temperature.

The Opti-MEM was aspirated from the cells and replaced, dropwise, by the plasmid mixture. The transfection was allowed to proceed overnight before the medium was replaced. The transfection was confirmed using the EVOS-FL microscope system (Invitrogen). Subsequently the cells were subcultured into Nunc 8-well glass cover slip dishes or MaTTek 35 mm glass cover slip dishes at 5×10^3 cells per cm^2 and given 24 hours to recover.

GLUT4 Translocation Study

The transfected C2C12 myoblasts were starved in 37°C PBS (supplemented with 1 mM MgCl$_2$ and 1 mM CaCl$_2$) for 30 minutes. Subsequently, the cells were exposed to 1 μL CellMask™ Orange and 10 μL Hoechst stains for a further 10 minutes. The cells were then washed twice with the 37°CPBS mixture before being imaged in the basal, unstimulated state. Once imaged, the cells were exposed to 100 nM of insulin for 30 minutes, before undergoing further imaging.

3.2.7 Imaging

The materials, equipment, reagents, and software which were used during these experiments may be found in Tables 3.6, 3.1, 3.2, and 3.7.

LADD Staining

The staining protocol was adapted from [326].

Cells were seeded in several six-well dishes at an initial density of 5×10^4 cells/cm^2 and then grown and differentiated as described in Section 3.2.2. Each six-well dish represented a single day along the differentiation time line and was split into three wells each representing *standard* and *updated* culturing conditions respectively.

On the day of the experiment, the cells were twice-washed with 37°C PBS and then fixed in 1 mL of 100% EtOH for 10 minutes. The EtOH was aspirated and replaced with 1 mL of the LADD stain (0.27 % m/v tolouidine blue and 0.73 % m/v fuchsin

dissolved in a 30 % v/v EtOH solution). The stain proceeded for one minute before being aspirated. The cells were washed with distilled water until the water was clear - in this instance, three times - and allowed to dry overnight.

Cells were visualised with an Olympus CKX 41 inverted microscope set to phase-contrast at $200\times$ magnification. Each well was randomly photographed in six separate areas. The images were imported into the ImageJ software suite and each image was further divided into nine quadrants. A random number generator was used to select three quadrants from each image. These quadrants were further analysed using the 'Cell Counter' plugin. Using this plugin, nuclei were assigned to myofibers (three or more nuclei per cell) or myocytes (a single nucleus per cell). Cells and nuclei near the edge of each image were ignored. Using these separate nuclei counts, a ratio of 'differentiated' nuclei (those in fibers) to 'undifferentiated' nuclei (those in myocytes) was calculated.

Confocal Microscopy

Since C2C12 myoblasts adhere to the material of the cell culture dishes, no chemical fixing was used in the preparation of the images. The cells were imaged with a Zeiss LSM 780 confocal microscope. Additionally, the stage temperature, CO_2 levels, and humidity were kept constant at $37^\circ C$, 5%, and approx. 80% resppectively. Cells were selected on a 'first-found' basis - in other words the first cell that exhibited GFP activity during a random scan of the dish. Each cell was imaged with a $63\times$ oil-immersion objective along the Z-axis - beginning and ending slightly out of focus. Resolution was set at 1024×1024 pixels with a step-size of 700 nm and an overlap of 10 nm with each vertical slice. The following wavelenghts: 350 nm, 395 nm, and 567 nm were used to excite the Hoechst stain, GFP, and CellMask™ Orange stain respectively. Cells were not imaged for longer than 60 minutes to ensure minimal photobleaching and dye cross-reactivity or internalisation. Similarly, laser intensity was kept to a minimum. The ZEN Lite software output a .lsm file which, when read into FiJi, separated each colour channel into a separate Z-stack.

3.3   Reagents, Apparatus, and Software

The reagents, apparatus, and software used for this project are summarised in the following tables.

Table 3.1: General Reagents

Reagent	Supplier	Catalogue #
Triton X-100	BDH Chemical	30632
Tris Hydroxy Aminomethane	Sigma-Merck	1.08382
PBS Tablets	Gibco	18912014
PhosSTOP Tablets	Sigma-Merck	4906845001
Na.Deoxycholate	Sigma-Merck	D6750
cOmplete™ Protease Inhibitor	Sigma-Merck	4693132001
NaCl	Sigma-Merck	1.02406
$MgCl.6H_2O$	Sigma-Merck	1.05833
$CaCl.2H_2O$	Sigma-Merck	1.02382
1x DPBS	Sigma-Merck	D8537
Fuchsin	Sigma-Merck	47860
Tolouidine Blue	Sigma-Merck	89640
Coomassie Brilliant Blue G250	Sigma-Merck	27815
SDS	Sigma-Merck	75746
Na.Ampicillin	Sigma-Merck	A9518
LB Broth	Sigma-Merck	L3022

Table 3.2: Cell Culture Reagents

Reagent	Supplier	Catalogue #
DMEM	Sigma-Merck	D6406
Glucose Solution	Gibco	A2494001
Equine Serum	Sigma-Merck	H1270
Foetal Bovine Serum	Gibco	10500-064
DMSO	Sigma-Merck	D2650
Insulin	Sigma-Merck	I9278
x-Treme GeneHP™	Sigma-Merck	6366236001
opti-MEM	Gibco	31985070
10x Trypsin-EDTA	Sigma-Merck	L2153
CellMask™ Orange	ThermoFisher C10045	
Hoechst 33258	abcam	ab228550

Table 3.3: Assay Reagents

Reagent	Supplier	Catalogue #
Hydrazine.H_2O	Sigma-Merck	207942
G6PDH	Sigma-Merck	G7877(*S. Cerevisiae*), G8404(*L. Mesenteroides*)
C^{14}-glucose	AEC Amersham	ARC 0122G
LDH	Sigma-Merck	L2625
ATP	Sigma-Merck	A9187
$NADP^+$	Sigma-Merck	N3139
NAD^+	Sigma-Merck	N7004
Na.L-Lactate	Sigma-Merck	L7022
BSA	Sigma-Merck	A7906
HXK	Sigma-Merck	H6380

Table 3.4: Western Blotting Components:

Component	Manufacturer	Catalogue #
Temed	Sigma-Merck	T9281
Acrylamide	Sigma-Merck	A3699
TCE	Sigma-Merck	T54801
DTT	Sigma-Merck	11583786001
$4\times$ Laemmli concentrate	Bio-Rad Laboratories	161-0747
Na.Arzide	Sigma-Merck	S2002
Tween®20	Sigma-Merck	P9416
Methanol (absolute)	Sigma-Merck	1.06007.2500
Immun-Blot® PVDF membrane	Bio-Rad Laboratories	162-0177
Sponge	Bio-Rad Laboratories	170-3932
Blotting Paper	Bio-Rad Laboratories	162-0118
Precision Plus Protein™	Bio-Rad Laboratories	161-0373
30% Acrylamide/Bis-Acrylamide Solution	Sigma-Merck	A3699
Clarity Western ECL Substrate	Bio-Rad Laboratories	170-5061

Table 3.5: Antibodies: all primary antibodies were diluted 1:999 in their respective diluents and 3mM sodium arzide. Secondary antibodies were freshly diluted 1:10 000 for each Western blot.

Antibody	Diluent	Manufacturer	Catalogue #
Akt^{total}	5% BSA	Cell Signaling Technology®	9272
Anti-Akt1^{S473}	5% skim milk	Abcam	81283
Anti-Akt123^{T308}	5% skim milk	Cell Signaling Technology®	13038
IR^{total}	5% skim milk	Abcam	69508
Anti-Phospho Tyrosine	5% BSA	Cell Signaling Technology®	9411
(Goat) Anti-mouse secondary	5% skim milk	Abcam	ab97051
(Goat) Anti-rabbit secondary	5% skim milk	Abcam	ab97023

Table 3.6: List of Equipment

Apparatus	Manufacturer	Model #
Incubator	NuAire	NU-5800
Spectrophotometer	BMG Labtech	SPECTROstar *Nano*
Scintillation Counter	Perkin Elmer	Tri-Carb 2810TR
Benchtop Centrifuge	Eppendorf	5804
Autoclave	Steridium	SD660
Confocal Miscroscope	Carl Zeiss	LSM 780
Haemocytometer	Marienfield	Neubauer-Improved 0.1 mm (0640010)
Spectrophotometer	Agilent Technologies	Cary 60
Swing-bucket rotor	Eppendorf	A-4-44
Fixed angle rotor	Eppendorf	F 45-30-11
Culture Dishes	Nest	708003(T75), 709003(T175), 704001(100 mm)
35 mm glass bottom dishes	MaTTek	P35G-1.5-14-C
GeneJET™ kit	ThermoFischer	K0481
EVOS™-FL Microscope	Invitrogen	AMF4300
MilliQ system	MerckMilliPore	C79625
dH$_2$O system	PurePro	EC105
F-bottom Microtitre 96-Well Plates	Greiner	P1PLA024C-000096
Rotary Shaker	Already Enterprise Inc.	LM-575D
Scale	Mettler Toledo	ME204
pH Meter	Crison	GLP 21
10 mm Quartz Cuvette	Hellma	105-201-15-40
Gel-Doc™ XR+	Bio-Rad	
Mini-PROTEAN® Tetra Cell Casting Module	Bio-Rad Laboratories	165-8016
Mini-PROTEAN® Tetra Vertical Electrophoresis Cell	Bio-Rad Laboratories	165-8004
Mini Trans-Blot® Cell	Bio-Rad Laboratories	
myECL™ Imager	Thermo Scientific™	13375071

Table 3.7: The varieties of software used and their purpose(s)

Purpose	Software	Developer
Initial data analysis and formatting	Excel 365	Microsoft Corporation
Detailed data analysis as well as the development and simulation of an ODE-based model	Wolfram Mathematica v. 11.x	Wolfram Research
Analysis of phase-contrast microscope images as well as Western blots	Fiji (ImageJ) v.1.52	GPL v.2
Further analysis of Western blots	Image Lab	Bio-Rad Laboratories
Capturing and initial analysis of confocal microscope images	ZEN Lite v.2.1	Carl Zeiss AG
Capturing of phase-contrast images	ScopeTek Devices v.1.2	Hangzhou Scopetek Opto-Electric Co.

Chapter 4

Optimisation of Growth Conditions

4.1   Introduction

The use of C2C12 cells in studying insulin signalling or glucose metabolism is well-documented [268, 271, 327]. These cells are widely used as a model for signal transduction pathways as well as muscle metabolism. C2C12 cells can be used in the undifferentiated stage as myoblasts, or once they have differentiated, as myotubes. Since myotubes are the dominant form of these cells in adult animals, the cells are often used in differentiated form. However, few studies attempt to quantify the degree to which their cells are differentiated. Studies that do track the degree to which cells are differentiated report values of between 10% [328] and 45% [326].

Although some consensus on medium composition exists (e.g. 25 mM glucose and 10% FBS), studies often neglect to mention the DMEM formulation that is used or the final glucose concentration of the media being used. Under these hyperglycaemic conditions, increases in glucose import upon the addition of insulin of up to 10-fold were reported [329, 330] as well as increases in glycolytic flux that ranged between 1.3- and 2-fold [331, 332]. In this study, evaluating the culturing conditions of C2C12 cells was motivated by the fact that high blood glucose concentrations are indicative, if not causative, of insulin resistance *in vivo* [333].

In vivo glucose concentrations in mice vary depending on lineage. However, concentrations of 120 - 300 mg/dL (6.6 - 16.7 mM) have been reported [334, 335]. In

59

diabetic (db/db) mice the fasting glucose concentrations can be as high as 470 mg/dL or 26 mM [336]. Similarly, the circulating concentrations of insulin range between 0.5 ng/mL and 1.7 ng/mL (80 - 300 pM) [334, 336]. The standard glucose concentration in most culture media of 4.5 g/L more closely resembles those found in the diabetic mice. Insulin concentrations in sera are generally not evaluated. However, in rat adipocytes (3T3-L1 cells), Foetal Bovine Serum (FBS) exhibits insulin-like effects on the translocation of GLUT4 to the plasma membrane while also stimulating glucose (2-Deoxy glucose) uptake [337].

Variations in culturing conditions may affect the insulin sensitivity of the cells. Firstly, high glucose concentrations are associated with increases in reactive oxygen species (ROS) [338, 339]. Secondly, the greater levels of glucose and ROS lead to decreases in cell differentiation in neural cells [340], cardiomyocytes [341], and mesenchymal stem cells [342]. Thirdly, in differentiated myotubes GLUT4 is expressed in greater quantities when compared with myoblasts [233]. Lastly, GLUT4 is the main insulin-responsive glucose transporter in skeletal muscle cells [343, 344]. Therefore, how cells are cultured may well affect their responsiveness to insulin. A recent review of C2C12 cells suggests that hyperglycaemia may indeed affect the insulin sensitivity of these cells [345].

Common culturing practices - high (>25 mM) glucose concentrations and a minimum of 10% v/v FBS - may therefore induce insulin desensitisation of *in vitro* C2C12 cells. Therefore, in order to more accurately determine the basal state of insulin signalling and glucose transport, it was necessary to determine the culturing conditions which best balanced the physiological state of *in situ* muscle cells, cells which would remain insulin sensitive, and a realistic culturing and experimental schedule. Further, the data from this study would be used to inform studies in Chapter 5 which sought to offer a proof-of-concept for the induction of insulin resistance in C2C12 cells. In pursuance of these objectives, the cells were grown at various glucose concentration and induced with insulin, FBS, or a combination of both and their glucose-lactate flux was evaluated as a proxy-measure for insulin sensitivity.

4.2   Materials and Methods

4.2.1   Cell Culture Protocol

Mouse skeletal myoblasts (C2C12, $\pm$ 500,000 cells) were thawed from liquid nitrogen storage and seeded in vented T75 culturing flasks which contained 10 mL of complete culturing media. Growth media was replaced every two days until a confluence of $\pm$ 80% was achieved - by the fifth day. Thereafter, the cells were either split or differentiated. The latter saw culture media supplemented with 2% v/v horse serum instead of FBS, whereas the former occurred according to protocols discussed in Chapter 3. Once again, differentiation media was replaced every second day until the cells were judged to be mostly differentiated - by the fifth day. The media formulations used are summarised as follows: 'standard' media contained 25 mM glucose DMEM and 10% FBS whereas the 'updated' media had the 25 mM glucose reduced to 15 mM. During differentiation, the 10% FBS was replaced with 2% horse serum (HS).

Differentiated cells were prepared for experimentation by transferring them into media containing no serum for an overnight (12 to 14 hours) serum-starvation period. Subsequently the cells were starved of glucose and serum for a further four hours in PBS which was supplemented to 1 mM $MgCl_2$ and 1 mM $CaCl_2$. This last step was undertaken to put the cells into a 'zero-glucose' state which meant that their internal stores of glucose were mostly depleted. This step was taken in order to ensure that the glucose flux or ^{14}C glucose-uptake that was observed was due to the 'actual' uptake of the glucose and minimally influenced by feedback inhibition or the internal concentration of glucose.

Half an hour before each experiment, the cells were stimulated with 100 nM of insulin, 10 % v/v FBS, or a combination of insulin and FBS for the induction of the signalling cascade. The cells were induced with FBS in order to determine whether this (often) undefined mixture of growth factors and proteins has an insulin-like effect on the glycolytic flux in C2C12 cells. Lastly, details regarding equipment, reagents, as well as the procedures for the enzymatic determination of lactate and glucose concentrations can be found in Chapter 3. While initially, half an hour was chosen based on

literature [346, 347], subsequent experiments (Chapter 5) will show that 15 minutes are sufficient.

4.2.2 LADD-staining and Image Analysis

The staining protocol was adapted from [326]. The LADD multiple stain contains a combination of fuchsin and toluidine blue. This stain is able to differentially stain the cytoplasm and nuclei of cells, thereby enhancing contrast and identification of organelles [348].

Cells were seeded in several six-well dishes at an initial density of $5 \times 10^4 \text{ cells/cm}^2$ and then grown and differentiated as previously described. The cells were split into seven, six-well dishes. Each six-well dish was divided into three wells which represented the 25 mM glucose (*standard*) culturing condition and three wells which represented the 15 mM glucose (*updated)* culturing condition. Beginning with the day *before* differentiation, each six-well dish was stained (*vide infra*) and photographed under a microscope.

Before staining, the cells were twice-washed with warm PBS and then fixed in 1 mL of 100% EtOH for 10 minutes. The EtOH was aspirated and replaced with 1 mL of the LADD stain (0.27 % m/v tolouidine blue and 0.73 % m/v of fuchsin dissolved in a 30 % v/v EtOH solution) for one minute, aspirated, and then washed with distilled water until the water was clear. In this instance, three washes were required. The cells were then allowed to dry overnight.

Cells were visualised with an Olympus CKX 41 inverted microscope set to phase-contrast at $200 \times$ magnification. Each well was photographed in six, randomly chosen, areas. The images were imported into the ImageJ software suite and each image was further divided into nine quadrants. A random number generator was used to select three quadrants from each image. These quadrants were further analysed using the 'Cell Counter' plugin. Using this plugin, nuclei were assigned to the fiber category (three or more nuclei per cell) or to the myocyte category (a single nucleus per cell). Cells and nuclei near the edge of each image were ignored. Using these separate nuclei counts, a ratio of 'differentiated' nuclei (those in fibers) to 'undifferentiated' nuclei

(those in myocytes) was calculated.

4.3 Results and Discussion

In tissue culture literature it is not often made explicit at which glucose (or metabolites such as pyruvate or glutamate) concentration the cells were cultured [349]. The general assumption is that, unless otherwise specified, cells are usually cultured at higher glucose concentrations. While this may be a good approach for the majority of cell lines, as the present chapter will illustrate, this may not be the best approach for *all* cell lines, or for all research questions.

4.3.1 Glycolytic Flux Measurement

Glucose concentrations during cell culturing were evaluated for their potential to generate cells that were responsive to insulin. This responsiveness was assayed by determining the glucose consumption and lactate production rates as well as their respective fold induction by insulin. Cells grown under standard, high glucose conditions were stimulated with 100 nM insulin, 10% FBS, or a combination of 100 nM insulin and 10% FBS. Water, as the carrier condition, was used for the control experiments. The glucose consumption and lactate production results are shown in Fig. 4.1. Glucose consumption remained linear throughout the experiment for all culturing conditions and no significant differences were observed between cells cultured with high glucose concentrations (Table 4.1).

However, cells grown under medium or low glucose conditions showed an induction of glucose consumption in response to insulin, FBS, or a combination thereof. In other words, these cells retained their insulin sensitivity and were able to upregulate glucose transport or glycolysis in response. For example, while the control glucose consumption was 0.025 μmol.min^{-1}.mg^{-1} (±0.002) for all culturing conditions, adding 100 nM insulin to the medium and low glucose cells increased their glucose consumption rate to 0.044 μmol.min^{-1}.mg^{-1} (±0.003) and 0.038 μmol.min^{-1}.mg^{-1} (±0.001) respectively. The difference between these two rates was not significant (p

= 0.55). In contrast, the glucose consumption rate of insulin stimulated cells grown at high glucose was essentially the same as the control value at 0.024 μmol.min^{-1}.mg^{-1} (± 0.0005), a difference which was not significant either (p = 0.24). Similarly, insulin stimulated the production of lactate, which remained linear in time for all culturing conditions. The induction of lactate production by insulin and FBS is evident under the medium and low glucose conditions. The rates were normalised to the total protein concentration in each experimental vessel and are presented in Table 4.1. The results indicate that in these C2C12 cells grown under standard, high glucose conditions, their responsiveness to insulin had been greatly diminished. When normalised to the control condition (high glucose), both glucose consumption and lactate production showed no induction by the addition of insulin, FBS, or the combination thereof (Table 4.1).

Comparing the glucose consumption and lactate production rates (0.0246 and 0.0514 μmol.min^{-1}.mg^{-1}respectively) of the medium glucose control (i.e. cells not induced with insulin) (Fig. 4.1) yielded no significant difference to the high glucose control (Table 4.1). However, the insulin-, FBS-, and insulin and FBS-stimulated consumption and production rates showed significant inductions. The insulin-stimulated cells showed a 1.7-fold induction of glucose consumption and a similar induction of lactate production. The FBS-only stimulated cells showed a more modest, 1.1-fold induction of both glucose consumption and lactate production. Lastly, stimulating the cells with both FBS and insulin had little advantage over stimulating with insulin exclusively, yielding a 1.61- and 1.55-fold induction of glucose consumption and lactate production respectively.

In addition to high and medium glucose culturing conditions, these experiments were repeated using cells cultured under low, but physiological, glucose (5.5 mM or 1 g/L) conditions. The glucose consumption and lactate production rates (Table 4.1,$\pm$ 0.025 and $\pm$0.047 μmol.min^{-1}.mg^{-1}respectively), without insulin induction, did not differ from cells grown under high or medium glucose conditions. Insulin did stimulate glycolytic flux in these cells; consumption and production rates achieved 1.5- and 1.44-fold induction when compared to the control (Table 4.1). These rates, however, did not achieve as strong an induction of flux as was seen in cells grown under
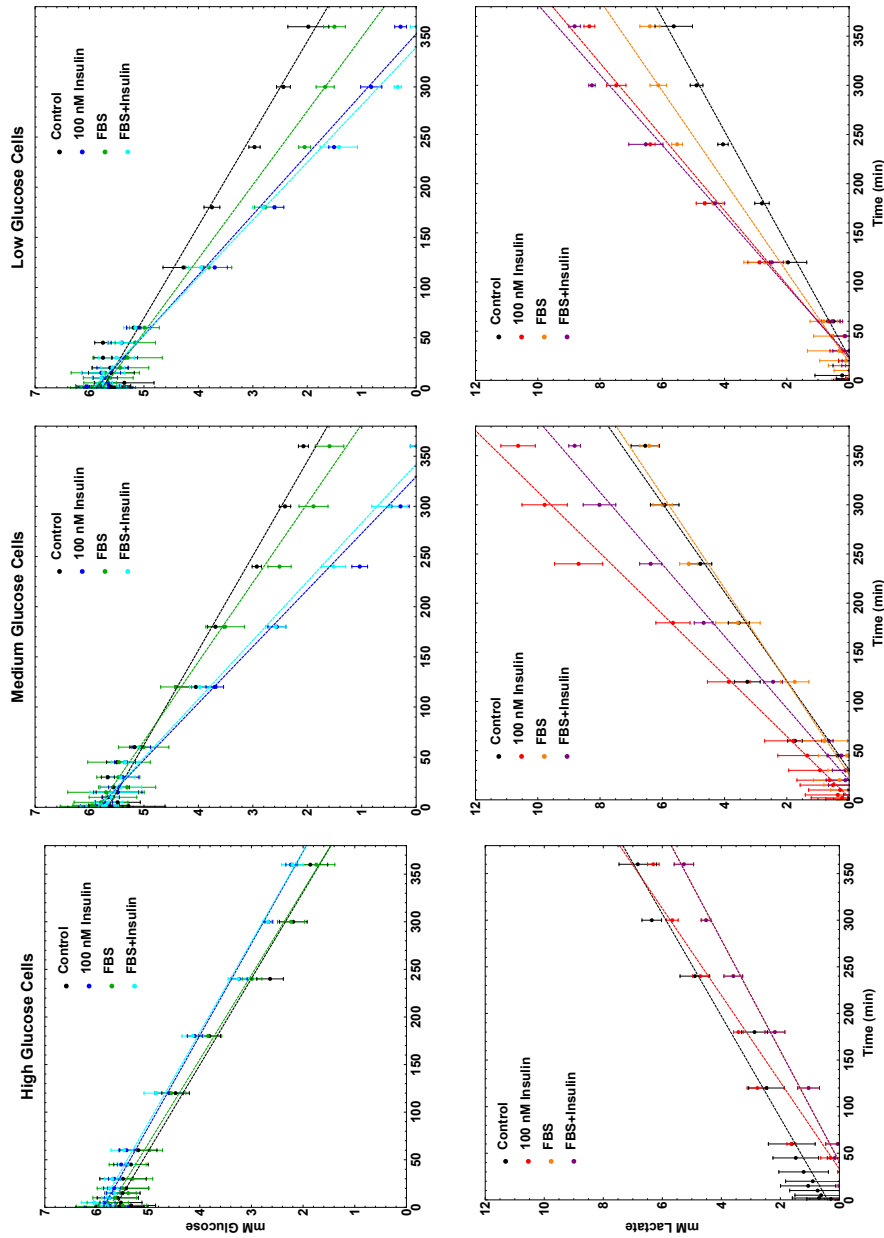
Figure 4.1: Glucose consumption (top) and lactate production (bottom) by cells which were cultured in high glucose (left), medium glucose (center), and low glucose (right), conditions. Cells were either induced with 100 nM insulin, 10% FBS, or 100 nM insulin and 10% FBS. Water, as the carrier condition, was used for the control experiments. The transport assays were all performed at the same (5mM) glucose concentration. The dashed lines indicate linear fits to the data which were used to determine the glucose consumption and lactate production rates presented in Table 4.1. The total protein was similar across all experiments at 8.70 mg ($\pm$ 0.13). Error bars indicate SEM, and each data point represents a biological triplicate (n = 3).

medium-level glucose conditions. A modest induction was seen with FBS-stimulated cells - approximately 1.2-fold for both glucose consumption and lactate production. The combination of insulin and FBS showed the greatest induction of glycolytic flux in these cells.
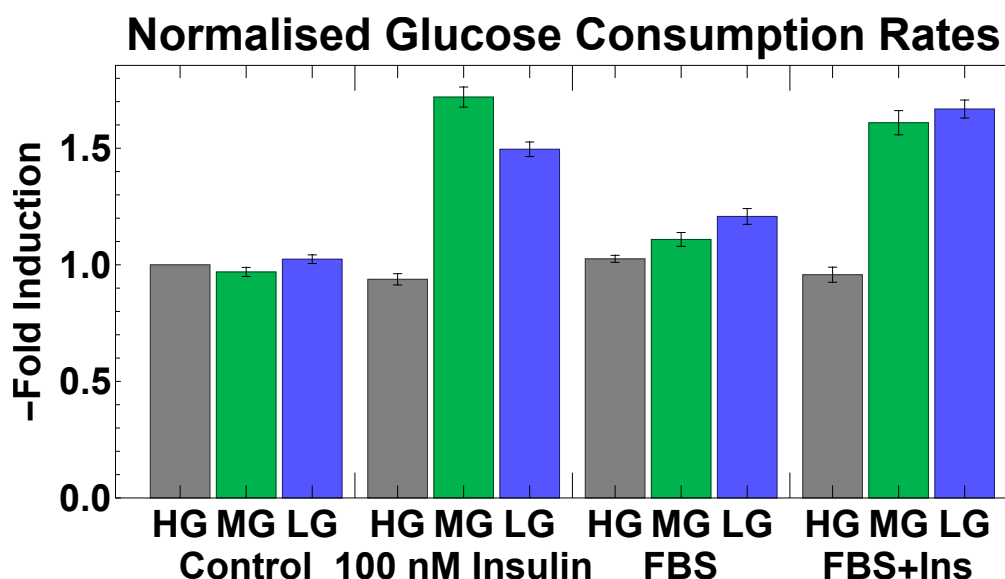
Figure 4.2: Glycolysis in terms of glucose consumption as induced by 100 nM insulin, 10 % v/v FBS, or both. Cells cultured in 25 mM (HG), 15 mM (MG), or 5 mM (LG), glucose are indicated as grey, green, or blue bars respectively. Error bars indicate SEM, and each bar represents a biological triplicate (n = 3).

The results further indicated discrepancies between the final glucose and lactate concentrations as well as their respective consumption and production rates Table 4.1. Glycolysis degrades one molecule of glucose into two molecules of lactate. Therefore, one would expect the steady-state rate of lactate production to be approximately twice that of glucose consumption. While the high glucose and medium glucose control conditions did achieve this two-fold conversion, the rest of the cells experienced a conversion of 1.5- to 1.7-fold. Since the rate of glycogen synthesis remains fairly low in *in vitro* cells [350], it is unlikely that this discrepancy in glucose-lactate conversion can be explained by glycogen synthesis. Assuming the $\pm 5 \mathrm{pmol.min}^{-1}.\mathrm{mg}^{-1}$ glycogen synthesis rate for C2C12 cells as per Abdelmoez et al (2020) [351], this would yield approximately 24 nmol or 16 μgof glycogen over the course of a 10 hour experiment.

Experiment	Glucose Consumption Rate	Induction	p value	Lactate Production Rate	Induction	p value
HG: Control	0.0254 ± 0.0012	1	-	0.0422 ± 0.0029	1	-
HG: Insulin	0.0238 ± 0.0005	0.94	0.24	0.0495 ± 0.0009	1.17	0.0036
HG: FBS	0.0261 ± 0.0009	1.03	0.31	0.0388 ± 0.0005	0.92	0.061
HG: FBS+Ins	0.0243 ± 0.0003	0.96	0.13	0.0389 ± 0.0005	0.92	0.061
MG: Control	0.0246 ± 0.0017	0.97	0.98	0.0514 ± 0.0026	1.22	0.003
MG: Insulin	0.0437 ± 0.0010	1.72	0.0019	0.0707 ± 0.0025	1.68	0.012
MG: FBS	0.0282 ± 0.0021	1.11	0.042	0.0470 ± 0.0039	1.12	0.019
MG: FBS+Ins	0.0409 ± 0.0006	1.61	0.0031	0.0655 ± 0.0010	1.55	0.0043
LG: Control	0.0260 ± 0.0008	1.02	0.61	0.0417 ± 0.0012	0.99	0.22
LG: Insulin	0.0380 ± 0.0010	1.50	0.0023	0.0608 ± 0.0016	1.44	0.0034
LG: FBS	0.0307 ± 0.0023	1.21	0.027	0.0521 ± 0.0039	1.23	0.02
LG: FBS+Ins	0.0424 ± 0.0010	1.67	0.0016	0.0678 ± 0.0016	1.61	0.0027

Table 4.1: Glucose consumption and lactate production rates (in $\mu\mathrm{mol}/(\mathrm{min.mg_{protein}})$) for all experimental conditions as well as their fold-induction values for glucose consumption and lactate production rates. HG, MG, and LG, refer to growth in 25 mM, 15 mM, and 5 mM glucose respectively.

Normalised Lactate Production Rates
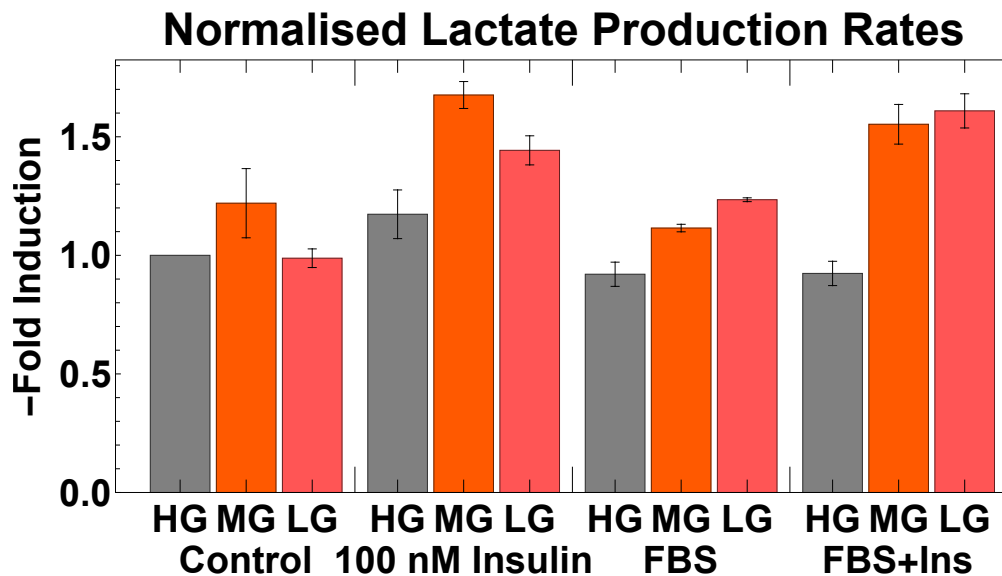
Figure 4.3: Lactate production as induced by 100 nM insulin, 10 % v/v, or both. Lactate production rates normalised to those observed in the high glucose control. Cells cultured in 25 mM (HG, 15 mM (MG), or 5 mM (LG) glucose are indicated as grey, orange, or pink bars respectively. Error bars indicate SEM, and each bar represents a biological triplicate (n = 3).

Reducing glucose concentrations during culturing therefore appears to improve the ability of cells to respond to insulin with an induction in glycolytic flux. The strongest induction of glycolytic flux was seen when cells were grown in medium-level glucose (Fig. 4.2, green) as opposed to more modest induction at low, but physiological, glucose conditions (Fig. 4.2, blue), or none at all under high glucose growth conditions (Fig. 4.3, grey). The combination of FBS and insulin appeared to have no significant advantage over only using insulin to induce glycolytic flux. However, it does appear that the prolonged exposure to the combination of high glucose and FBS attenuates the ability of C2C12 myotubes to upregulate glycolytic flux in response to insulin. Considering that, under medium and low glucose conditions FBS has a modest pro-insulinic effect, it is possible that prolonged exposure to hyperglycaemic conditions and FBS induces an insulin resistant-like state in these cells.

The glucose-lactate flux was a reliable measure by which the insulin response of cells could be evaluated. Therefore, insulin dose-dependent induction of glucose consumption and lactate production were subsequently tested in cells grown at medium glucose concentrations.

(a)   **(b)**
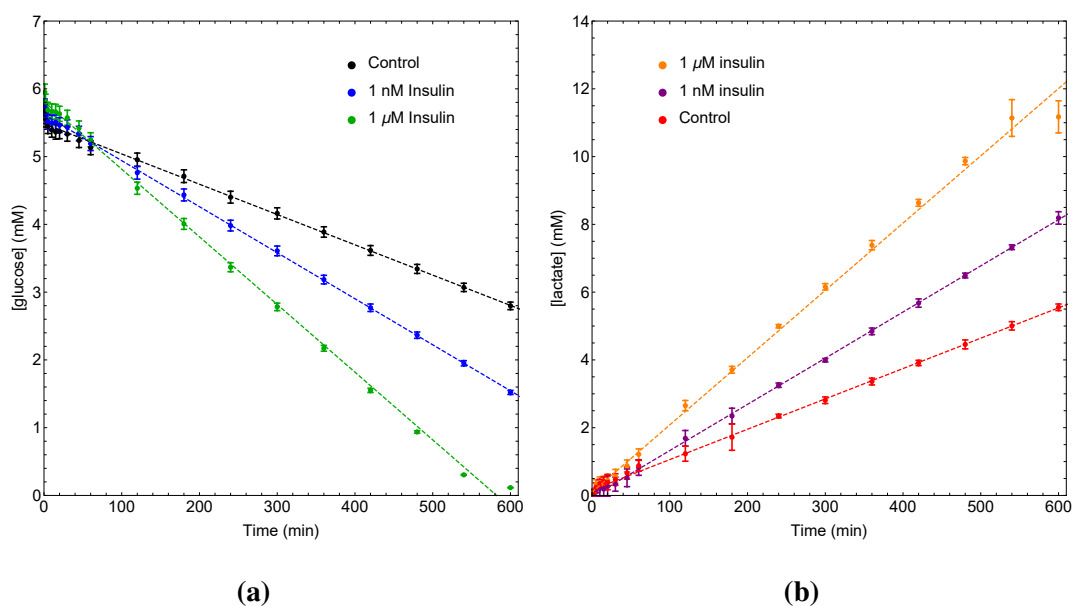
Figure 4.4: Glucose consumption (A) for control (black) cells and cells treated with 1 nM (blue) and 1 μM (green) insulin and lactate production (B) for control (red), 1nM insulin (purple), and 1 μM insulin (orange). The biomass yield was similar (8.6 mg $\pm$ 0.1) for all experiments. Error bars indicate SEM, and each data point represents a biological triplicate (n = 3).

Glucose consumption is shown in Fig. 4.4 for three insulin concentrations - 0 nM, 1 nM, and 1000 nM. These concentrations were chosen as 1000 nM of insulin would ensure full-stimulation of the insulin signalling pathway. On the other hand 1 nM of insulin would ensure a significant insulin response while still within the physiological range reported in mice [352], albeit at the upper end of the spectrum. A dose-dependent stimulation was observed with an overall induction of glucose consumption between control and 1000 nM insulin by a factor of approximately 2.2.

While not conclusive evidence for insulin resistance or type two diabetes, these results do indicate that, under standard culturing conditionsm, C2C12 cells appear unable to upregulate glycolytic flux in response to insulin. Taking into consideration the role of high glucose concentrations in the ætiology of insulin resistance and type two diabetes, it was decided that further efforts would not evaluate cells grown at 25 mM glucose concentrations. Rather, a concentration of 15 mM glucose was chosen as is still within the physiological range reported in mice [334, 335] and would not

deplete as rapidly as a concentration of 5 mM of glucose would.

4.3.2   Quantifying C2C12 Differentiation

In addition to testing the insulin sensitivity as a function of media glucose concentration, further experiments were necessary to determine the effect of glucose concentration on cell differentiation. The method developed by McColl et al (2016) was adapted for this purpose [326].

The modified LADD-staining method, discussed in Section 4.2, resulted in the images shown in Fig. 4.5. What is apparent *prima facie* is the greater coverage by myotubes in cells cultured at 15 mM glucose (Fig. 4.5b) as opposed to cells cultured at 25 mM glucose (Fig. 4.5a). Myotubes cultured at 15 mM are thicker, longer, and more numerous. Conversely, cells cultured at 25 mM glucose seem less differentiated as indicated by the numerous, unaligned cells present as single clusters rather than fibres. Additionally, the LADD stain was present in greater amounts in myotubes as these had more nuclei and cytoplasmic volume to stain. Since Fig. 4.5b appears to exhibit stronger pink and purple hues than Fig. 4.5a it seems likely that greater quantities of the LADD stain have been retained, which in turn implies the presence of more myotubes. However, for the purposes of this investigation, it is sufficient to enumerate the nuclei present *within* distinct myotubes and those that remained as myoblasts.

The images were analysed in the FiJi distribution of ImageJ. The optional 'Cell-Counter' plug-in was used to manually count the nuclei present in single cells (black arrows in Fig. 4.5a and 4.5b) or the nuclei present in myotubes (yellow arrows). Cells that were too close to the edge of the image as well as multi-nucleated cells with fewer than two discernible nuclei were discounted.

Since, during differentiation, myotubes result from the fusion of several myoblasts, it stands to reason that the greater the extent of differentiation one sees in these cells, the more nuclei would be included *within* myotubes. Similarly, one would expect to see fewer individual nuclei in individual myoblasts. As seen in Fig. 4.6 cells grown under high glucose conditions showed a mean of 58% ($\pm$ 2%) of nuclei that were included in myotubes. Greater inclusion of nuclei in myotubes was seen in cell cultured

(a)

(b)
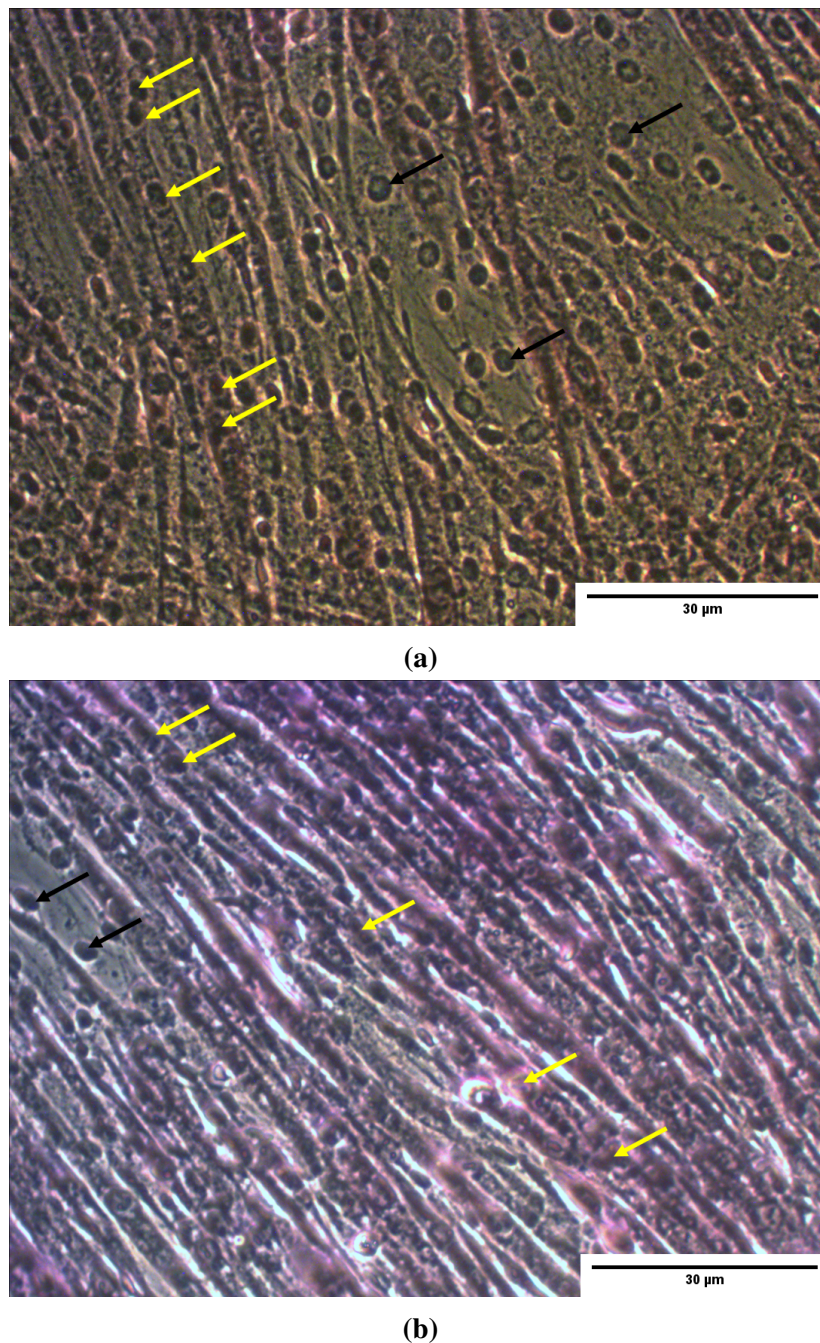
Figure 4.5: Phase constrast images of C2C12 cells grown under high glucose conditions (A) and under medium glucose conditions (B). Cells were fixed with 100% ethanol and stained with fuchsin and toluidine blue to differentiate between the cell membrane and the nucleus (as described in Section 4.2). Thereafter ImageJ was used to analyse the images and assign nuclei as belonging either to myoblasts or myotubes. Yellow arrows indicate nuclei that were assigned to a single myotube whereas black arrows indicate nuclei in single myoblasts. These images were used to generate the data found in Fig. 4.6 and Table 4.2.
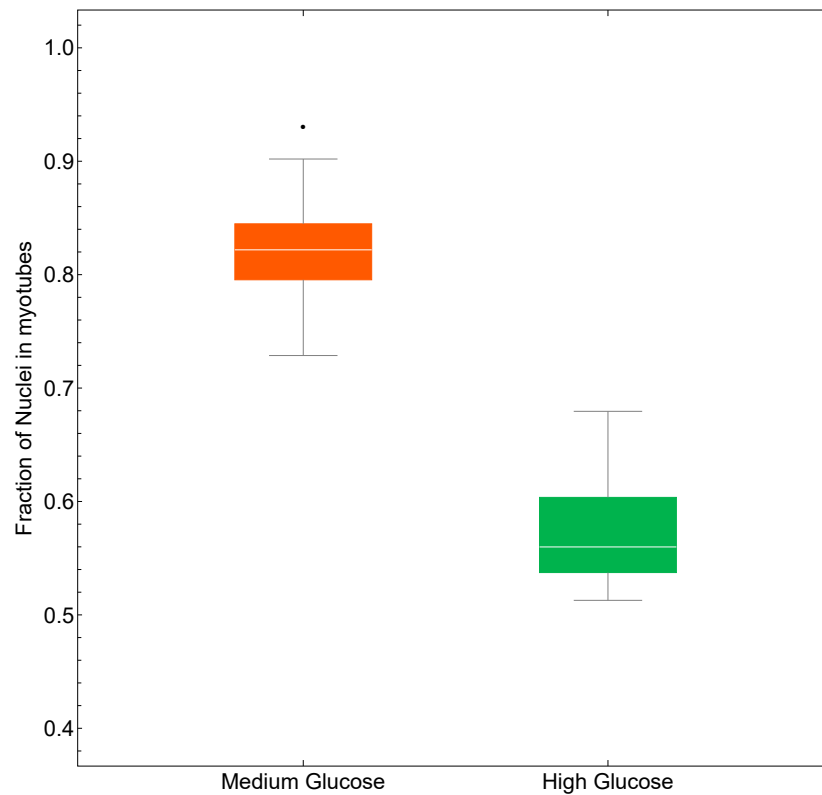
Figure 4.6: A box-whisker plot which shows the differences in the fraction of differentiated nuclei among high glucose culturing protocols (green) and the updated, medium glucose protocol (orange) after six days of culturing. Error bars indicate SEM, n = 9.

under medium glucose conditions. Further, a mean of 82% of nuclei ($\pm$ 1.5%) were included in myotubes in these cells - with one sample showing as many as 93% of nuclei included in myotubes (Table 4.2). This accords a significant ($p < 0.05$) difference in the degree to which the cells are differentiated. These data therefore indicate that reducing the glucose concentration in culturing media has a discernible effect on the degree to which C2C12 skeletal muscle differentiate.

Table 4.2: A comparison of the fraction of nuclei present in differentiated cells cultured according to the high glucose or medium glucose culturing conditions. Values represent three images taken from each of three biological samples for each culturing condition (error bars indicate SEM, n = 9).

Media	Mean	Median	25%	75%	Min	Max
High glucose	0.575 $\pm$0.017	0.56	0.54	0.60	0.51	0.73
Medium glucose	0.816$\pm$0.015	0.82	0.80	0.84	0.68	0.93

4.4 Conclusion

Reducing the glucose concentration from 25 mM to 15 mM in the culturing medium has marked effects on C2C12 cells. Firstly, cells cultured at the reduced glucose concentration appear to regain their insulin sensitivity, or not lose it in the first place. This is indicated by the increased glucose consumption and lactate production when these cells are stimulated by insulin. Conversely, cells which were cultured at 25 mM glucose showed no significant induction of glucose consumption upon stimulation by insulin, FBS, or both.

Secondly, C2C12 cells cultured at 15 mM glucose differentiate to a greater degree. Cells which were cultured at 15 mM glucose were 26 % more differentiated than cells grown in 25 mM glucose. Since the amount of insulin-sensitive GLUT4 correlated with the degree of differentiation [353], cells which exhibit greater differentiation will show greater glucose uptake than their hyperglycaemic counterparts.

Inducing a diabetic state in cultured cells often relies on a combination of hyperinsulinemia and hyperglycaemia. Current, 'standard' cell culture methodology for C2C12 cells relies on 25 mM glucose in the media which satisfies the hyperglycaemic condition. Supplementing these cells with 50 to 500 nM insulin before experimentation often leads to perceived insulin insensitivity in C2C12 cells. However, under *in situ* conditions, insulin insensitivity is a progressive disease [354, 355]. Therefore, prolonged exposure to lower, but above normal, concentrations of insulin may result in an insulin insensitive state. In support of this, data presented in this chapter indicates that the 10 % v/v FBS supplementation appears to have a mild pro-insulinic effect on cells. Cells which were cultured either at 15 mM or 5 mM glucose and then induced with FBS showed above-normal glucose consumption and lactate production. This indicates that FBS contains either insulin or an insulin-like factor which stimulates glucose consumption. Since this increase in glucose consumption and lactate production was absent in cells cultured at 25 mM glucose and then stimulated with FBS, it is possible that the combination of persistent FBS and high glucose concentrations in most standard media may reduce the sensitivity of C2C12 cells to insulin.

One of the challenges in molecular biology is reproducibility [356, 357]. Studies

often do not make explicit the metabolite concentrations or specific formulations of DMEM that are being used for cell culture. As this data in this chapter demonstrate, minor changes such as reducing the glucose concentration in cell culture media, can drastically affect the outcomes of an experiment. If there is no clarity or uniformity in how cells are cultured, then there can be no reproducibility in the results which are obtained. It is therefore imperative that glucose and metabolite concentrations are made explicit in ongoing and future molecular biological research.

Chapter 5

Integrating Insulin Signalling and Glucose Transporter Data: Constructing a Minimal Model

This chapter presents the results on the insulin concentration and time responses of the IR and Akt protein phosphorylation as well as the GLUT4 glucose transporter activity to insulin. Further, this chapter will attempt to construct a minimal model which integrates these data in order to describe the first and second modules as presented in Section 1.1.

5.1   The Minimal Modelling Strategy

The minimal modelling strategy is based on the 'three modules' approach outlined in Section 1.1. The model described in this section attempts to describe the dynamics of the signal transduction and glucose transporter modules. A second project by Dr. Cobus van Dyk and colleagues will describe the glucose metabolism module.

A minimal, ODE-based modelling approach was best suited to the type of data which could be gathered given the experimental constraints. The insulin signalling pathway consists of dozens of proteins each of which interact with components from other pathways as well which makes studying them in detail prohibitive for a single

project. Therefore, in order to align the modelling strategy, experimental approaches, and complexity with one another, several choices were made.

The first choice was made to limit the insulin signalling pathway to those components which lead from the IR to GLUT4 by the shortest path (see: Section 2.1.9. This is not to negate the effect of the various other components which act upon the insulin signalling pathway or as a result of its activation. Rather this would focus on those components, leading up to GLUT4, which are most likely to be affected as a result of insulin stimulation.

The second choice was to further limit the components which were measured in accordance with the 'three module' approach which defined each module as an input-output relationship between two components. The insulin receptor and Akt proteins were the respective inputs and outputs for the insulin signalling module as these components could be measured through Western blotting, they are crucial to the normal induction of the glucose transporter in response to insulin [27, 358], they are known to be defective in insulin resistant states [359, 360], and they are sensitive to insulin concentrations [361, 362]. The glucose transporter module was defined by the phosphorylated Akt as its input and the glucose transporter activity as output. The glucose transporter activity was assayed by measuring how much ^{14}C was internalised by the cell in response to the given experimental conditions.

Thirdly, the dose response data were used for a steady-state analysis of the model (Section 5.2)in order to constrain model parameters such as the forward and reverse reaction constants. These constraints were incorporated into the model which was then used to fit simulations to the time dynamic experimental data (Section 5.3). This step was used to validate the steady-state parameter estimations.

This modelling approach may not lead to the best possible fits since the model parameters were constrained to their steady-state estimations which were in turn based on mass-action kinetics and a limited data set. This approach does not require large sets of parameters as one would need for a more detailed model. However, the goal was not to create a detailed model. The goal with the three-module and minimal modelling approach was to characterise the 'normal' - non insulin-resistant state of the insulin

signalling and glucose transporter modules. Understanding how these modules react under normal conditions will help understanding *where* in the insulin signalling cascade dysregulation occurs, should it occur. In other words, aberrant behaviour could be traced to the signalling, glucose transporter, or metabolism modules with a small set of experimental perturbations. This will allow more detailed investigations at the appropriate module instead of needing to investigate the entire insulin signalling system.

5.2   Insulin Response Characteristics of the Insulin Signalling Pathway

AktS473concThe effect of varying the insulin concentration on the authosphorylation of the IR as well as the phosphorylation of both Akt serine 473 and threonine 308 was analysed. For this, the cells were grown under the updated, 15 mM glucose, conditions, starved, and then exposed to different insulin concentrations ranging from 0 nM to 1000 nM (for further details on all methods, see Chapter 3. After 30 minutes the cells were harvested, lysed, and stored for Western blot analysis. The degree of phosphorylation of cells exposed to 100 nM insulin after 30 minutes was used as the reference state and all samples were normalised to this value.

Physiological, basal insulin concentrations in mice can be as low as $\pm$ 40 pM or as high as 1.7 nM [334, 336, 352]. Insulin concentrations were chosen to represent the control at 0 nM of insulin, a minimum at 10 pM of insulin, and a maximum at 1000 nM of insulin. Intermediate ranges were used to determine the insulin dose-dependent phosphorylation of the insulin signalling intermediates. While some concentrations are indeed supraphysiological, they were nonetheless useful in parameterising the model. The 30 minutes, 100 nM state was used as a reference state since it is commonly used in literature [363–365] as well as reportedly eliciting a maximal response in signalling [366].

5.2.1 The Dose-Response Characteristics of the Insulin Signalling Module

The response of the insulin signalling module (Section 1.1) in response to varying insulin concentrations is investigated in this section. The insulin receptor is phosphorylated in a dose-dependent manner in response to insulin (Fig. 5.1). It achieved maximal phosphorylation at 100 nM insulin and no increase in phosphorylation was observed when the insulin concentration was increased to 1000 nM. The decrease in IR phosphorylation observed at the 1000 nM insulin concentration is likely due to a combination of insulin and stress induced cytotoxicity [278, 367]. However, this would need to be tested in future studies. The total level of IR was independent of the insulin concentration (Fig. 5.1 - black points).

The levels of the phosphorylated proteins, Akt_{S_P} and Akt_{T_P}, also depended on insulin over a wide concentration range (Figs. 5.2 and 5.3 respectively). The phosphorylation of Akt_S showed a linear increase with Log[insulin] up to 1 μM (Fig. 5.2). Akt_{T_P} was not detectable at insulin concentrations below 20 nM, but showed a strong dependence on insulin at concentrations greater than 100 nM - for example, a nearly 4-fold increase in phosphorylation at 1 μM (Fig. 5.3). However, this is likely due to the artificial constraint of setting the phosphorylation of the 100 nM condition as '1' for the purposes of constructing the model. As observed for the IR, the total Akt levels were similar across all samples for the different insulin doses.

After the initial observations, a set of rate equations were developed for the forward (phosphorylation) and reverse (dephosphorylation) reactions of the minimal signalling. The rate equations are based on simple mass-action kinetics which described the change in concentrations of the IR and Akt proteins as a function of their respective phosphorylation and dephosphorylation reactions. Afterwards, the rate equations were rewritten as a single, balanced ordinary differential equation (ODE). Experimentally, the data were gathered in two stages, a dose-response and a time-response. The dose-response data were assumed to be in steady-state to fit for the ratio of the phosphorylation constant (k_p) over the dephosphorylation constant (k_{dp}).

(a)

(b) The phosphorylation of the IR at selected insulin concentrations in nM.
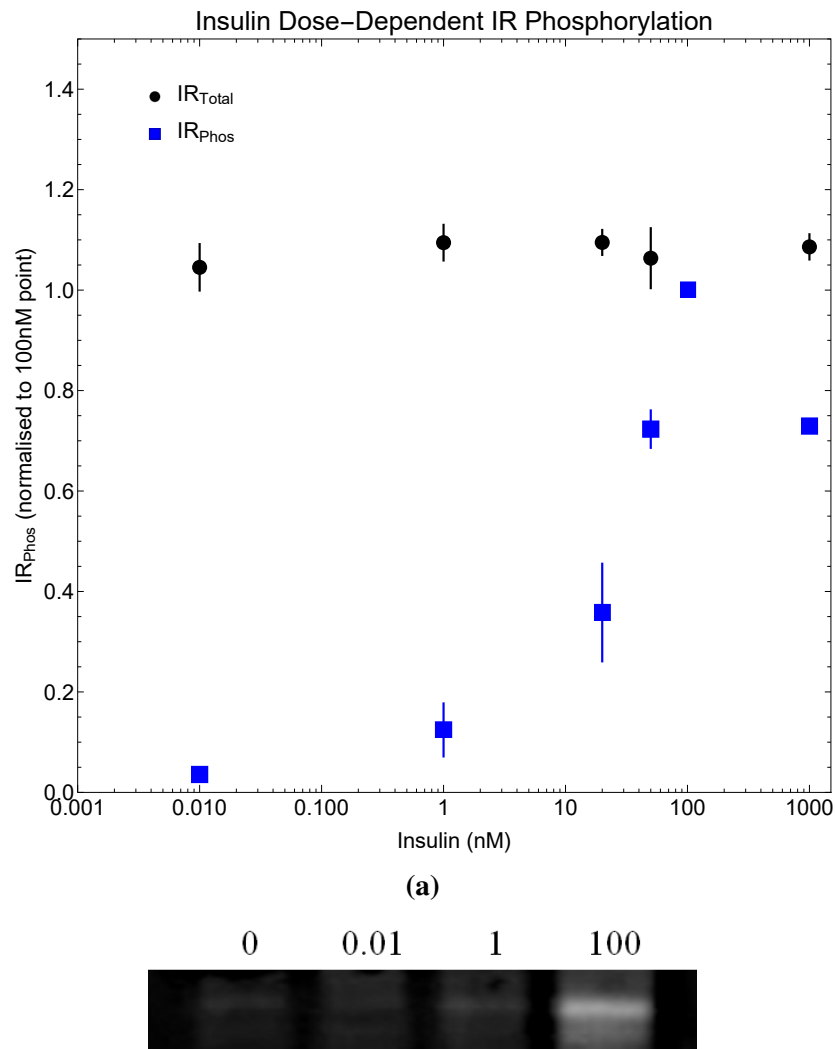
Figure 5.1: A semi-log graph of the concentration of total IR (black) and phosphorylated IR (blue) as a function of insulin concentration after a 30 minute incubation. The C2C12 cells were exposed to varying insulin concentrations for 30 minutes, harvested, and then they underwent Western blotting to determine the relative induction of phosphorylation. Error bars indicate SEMs and each data point represents the average of a biological triplicate (n = 3).

$$\frac{\mathrm{d}IR}{\mathrm{d}t} = -insulin \times k_{\mathrm{pIR}} \times IR(t) + k_{\mathrm{dpIR}} \times (IR_{\mathrm{total}} - IR(t)) \qquad (5.1)$$

$$\begin{aligned}\frac{\mathrm{d}AKTS}{\mathrm{d}t} &= -k_{\mathrm{pAKTS}} \times (IR_{\mathrm{total}} - IR(t)) \times AKTS(t) \\ &\quad + k_{\mathrm{dpAKTS}} \times (AKT_{\mathrm{total}} - AKTS(t))\end{aligned} \qquad (5.2)$$

(a)
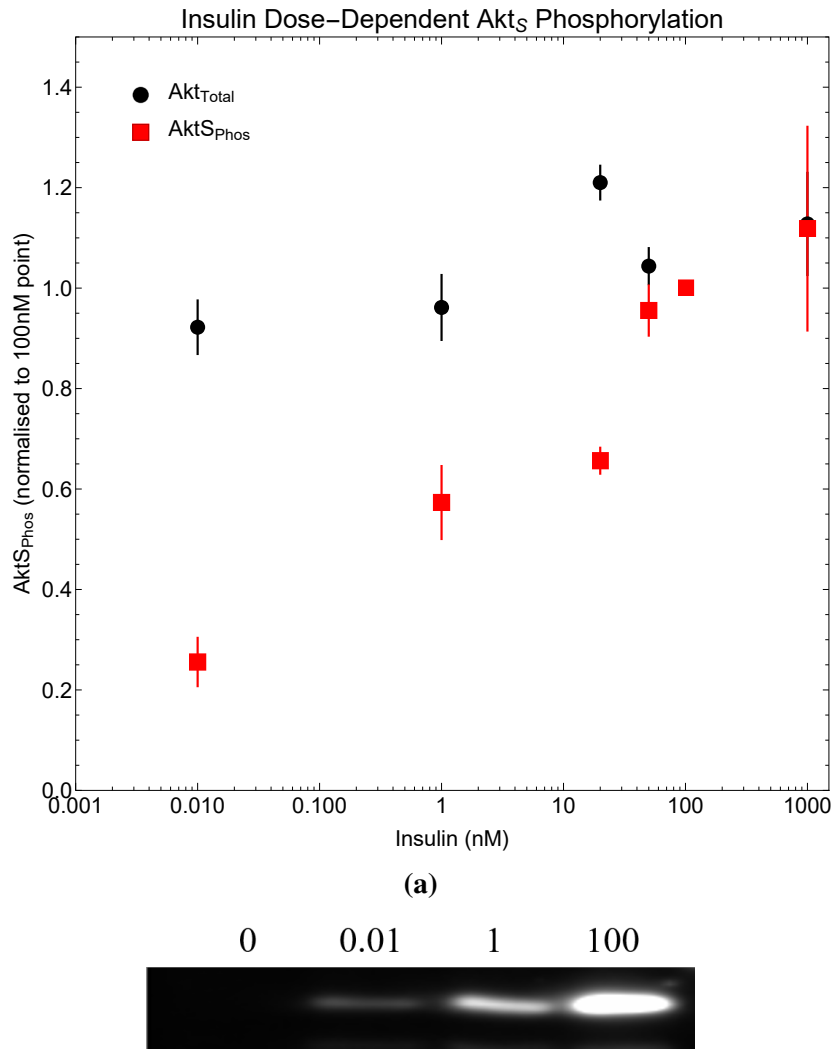
(b) The phosphorylation of Akt at serine 473 at selected insulin concentrations in nM.

Figure 5.2: The phosphorylation of AKT serine 473 due to increases in insulin concentration. The total level of AKT is shown in black while Akt_{S_P} is indicated in red. The C2C12 cells were exposed to varying insulin concentrations for 30 minutes, harvested, and then they underwent Western blotting to determine the relative induction of phosphorylation. Error bars indicate SEMs and each data point represents the average of a biological triplicate (n = 3).

$$\frac{\mathrm{d}AKTT}{\mathrm{d}t} = -k_{\mathrm{pAKTT}} \times (IR_{\mathrm{total}} - IR(t)) \times AKTT(t)$$
$$+ k_{\mathrm{dpAKTT}} \times (AKT_{\mathrm{total}} - AKTT(t)) \tag{5.3}$$

The Western blotting data allowed for the estimation of the steady-state parameters of the insulin-IR interaction. The steady-state levels of the IR were derived from Eq. (5.1) as follows:

80

(a)
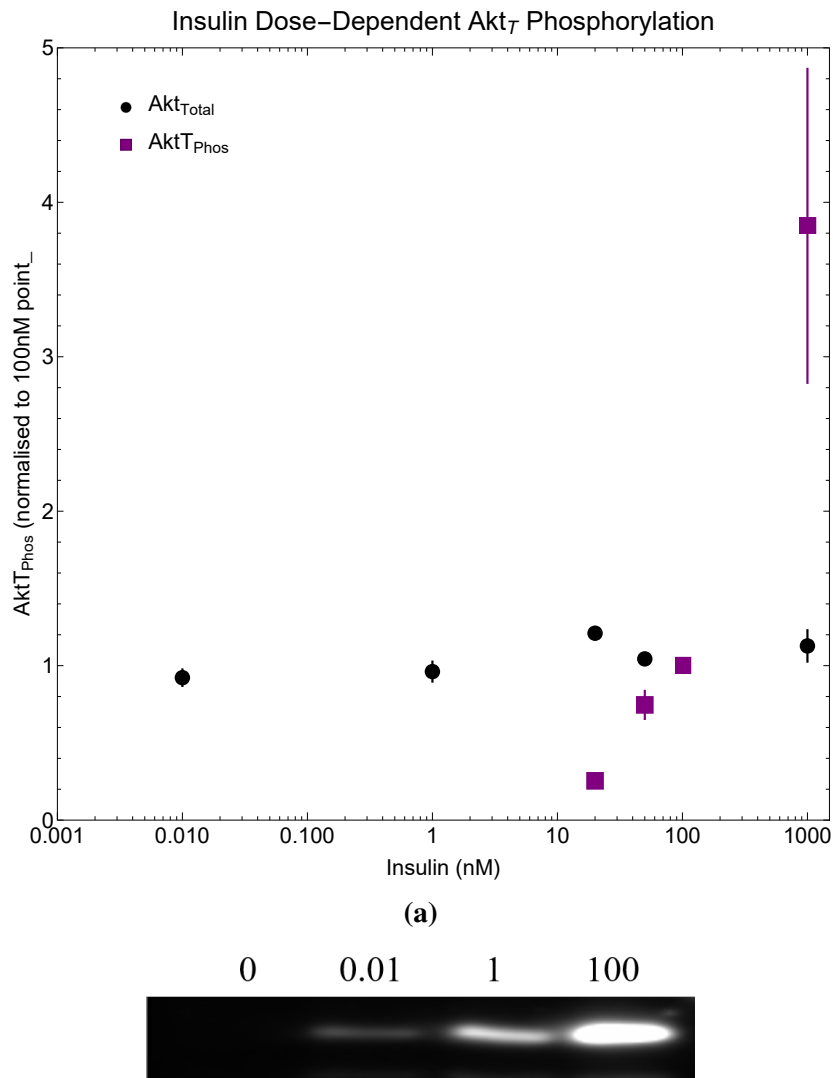
(b) The phosphorylation of Akt at threonine 308 at selected insulin concentrations in nM.

Figure 5.3: The levels of Akt_{T_P} (purple) in relation to the total levels of Akt (black). At lower concentrations of insulin, Akt_{T_P} could not be detected. However, at insulin levels in excess of 100 nM, Akt_{T_P} appears to still have capacity to phosphorylate. The C2C12 cells were exposed to varying insulin concentrations for 30 minutes, harvested, and then they underwent Western blotting to determine the relative induction of phosphorylation. Error bars indicate SEMs and each data point represents the average of a biological triplicate (n = 3).

$$0 = -insulin \times k_{\text{pIR}} \times \overline{IR} + k_{\text{dpIR}} \times (IR_{\text{total}} - \overline{IR}) \tag{5.4}$$

$$\overline{IR} = \frac{k_{\text{dpIR}} \times IR_{\text{total}}}{insulin \times k_{\text{pIR}} + k_{\text{dpIR}}} = \frac{IR_{\text{total}}}{insulin \times \dfrac{k_{\text{pIR}}}{k_{\text{dpIR}}} + 1} \tag{5.5}$$

Further, $\overline{IR} = IR_{\text{total}}$ when $insulin = 0$ and, when $insulin = 100$, $IR = 1$. This leads to the following equations for IR_{total}:

$$1 = IR_{\text{total}} - \overline{IR} = IR_{\text{total}} - \frac{IR_{\text{total}}}{100 \times \dfrac{k_{\text{pIR}}}{k_{\text{dpIR}}} + 1} \tag{5.6}$$

Therefore, solving for IR_{total} yields:

$$IR_{\text{total}} = 1 + \frac{1}{100} \times \frac{k_{\text{dpIR}}}{k_{\text{pIR}}} \tag{5.7}$$

Lastly, the phosphorylation of IR in response to insulin can be described as:

$$\overline{IR} = 1 + \frac{1}{100} \times \frac{k_{\text{dpIR}}}{k_{\text{pIR}}} - \frac{1 + \dfrac{1}{100} \times \dfrac{k_{\text{dpIR}}}{k_{\text{pIR}}}}{\dfrac{k_{\text{pIR}}}{k_{\text{dpIR}}} \times insulin + 1} \tag{5.8}$$

In Fig. 5.4 the dose-reponse fits for the phosphorylation of IR and Akt_S are shown. The fit is not particularly good; two data points for the IR, and one data point for the Akt_S fit have significantly lower experimental levels of phosphorylation than obtained for the fit. The simplicity of the model, (for this curve only one parameter was fit to the data), restricts the shape of the response curve strongly, however the advantage of the small number mean that the fit was considered good enough to allow further analysis. The Akt_S responds stronger to insulin at lower concentrations, for example at insulin concentrations that elicit 35% of maximal IR phosphorylation, the Akt_S is 65% phosphorylated. This might appear counter-intuitive since AktS phosphorylation is dependent on IR phosphoryation. However, it should be noted that Fig. 5.4 represents a steady-state response and not a temporal response (for which one would expect the IR to phosphorylate more rapidly than Akt). Additionally, the phosphorylation levels are all relative which means that Akt_S and IR responses cannot be compared in absolute sense. Lastly, it is not unusual to see amplification in signal transduction pathways [368, 369].

Therefore, the phosphorylation of both Akt sites was expressed as a function of the phosphorylation of IR (Fig. 5.5). It may seem counter-intuitive to express one variable as a function of another variable. However, this method of visualising the data allows
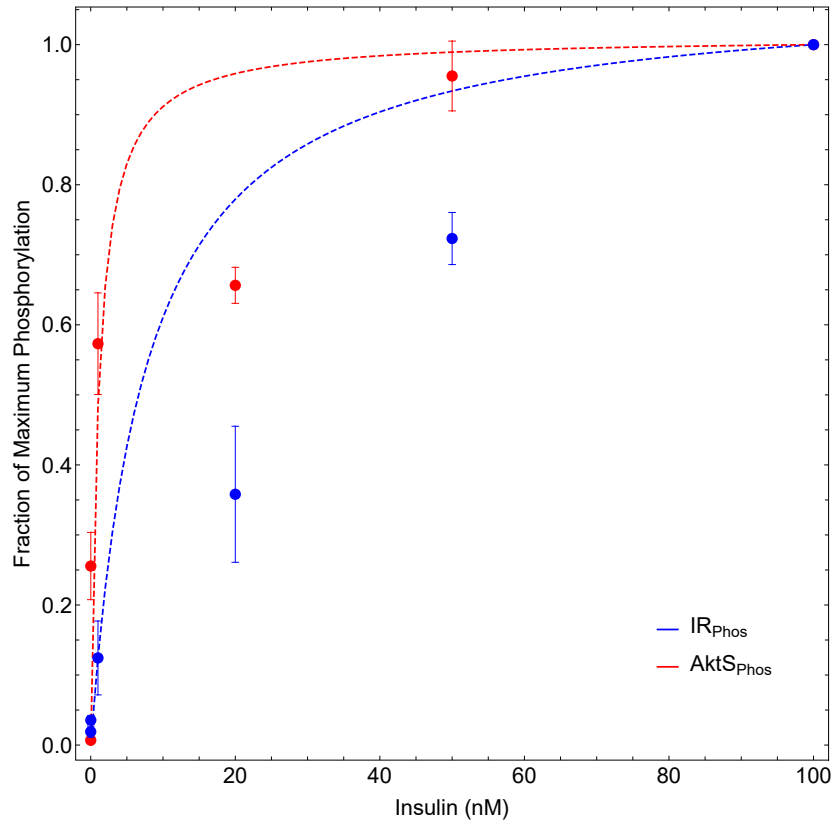
Figure 5.4: Model fits of the insulin concentration-dependent phosphorylation of the IR (blue) and Akt_S (red) data as seen in Figs. 5.1 and 5.2. These curves are predictions of the phosphorylation of Akt_S as determined by the ODEs. Akt_S phosphorylation appears more sensitive to insulin than IR. Error bars indicate SEMs and each data point represents the average of a biological triplicate (n = 3).

one to directly relate one module (or part thereof) of the insulin signalling cascade to the preceding module, and in their co-response analysis Hofmeyr and Cornish-Bowden [370] have shown that this contains much information about control and regulation and in the absence of a feedback loop, a co-response relation equals a cause effect relation [369]. When comparing normal cells to insulin resistant cells, it would then become apparent *where* in the cascade dysfunctions occur instead of merely showing the response of each module to insulin.

$$\overline{AKTS}_P = 1 + \frac{k_{\text{dpAKTS}}}{k_{\text{pAKTS}}} - \frac{1 + \dfrac{k_{\text{dpAKTS}}}{k_{\text{pAKTS}}}}{\dfrac{k_{\text{pAKTS}}}{k_{\text{dpAKTS}}} \times (IR_{\text{total}} - IR(t)) + 1} \tag{5.9}$$

$$\overline{AKTT}_P = 1 + \frac{k_{\text{dpAKTT}}}{k_{\text{pAKTT}}} - \frac{1 + \dfrac{k_{\text{dpAKTT}}}{k_{\text{pAKTT}}}}{\dfrac{k_{\text{pAKTT}}}{k_{\text{dpAKTT}}} \times (IR_{\text{total}} - IR(t)) + 1} \tag{5.10}$$

The steady-state equations (Eqs. 5.8, 5.9, and 5.10) and the Western blotting data were used to parameterise the model in a single optimised fitting step. This yielded values for the $\dfrac{k_p}{k_{dp}}$ ratios of the IR_P, $AKTS_P$, and $AKTT_P$ steady-state equations. These values (Table 5.1) were those that best fit the dose-response data for the whole model.

Table 5.1: Fitted parameters. k_{endo} refers to the rate constant of GLUT4 endocytosis from the PM into the cell. k_{exo} is the rate constant for GLUT4 exocytosis from the cell into the PM. The value for the $\dfrac{k_{\text{dpAKTT}}}{k_{\text{pAKTT}}}$ ratio was constrained to be equal to or less than 10 since it was unable to determine a value for this ratio without such a constraint. The $\dfrac{k_{\text{endo}}}{k_{\text{exo}}}$ ratio was fit to data which took into account the effect of both the Akt_S and Akt_T phosphorylation sites.

Parameter	Value
$\dfrac{k_{\text{dpIR}}}{k_{\text{pIR}}}$	7.62
IR_{total}	1.08
$\dfrac{k_{\text{dpAKTS}}}{k_{\text{pAKTS}}}$	0.18
$\dfrac{k_{\text{dpAKTT}}}{k_{\text{pAKTT}}}$	10.0
AKT_{total}	1.18
$\dfrac{k_{\text{endo}}}{k_{\text{exo}}}$	1.01

The Akt_S (red) and Akt_T (purple) phosphorylation responses as a function of IR phosphorylation are shown in Fig. 5.5. The Akt_S site responds more strongly to IR phosphorylation and achieves maximum phosphorylation once the IR is fully phosphorylated. The Akt_T, however appears to not to be maximally phosphorylated. It responds linearly to an increase in IR phosphorylation. However, given the data in Figs. 5.1 and 5.3, Akt_T phosphorylates quite strongly in response to insulin concentrations beyond 100 nM - which is already several times the physiological concentration. Sim-

ilarly, since the IR seemingly dephosphorylates at such high insulin concentrations, it might be that the phosphorylation of Akt_T at such high concentrations of insulin is due to an IR-independent mechanism. It is possible that the spare phosphorylation capacity of Akt_T at high insulin concentrations is an adaptive mechanism which could ameliorate the consequences of insulin resistance.
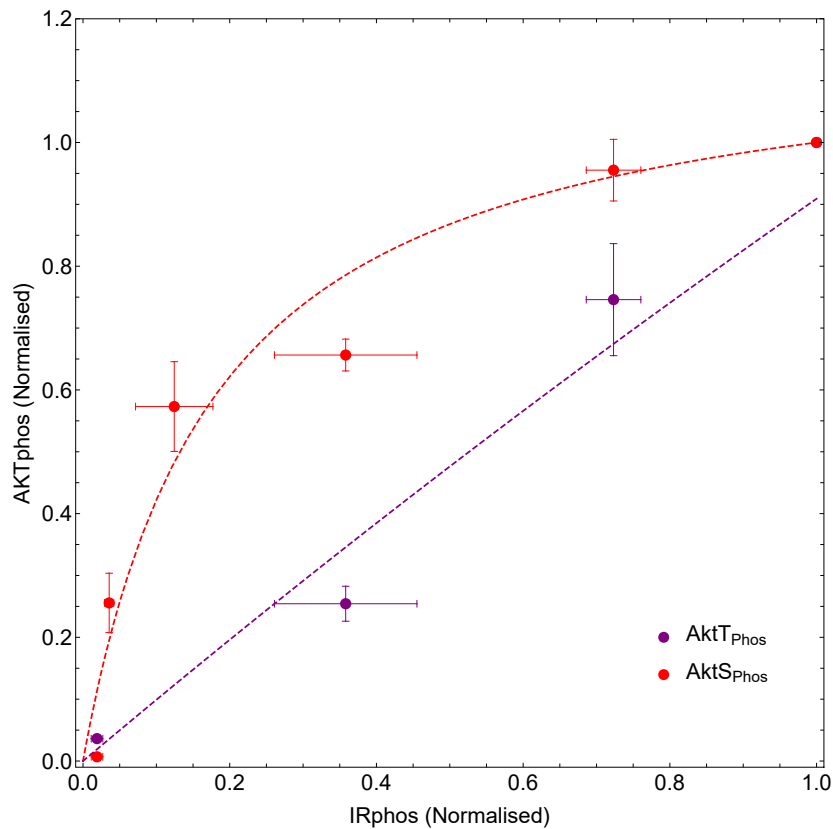
Figure 5.5: The phosphorylation of Akt_S (red) and Akt_T (purple), in response to increases in IR phosphorylation. The fitted equations (Eq. (5.9) and 5.10) are shown with dashed lines. The C2C12 cells were exposed to varying insulin concentrations for 30 minutes, harvested, and then they underwent Western blotting to determine the relative induction of phosphorylation (as seen in Figs. 5.1, 5.2, and 5.3). Error bars indicate SEMs and each data point represents the average of a biological triplicate (n = 3)

5.2.2   The Dose-Reponse Characteristics of the Glucose Transporter Module

The first set of C^{14} glucose-uptake experiments sought to establish the relationship between glucose transporter activity and insulin concentration. The cells were grown under the previously established conditions and starved as indicated in Chapter 3. The cells were then exposed to insulin at concentrations which ranged from 0 nM to 1000 nM for 30 minutes. Thereafter a 2 second ^{14}C glucose-uptake assay was performed. When no insulin has been added to the cells, *basal* glucose uptake of 0.81 μmol.min^{-1}.mg^{-1} was measured. An almost linear relationship between insulin concentration and glucose uptake was observed on a semi-log scale (see Fig. 5.6). The maximum glucose transport rate was 1.91 μmol.min^{-1}.mg^{-1}$_{\text{protein}}$ at 1000 nM insulin.

Induction of GLUT4 activity was modelled using mass-action kinetics which depended on the Akt phosphorylation. In this case, 'Akt phosphorylation' was described by combining the Akt_S and Akt_T phosphorylation states. Since the *precise* role of either phosphorylation site is not known in detail, the assumption was that they both contribute to the induction of glucose transport activity.

Mass-action kinetics is the simplest form with which to model the induction of GLUT4 activity by insulin and follows the same principles that were used in modelling the signal transduction pathway. When insulin, and therefore AKT phosphorylation are set to 0, there will still be basal glucose uptake owing to insulin-independent transporter activity such as that of GLUT1. The maximum induction level of glucose transporter was assumed equal to the maximum activity of 1.91 μmol.min^{-1}.mg^{-1}. Consequently, if '1' is the *maximum* normalised glucose transport, then 0.42 is the *basal* normalised glucose transport. This then leads to the fraction of *inducible* glucose transporter being $1-0.42 = 0.58$. In order to describe glucose transporter activity, k$_{\text{exo}}$ is the rate constant for the *exocytosis* of GLUT4 from the intracellular space to the PM whereas k$_{\text{endo}}$ is used to describe the *endocytosis* of the GLUT4 from the PM into the cell. Since the mass action kinetics apply to the inducible or 'responsive' elements in the insulin signalling cascade, they were adapted as follows to take into account the different dynamics of glucose transport:
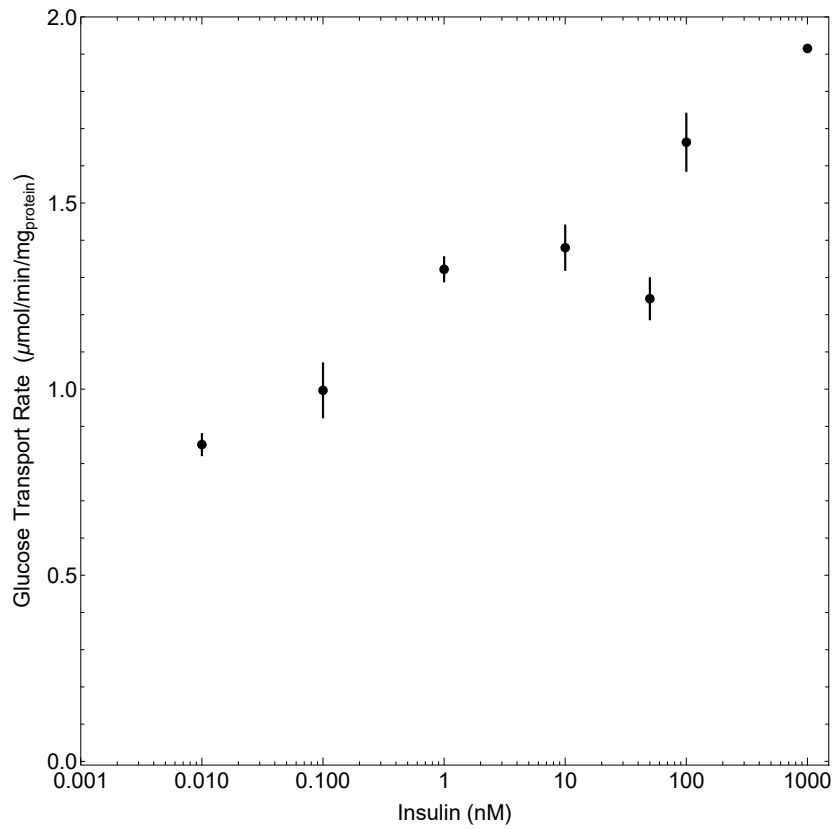
Figure 5.6: Glucose transport activity (in μmol.min^{-1}.mg^{-1}) as a function of insulin concentration.The C2C12 cells were exposed to varying insulin concentrations for 30 minutes and then subjected to a ^{14}C glucose uptake assay to determine the dose-dependent induction of glucose uptake by insulin-stimulated glucose transporters. Error bars indicate SEMs and each data point represents the average of a biological triplicate (n = 3)

$$\frac{\mathrm{d}GLUTM}{\mathrm{d}t} = -k_{\text{endo}} \times GLUTM(t) + k_{\text{exo}} \times (AKT_{\text{total}} - AKT[t])$$
$$\times (GLUTmax - GLUTM[t]) \tag{5.11}$$

Where GLUTM represents the portion of glucose transporter at the membrane. Solving for the steady-state levels of GLUTM yields the following:

$$\overline{GLUTM} = (1 + \frac{k_{\text{exo}}}{k_{\text{endo}}} - \frac{1 + \frac{k_{\text{exo}}}{k_{\text{endo}}}}{\frac{k_{\text{endo}}}{k_{\text{exo}}} + \overline{AKT_p}}) \times 0.5759 + 0.4241 \tag{5.12}$$

Where $\overline{AKT}_{\text{p}}$ represents the sum of AKT serine and Akt threonine phosphorylation and the numbers refer to the basal and inducible activities as determined previ-

ously. Fitting the $\dfrac{k_{\text{exo}}}{k_{\text{endo}}}$ ratio yields a value of 1.01 (Table 5.1). This was used to simulate the glucose transporter activity as a function of Akt phosphorylation as shown in Fig. 5.7.

In Fig. 5.7, the fraction of total glucose transporter in the plasma membrane is given as a function of various Akt phosphorylation states. Insulin does not directly affect the glucose transporter, rather it leads to the activation of a phosphorylation cascade which culminates in the phosphorylation of Akt residues. Therefore, the activity of the glucose transporter is shown as a function of Akt phosphorylation. Figure 5.7 shows the effect that Akt_S (red), Akt_T (purple), or the combination of Akt_S and Akt_T (black) would have on the glucose transporter. Since the response of the glucose transporter under the influence of both Akt sites was sensitive to the Akt_T site, the glucose transporter would be fit to the data which incorporates both Akt phosphorylation sites. The Akt_S site should not be ignored since at lower levels of IR phosphorylation (i.e. lower insulin concentrations), Akt_S is phosphorylated whereas Akt_T is not (Fig. 5.5).

After $\dfrac{k_{\text{exo}}}{k_{\text{endo}}}$ was fit to the data, the complete model was used to predict glucose transporter activity in response to insulin concentration by varying k_{pIR} and k_{pAKTS}. The sigmoidal graph in Fig. 5.8 constituted the best fit of the complete model of IR and Akt_S phosphorylation as well as glucose transport to the glucose transport data. The GLUT4 transporter may not conform strictly to mass-action kinetics, however given the available data and the modelling strategy, this represents the best approximation of the GLUT4 transport activity.
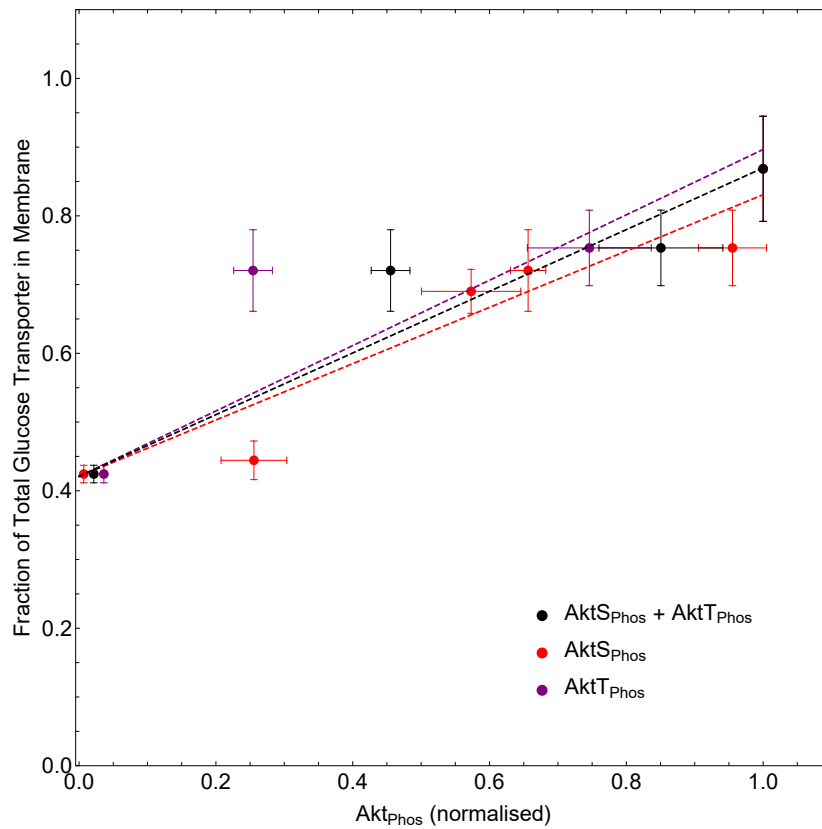
Figure 5.7: The fitted functions for Akt_{S_P} (red, dashed), Akt_{T_P} (purple, dashed), and the combined effect of the phosphorylation sites (black, dashed) and their effect on glucose transporter activity. Error bars indicate SEMs and each data point represents the average of a biological triplicate (n = 3).
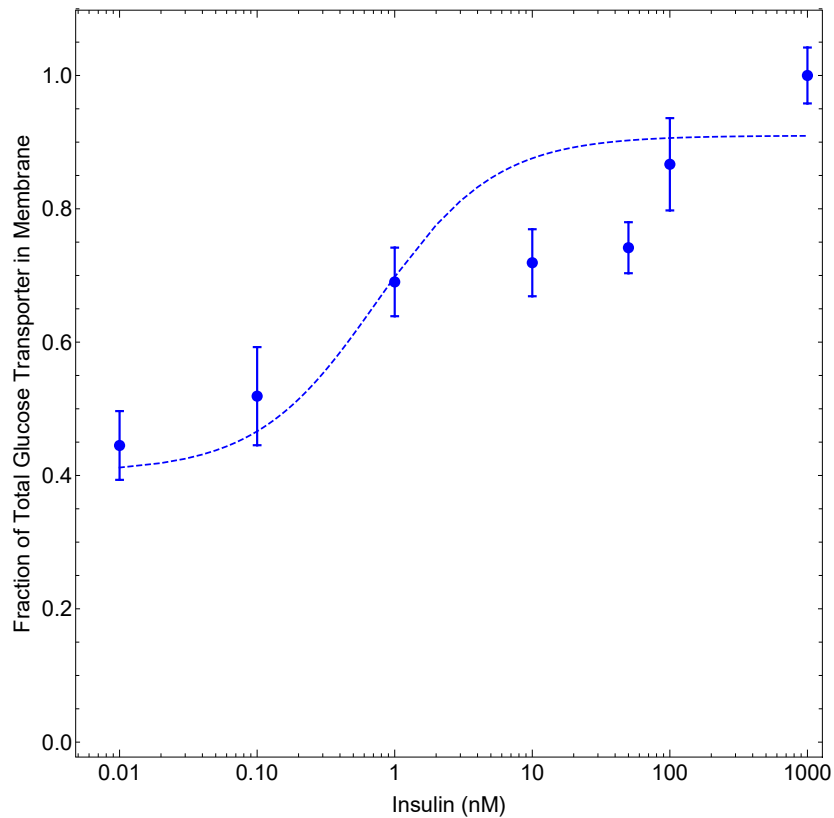
Figure 5.8: The simulated induction of glucose transport (dashed line) overlaid with the data used to generate this fit (circles). The C2C12 cells were exposed to varying insulin concentrations for 30 minutes and then subjected to a ^{14}C glucose uptake assay to determine the dose-dependent induction of glucose uptake by insulin-stimulated glucose transporters. Error bars indicate SEMs and each data point represents the average of a biological triplicate (n = 3).

5.3   Time Dynamics of the Insulin Signalling Pathway

5.3.1   Investigating Time-Dependent Phosphorylation of the Insulin Signalling Module

The time-dependent behaviours of IR phosphorylation, Akt serine phosphorylation, and glucose transport under 100 nM insulinic conditions were investigated. The first phase of experiments established the 'on' behaviour of the insulin signalling cascade. Cells were cultured as before, starved, and stimulated with 100 nM insulin for a given period. Thereafter cells were harvested, frozen in liquid nitrogen, and stored until Western blot analysis. These experiments were repeated with 1 nM insulin for the IR and Akt proteins. The datapoints in Figs. 5.9a and 5.10a were scaled according to the dose-response dose-response experiments discussed in Section 5.2 which showed that when IR and Akt_{S_P} were exposed to 1 nM of insulin, they only achieved 12% and 57% of their maximal phosphorylation (i.e. when compared to the 100 nM condition). Therefore, the IR and Akt_{S_P} data for the timecourse experiments in Figs. 5.9a and 5.10a were scaled by 12% and 57% respectively. Neither IR_{total} nor Akt_{Total} showed an increase in their concentrations for the duration of these experiments (Figs. 5.9a and 5.10a, solid, black circles).

There is a marked difference in the speed with which the IR and Akt serine phosphorylate. The IR achieves near-maximal phosphorylation by the earliest measured time point (1 minute). It is likely therefore, that the IR achieves 50% of its maximum phosphorylation in under a minute. The Akt serine achieves its half-maximum phosphorylation at the two-minute mark. The levels of IR_{total} and AKT_{total} remain constant for the duration of either experiment. As a result, it is unlikely that observed increases in IR or Akt phosphorylation are due to increases in the expression of total IR or Akt.

(a)
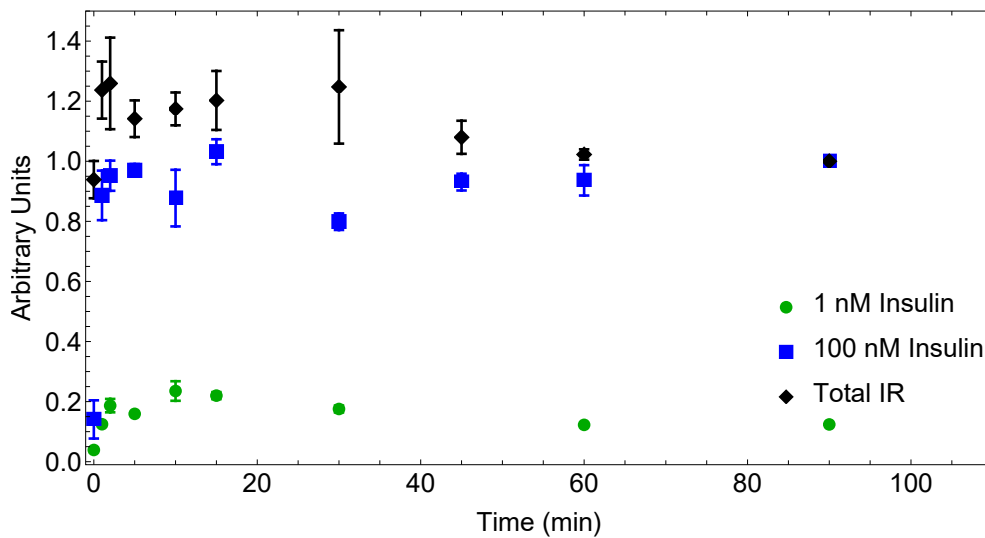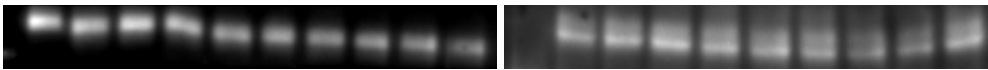
(b) The Western blot of the total amount of IR for the duration of the experiment.

(c) The Western blot for the amount of IR_{Y_P} for the duration of the experiment.

Figure 5.9: The time-dependent phosphorylation of the IR under 100 nM (blue) and 1 nM (green) insulinic conditions. The IR_{total} is shown in black and appears to remain relatively constant throughout the experiment. The data for the 1 nM insulinic condition (green) are scaled to 12% of their observed values. This was done since directly comparing 'full' induction of IR phosphorylation exposed to 100 nM or 1 nM insulin after 30 minutes showed that the 1 nM condition only achieved 12% of the phosphorylation of the 100 nM condition. The C2C12 cells were exposed to 100 nM insulin varying time points, harvested, and then they underwent Western blotting to determine the relative induction of phosphorylation. The IR_{total} values were obtained at 100 nM insulin exposure. Error bars indicate SEMs and each data point represents a biological triplicate (n = 3).

5.3.2 Determining the Time-Dependent Activity of Glucose Transporter Module

A set of time course experiments were performed for glucose transport. Once starved, the cells were exposed to 100 nM insulin for time points ranging from 1 to 45 minutes. The cells then underwent a 2 second ^{14}C glucose-uptake assay as described in Chapter 3. These samples were then analysed in a scintillation counter and the data were used to calculate the glucose uptake rate in μmol.min^{-1}.mg^{-1}. At time-point 0 min - much in during the absence of insulin - the cells exhibited some level of basal glucose transport activity (Fig. 5.11). However, the longer incubations with insulin elucidated

(a)
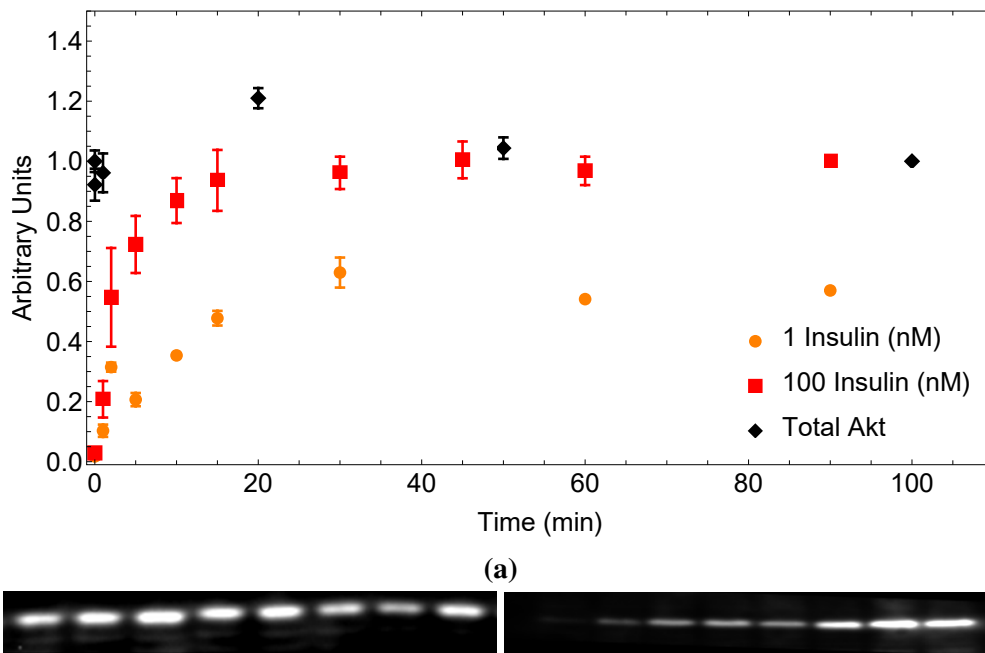
(b) The Western blot of the amount of Akt_{Total} for the duration of the experiment.

(c) The Western blot results of the amount of Akt_{S_P} for the duration of the experiment.

Figure 5.10: Akt serine 473 phosphorylation over 90 minutes in response to 100 nM (red) and 1 nM (orange) insulin. The reponses by Akt serine *vis a vis* 1 nM insulin has been scaled to 57% of the maximal response at 100 nM insulin as per Fig. 5.2. The C2C12 cells were exposed to 100 nM insulin varying time points, harvested, and then they underwent Western blotting to determine the relative induction of phosphorylation. The Akt_{total} values were obtained at 100 nM insulin exposure. Error bars indicate SEMs and each data point represents a biological triplicate (n = 3).

the temporal behaviour of glucose transport activity. The induction of glucose transport closely mirrored that of Akt serine phosphorylation in that both increase more slowly when compared to the phosphorylation of the IR *and* both glucose import and Akt serine phosphorylation achieve their relative maxima after 15 minutes at 100 nM insulin and then remain constant.

The most-commonly investigated aspect of insulin signalling is the 'on' behaviour. In other words, the effect that insulin has on the phosphorylation of signalling intermediates or on the induction of glucose transport or other molecular activity. However, considering the pulsatile nature of insulin release *in vivo*, the 'off' behaviour - dephosphorylation of signalling molecules or reduction of glucose transport - must be investigated as well. If dysregulation of the insulin signalling cascade can occur dur-

ing phosphorylation or transport induction, then it is possible that such dysregulation would present itself during dephosphorylation or transport reduction.

Therefore, the second phase of experiments was set up as follows: the cells were grown and exposed to 100 nM insulin as previously detailed. Once the 30 minute insulin stimulation was over, the cells were carefully washed, thrice, with warm PBS, supplemented with 1 mM of $CaCl_2$ and 1 mM of $MgCl_2$. The cells were then left to incubate in warm, supplemented PBS for time points ranging from 0 to 60 minutes whereafter they were either subjected to a 2 second ^{14}Cglucose-uptake assay or harvested for Western blotting.

As one can see in Fig. 5.12, the phosphorylation of the IR dropped by approximately 90% (0.08 ± 0.05 of maximum) in the first sample, taken two minutes, after washing off the insulin. It maintained this low level for the remainder of the experiment. The dephosphorylation of Akt_{S_P} occured somewhat more slowly; after 2 minutes it had only reduced by approximately 40% (0.6 ± 0.1 of maximum). It reached its minimum by the 135 minute mark (0.06 ± 0.028 of maximum) which it then maintained for the duration of the experiment (Fig. 5.12, red). The IR therefore dephosphorylates faster than it phosphorylates.

The changes in glucose transporter activity in response to the removal of insulin were also assayed. Upon removing insulin from the cells, the glucose import activity decreased rapidly from its maximum steadily until it returned to basal levels 60 minutes after the insulin was removed (Fig. 5.11). The glucose transport dynamics, particularly the endocytosis of GLUT4, are thereby slower than the IR and Akt phosphorylation dynamics.

The steady-state analysis in Section 5.2 yielded the ratios of the phosphorylation and dephosphorylation constants for the IR and Akt molecules as well for as the endo- and exocytosis constants for glucose transporters (shown in Table 5.1). The dynamic data for the 100 nM insulin exposure were used to fit the individual rate constants. The values were constrained so as to be consistent with the ratios that had been determined during the dose-response experiments. Owing to the rapid phosphorylation of the IR (Fig. 5.9a), it was not possible to estimate an upper bound for k_{pIR}, which was therefore
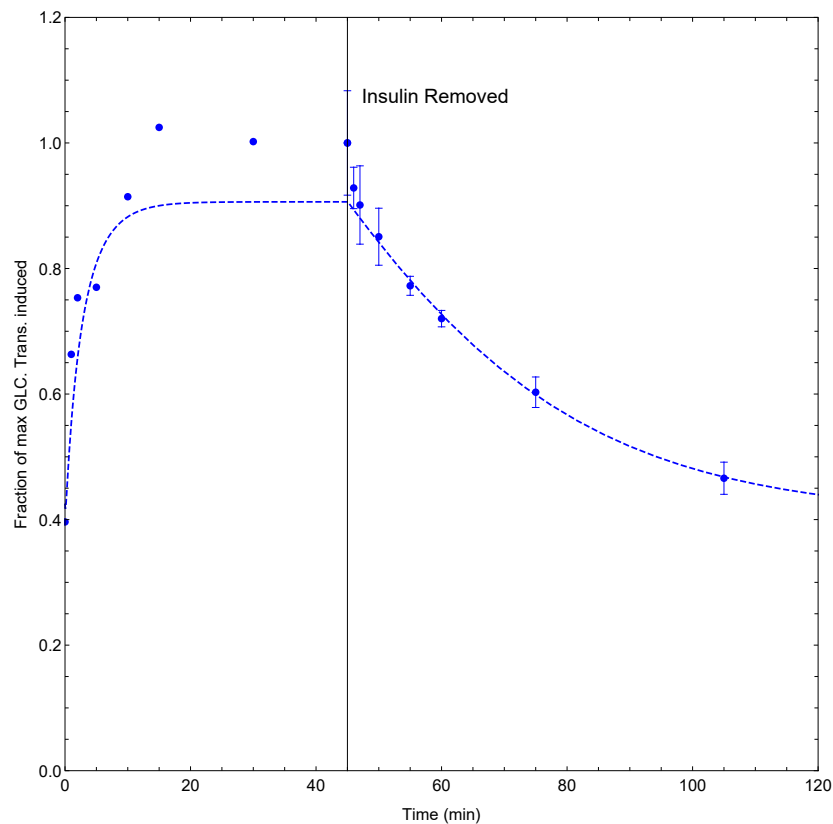
Figure 5.11: After the removal of insulin at 45 minutes, glucose transporter activity steadily decreases over time until it reaches basal levels at 60 minutes. The increase in glucose transporter activity in response to insulin stimulation occurs within the first 15 minutes of the experiment. However, the reduction in transporter activity requires nearly 60 minutes after insulin has been removed in order to return to basal levels. The C2C12 cells were exposed to 100 nM insulin varying time points and after 45 minutes, the insulin was removed. At each timepoint, the cells underwent a ^{14}C glucose assay to determine their insulin-stimulated glucose transport rate. Error bars indicate SEMs and each data point represents a biological triplicate (n = 3).

fixed at an arbitrary value of 10.

Equations 5.1, 5.2, and 5.11 were fit to the available data. These fits determined the 'off'/'on' ratios shown in Table 5.1. The ratio for Akt_T was constrained to a value of 10 since this was the lowest value at which no change in the fit of the curve was observed. These ratios were used to parameterise the model and obtain steady state solutions for the phosphorylation and dephosphorylation of the IR and Akt_S (Fig. 5.12). The same ratio values were used for the 100 nM and 1 nM simulations (Fig. 5.12 red and orange respectively). The model was also able to adequately simulate the behaviour of the glucose transporter in response to the addition or removal of insulin.

95
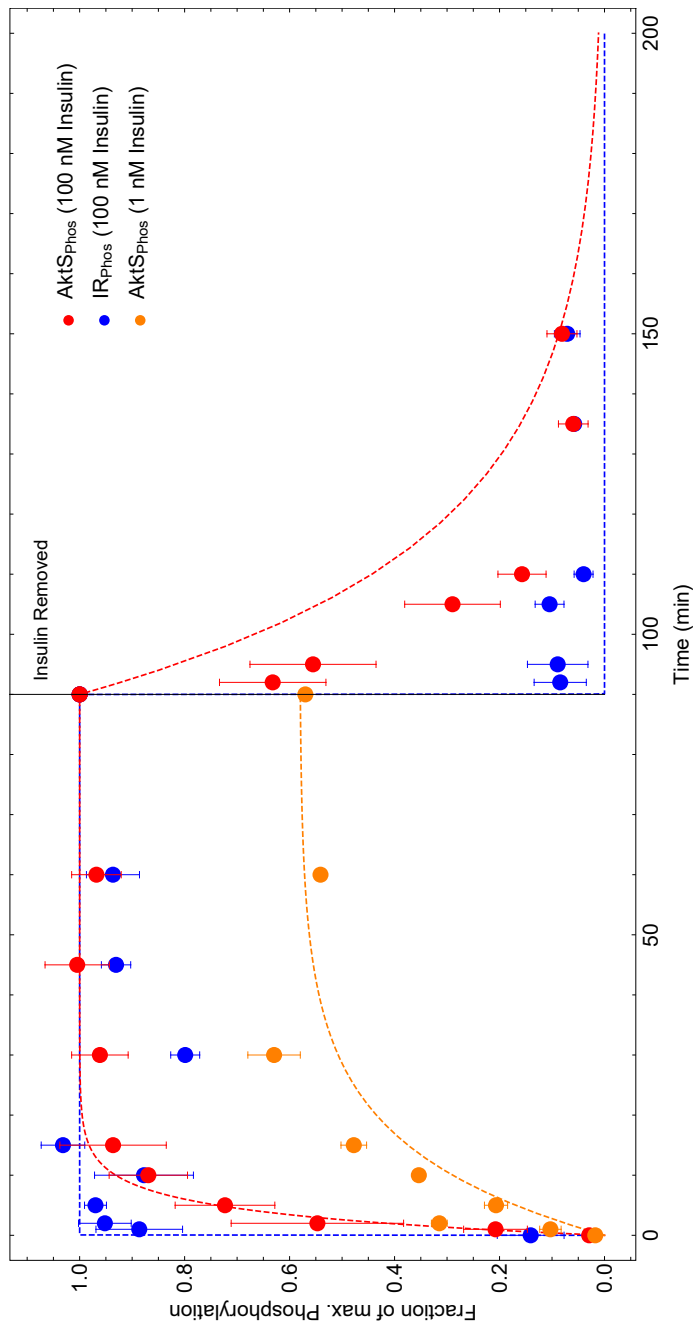
Figure 5.12: The model fits (dashed lines) combined with the experimental data (solid circles) are shown here. Akt serine phosphorylation and dephosphorylation at 100 nM insulin (red) occur much slower than that of the IR at 100 nM insulin (blue) which appears to have an almost 'instantaneous' on/off switching. This may, of course, be due to the limitations in sampling and it is likely that with more granular data, the IR behaviour would appear less step-wise. Lastly, the model was able to accurately simulate the phosphorylation of Akt serine at 1 nM insulin (orange). The C2C12 cells were exposed to 100 nM insulin varying time points and after 45 minutes, the insulin was removed. At each timepoint, the cells were harvested and subjected to Western blotting in order to determine their relative phosphorylation states. Error bars indicate SEMs and each data point represents a biological triplicate ($n = 3$).

This model integrates data from modules one and two of the 'three module' approach which is described in Section 1.1. It is therefore possible use this model to simulate the phosphorylation of the insulin signalling cascade (module one) and the activation of glucose transporter activity (module two) in response to both insulin concentration and time.

5.4 Inducing Insulin Resistance *in vitro*: A Proof of Concept

The idea that persistent insulinemia and hyperglycemia might lead to insulin-resistant states was first explored in Chapter 4 where such culturing conditions led to an abbrogation of insulin induction of glucose flux. The link between over-exposure to insulin and high circulating glucose concentrations on the one hand and insulin resistance on the other is further supported by literature [371, 372]. This section therefore presents a *preliminary* exploration of insulin signalling and glucose transport behaviour under culturing conditions that were designed to mimic insulin resistance.

In order to examine a *pseudo* insulin resistant state to compare against the reference state of insulin signalling, the cells were grown and differentiated in either 'high' glucose (25 mM) or 'medium' glucose (15 mM) conditions with perpetual exposure to 1 nM insulin. The cells were grown under these two glycaemic conditions in order to assess whether the media glucose concentration had any effect on the insulin sensitivity of the cells. Similarly, the addition of 1 nM of insulin to the growth medium was to simulate perpetual hyperinsulinaemia and consequently to examine whether this would induce an insulin resistant state.

Subsequently, the cells were starved as before (see Chapter 3) and then stimulated with 100 nM insulin and either 5 mM (reference condition) or 25 mM (experimental condition) glucose in order to assess the phosphorylation behaviour of the IR and Akt. Cells that had been grown at 15 mM glucose and without perpetual insulin were used as controls - in other words, these cells yield the reference state of insulin signalling. The phosphorylation levels of the IR or the Akt serine site after 30 minutes of exposure
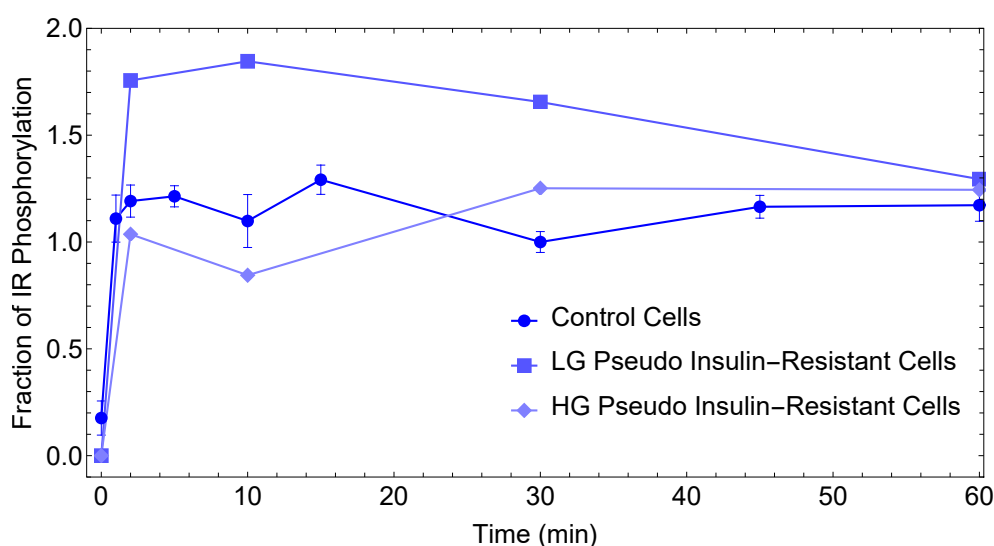
Figure 5.13: The kinetic behaviour of IR phosphorylation in response to 100 nM insulin, under 5 mM glucose and insulin resistant conditions (squares), 25 mM glucose and insulin resistant conditions (diamonds), and under control conditions (circles). Control cells (circles) were grown and differentiated as described in Section 3.2.2. Cells that were challenged with 5 mM glucose and 100 nM insulin (squares) were grown and differentiated at 15 mM glucose, 10% v/v FBS, and 1 nM insulin. Cells that were challenged with 25 mM glucose and 100 nM insulin (diamonds) were grown and differentiated at 25 mM glucose, 10% v/v FBS, and 1 nM insulin. At each time point, the cells were harvested and subjected to Western blotting in order to determine their relative phosphorylation state. The experimental conditions reflect data from a single experiment.

of these cells to 100 nM insulin were set to 1 (see Fig. 5.13, Fig. 5.14, and Fig. 5.15). This value was used to normalise all other results and will serve as the reference value for IR and Akt phosphorylation. The dynamic phosphorylation results of the insulin-resistant cells were normalised to and expressed as a fraction of the reference value. In order to control experimental error, the samples for each were loaded on the same gel and at the same total protein concentration.

The first set of experiments assessed the phosphorylation of the IR and Akt in *pseudo* insulin resistant cells by stimulating the cells with 100 nM of insulin and either 5 mM or 25 mM of glucose. Under both glucose conditions, the IR phosphorylated in a similar manner to the control cells. The cells cultured under low-glucose insulin-resistant conditions (Fig. 5.13, squares) perhaps even hyperphosphorylating (to 1.5-fold of control) within the first 10 minutes. Under hyperglycaemic conditions, the IR in pseudo-insulin resistant cells exhibited phosphorylation dynamics similar to those
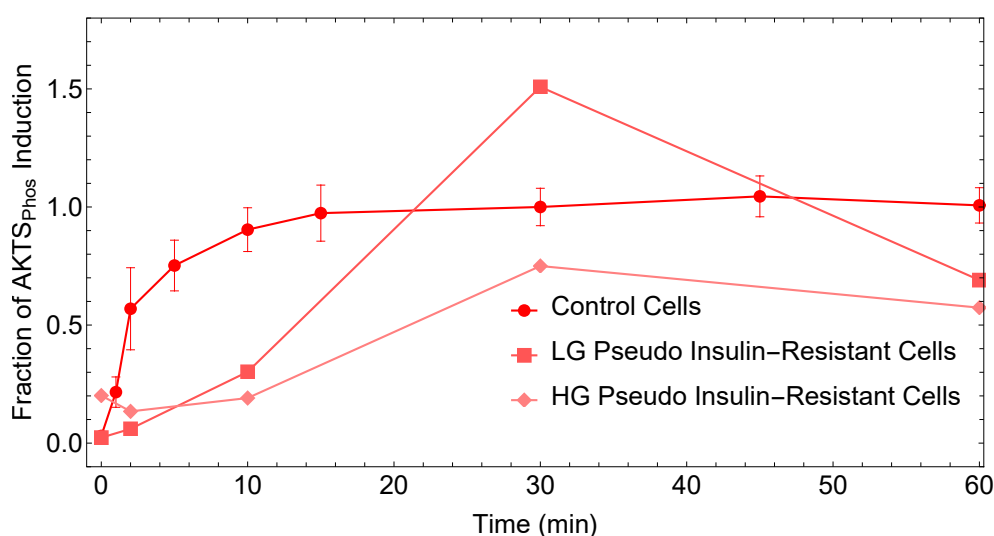
Figure 5.14: The phosphorylation of Akt_{S_P} in pseudo insulin-resistant cells after 100 nM insulin exposure. Control cells (circles) were grown and differentiated as described in Section 3.2.2. Cells that were challenged with 5 mM glucose and 100 nM insulin (squares) were grown and differentiated at 15 mM glucose, 10% v/v FBS, and 1 nM insulin. Cells that were challenged with 25 mM glucose and 100 nM insulin (diamonds) were grown and differentiated at 25 mM glucose, 10% v/v FBS, and 1 nM insulin. Both insulin resistant states showed altered dynamic behaviour of Akt_{S_P} phosphorylation with a peak occurring at 30 minutes, and a final phosphorylation state between 60 and 70% of control. At each time point, the cells were harvested and subjected to Western blotting in order to determine their relative phosphorylation state. The experimental conditions reflect data from a single experiment.

of the reference state (Fig. 5.13, diamonds).

Similarly, in cells grown with low glucose and 1nM insulin, Akt_{S_P} appears to hyperphosphorylate after 30 minutes to nearly 1.5-fold of normal induction (Fig. 5.14, squares), after which it returned to consistent below-reference ranges of phosphorylation (0.66 to 0.72-fold of reference) for the duration of the experiment. However, given the trend of the remaining data as well as the data from those cells cultured under high glucose insulin-resistant conditions, it is likely that this is an outlier.

The phosphorylation of Akt_{S_P} in cells that had been exposed to 25 mM glucose *and* persistent 1nM insulin (Fig. 5.14, diamonds), also achieved its maximum phosphorylation after 30 minutes, however the peak was substantially subdued when compared to the dynamic behaviour of control cells (Fig. 5.14, circles) and low glucose, insulin resistant cells (Fig. 5.14, squares).

The phosphorylation of Akt_{T_P} was significantly diminished in cells which had been
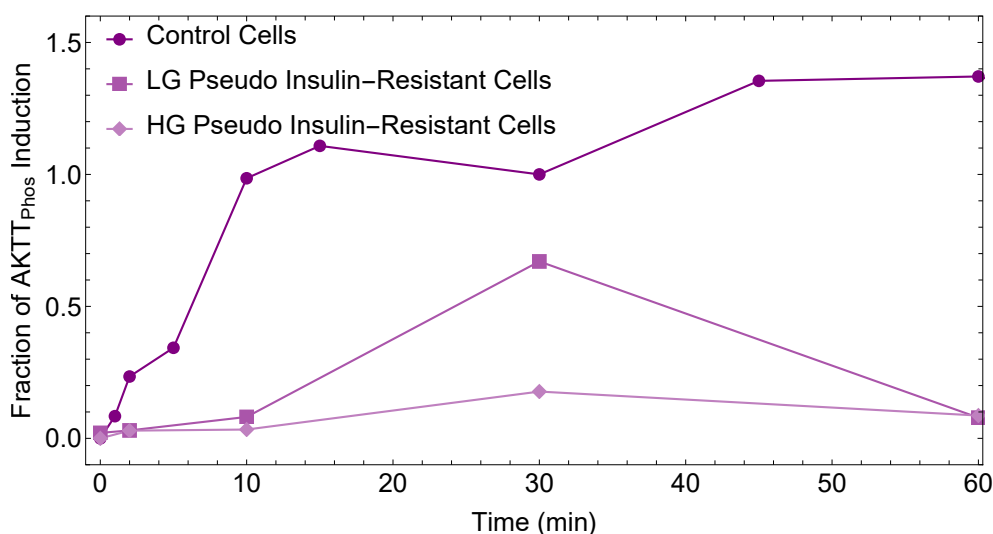
Figure 5.15: The phosphorylation dynamics of Akt_{T_P} under control (circles), low glucose pseudo insulin-resistant (squares), and high glucose pseudo insulin-resistant (diamonds), states. Control cells (circles) were grown and differentiated as described in Section 3.2.2. Cells that were challenged with 5 mM glucose and 100 nM insulin (squares) were grown and differentiated at 15 mM glucose, 10% v/v FBS, and 1 nM insulin. Cells that were challenged with 25 mM glucose and 100 nM insulin (diamonds) were grown and differentiated at 25 mM glucose, 10% v/v FBS, and 1 nM insulin. At each time point, the cells were harvested and subjected to Western blotting in order to determine their relative phosphorylation state. The experimental conditions reflect data from a single experiment.

incubated in the presence of insulin. Hyper- and normo-glycaemic states showed a marked reduction in phosphorylation (Fig. 5.15, squares and diamonds respectively). After 60 minutes, neither insulin-resistant condition were able to maintain much of a phosphorylated state. This is in stark contrast with the normal Akt_{T_P} signalling which was able to maintain maximal posphorylation for at least 60 minutes (Fig. 5.15, circles). However, given that these experiments which explore the signalling cascade have yet to be repeated, it is not possible to draw any strong inferences from these data.

The behaviour of the glucose transporter under insulin resistant states was determined. First, the cells were grown under insulin resistant and 15 mM or 25 mM glucose states and then they were exposed to 100 nM insulin and low (5 mM) or high (25 mM) glucose for 30 minutes before undergoing a ^{14}C glucose-uptake assay. These results are shown in Fig. 5.16. Both the high and low glucose experiments showed some induction in glucose transporter activity, however neither achieved the 2-fold induction
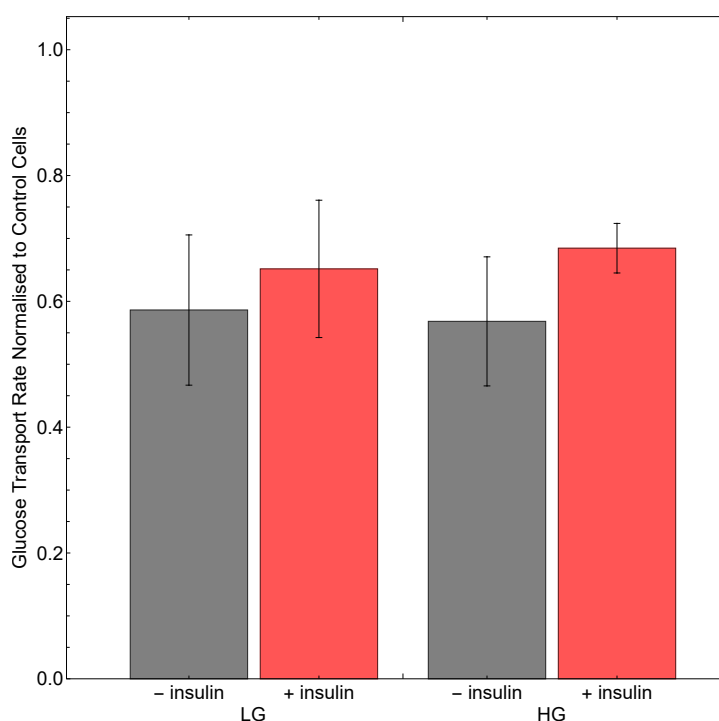
Figure 5.16: The fraction of total glucose transport rate in high (red) and low (grey) glucose insulin resistant cells. After the cells were exposed to 100 nM insulin for 30 minutes, they were subjected to a ^{14}C glucose uptake assay in order to determine their glucose transporter activity. The initial glucose transporter activity (before the addition of insulin) are elevated above normal (0.4) for both glycemic conditions. However, their induction response of glucose transport is severely impaired, with only minor increases in glucose transport being recorded in response to insulin induction. Error bars indicate SEMs and each experiment represents a biological triplicate (n = 3).

thereof as one sees with control cells.

Based on the results in Fig. 5.16, the next experiments explored the time dynamics of the glucose transporter activity when exposed to 100 nM insulin and either 5 mM or 25 mM of glucose. The cells for the 'low glucose' experiments were cultured at 15 mM of glucose, 10% v/v FBS, and 1 nM of insulin until fully differentiated upon which they were washed with $37°$CPBS (inclusive of 1 mM of both $CaCl_2$ and $MgCl_2$). Thereafter the cells were challenged with 5 mM of glucose and 100 nM of insulin. Conversely, the cells for the 'high glucose' experiments were cultured at 25 mM of glucose, 10% v/v FBS, and 1 nM of insulin until fully differentiated whereupon they were washed with $37°$CPBS (inclusive of 1 mM of both $CaCl_2$ and $MgCl_2$). The cells were then challenged with 25 mM of glucose and 100 nM of insulin.
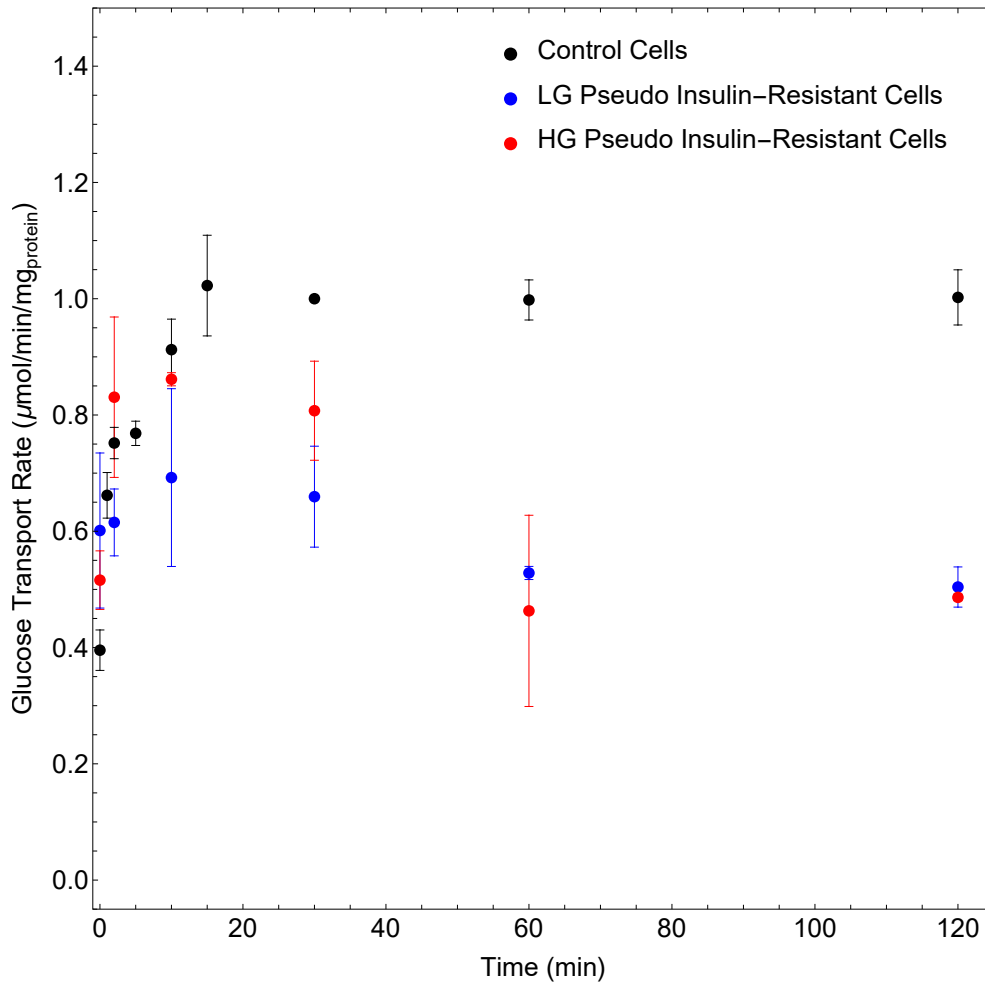
Figure 5.17: The glucose transport dynamics in pseudo insulin resistant cells which were challenged with 100 nM of insulin and either 5 mM of glucose (blue) or 25 mM of glucose (red) after which they underwent a ^{14}C glucose uptake assay to determine their glucose transporter activity. The cells in blue were grown and differentiated at 15 mM of glucose, 10% v/v/ FBS, and 1 nM of insulin whereas the cells in red had their glucose concentration increased to 25 mM. Control cells are shown in black. Error bars indicate SEMs and all data points represent three biological repeats (n = 3).
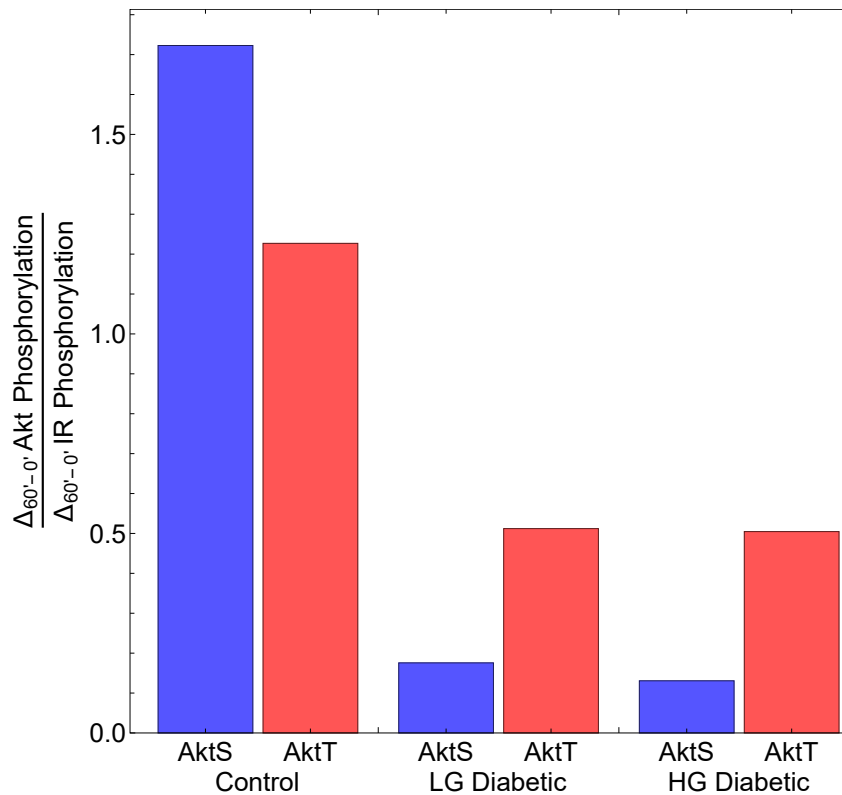
Figure 5.18: The ratios of the 60 minute changes in Akt_S (blue) and Akt_T (red) phosphorlation to IR phosphorylation, in control, low glucose (LG) diabetic, and high glucose (HG) diabetic cells. The change across 0 and 60 minutes was chosen as it spans a period before insulin was added to after the glucose transporter activity and Akt phosphorylation had stabilised.

The initial glucose transporter activity (before the addition of 100 nM insulin), for both the high and low glucose insulin resistant cells was elevated when compared to the control cells (Fig. 5.17 red, blue, and black, respectively). However, unlike the control cells, the insulin resistant cells are unable to respond to insulin by upregulating glucose import to the degree ($\pm$ 2-fold) that was established in Section 5.3). The glucose transporter induction in insulin resistant cells is also more temporary than that of control cells. Glucose transporter activity remains induced for at least two hours in control cells whereas insulin resistant cells appear to lose their glucose induction after 20 to 30 minutes.

Once the preliminary data were collected, the next was to determine with which module the error lay. In order to to this, the ratios of the changes (from 0 to 60 minutes) in Akt phosphorylation to IR phosphorylation and glucose transporter activity to Akt phosphorylation were graphed as seen in Figs. 5.18 and 5.19. This does bear the risk that incredibly small changes in the independent variable (i.e. the denominator) can bias the ratios. However, in Figs. 5.14, 5.15, and 5.17 one can see that Akt phosphorylation and the induction of glucose transporter activity changes from the 0 to 60 minute point are both low. Therefore, since both Akt and glucose transporter activity are significantly diminished and display similarly small changes, such ratios can be useful when determining which of these modules respond differently to the control values.

Larger ratios indicate that the independent variable is more sensitive to the dependent variable whereas smaller values indicate a loss of sensitivity to the independent variable. In other words, in Fig. 5.18 one can see that the ratio of IR_P to Akt_{S_P} is 1.7. This indicates that Akt_{S_P} increases at disproportionately higher levels in response to IR phosphorylation. Similarly, in the pseudo insulin-resistant condition, the phosphorylation of Akt_S is seemingly nearly entirely diminished. The levels of Akt_{T_P} are reduced as well, although not as strongly as the Akt_{S_P} levels.

In Fig. 5.19 one can see that glucose transporter activity is moderately sensitive to Akt_{S_P} and Akt_{T_P}. However, in the pseudo insulin-resistant cells, there is a marked reduction in glucose transporter sensitivity to Akt_{S_P} whereas the sensitivity to Akt_{T_P} remains unchanged, with perhaps a slightly reduced sensitivity to Akt_{T_P} in pseudo insulin-resistant cells cultured under high glucose conditions.

This does not mean that glucose transporter activity has become uncoupled from Akt phosphorylation. Rather, taking the data in Figures 5.14, 5.15, and 5.17 into account, one can see that under pseudo insulin-resistant conditions, glucose transporter activity is significantly diminished. Akt phosphorylation at the 60 minute mark is similarly reduced whereas there appears to be no significant change in IR phosphorylation at the same timepoint (Fig. 5.13).

Additionally, with Fig. 5.18 these data implicate the signalling module as the com-
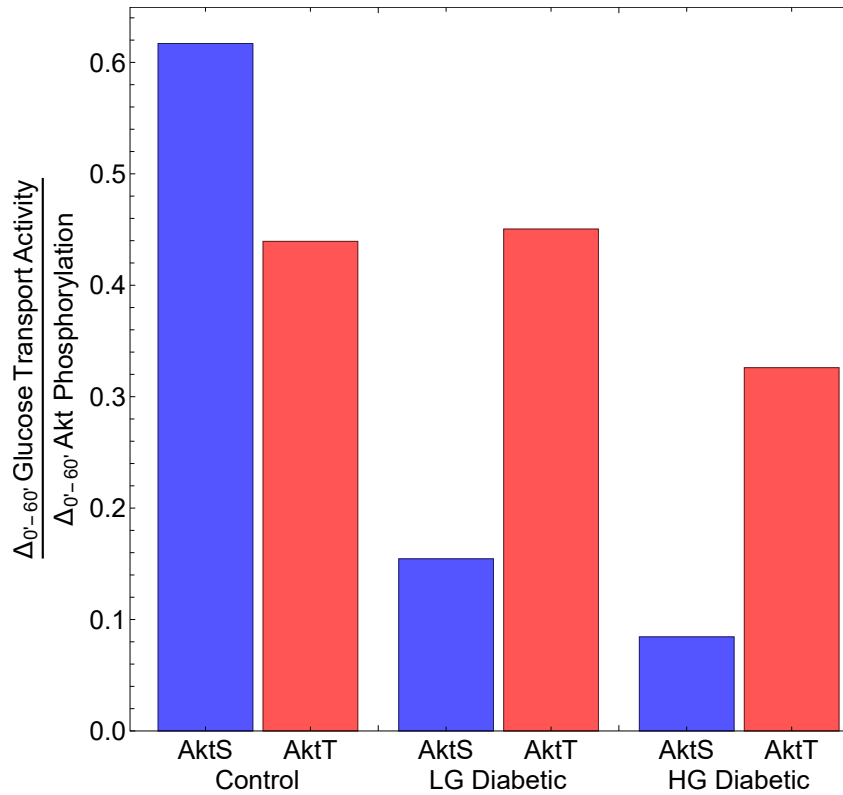
Figure 5.19: The ratios of the 60 minute changes in glucose transporter activity to Akt_{S_P} (red) and Akt_{T_P} (purple) in control, low glucose (LG) diabetic, and high glucose (HG) diabetic cells. The change across 0 and 60 minutes was chosen as it spans a period before insulin was added to after the glucose transporter activity and Akt phosphorylation had stabilised.

ponent responsible for reduced glucose transporter activity in pseudo insulin-resistant cells. More specifically, the fault could be within one of the intermediates between IR and Akt since the signal from IR to Akt is already diminished. This would lead to a lower output of the signalling module - in other words, lower Akt phosphorylation which in turn impacts glucose transporter activity as seen in Fig. 5.19. However, despite these initial results, more conclusive data is required before these data can be used for reliable model simulations.

5.5 Discussion

The insulin receptor and Akt proteins both phosphorylate in response to stimulation by insulin (Section 5.2). The Akt_S site responds more strongly at lower concentrations of insulin than the insulin receptor does. At an insulin concentration of 10 pM, the Akt serine site is already phosphorylated to 25% of its maximum value (Fig. 5.2) whereas the insulin receptor only achieves approximately 5% of its maximum phosphorylation (Fig. 5.1). Similarly, at insulin concentrations of 1 nM, 10 nM, 20 nM, and 50 nM, Akt_S is consistently phosphorylated to a greater degree of its maximum than the IR is.

However, in reality, Akt does not directly phosphorylate in response to insulin since these molecules do not interact. Rather, Akt is phosphorylated by upstream agents such as MTORC1/2 or PDK1. In this study, the insulin receptor is used as a proxy for these intermediates. While not entirely accurate, these data indicate that relatively small increases in the degree of phosphorylation of the IR are amplified downstream and ultimately lead to a stronger response from molecules such as Akt. This is further evidenced by phosphorylation of the Akt_T site (Fig. 5.3). While this site does not appear to detectably phosphorylate at insulin concentrations under 20 nM, it does seem to have significant capacity for phosphorylation at insulin concentrations beyond 100 nM. While the IR and Akt_S sites both exhibit slight decreases in phosphorylation, the Akt_T site phosphorylates to between two and three times its control value. This possibly indicates that the phosphorylation of Akt_T could be a mechanism by which the cell attempts to regulate extreme hyperinsulinemia and hyperglycaemia. It is also likely that this could be a mechanism through which the cell seeks to compensate for the apparent desensitising of the IR and Akt_S at extremely high concentrations of insulin.

The glucose transporter reacts to concentration increases of insulin in a similar, dose-dependent manner as the phosphorylation of the IR and Akt proteins (Fig. 5.6). However, much like Akt does not react directly to insulin, neither does the glucose transporter. The glucose transporter will react to increases in upstream intermediaries (notably AS160) for which the Akt will serve as a proxy. With this in mind, the response of the glucose transporter activity to Akt phosphorylation is shown in Fig. 5.7.

Since Akt_S and Akt_T may be responsible for the activation of glucose transporter translocation, the combined effect of these phosphorylated sites is shown in addition to their singular effects. It appears that the combined impact of Akt_S and Akt_T phosphorylation closely resembles that of Akt_T on its own. This possibly indicates that Akt_T is a stronger determinant of glucose transporter induction - especially at greater insulin concentrations - than Akt_S phosphorylation.

The full phosphorylation and dephosphorylation of the IR occur rapidly - within one minute of either adding or removing the insulin (Fig. 5.12). The Akt protein however phosphorylates and dephosphorylates much slower, requiring at least 15 minutes to fully phosphorylate and nearly an hour to dephosphorylate. These dynamics are mirrored by the induction and reduction of glucose transporter activity (Fig. 5.11). This may indicate that the IR is more sensitive to *in situ* oscillations in insulin concentration. Should the IR be too strongly induced or induced for too long, this may over-activate glucose transporter activity with respect to the metabolic demands or available glucose at that time. Therefore, given the 'amplification' of the IR phosphorylation on to the Akt phosphorylation, it is likely that the rapid 'on-off' dynamics of the IR are a mechanism by which the Akt-dependent pathways and glucose transporter activities are regulated.

The data from the insulin dose-dependent experiments were used to estimate the steady-state parameters of the forward and reverse reactions which constituted the ODEs. These steady-state parameters were used as model constraints in order to simulate the time dynamic phosphorylation and dephosphorylation of the signalling module components as well as the induction and reduction of glucose transporter activity. The goal at the outset of this chapter (Section 5.1) was to develop a minimal mathematical model which is able to simulate the phosphorylation and glucose transporter activity dynamics of the insulin signalling and glucose transporter modules. This approach, by its nature, is limited in that it does not account for the significant complexity and numerous parameters that the entire insulin signalling system would contain.

However, the model was able to produce predictions for the 'on-off' behaviour of the insulin signalling and glucose transporter modules. In contrast to the complex-

ity of models such as those of Sedaghat [292] or Brännmark et al [315], this model can provide insight into the signalling and glucose transporter modules by perturbing one or two carefully selected molecules and examining the systemic behaviour of the signalling cascade. The fits generated herein are not the best-possible fits for such a system, but they offer an experimentally and computationally straightforward method by which one can assess the functioning of each module.

The pseudo insulin-resistant cells the phosphorylation responses of the IR, Akt_S and Akt_T upon insulin induction in pseudo insulin-resistant cells were compared with those of control cells. For the IR there was no significant difference, or even a small increase in the phosphorylation, while both the Akt_S and particularly the Akt_T seemed to have a lower induction level then the control cells. However, it does appear as if those cells grown with 25 mM have a consistently lower degree of phosphorylation than cells grown with 15 mM glucose.

The effect of insulin resistance on glucose transporter activity is shown in Figs. 5.16 and 5.17. In Fig. 5.16, the pseudo insulin-resistant cells indicated an inability to induce glucose transport activity in response to 100 nM insulin. Similarly, the dynamic induction of glucose transporter activity in insulin resistant cells differed significantly from control cells (Fig. 5.17). While glucose transporter activity can be induced with 100 nM insulin, it does not achieve the expected two-fold induction, nor are insulin resistant cells able to maintain this induction of glucose transport activity for as long as control cells.

Chapter 6

Insulin Induced GLUT4 Clustering

6.1   Introduction

In mature, insulin-sensitive tissues, GLUT4 is the primary insulin-responsive glucose transporter [182]. The exposure of skeletal muscle or adipose tissue to insulin results in the translocation of GLUT4-containing vesicles such as endosomes or, the more specialised, GLUT4 storage vesicles (GSVs), from the perinuclear and perimembrane spaces to the plasma membrane (PM) [31]. Exposure to insulin also alters the dynamics of GLUT4 endo- and exocytosis. Typically, when the cells are at rest, there is a slow, yet persistent recycling of GLUT4 between the endosomes and the plasma membrane [201]. This 'recycling' - rate by which GLUT4 enters and exits the PM - increases by as much as 60-fold whereas the retention of GLUT4 in the PM can increase by as much as ten-fold in response to insulin [201, 373, 374]. However, since evidence suggests that the translocation of GLUT4 and its activation are distinct processes, an increase in GLUT4 at the PM does not imply an increase in glucose import [375]. In support of this, experiments by Ishiki *et al* (2005) showed that while either $PI(3,4,5)P_3$ and PI3P are sufficient for the mobilisation of GLUT4 to the membrane, the former mediates fusion *without* activation whereas the latter mediates activation, but not fusion with the PM [108].

Under *basal* conditions, GSVs are localised to the apex of the perinuclear space and are thereby found in relatively dense clusters [108, 376]. Due to the rapid decay

or degradation of solitary GLUT4 molecules, it is mostly distributed among larger endosomes, smaller GSVs, and the *trans*-Golgi network [377–379]. The balance of this distribution shifts from a mostly-endosome to a mostly GSV distribution as the cells mature and differentiate [380]. The location of these vesicles coincides with the the microtubule organising center (MTOC) [374, 381]. This centrosomal structure forms a hub where actin and tubulin filaments attach to and nucleate from [382].

The translocation of GSVs to the PM has been shown to co-localise with microtubules in undifferentiated cells [374]. Here a problem is that many studies that rely on fluorescent microscopy to reach these conclusions are unable to differentiate between GSVs that are *near* the membrane and those that are *within* the membrane. While the cytoskeleton may not be necessary for the translocation of GSVs, it may play an important role in the direction or targeting of GSVs to specific sites on the PM [374].

This question - whether MTs aid in the directing of GSVs - was explored by Stenkula *et al* (2010). They found that the distribution of GLUT4 in response to insulin (70 nM, 30 min), was inhomogenous and organised in clusters along the plasma membrane [373]. Later work by Dawicki-McKenna et al (2012) showed that such clusters occur near the membrane-associated ends of microtubules [374]. Lastly, superresolution microscopy of 3T3-L1 adipocytes indicated that exposure to insulin results in more, but smaller clusters distributed along the PM [202].

6.1.1 Clustering Methods: An Overview

While no strict definition of a 'cluster' has been agreed on, a cluster - or set thereof - can be identified by at least three features [383]. Firstly, data *within* a cluster should be as similar as possible. In practical terms, for this study, this similarity was determined by calculating the euclidean distances between each point and every other point, the distances between each point and the cell nucleus, and the variances across those distances. The second feature suggests that data in *different* clusters should be as different as possible. For any cluster this was assured by excluding data that was displaced from the centre of the emerging cluster by more than three times the mean euclidean distance of the points already in the emerging cluster. The third feature requires that the simi-

larity and dissimilarity measures are explicit and transparent and that these measures can be quantified and implemented computationally [383].

Three clustering methods were considered for the analysis of the data: *K*-means methods, density-based methods, and hierarchical methods. *K*-means clustering was an initial candidate due to its lower computational intensity and time-dependence [384]. However, this type of clustering requires foreknowledge of the numbers of clusters one wishes to find [385]. *K*-means methods are useful for partitioning data according to a specific aim or design. Since the data in this study provided no indication as to the number of clusters one expected to find and in an effort to avoid bias, *K*-means, and partitioning methods in general, were put aside.

Density-based algorithms such as DBSCAN were considered as they rely on nearest-neighbour density of data points [386]. The data generated in Section 6.3 appeared sufficiently densely populated to warrant density-based clustering. However, density-based methods suffer when presented with data of highly uneven densities [383]. This meant that data with punctate clusters dispersed across an arbitrary space might compromise the algorithm. Additionally, such methods are computationally intensive [387].

Hierarchical clustering methods were selected by relating the data back to a biological context. Current theory holds that GLUT4 not at the PM is primarily found in GSVs and endosomes. These vesicles are, in turn, co-located around the MTOC in the perinuclear region [388]. Therefore, GLUT4 is already present in a 'cluster of clusters'. Bottom up hierarchical clustering methods assume that each individual data point is a cluster [389]. The algorithm then seeks to merge clusters based on the distances between each cluster and the density within each cluster until a minimum number of clusters has been achieved.

6.1.2 Motivation and Aim

The data generated by overexpressing a GLUT4-GFP construct in C2C12 cells, staining the nucleus and membrane, and confocal microscopy were kindly used by Prof. J. L. Snoep of Stellenbosch University to generate the images in Fig. 6.1. In these

images, one can see that in the pre-insulinic cells, the GFP signal is located in the perinuclear region (Fig. 6.1a). More specifically, it is concentrated to one apex of the nucleus. It is likely that this is where the MTOC is located, since GSVs are known to concentrate here [374]. Conversely, in the post-insulinic cell, the GFP signal is more distributed throughout the cell (Fig. 6.1b).

These observations led to the development of two aims: firstly, to investigate whether clustering analyses can be applied to the types of images and data generated from the imaging studies. Secondly, to examine whether such analyses could lead to novel, meaningful insights into the clustering behaviour of GLUT4 between pre- and post-insulinic C2C12 myoblasts.

In order to fulfil the demands of the first aim one would need to know whether there are differences in the number of clusters between the pre- and post-insulinic cells and whether the number of GFP signals (pixels) had an impact on the number of clusters that were identified. Once these questions are answered, focus shall shift on to the second aim where the following questions may be addressed:

1. Are the differences in cluster quantity between the different insulinic conditions a real phenomenon or due to chance?

2. Do the post-insulinic clusters differ from the pre-insulinic clusters with regards to the number of pixels they contain?

3. Is there a difference in the proportion of pixels that are assigned to clusters between the insulinic conditions? This would establish whether insulin has an effect on the dispersion of pixels throughout a cell.

4. If insulin has a dispersive effect on the GFP-tagged GLUT4, can this be determined both on a cluster and on an individual pixel level? In other words, are clusters and pixels in post-insulinic cells more distant from the perinuclear space than in post-insulinic cells?

5. What are the differences in cluster densities between pre- and post-insulinic cells?

(a)

(b)
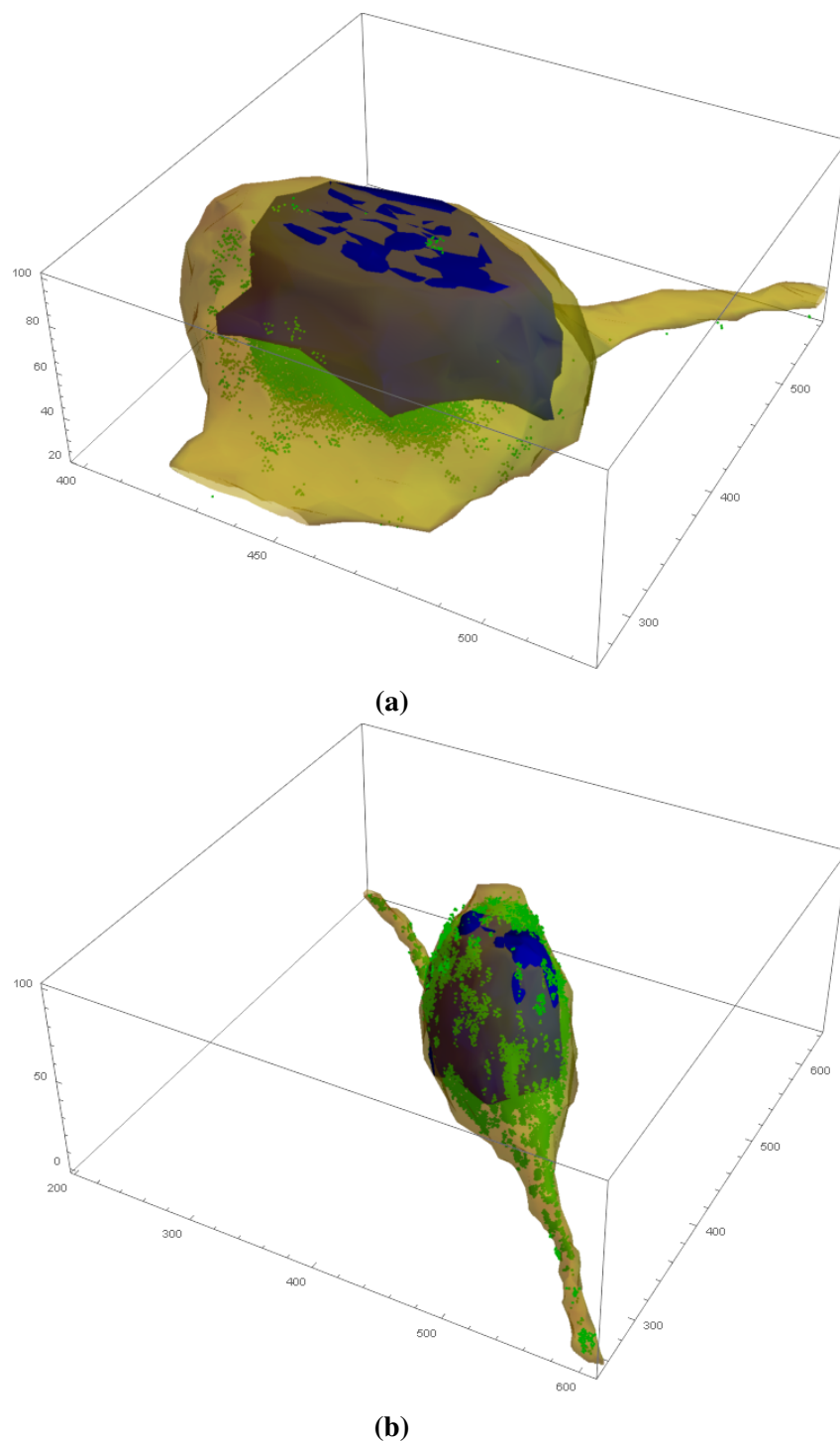
Figure 6.1: Three-dimensional reconstructions of pre-insulinic (Fig. 6.1a) and post-insulinic (Fig. 6.1b) cells from GLUT4-GFP, Hoechst stain, and membrane-staining data. The GLUT4-GFP signal is shown in green whereas the nucleus and membrane are shown in blue and yellow respectively. The pre-insulinic cell (Fig. 6.1a) has dimensions of $160 \times 280 \times 90$ pixels which corresponds to a length of 21 μm, a breadth of 37 μm, and a height of 12 μm. Similarly, the post-insulinic cell (Fig. 6.1b) has dimensions of $410 \times 360 \times 90$ pixels which corresponds to a length of 54 μm, a breadth of 47 μm, and a height of 12 μm.

6.2 Methods

The C2C12 myoblasts were transfected as discussed in Chapter 3. Images were acquired as described in Chapter 3. Myoblasts were used for these experiments since the plasmid was rejected during differentiation and myofibers did not transform. Two sets of images were acquired: those representing a pre-insulinic state, and those representing a post-insulinic state. The images were pre-processed in the FiJi implementation of ImageJ. The .lsm files were separated into individual .tiff files according to colour channel and Z-position. Further, the background for each image was subtracted with the 'Rolling Ball' method. The images were then imported into Mathematica where they were deconvoluted using Mathematica's 'ImageDeconvolve' function. The images were then manually examined and a rectangular border was drawn around each cell. All further analyses occurred within these pre-determined boundaries.

For the purposes of these analyses, the pixel intensity values were used. Mathematica was tasked with finding the 2-dimensional coordinates of every green pixel in every image for every cell. This was performed for various intensities of green. The software categorised these intensities according to a 'dissimilarity' score where 1 is the most dissimilar to green and a null value is the most similar. For the purpose of this study, values from 0.5 to 0.99 - in other words 50% to 99% - were used.

The dimensions of each pixel were calculated to be 136 nm by 136 nm since each 1024×1024 image was 139.8 μm $\times$ 139.8 μm according to the instrumentation. Similarly, since each Z-slice represented a depth of 690 nm, each slice was calculated to be approximately 5 pixels deep. However, since each image is two-dimensional, the three dimensional position of each pixel had to be estimated. In order to do this, the highest and lowest possible position for a pixel in each Z-stack were estimated. For example, the lowest point for the *first* slice was set to '0' whereas the highest point was set to 5 pixels. Thereafter, within each pixel range for any z-slice, the position of each pixel was assigned a random z value based on Mathematica's 'RandomReal' function and the depth constraint of 5 pixels since the z value was not known for the pixels.

After the 3-dimensional pixel positions were identified, they were fed into a custom algorithm that calculated the number of clusters and defined certain exclusion criteria

by which 'true' clusters were identified. The clustering made use of Mathematica's 'FindClusters' function and it was specified to calculate the Euclidean distances between each pixel in each image. Based on the distances between each pixel in each image, the function then made use of the 'Agglomerate' option which determined the number of clusters based on a hierarchical algorithm.

Hierarchical clustering was appropriate for this problem from a biological viewpoint. GLUT4 is already arranged into 'mini'-clusters of up to 25 molecules per GSV [31]. These GSVs are in turn clustered around the perinuclear space - more specifically, the MTOC [390]. Further, once translocation of the GSVs occurs, they move along the cytoskeleton. Since there are a limited number of cytoskeletal filaments in a cell in relation to the number of GSVs, this will further contribute to clustering of GSVs along the cytoskeleton. This has been observed in [202] who show that, not only do GLUT4 molecules co-locate with the ends of microtubules, the density of GLUT4 decreases significantly with increasing distance from the MTs. This led to the decision that, since GSVs appeared to be organised as clusters within clusters which translocate as clusters, using hierarchical clustering function was appropriate (see Section 6.1.1).

The algorithm was further designed to exclude certain pixels or clusters from the final results based on certain criteria. In both the pre-insulinic and post-insulinic cells, clusters with fewer than the median number of members (3 and 11 respectively) were excluded in order to control for skew in the data. Additionally, due to the inefficient transformation, blebbing, or lysis of some cells it was possible for small quantities of GFP-tagged GLUT4 to present beyond the boundaries of the cell under investigation.

In order to account for these outliers, the Euclidean distances between each pair of pixels were calculated and pixels which were more than three times the mean distance were excluded. Lastly, the logarithm of the total variance of the Euclidean distances between the pixels within a cluster was calculated in order to account for skewed data. This was then normalised to the total number of members of the cluster to serve as a proxy measure for the density of a cluster. Clusters which had a density of three standard deviations from the mean density of the clusters within a cell were excluded from further analysis.

Considering that, at this point, each experimental condition was defined by a set of Z-stacks for each pixel intensity value, the question arose: at which pixel intensity value was the data most significant? Since the data were non-normally distributed, a Mann-Whitney U test was used to compare the numbers of clusters in the pre-insulinic cells with those in post-insulinic cells in order to determine whether the differences in cluster numbers were statistically significant. Similarly, Spearman Rank correlation tests were applied to each set of 3-dimensional points to test whether the number of clusters depended on the number of pixels in a set of images. This was important since the numbers of pixels differed by as much as a factor of three between some images.

The final set of 3-D positions were selected according to *p*-values and the spread of the Euclidean distances within each cluster. The latter was assessed using the variances, standard deviations, mean deviations, and numbers of outliers for each experimental condition and pixel intensity values. Using these 3-dimensional pixel positions as well as their clustering characteristics, Mathematica was asked to discretise these into distinct regions with the 'ConvexHullMesh' function. Thereafter, the center point of each cluster was determined using 'RegionCentroid'. This served a two-fold purpose. Firstly, the Euclidean distances between the centers of each combination of clusters were determined and the total variance among these distances was used as a proxy for the overall dispersion of the clusters. Secondly, the center point of each nucleus was determined by manually defining the nuclear region and using 'ConvexHullMesh' and 'RegionCentroid'. These data were then used together with the center points of each cluster in order to determine whether the Euclidean distances between each cluster and the nucleus had increased in response to insulin.

6.3 Results

The following section discusses the results in two separate phases of analysis. First it was necessary to determine which pixel intensities were suitable for further analysis and then sort these into clusters. These intensities are inverse to how strongly the GFP fluoresced and represent a threshold which excludes pixels above the designated value

(as discussed in Section 6.2). Larger values would therefore include more pixels and lower values would include fewer pixels. The number of pixel positions that are subsequently analysed by the algorithm has an effect on the accuracy of the analyses that are generated. Therefore, before delving into the analyses of the clusters themselves, it is important to ensure that the data are appropriate for such analyses. Secondly, the clusters themselves will be analysed with regards to their density and distribution in order to determine whether there are differences between pre- and post-insulinic cells.

Mathematica was used to determine the clusters by using its integrated 'FindClusters' function. This function made use of the 'Agglomerate' method and evaluated the Euclidean distances between each pixel in order to determine the numbers of clusters. Agglomerative methods are a subset of a hierarchical clustering method that make use of a 'bottom-up' approach. Each cluster begins as a single observation and is then iteratively sorted into ever larger clusters [389]. This method allowed a blind determination of clusters whereas methods based on K-means clustering requires foreknowledge of the numbers of clusters one expected to find and was therefore not used.

6.3.1   Determining the Number of GFP Clusters in C2C12 Myoblasts

Images were captured from two sets of 12 cells that were equally divided among the pre-insulinic and post-insulinic experimental groups. The data generated by the imaging analyses and clustering algorithm were binned as follows: first they were categorised according to pre- or post-insulinic conditions. Thereafter, within each experimental condition, the pixel positions were binned according to the pixel intensity that was used to generate them. These data were then used to generate box plots of the pre- and post-insulinic cells (Figs. 6.2 and 6.3 respectively) which indicate the spread of data, the medians of each set of data, and the number of outliers (five number summaries can be found in Table 6.1). The pre-insulinic cells showed greater variability in the number of clusters as the pixel intensity increased above 75% (Fig. 6.2). The variability in cluster numbers for the post-insulinic cells remained stable for pixel intensities between 70% and 85% (Fig. 6.3). Including too many or too few pixels
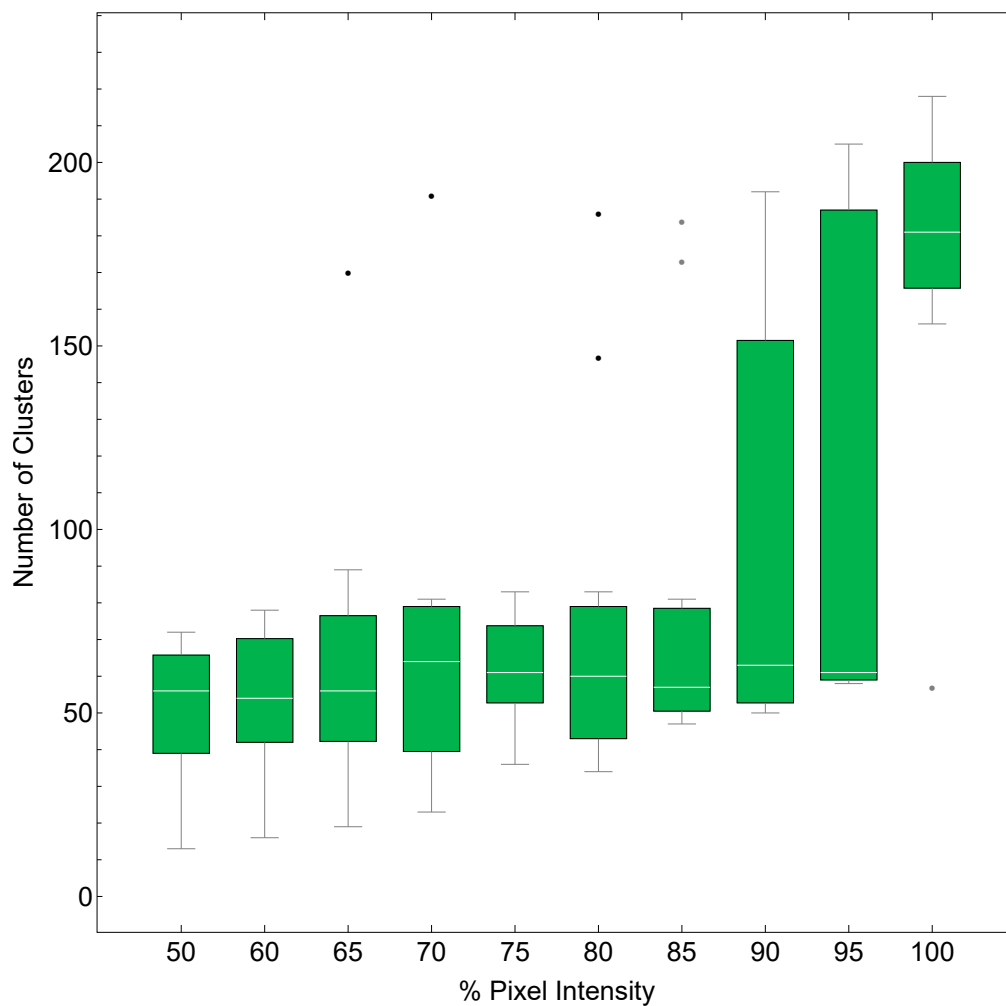
Figure 6.2: Box whisker plots of the clustering data in pre-insulinic cells which indicate the five number summaries of the clustering data: smallest clusters, largest clusters, median number of clusters, and the 25th and 75th quartiles. Pixel intensities above 75% resulted in greater variability in the data. Therefore values of 75% and lower were considered for further analysis. Outliers are presented as gray dots. See Table 6.1 for the relevant five number summaries of these data. These data were gathered from 12 individual cells (n = 12).

resulted in less reliable data. Therefore, taking the variability of all data into account, this limited the range of acceptable pixel intensities to between 65% and 75%.

Barring a single outlier in the pre-insulinic condition at 100% pixel intensity, the median number of clusters that was identified for each experiment and intensity value, remained fairly constant (Figs. 6.2 and 6.3). This further mitigated any impact that the choice of pixel intensity may have had on the number or the distribution shift of the clusters in either experimental condition. Similarly, a disconnect between pixel
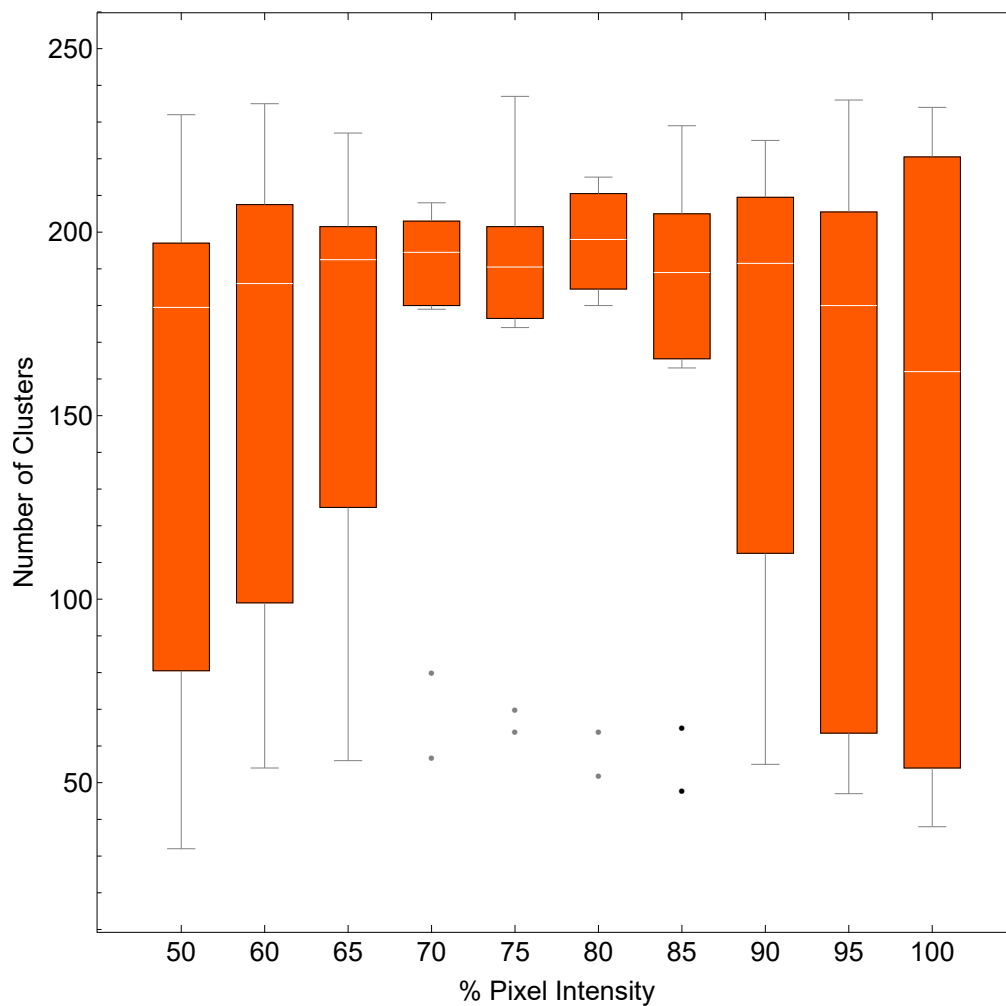
Figure 6.3: The spread of clustering data in post-insulinic cells as visualised using box whisker plots. These pots indicate the five number summaries of the clustering data: smallest clusters, largest clusters, median number of clusters, and the 25th and 75th quartiles. Lower (50 and 60) as well as higher (95 and 100) percent pixel values present with greater variability in the data. Despite this, however, the median values remained relatively constant. Values between 65 and 90% were considered for further analysis. Gray spots represent outliers in the data. The relevant five number summaries of each percent pixel intensity can be found in Table 6.1. These data were gathered from 12 individual cells (n = 12).

intensity and median numbers of clusters further reduced the impact of any bias that could be present in the analysis. The final decision to use the 75% value was based on the observation that this had the fewest outliers (2), compared to the 70% and 65% values (4 and 8 respectively) as seen in Table 6.2.

Since the pixel intensities correlated positively with the number of pixels that were ultimately analysed, the need arose to investigate whether pixel intensities correlated

Table 6.1: The five number summaries which contain the: Q_1 (25th and 75th percentile respectively), Q_3, median, minimum, and maximum values of the cluster data generated for the box-whisker plots shown in Fig. 6.2 and Fig. 6.3.

		50%	60%	65%	70%	75%	80%	85%	90%	95%	100%
						Pixel Intensity					
Pre-insulinic	Q_1	43	39	34	35	50	42.75	52	52	59	161
	Q_3	63	65	76	77	77	99	104	180	185	200
	Median	56	53	56	64	57	60	57	63	61	181
	Min	13	16	19	23	36	34	47	50	58	57
	Max	67	76	170	191	83	186	184	192	205	215
Post-insulinic	Q_1	81	99	125	180	178	185	166	113	64	54
	Q_3	197	208	202	203	202	211	205	210	206	221
	Median	180	186	193	195	191	198	189	192	180	162
	Min	32	54	56	57	64	52	48	55	47	38
	Max	232	235	227	208	237	215	229	225	236	234

Table 6.2: The average numbers of clusters found in pre- and post-insulinic cells for each pixel intensity as well as the number of cells which were considered statistical outliers. Outliers where those cells where the number of clusters differed by three standard deviations from the mean number of clusters among all cells for the insulinic condition. The p values indicate the significance of the differences between the number of clusters in pre and post-insulinic cells.

% Pixel Intensity	#Clusters Insulinic	Pre- #Clusters Insulinic	Post- Outlying pre- or post- insulinic cells	p value
50	60	151	0	0.0002
60	74	162	1	0.007
65	83	177	8	0.03
70	88	186	4	0.0002
75	80	186	2	0.0005
80	84	190	1	0.03
85	79	194	0	0.003
90	90	186	1	0.0004
95	102	154	0	0.1
100	166	136	1	0.2

121

with the *number* of clusters. In other words, does a greater number of pixels to be analysed, result in the identification of more clusters? In order to test whether the number of points influenced the number of clusters, a Pearson's correlation test was used. The test showed very weak correlation among the post-insulinic cells. At a correlation coefficient of 0.067, this indicated that approximately 7% of the increase in the number of clusters could be attributed to the greater numbers of pixels. The pre-insulinic cells however, showed greater - albeit weak - correlation between their pixel numbers and the number of clusters. The correlation coefficient in this instance was 0.33. This indicates that the number of clusters somewhat dependent on the number of pixels used for the analysis. The number of clusters in pre-insulinic cells may therefore be slightly overestimated.

Insulin might stimulate the synthesis of new GLUT4 proteins. However, previous studies have shown that exposure to insulin shows no significant increase in GLUT4 mRNA or protein levels [391, 392]. Additionally, the plasmid is constitutively expressed and the promotor is insensitive to insulin. Finally, no change in overall fluorescence was noticed throughout the experiment. It was therefore assumed that the differences in the amount of GFP signal were due to either the greater dispersion of GFP-tagged GLUT4 or due to inherent biological variation in the cells. A Mann-Whitney U test was used to determine whether the differences in GFP signal between pre- and post-insulinic cells could be due to chance or whether they represented a statistically significant difference. The results indicated that the differences in GFP signal were a real - biological - phenomenon, and not due to chance ($p < 0.01$). The differences in pixel number is thought to be due to the greater dispersion of GFP-tagged GLUT4 as a consequence of insulin exposure. More dispersed GFP signal could give the impression that more GFP-tagged GLUT4 is present in a cell since the diffraction limit of the confocal microscope would obscure more densely clustered GFP-tagged GLUT4.

6.3.2 Analysing the Cluster Characteristics: Differences, Dispersion, and Densities

The cluster data lead to the development of several questions. Firstly, are the differences between the number of clusters found in pre- and post-insulinic cells significant? Secondly, do these clusters, on average, differ significantly with regards to the number of pixels included within them? Thirdly, is there a difference between the proportion of pixels that have been included and excluded from clusters among the different insulinic conditions? Fourth, are the clusters and pixels more dispersed - distant from the nucleus - in post-insulinic cells than in pre-insulinic cells? Finally, are there differences with regard to the densities of the clusters in pre- and post-insulinic cells?

Table 6.2 shows the differences among the numbers of clusters between pre- and post-insulinic cells. However, the question arose whether these differences were biological features, whether they were systematic artefacts of the imaging or data analysis, or whether they were due to random error. In order to test whether these differences were real or due to chance, a Mann-Whitney U test was used to compare the numbers of clusters with one another. The Mann-Whitney U test compared the numbers of clusters in the pre- and post-insulinic cells across the range of pixel intensities. The 75% value displayed the lowest p-value at 9.73E-05 which further supported this as being the appropriate pixel value to use. Therefore, the differences in the numbers of clusters was due to the effect of insulin. The only instances where the differences in cluster numbers between the insulinic states was *not* significant ($p>0.05$), was with the 95% and 100% pixel intensities. This is most likely due to the large degree of 'noise' that is included in the data when using these values.

Another question that emerged from comparing the two data-sets was whether the differences in cluster numbers between the two insulinic states was due to the effect of the insulin or due to random, biological variation in the cells.

The sizes of the clusters, in terms of the number of pixels included as members of a cluster, did not differ significantly ($p > 0.05$) among the pre-insulinic (205 ± 448) and post-insulinic (237 ± 375). These numbers may indicate that the cluster size is *not* impacted by insulin. However, there are several caveats to consider. Firstly, both

insulinic conditions showed correlation coefficients greater than 0.98 between the total number of pixels and the number of pixels found *within* clusters. Secondly, the total number of pixels identified in post-insulinic cells is nearly thrice that of those identified in pre-insulinic cells. Thirdly, it is very likely that the number of clusters in the pre-insulinic cells has been overestimated by as much as 33%. Lastly, the diffraction limited nature of confocal microscopy means that it is likely that a portion of the GFP signals were not identified in the pre-insulinic cells due to the lower dispersion of the signal. Therefore, it is quite likely that the numbers of pixels per cluster in pre-insulinic cells has been underestimated in pre-insulinic cells. This would indicate that the *real* number of pixels per cluster may in fact be greater than what the data indicates.

Whether the ratio of clustered to unclustered pixels differed significantly between pre- and post-insulinic cells (Fig. 6.6) was tested by calculating the ratio of included vs.
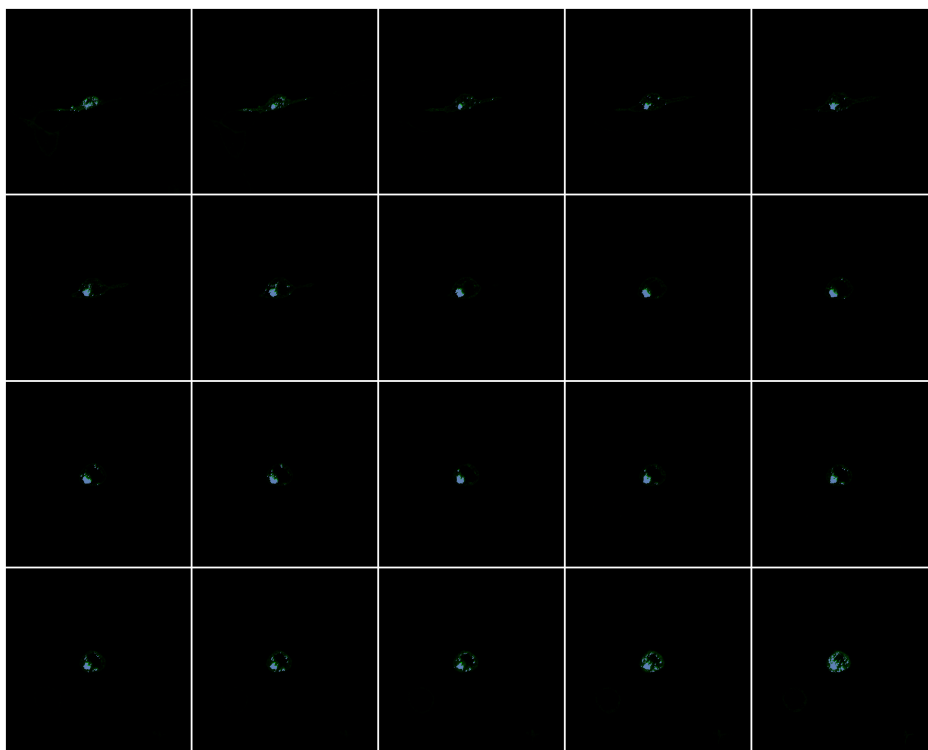
Figure 6.4: An overlay of the accepted pixel data and confocal images in pre-insulinic cells. Each set of 2-dimensional pixel positions was overlayed with its corresponding z-slice of a sample set of confocal images for C2C12 myoblast. What is apparent is the typical clustering of GLUT4 molecules in the perinuclear region in cells which have not been insulin-stimulated. Each image is 600×400 pixels which corresponds to a length of 79 μm and a height of 52 μm. For more images, please see Chapter A.
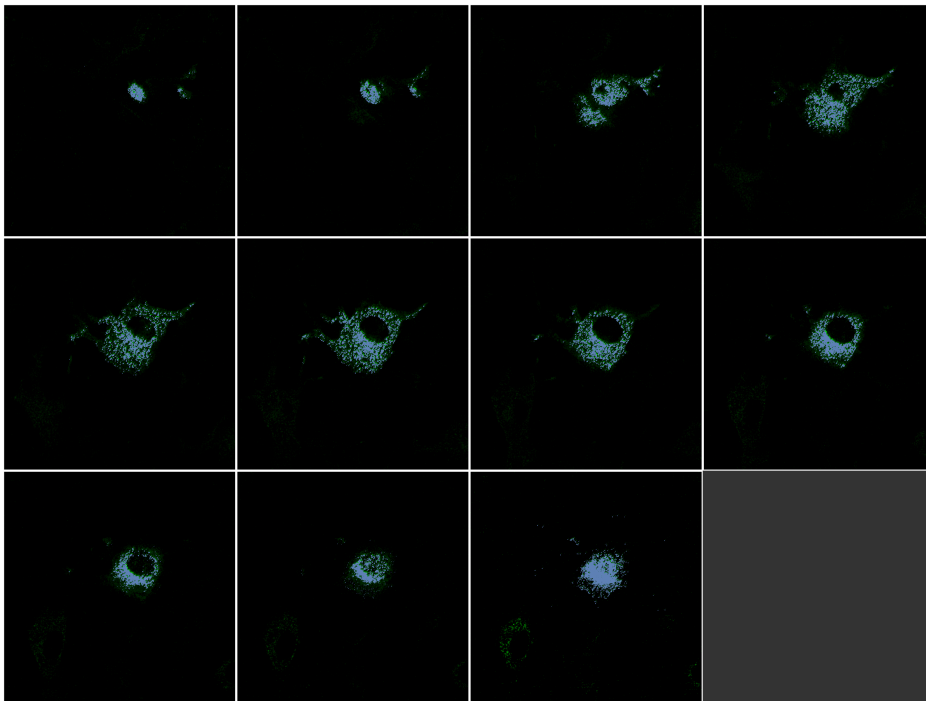
Figure 6.5: An overlay of the accepted pixel data and confocal images in post-insulinic cells. Similar to Fig. 6.2, the pixel positions were superimposed on each z-slice confocal image of the corresponding post-insulinic C2C12 myoblast. In these cells, the GFP signal (and thus the GLUT4) appears more dispersed within the internal volume of the cell after insulin stimulation. Each image is 640×520 pixels which corresponds to a length of 84 μm and a height of 68 μm. For more images, please see Chapter A.

excluded pixels for each cell and comparing these values by using a Mann-Whitney U test. Pre-insulinic cells showed a significantly ($p < 0.01$) higher percentage of pixels in clusters ($74\% \pm 6\%$) when compared to post-insulinic cells ($62\% \pm 7\%$). Therefore, the dispersion of GFP signals in post-insulinic cells was significantly greater than pre-insulinic cells. Together with the greater number of *total* signals and clusters in post-insulinic cells this indicates that insulin may have a marked effect on the distribution of GSVs within a cell. GSVs in pre-insulinic cells tend to be found mostly in clusters as opposed to those in post-insulinic cells. This is likely due to the MTOC-associated 'superclusters' splintering into smaller, more distributed clusters throughout the cell.

In order to test whether the dispersion of the clusters within a cell differed among pre- and post-insulinic cells, the two-dimensional positions of the pixels were superimposed on their original images. Sample images can be seen in Fig. 6.4 and Fig. 6.5 which describe the pre-insulinic and post-insulinic cells respectively. Further images
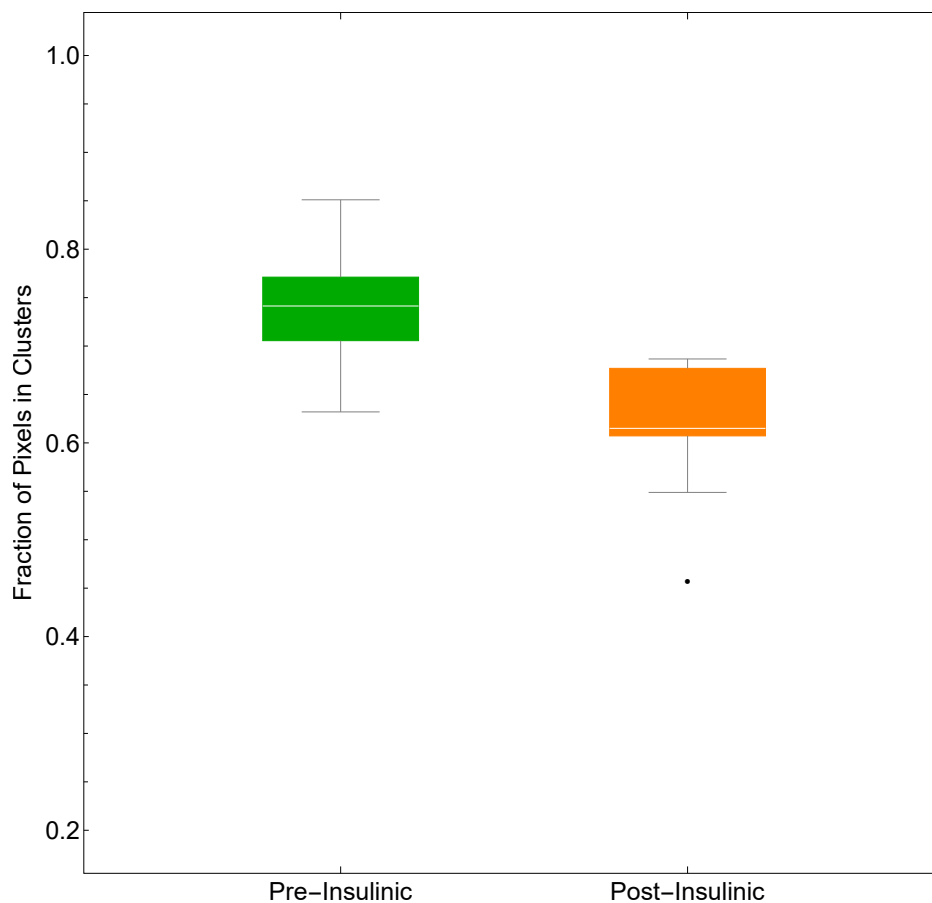
Figure 6.6: The differences between pre-insulinic (green) and post-insulinic (orange) cells with regards to the fraction of GFP signal that could be assigned to a cluster.

may be found in Appendix A. However, what is apparent from these images already is that the post-insulinic cell (Fig. 6.5) exhibits much greater *dispersion* of GFP when compared to the pre-insulinic cell (Fig. 6.4). This suggests that GLUT4 itself has moved from the perinuclear space to the perimembrane space, if not having fused with the membrane itself.

Further, each cluster was defined as a three-dimensional region. Thereafter, the central point of each cluster was determined and the Euclidean distances between the centers of each cluster within each cell were then calculated. A greater mean distance would indicate that, on average, the cluster centers are further apart from one another. In turn this would suggest that clusters have moved from a localised formation, to a more decentralised formation within a cell. In post-insulinic cells, clusters were a mean distance 117 pixels ($\pm$ 85) apart from one another. Pre-insulinic cells were, on

average, 53 pixels ($\pm$ 34) apart from one another. These differences were significant ($p < 0.05$). Therefore, taking into account previous results that indicate the significant biological action of insulin on these cells, these results suggest that insulin is the causal agent for the greater dispersion of clusters within a cell.

However, these data suggest only that the *center* of a cluster has moved. This does not mean that the cluster members themselves are more dispersed. In order to test this, the Euclidean distances between each pixel and the center of their respective nuclei (Section 6.2) were calculated. Greater mean distances between pixels and nuclei would indicate that the GFP signal has dispersed more widely within the cell from its initial, peri-nucleic location. The pixels in the pre-insulinic cells were closer to the nuclear region (81 pixels, $\pm$ 31) when compared to those in post-insulinic cells (94 pixels $\pm$ 59). This further supports a significant ($p < 0.05$) effect of insulin on the dispersion of GSVs within the cell.

Lastly, the cluster densities were evaluated across pre- and post-insulinic cells. The same clustering score that was used in Section 6.3.1 was used in order to determine the density of each cluster. The motivation for this was to determine whether the density of clusters changed in response to insulin exposure. The results indicate that pre-insulinic clusters were less dense (0.079 ± 0.0035). This represented an almost 1.5-fold greater dispersion *within* a cluster than in post-insulinic clusters (0.053 ± 0.0024). This supports previous analyses that indicate smaller clusters splitting off from larger super clusters. Further, this is in line with previous observations in literature which indicate that GSVs translocate to punctate clusters around the termini of MTs [202].

6.4 Conclusion

The aim of this chapter was two-fold. First, to determine whether clustering algorithms could be applied to the types of confocal images generated herein. Secondly, to establish what types of questions could be answered by the resulting data and whether these questions yielded novel, meaningful insights to the clustering behaviour of GLUT4 molecules in pre- and post-insulinic cells.

In service of the first aim, Section 6.3.1 explored several aspects of the clustering algorithm itself. The first finding was that there was a difference in the number of clusters between cells which where stimulated with insulin and those which were not. Further, considering that the post-insulinic cells appeared to present more GFP signal, it was important to determine whether the quantity of GFP signal would affect the number of clusters. The number of clusters weakly correlated with the amount of GFP signal in pre-insulinic cells and could be overestimated by as much as 33%. However, in post-insulinic cells, this overestimation dwindled to 6.7%.

Considering that there was a marked increase in the number of pixels identified in post-insulinic cells over the pre-insulinic cells it was necessary to determine whether this was due to chance or a real phenomenon. The results detailed in Section 6.3.1 indicate that the difference in GFP signal was a real phenomenon and not due to chance. However, there are several caveats to these findings. Firstly, despite the difference being real, it is unknown whether this represents a difference in the quantity of signal. In other words, whether one cell expresses GFP-tagged GLUT4 over another is currently unknown. It is unlikely that insulin induces greater expression of GFP-tagged GLUT4 since it does not induce GLUT4 expression. Secondly, the diffraction limited nature of the confocal microscope makes isolating individual GLUT4 molecules unlikely in this study. This means that when the GFP-tagged GLUT4 was densely clustered, it was not possible to isolate individual signals. There may have been loss or overlap of signal which would obscure the true number of GFP signals in pre-insulinic cells. Therefore, if insulin induces greater dispersion among GLUT4 molecules, it is likely that this may appear like a real difference in GFP signal among pre- and post-insulinic cells.

In order to fulfil the second aim, several aspects of the clusters identified in Section 6.3.1 were analysed. It was determined that the amount of clusters was significantly different between pre-insulinic and post-insulinic cells. Where the previous analysis dislocated the number of clusters from the number of pixel, this result supports the notion that insulin effects the splintering of a few clusters into more. Next, the size of these clusters with regard to the number of pixels they contained was investigated. The results in Section 6.3.2 indicate that there is no significant difference

among the sizes of the clusters. However, in light of the limitations of the confocal microscope and the highly localised nature of pre-insulinic clusters, the reliability of this result is not sure.

In light of this, the next step was to determine whether the proportions of pixels included or excluded from clusters different between the insulinic cells. It was found that post-insulinic cells had fewer pixels which could be assigned to a cluster. Based on this, the next step was to determine whether this was due to the greater dispersion of the clusters and pixels in post-insulinic cells. Considering the exclusion criteria discussed in Section 6.2, greater dispersion of the pixels would mean that fewer pixels would be included in clusters as they would be too distant to their nearest neighbours. The results indicated that the clusters in post-insulinic cells more dispersed - in other words more distant from the nucleus. Similarly, the pixels within the post-insulinic cells are also more distant from the nucleus. This means that it is indeed likely that the difference in the proportions of pixels assigned to clusters is likely due to the greater dispersion of the GFP signal in post-insulinic cells.

Lastly, the densities of the clusters was examined. The post-insulinic clusters were denser than the pre-insulinic clusters. As discussed in Section 6.3.2, this is likely due to the nature of GSV translocation. Smaller clusters of GSVs break away from the larger, perinuclear clusters and travel along the microtubule network to ultimately fuse in denser, punctate clusters at the terminus of each microtubule [202]. However, once again one cannot ignore that, due to the diffraction limit, it is likely that the true number of pixels within each cluster is not fully known. It could very well be that the pre-insulinic clusters are denser, but since the true number of pixels is not known, this remains speculation. It may be possible to overcome this hindrance through the use of super-resolution microscopy such as a STORM (stochastic optical reconstruction microscopy) or a combined confocal and scanning electron microscopy based approach which would provide the necessary resolution and more detailed 3-dimensional information on the location of individual molecules [393–395].

In conclusion, this study demonstrated that cluster analysis is a viable method with which to investigate certain aspects of biological imagery. Further, it determined that

insulin has a notable effect on the number, dispersion, and density of GLUT4 clusters in C2C12 myoblasts. This means that one can use clustering data to generate novel, meaningful answers with respect to certain biological phenomena. This knowledge could assist investigations which wish to determine how different states such as disease or stress affect the behaviour of certain molecules.

Further work would investigate the time-dependent movement of GSVs in response to insulin stimulation. It would also be important to investigate the clustering behaviour of GSVs under conditions where the cytoskeleton has been disrupted. This would need to be paired with glucose transport or flux data in order to elucidate the effect that GSV clustering may have on glucose dynamics in cells. Additionally, repeating these experiments in differentiated muscle tissue would provide insight into the behaviour of GSVs in mature cells. Lastly, super-resolution microscopy would be necessary to better define the number of GLUT4 molecules *within* the membrane as well as determine their clustering charactersistics.

Chapter 7

Conclusion and Final Remarks

The present work examined insulin signalling from a variety of perspectives. Firstly, the impact that so-called standard cell culturing practises has on the differentiation and insulin sensitivity of C2C12 myotubes. Secondly, this work integrates the insulin signalling and glucose transport modules (Section 1.1) into a data-driven, minimal mathematical model. Thirdly, the impact that insulin has on the clustering and distribution of GLUT4 in C2C12 myoblasts.

7.1 Concerning the Optimisation of Growth Conditions

The first aim of this study was to re-establish, standard, physiologically relevant culturing conditions upon which all further experiments would be based. High glucose concentrations (25 mM) have been linked to the development of insulin resistance [396, 397], metabolic dysfunction [398], or reduced differentiation [279]. Therefore, it was necessary to determine *to what degree* these impacts were present in C2C12 cells and what steps could be taken to remedy this.

In Chapter 4, it was shown that standard, high glucose culturing protocols dysregulated the glucose metabolism and differentiation of C2C12 myoblasts. Cells cultured with 25 mM glucose showed a consistently lower induction of glucose-lactate flux in response to insulin stimulation than cells cultured with 15mM or 5 mM of glucose

(Fig. 4.1). Cells that were cultured with 15 mM or 5 mM glucose in their media responded to insulin induction and showed a greater glucose-lactate flux when compared to their respective controls. This indicates that persistent, high glucose culturing conditions have an adverse effect on either the insulin signalling or the glycolytic machinery. However, since these studies only evaluated the glucose-lactate flux, it is unclear from these results with which of these aspects the dysregulation lies.

A clue may be found in the second aspect of this particular study. The degree to which C2C12 myoblasts differentiate to myotubes in media which contained either 25 mM or 15 mM glucose was investigated. As seen in Fig. 4.6 and Table 4.2, cells which were grown with 15 mM of glucose showed an approximately 1.4-fold increase in differentiation when compared to those cultured in 25 mM of glucose. Considering the greater expression of GLUT4 [233] in differentiated cells, a greater degree of differentiation is desirable when investigating aspects of insulin signalling and glucose transport. Despite this, the lack of *direct* evidence of GLUT4 expression in Chapter 4 remains its most obvious shortcoming. However, future studies such as the image and cluster analyses presented in Chapter 6 could be used to elucidate this.

The standard culturing conditions were evaluated with the specific aim of ensuring their suitability for the insulin signalling and glucose transport studies which followed. In doing so it was discovered that lower glucose concentrations in the culturing and differentiation media resulted in cells that exhibited a greater degree of differentiation *and* were more sensitive to insulin induction of glucose transport and flux.

7.2 Concerning the Integration of Insulin Signalling and Glucose Transporter Data: the Construction of a Minimal Model

The second aim of this study was to develop a kinetic description of the phosphorylation of the IR and Akt proteins as well as the induction of GLUT4 activity. These data, which represented the insulin signalling and glucose transporter modules (Sec-

tion 1.1) respectively, were then included in a minimal model. Further, while not part of the original aims, Chapter 5 included a preliminary investigation of the IR, Akt, and GLUT4 activities under a pseudo insulin-resistant state.

7.2.1 Characterisation of the Insulin Signalling and Glucose Transport Modules

The first two modules - signalling and glucose transport - in the 'three module' module framework (outline in Section 1.1) were characterised. The signalling and glucose transport responses of C2C12 cells were characterised according to their insulin dose responses as well as their temporal dynamics.

How the IR and Akt phosphorylation dynamics and GLUT4 activity change in response to insulin concentrations between 10 pM and 1 μM was tested (Chapter 5). The phosphorylation of the IR and Akt achieved their maxima at 100 nM and 1 μM respectively. The Thr308 site on Akt displayed greater responsiveness to insulin at concentrations greater than 20 nM, and showed a remarkable 4-fold induction at 1 μM insulin. This is in contrast with the IR and Akt Ser473 whose phosphorylation state only increased two-fold in response to insulin concentrations of 100 nM and above. Similarly, the activity of the GLUT4 transporter (as measured by the uptake of radio-carbon glucose) increased linearly (on a logarithmic scale) with insulin concentration until it achieved a maximal induction of approximately 2-fold at insulin concentrations of 100 nM or greater. While no increase in total IR or Akt signal was observed, similar data was lacking for the GLUT4 transporter.

Secondly, the dynamic behaviour of IR, Akt, and GLUT4 activity were examined in response to a 100 nM insulin pulse (Chapter 5). The first component to achieve its maximum of a 2-fold induction of phosphorylation is the IR after two minutes. Thereafter, both the levels of Akt_{S_P} and GLUT4 activity reach their maxima after 15 minutes. In each case, these levels are maintained for the duration of the experiment. This represents the 'on' dynamics of insulin signalling. The 'off' dynamics were determined by a series of experiments which evaluated the dephosphorylation and reduction of GLUT4 activity as described in Chapter 5. With the exception of the IR, the 'switch-

ing off' of Akt_{S_P} and GLUT4 activity was slightly slower than the switching on. The k_{on}andk_{off} constants determine the insulin signalling dynamics and they need to be balanced with similar values in the glucagon system since it is not likely that cells would operate two antagonistic pathways at a maximum rate. Similarly, other possible explanations for these 'on - off' dynamics could be that they are an emergent feature or specific dynamics which are adapted to the pulsatile release of insulin as seen *in situ* [305, 399]. Whether the 'off' dynamics are altered in pseudo insulin-resistant cells or whether they are dependent on the culturing conditions will be the subject of future work.

7.2.2 Integration of Insulin Signalling and Glucose Transport Modules: A Minimal Mathematical Model

A minimal, ODE-based model was built which incorporated the two modules - insulin signalling and the GLUT4. The insulin signalling module was represented by IR and Akt phosphorylation dynamics as outputs and insulin as an input. The GLUT4 module used phosphorylated Akt as an input and yielded the glucose transport activity as an output which was measured by ^{14}C uptake assays.

Each of these components was described with a set of reversible mass-action equations. The experimental data were used to determine the ratios of the 'on' and 'off' constants for each equation in a single optimisation step. The division of the insulin signalling cascade into three distinct modules (as discussed in Section 1.1) meant that one could portray this pathway as a series of input-output relationships which relegated much of the complexity to so-called 'black boxes'.

When one compares this approach to those discussed in Section 2.3 several aspects stand out. The model presented here is less complex than the approach favoured by Sedaghat et al [292] or Brännmark et al [315]. However, despite this, the model could successfully simulate the normal state of insulin signalling. Further, this 'core' modelling approach attempts to blend a top-down approach (as described in [33]) with molecular data. In other words, insulin signalling and glucose transport modules were defined as functions on their inputs and outputs. The model relied on two sets of exper-

imental data: insulin dose-response data and the time dynamics in response to 100 nM insulin exposure. The complete model fit the dose-response and time-dynamic data of the IR and Akt phosphorylation as well as the glucose transporter activity to the available data. The fits for the dose-response data were less precise than those for the time-dynamic data.

7.2.3 Disruptions in Insulin Signalling, Which Module is Responsible?

The final component in Chapter 5 was a preliminary investigation into a dysfunctional insulin signalling pathway. Based on work in Chapter 4, the glucose-lactate flux responses were used to determine which cell culturing conditions would lead to an insulin resistant-like state. If neither glucose consumption nor lactate production increased in response to insulin, the cells were considered insulin insensitive.

Once the cells were grown to mimic insulin resistant states their IR and Akt phosphorylation dynamics as well as their GLUT4 transporter activity were determined. The response of the IR was counter-intuitive if one thinks that excess insulin would down-regulate the expression or activity of the IR (Fig. 5.13). Those cells which were grown with high-glucose, insulin resistant conditions showed a normal IR phosphorylation response to insulin. The insulin resistant cells grown at 15 mM glucose seemingly phosphorylated to a greater degree than control cells. These experiments need to be repeated in order to confirm these results. However, it does seem likely that the insulin resistant state induced in these cells had little effect on the phosphorylation of the IR.

A greater effect of insulin resistance on Akt phosphorylation is seen in Figs. 5.14 and 5.15 and more specifically in Fig. 5.18. This indicates that, while IR phosphorylation may proceed normally (Fig. 5.13), the signal from the phosphorylated IR does not result in adequate Akt phosphorylation. This in turn has the knock-on effect of abrogating glucose transporter activity (Fig. 5.19).

In pseudo insulin-resistant cells there is a clear reduction in Akt phosphorylation at the 60 minute mark and the reduction in glucose transporter activity appears to coincide

with the reduction in Akt_S phosphorylation. Conversely, Akt_{T_P} does appear to be similarly impacted by the pseudo insulin resistance since, glucose transporter activity does not appear to respond strongly to this decrease. However, both Akt_{S_P} and Akt_{T_P} levels are diminished by the 'loss' of signal coming from the phosphorylated IR.

While the data are incomplete, this analysis indicates that the reduced glucose transporter activity seen in pseudo insulin-resistant cells may originate from a fault in the signalling module, and more specifically one which occurs between IR and Akt. While it may be tempting to consider Akt_{S_P} the culprit for the reduced glucose transporter activity, it is not certain from these data whether the reduced Akt_{S_P} levels are the cause for this diminished activity or whether they are the result of a fault which lies further upstream.

The direct relationship between Akt phosphorylation and glucose transport activity induction discussed in Chapter 5 indicates that a reduction in Akt phosphorylation should bring about a decrease in glucose transporter induction. This likely has a knock-on effect which results in the reduced glucose-lactate flux as seen in Chapter 4. Since the signalling module is the first to respond to insulin, the reduced Akt phosphorylation indicates that the observed reduction in activity of the glucose transport and metabolism modules may originate with the apparent dysregulation of the signalling module.

Future work should focus on further exploring the dynamics of insulin resistant cells in order to strengthen the applications of the minimal model approach. Similarly, work that examines faults or dysregulation in the insulin signalling pathway may make use of this model to determine *which* module specifically was dysfunctional thereby focussing further efforts on that module or components thereof. Further, it would be worthwhile to expand the dataset used by the minimal model to incorporate one or more of the 'nodes' as shown in Fig. 1.1. Lastly, determining the concentration of GLUT4 as well as the expression levels of IR and Akt may shed further light on the long-term consequences of insulin exposure in C2C12 cells.

7.3   Concerning Insulin Induced GLUT4 Clustering

This aspect of the study investigated how GFP-tagged GLUT4 responded to insulin exposure. Specifically, focus was drawn to the clustering and distribution of these molecules within cells either *before* or *after* they were exposed to insulin.

Chapter 6 explored several questions with regard to the clustering of GLUT4 in response to insulin in C2C12 myoblasts. Firstly, does insulin stimulation increase the number of GLUT4 clusters? Cells that were exposed to 100 nM insulin for 30 minutes had more than twice the number of clusters when compared to cells not stimulated with insulin (Table 6.2). Secondly, are there differences among the pre- and post-insulinic cells in regard to the size and density of their clusters? While differences in cluster size - as determined by the number of members - were not evident, post-insulinic cells had clusters which were more dense than their pre-insulinic counterparts. Thirdly, does insulin stimulation results in the greater distribution of clusters? Cluster in insulin-stimulated cells were more distant from the nucleus and from each other. Considering that GSVs originate in the perinuclear space, this evidences that, not only are clusters further away from each other, they are further away from their point of origin. This indicates that insulin induces not only the translocation of GSVs and GLUT4, but also the dispersion throughout the plasma membrane into greater numbers of denser clusters. This chapter therefore highlights two aspects: the viability of an image and cluster-based analysis of GLUT4 in living cells and the ability of this approach to generate insights into the mechanisms by which insulin distributes GLUT4 throughout the cell.

Future work would need to address several shortcomings of this approach, specifically with regards to the scope of this project. Firstly, one would need to clarify whether this clustering behaviour is tied to an increase in GLUT4 activity. Secondly, it would be prudent to repeat this study in myocytes instead of myotubes. Lastly, videos which capture the translocation of GLUT4 from the perinuclear to the perimembrane space would further assist in correlating these results with those in Chapter 5.

7.4 Limitations and Possibilities

In conclusion, the present work considered several key aspects:

The importance of evaluating standard experimental protocols for their applicability to the research question(s) at hand. Investigating insulin signalling and GLUT4 activity in cells that are insulin resistant or sub-optimally differentiated may yield results that are not entirely accurate. Similarly, when doing such studies, it is important to include, in the methodologies glucose concentration in the cell culturing medium and degree of differentiation that was used for the ongoing experiments.

Throughout this thesis a core modelling technique was applied to describe the three modules of the system under study: the insulin signalling pathway, glucose transporter induction, and metabolism. An advantage of such a minimal modelling technique is that only a few parameters must be determined, since very simple rate equations are used. However these rate equations are not necessarily mechanistic and this can result in non-optimal fits. In particular for the insulin dose response curves the description of the model for the system was not very good. However, the functional relation between Akt phosphorylation and insulin concentration, for example, is not described directly by the model, but indirectly since the IR is the component which links the two. For the model the direct input-output relations are more important, and these could be described reasonably well by the core model, (with the exception of the insulin induced phosphorylation of IR). In other words the IR_P induced AktS and AktT phosphorylation, and the Akt_P induced glucose transport induction were described quite well. Moreover the time response of insulin induction was well described by the model, and it is noteworthy that these dynamic experiments obey the steady state constrained parameter relations as determined for the dose response experiments. The good description is therefore a partial validation for the k_{off}/k_{on} rate constants. On the basis of these considerations it was decided that the core model was good enough to use it for further analysis of the system.

Such an approach can, in future, be rapidly adapted for other signalling pathways, other organisms, or it could be expanded into a more complex model. Further, the data gathered in Chapter 5 suggests more modest increases in glucose uptake

when compared to the rather large increases sometimes reported in literature. The use of metabolisable glucose as well as the rapidity of the assay is likely to provide a more accurate estimate of glucose transporter activity than methods which use non-metabolisable glucose analogues such as 2-Deoxy-glucose. Glucose analogues such as 2-Deoxy-glucose are metabolised by hexokinase only. This means that the product is often not a substrate for phosphoglucose isomerase or phosphofructo-kinase. However, these molecules still act as inhibitors for hexokinase. Consequently, methods which rely on glucose analogues likely measure a interplay of glucose transport, dwindling hexokinase activity, and the eventual equilibration of analogue concentrations across the membrane.

Lastly, this work further supports the use of imaging studies to investigate the behaviour of specific elements in signalling pathways. Additionally, the clustering and dispersion behaviour of GLUT4 molecules in response to insulin remains a little-studied phenomenon. However, despite more work still being necessary, the study presented in Chapter 6 was able to partially explain and quantify the degree to which the clustering and motile behaviour of GLUT4 molecules is affected by insulin.

Appendix A

Supplementary Figures: Imaging Study

Figure A.1: Supplementary figure which depicts the overlay of accepted pixels and the original image for a post-insulinic cell. Each image is 650×750 pixels which corresponds to a length of 85 μm and a height of 98 μm. The green pixels represent positive GLUT4-GFP signal while the light blue points represent a subset of these pixels that were subsequently assigned to clusters based on the methods described in Chapter 6.

Figure A.2: Supplementary figure which depicts the overlay of accepted pixels and the original image for a post-insulinic cell. Each image is 400×750 pixels which corresponds to a length of 52 μm and a height of 98 μm. The green pixels represent positive GLUT4-GFP signal while the light blue points represent a subset of these pixels that were subsequently assigned to clusters based on the methods described in Chapter 6.

Figure A.3: Supplementary figure which depicts the overlay of accepted pixels and the original image for a post-insulinic cell. Each image is 650×630 pixels which corresponds to a length of 85 μm and a height of 83 μm. The green pixels represent positive GLUT4-GFP signal while the light blue points represent a subset of these pixels that were subsequently assigned to clusters based on the methods described in Chapter 6.
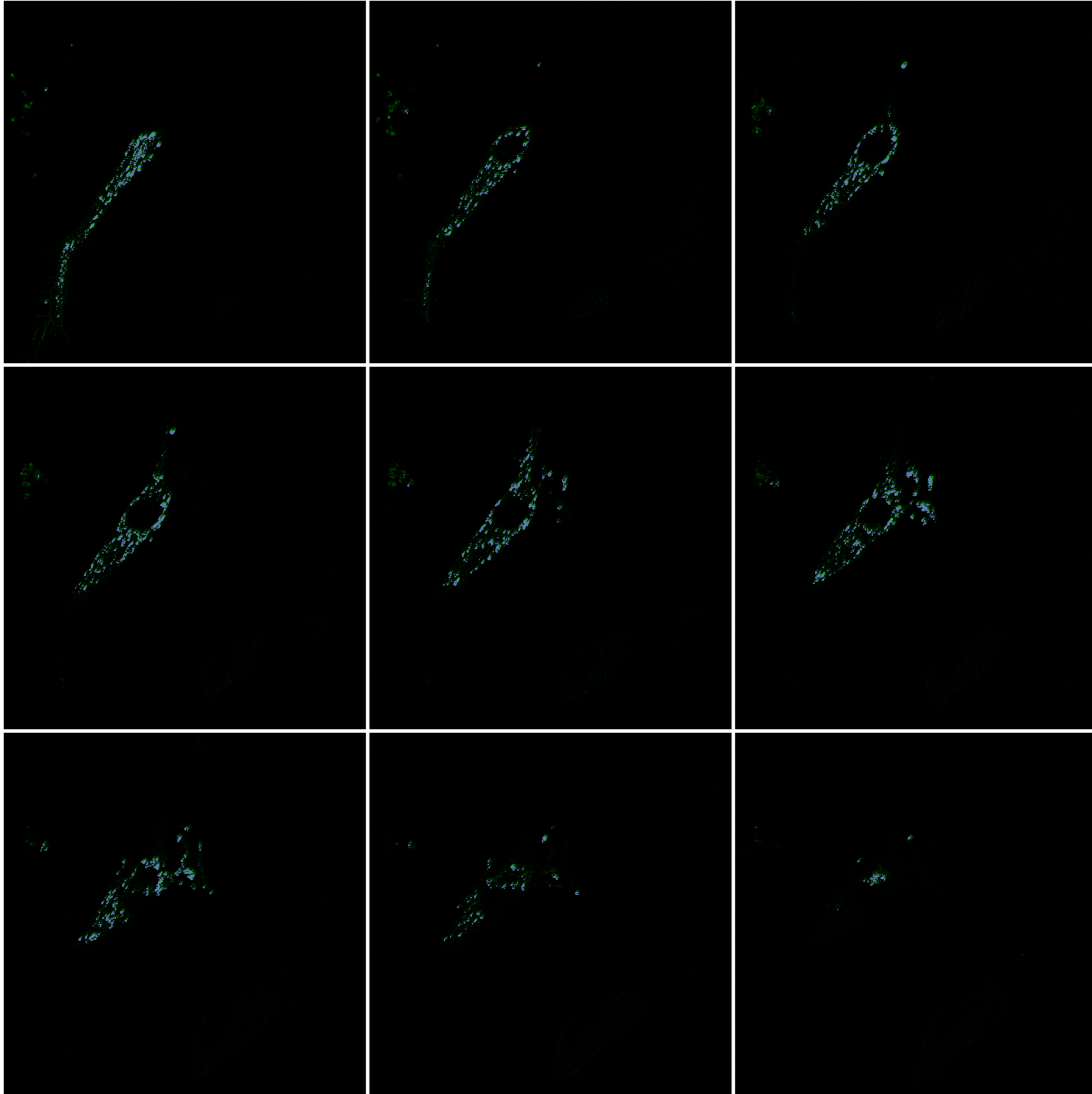
Figure A.4: Supplementary figure which depicts the overlay of accepted pixels and the original image for a post-insulinic cell. Each image is 710×400 pixels which corresponds to a length of 93 μm and a height of 52 μm. The green pixels represent positive GLUT4-GFP signal while the light blue points represent a subset of these pixels that were subsequently assigned to clusters based on the methods described in Chapter 6.

Figure A.5: Supplementary figure which depicts the overlay of accepted pixels and the original image for a post-insulinic cell. Each image is 400×900 pixels which corresponds to a length of 52 μm and a height of 118 μm. The green pixels represent positive GLUT4-GFP signal while the light blue points represent a subset of these pixels that were subsequently assigned to clusters based on the methods described in Chapter 6.
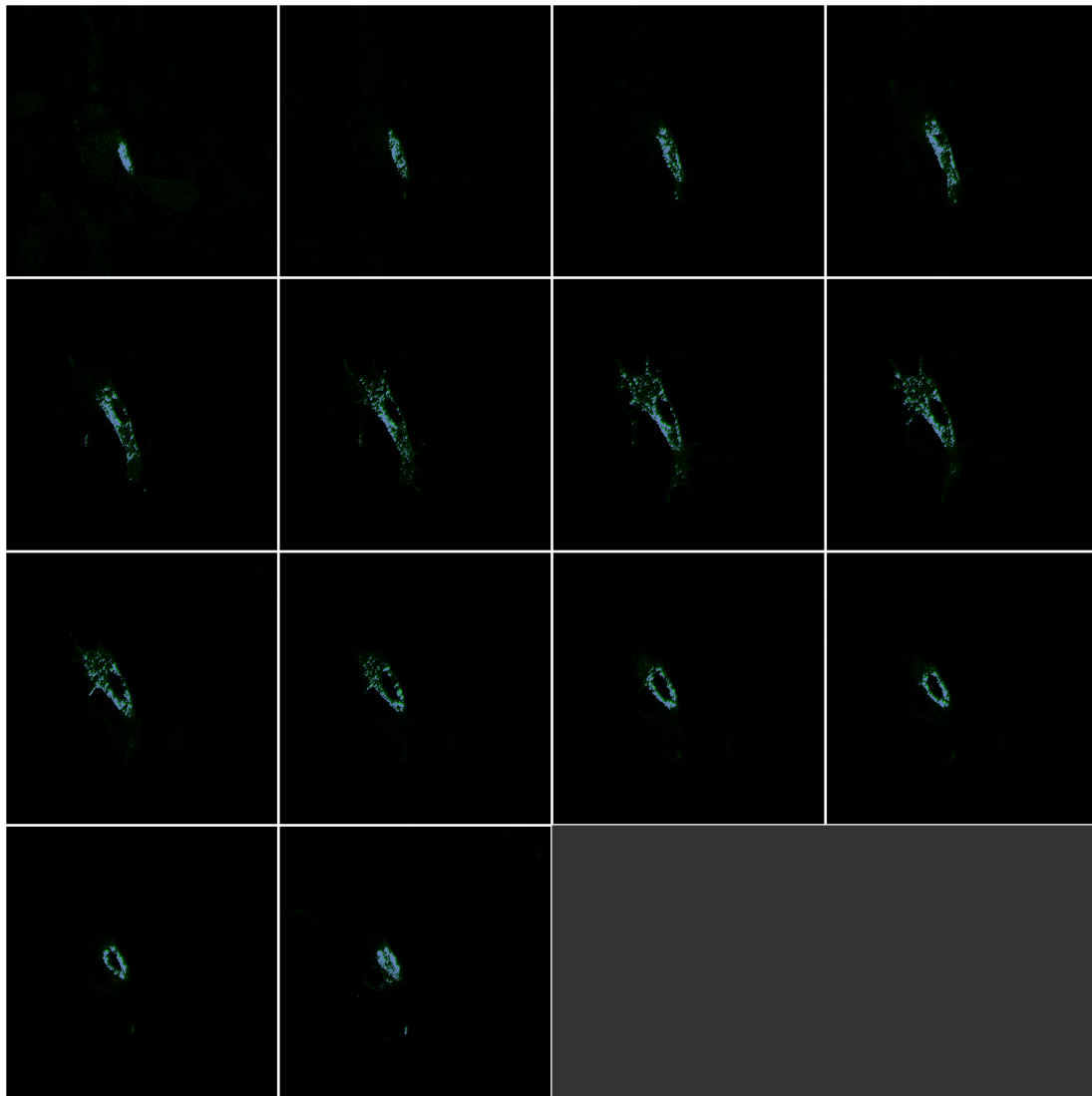
Figure A.6: Supplementary figure which depicts the overlay of accepted pixels and the original image for a post-insulinic cell. Each image is 480×750 pixels which corresponds to a length of 63 μm and a height of 98 μm. The green pixels represent positive GLUT4-GFP signal while the light blue points represent a subset of these pixels that were subsequently assigned to clusters based on the methods described in Chapter 6.
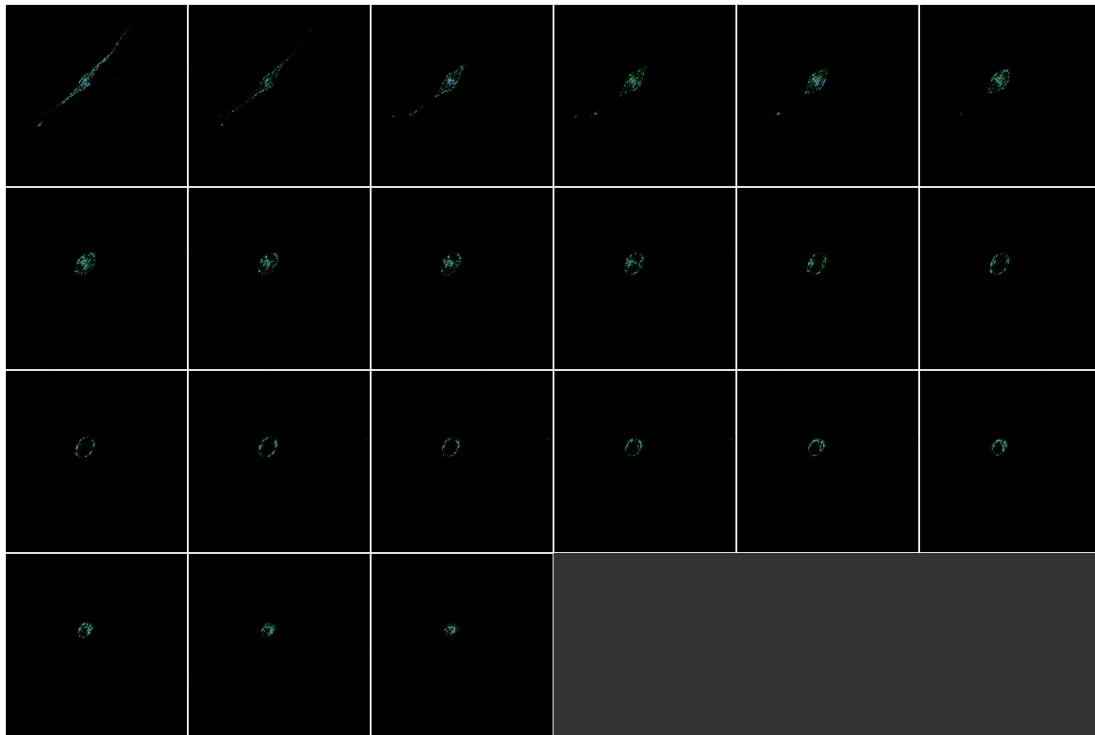
Figure A.7: Supplementary figure which depicts the overlay of accepted pixels and the original image for a post-insulinic cell. Each image is 370×670 pixels which corresponds to a length of 48 μm and a height of 88 μm. The green pixels represent positive GLUT4-GFP signal while the light blue points represent a subset of these pixels that were subsequently assigned to clusters based on the methods described in Chapter 6.
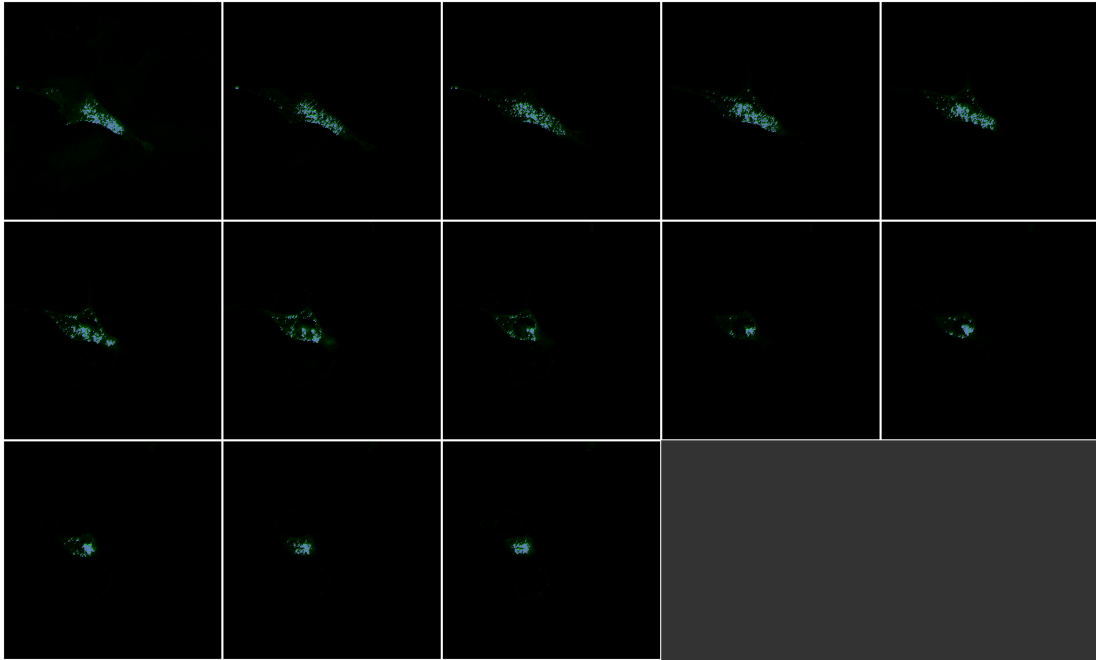
Figure A.8: Supplementary figure which depicts the overlay of accepted pixels and the original image for a post-insulinic cell. Each image is 490×824 pixels which corresponds to a length of 64 μm and a height of 108 μm. The green pixels represent positive GLUT4-GFP signal while the light blue points represent a subset of these pixels that were subsequently assigned to clusters based on the methods described in Chapter 6.

Figure A.9: Supplementary figure which depicts the overlay of accepted pixels and the original image for a post-insulinic cell. Each image is 500×1024 pixels which corresponds to a length of 66 μm and a height of 134 μm. The green pixels represent positive GLUT4-GFP signal while the light blue points represent a subset of these pixels that were subsequently assigned to clusters based on the methods described in Chapter 6.
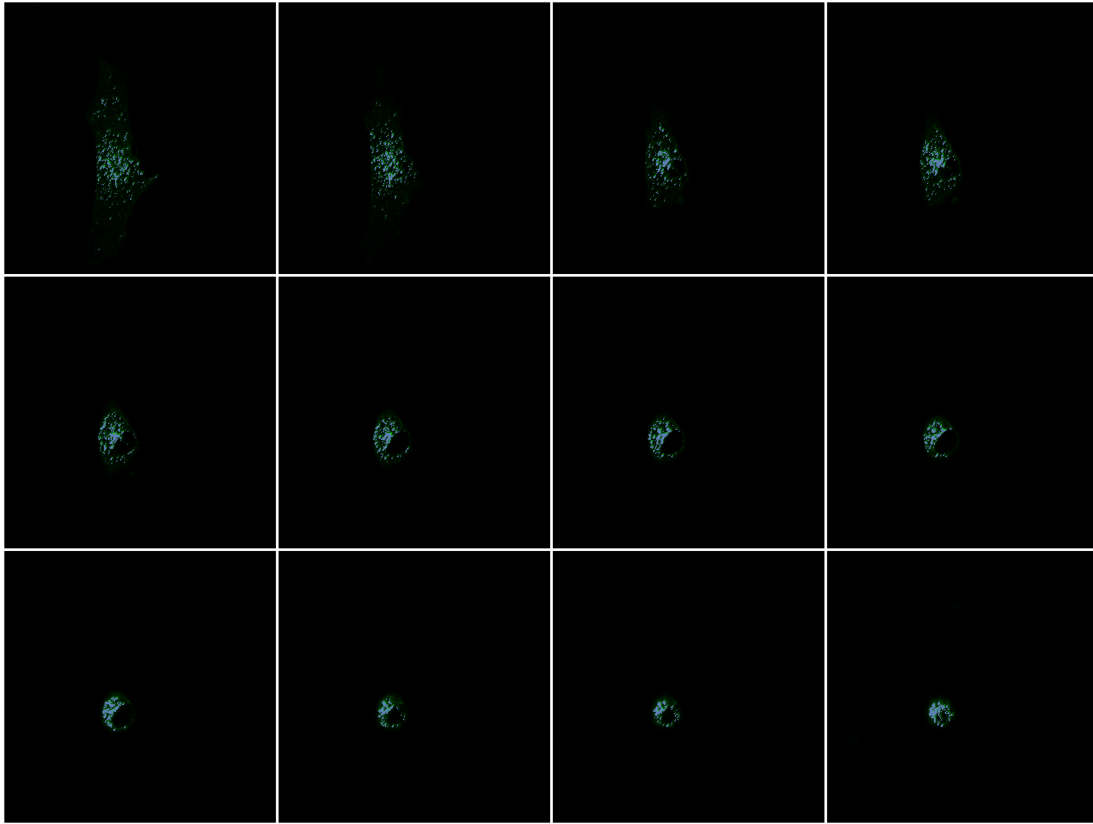
Figure A.10: Supplementary figure which depicts the overlay of accepted pixels and the original image for a post-insulinic cell. Each image is 850×550 pixels which corresponds to a length of 111 μm and a height of 72 μm. The green pixels represent positive GLUT4-GFP signal while the light blue points represent a subset of these pixels that were subsequently assigned to clusters based on the methods described in Chapter 6.
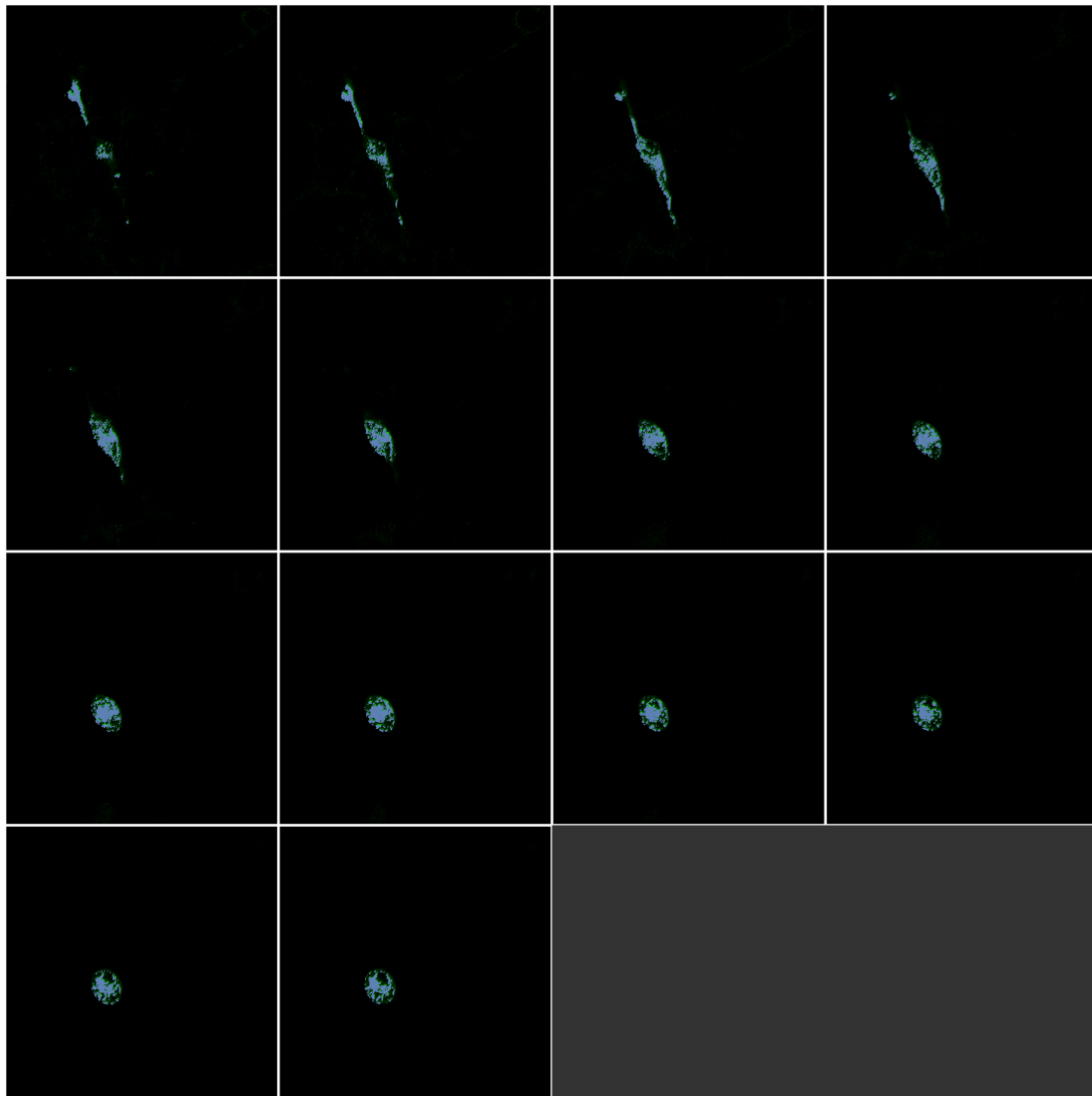
Figure A.11: Supplementary figure which depicts the overlay of accepted pixels and the original image for a post-insulinic cell. Each image is 850×450 pixels which corresponds to a length of 111 μm and a height of 59 μm. The green pixels represent positive GLUT4-GFP signal while the light blue points represent a subset of these pixels that were subsequently assigned to clusters based on the methods described in Chapter 6.
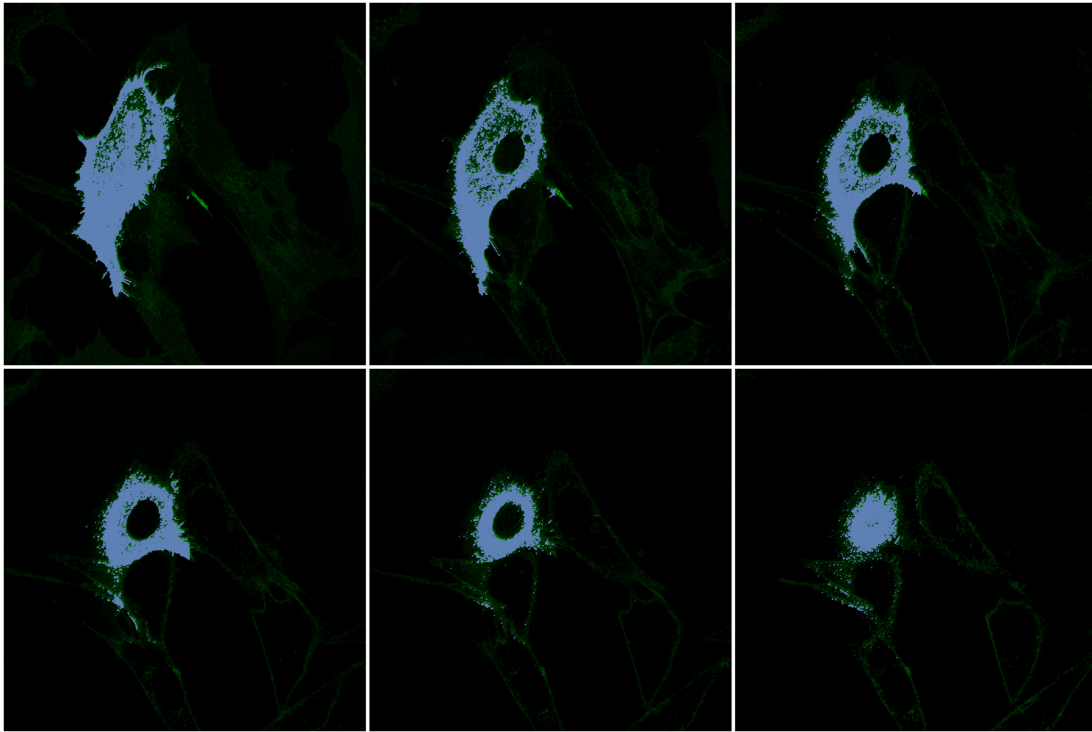
Figure A.12: Supplementary figure which depicts the overlay of accepted pixels and the original image for a pre-insulinic cell. Each image is 1400×10 pixels which corresponds to a length of 183 μm and a height of 131 μm. The green pixels represent positive GLUT4-GFP signal while the light blue points represent a subset of these pixels that were subsequently assigned to clusters based on the methods described in Chapter 6.

Figure A.13: Supplementary figure which depicts the overlay of accepted pixels and the original image for a pre-insulinic cell. Each image is 350×400 pixels which corresponds to a length of 46 μm and a height of 52 μm. The green pixels represent positive GLUT4-GFP signal while the light blue points represent a subset of these pixels that were subsequently assigned to clusters based on the methods described in Chapter 6.
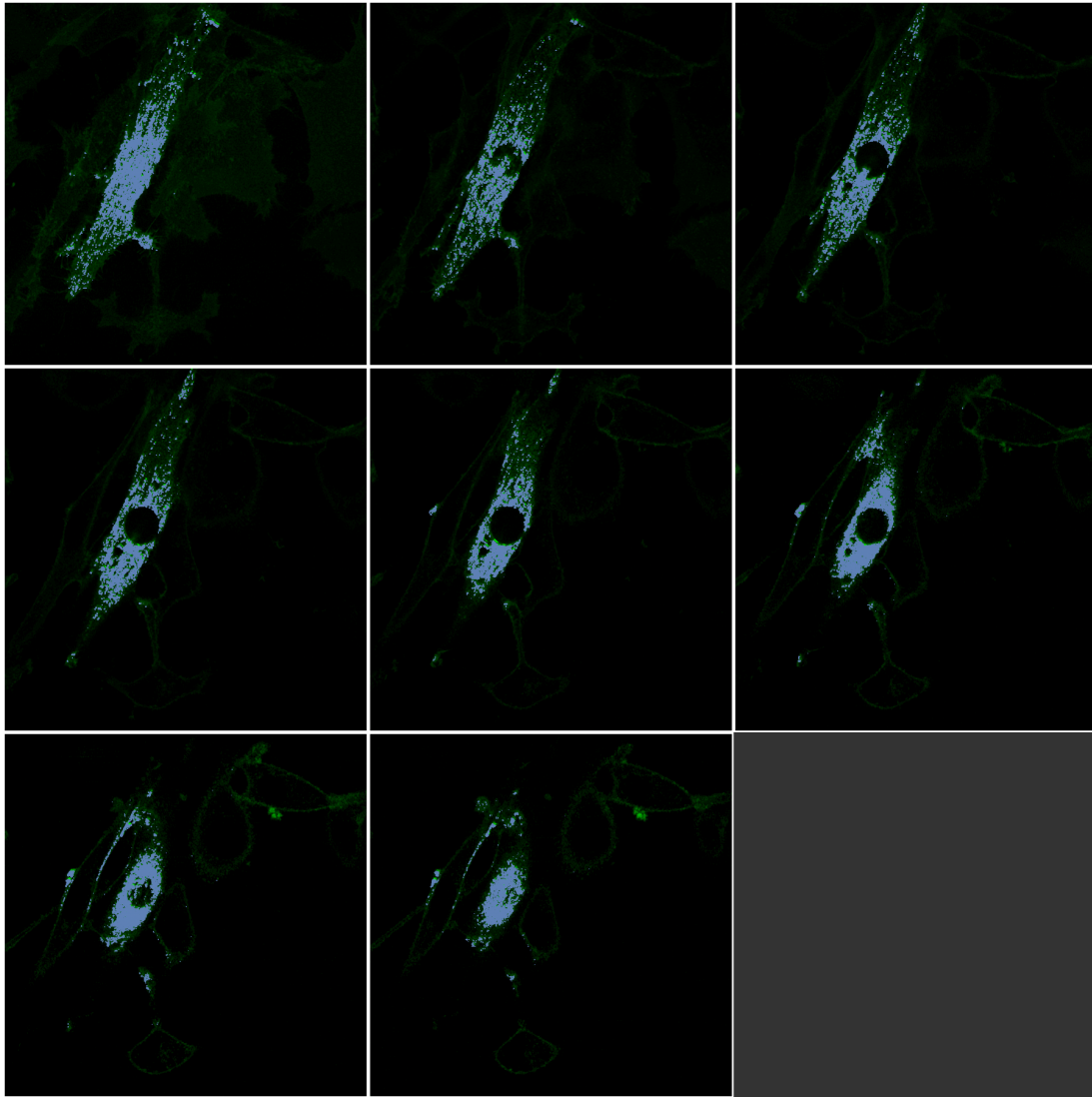
Figure A.14: Supplementary figure which depicts the overlay of accepted pixels and the original image for a pre-insulinic cell. Each image is 250×500 pixels which corresponds to a length of 33 μm and a height of 66 μm. The green pixels represent positive GLUT4-GFP signal while the light blue points represent a subset of these pixels that were subsequently assigned to clusters based on the methods described in Chapter 6.
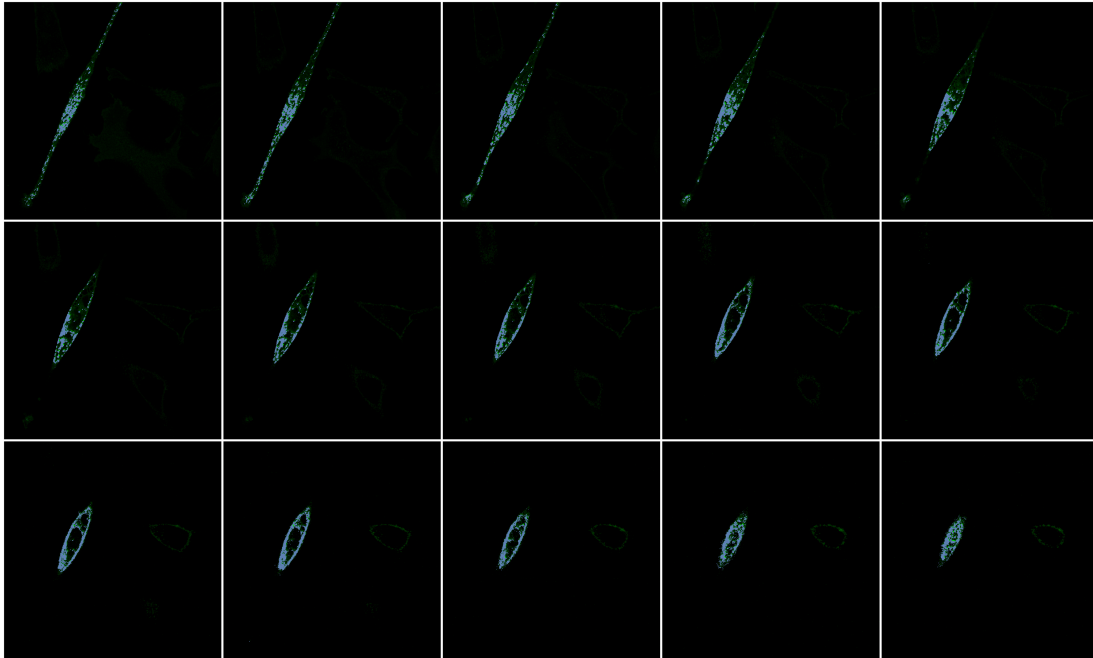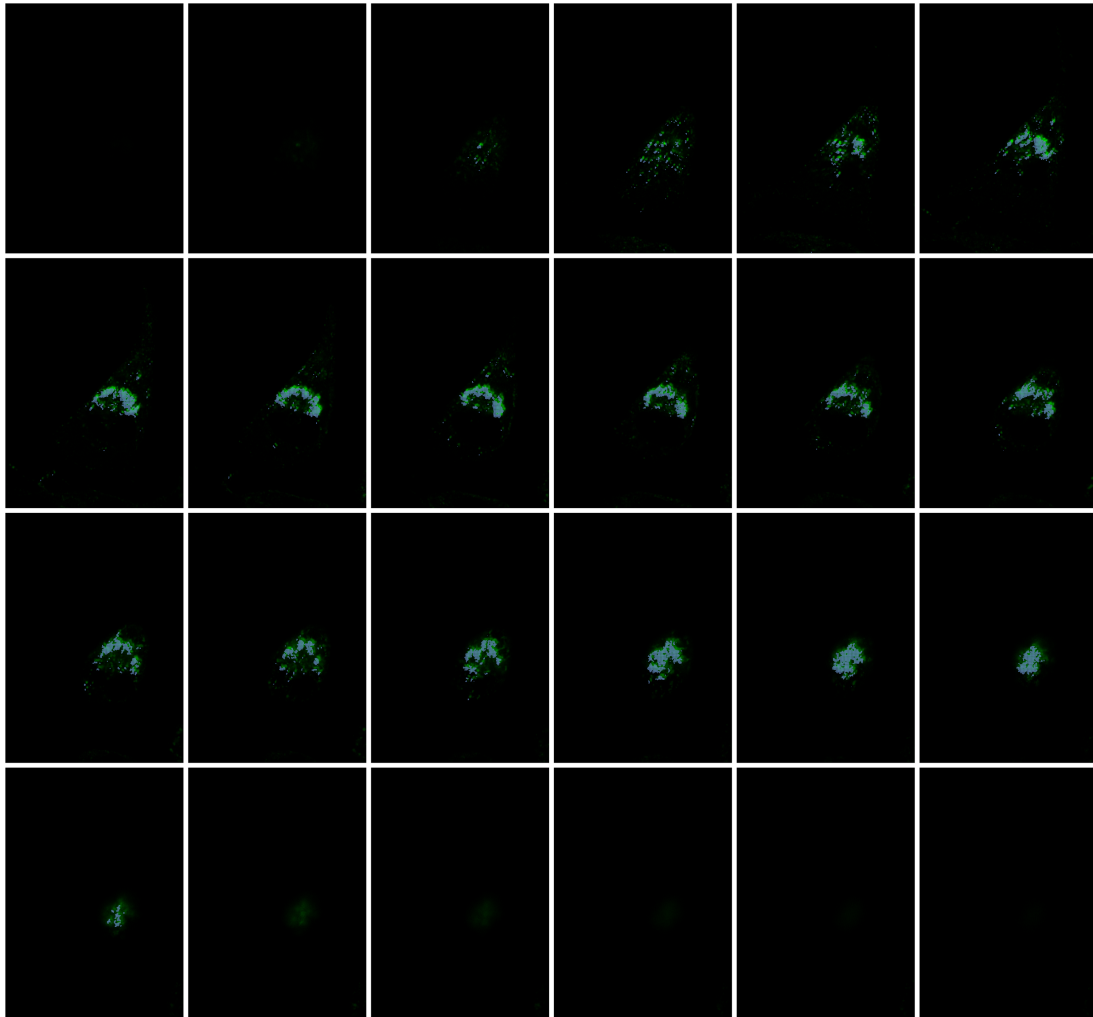
Figure A.15: Supplementary figure which depicts the overlay of accepted pixels and the original image for a pre-insulinic cell. Each image is 320×500 pixels which corresponds to a length of 42 μm and a height of 66 μm. The green pixels represent positive GLUT4-GFP signal while the light blue points represent a subset of these pixels that were subsequently assigned to clusters based on the methods described in Chapter 6.
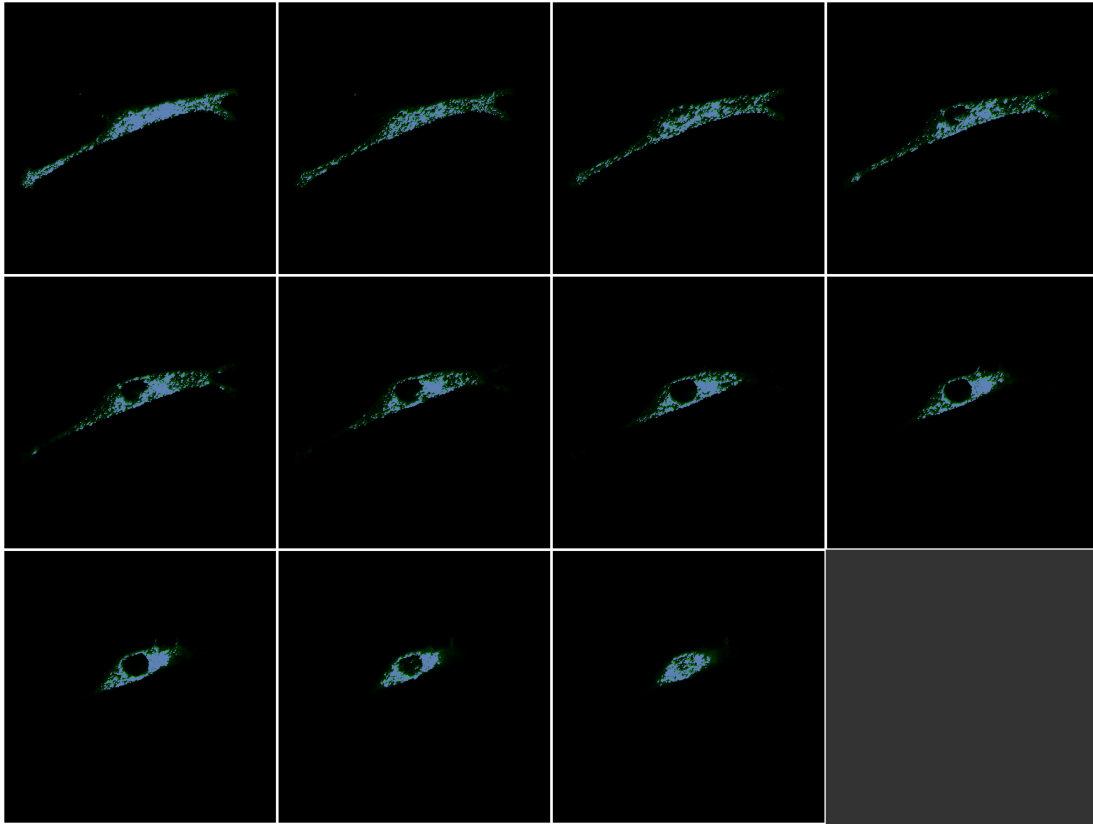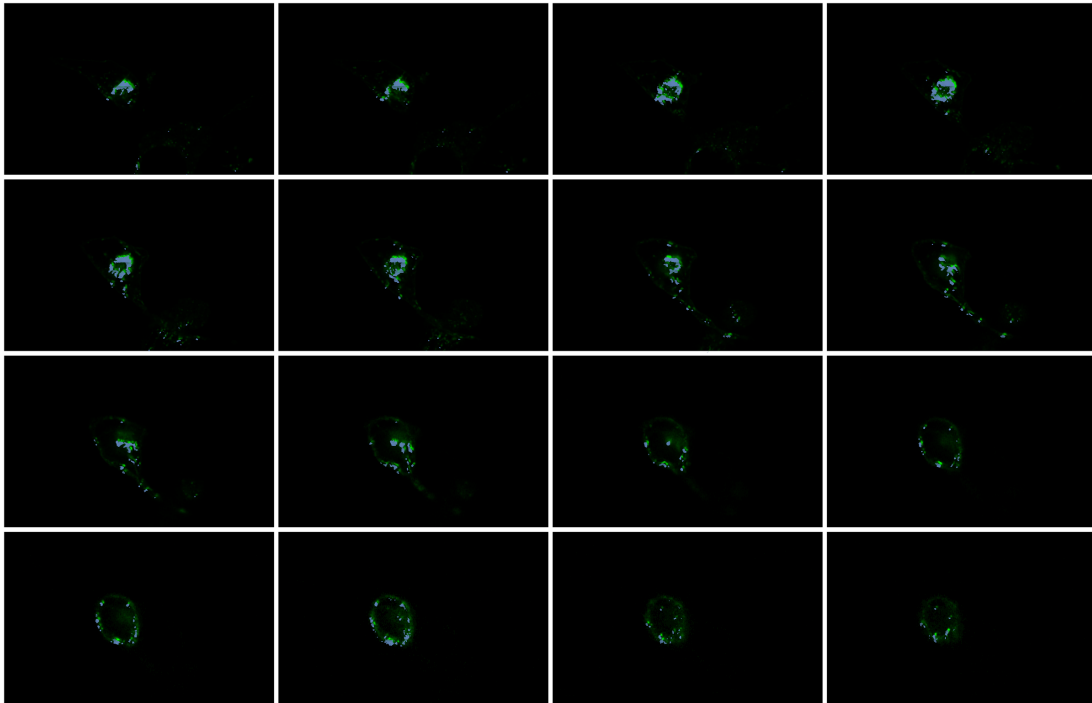
Figure A.16: Supplementary figure which depicts the overlay of accepted pixels and the original image for a pre-insulinic cell. Each image is 520 × 300 pixels which corresponds to a length of 68 μm and a height of 39 μm. The green pixels represent positive GLUT4-GFP signal while the light blue points represent a subset of these pixels that were subsequently assigned to clusters based on the methods described in Chapter 6.
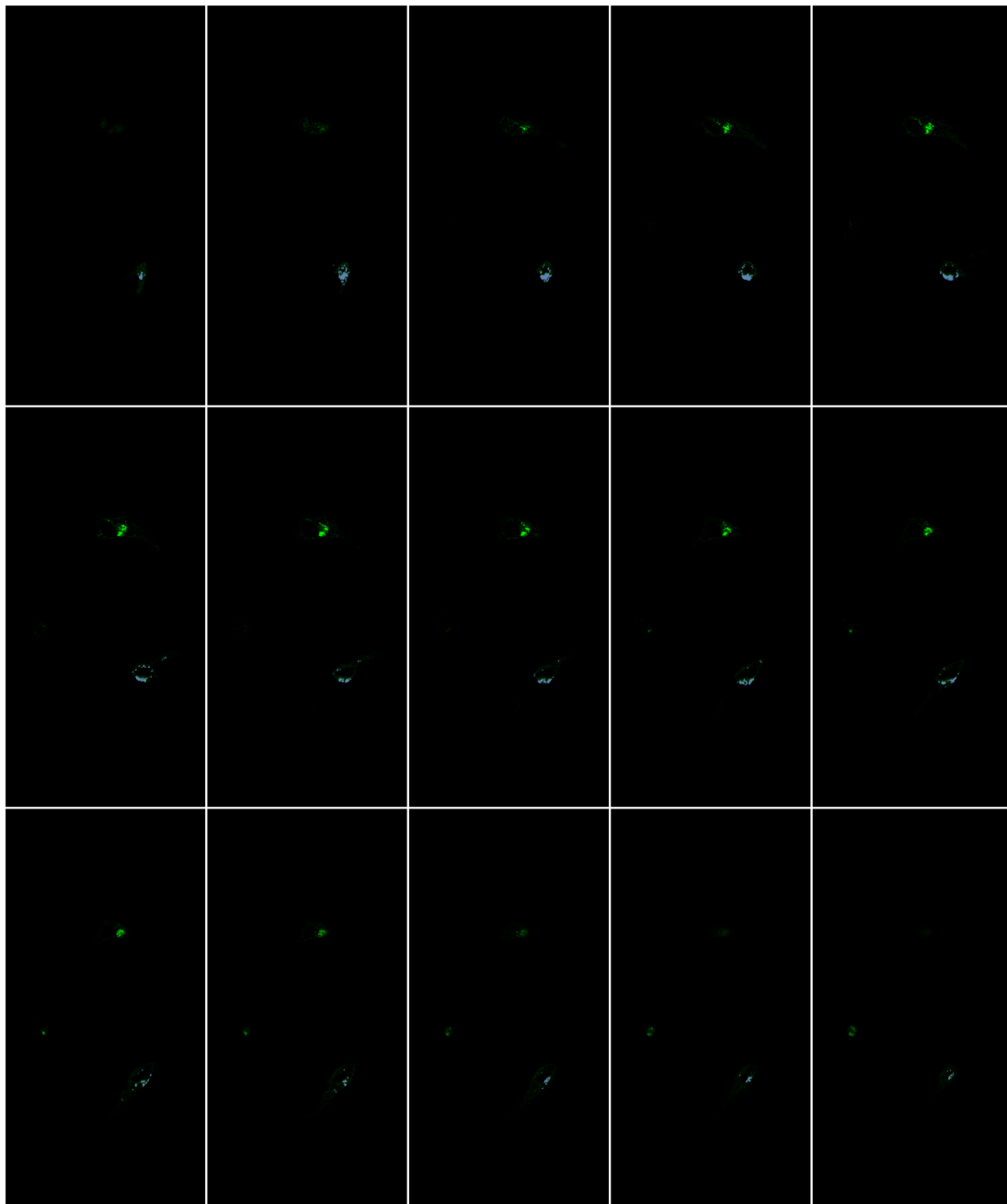
Figure A.17: Supplementary figure which depicts the overlay of accepted pixels and the original image for a pre-insulinic cell. Each image is 400 × 520 pixels which corresponds to a length of 52 μm and a height of 68 μm. The green pixels represent positive GLUT4-GFP signal while the light blue points represent a subset of these pixels that were subsequently assigned to clusters based on the methods described in Chapter 6.
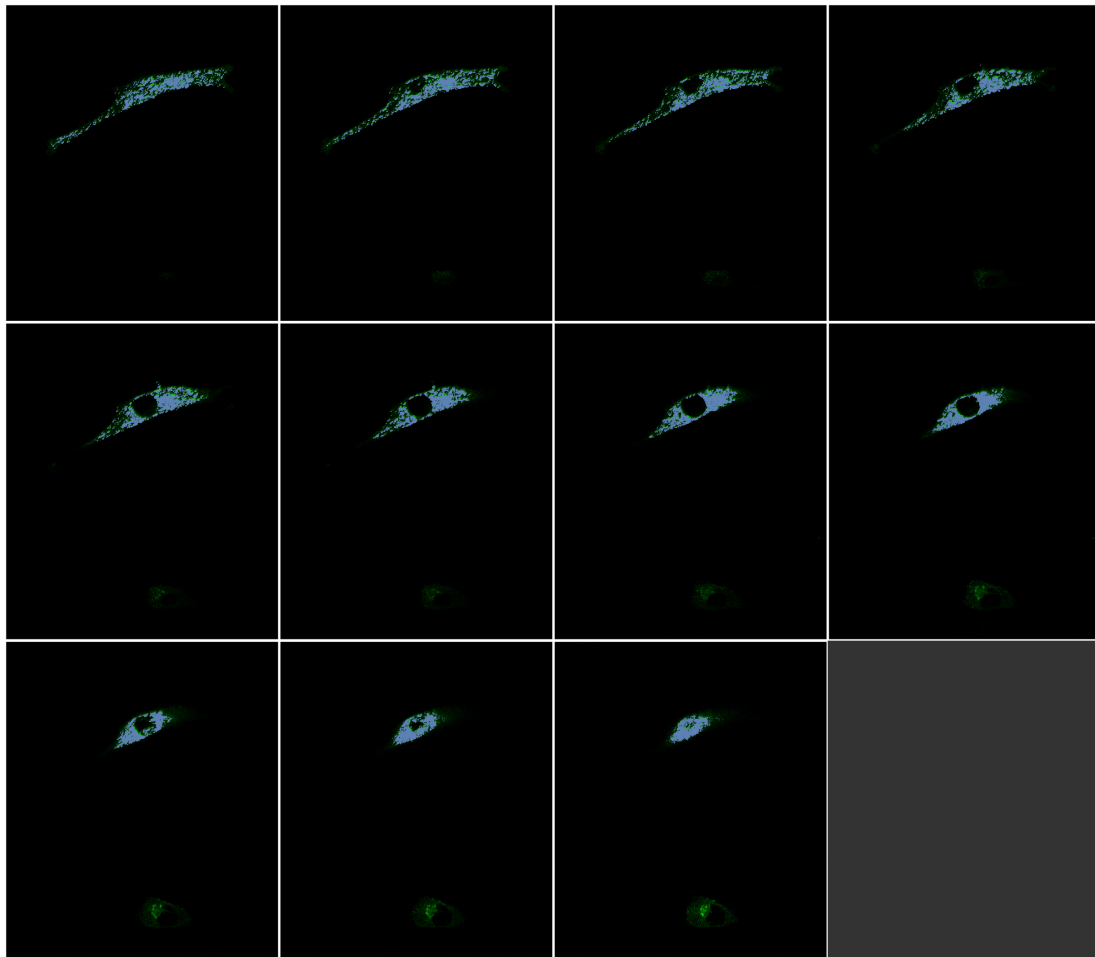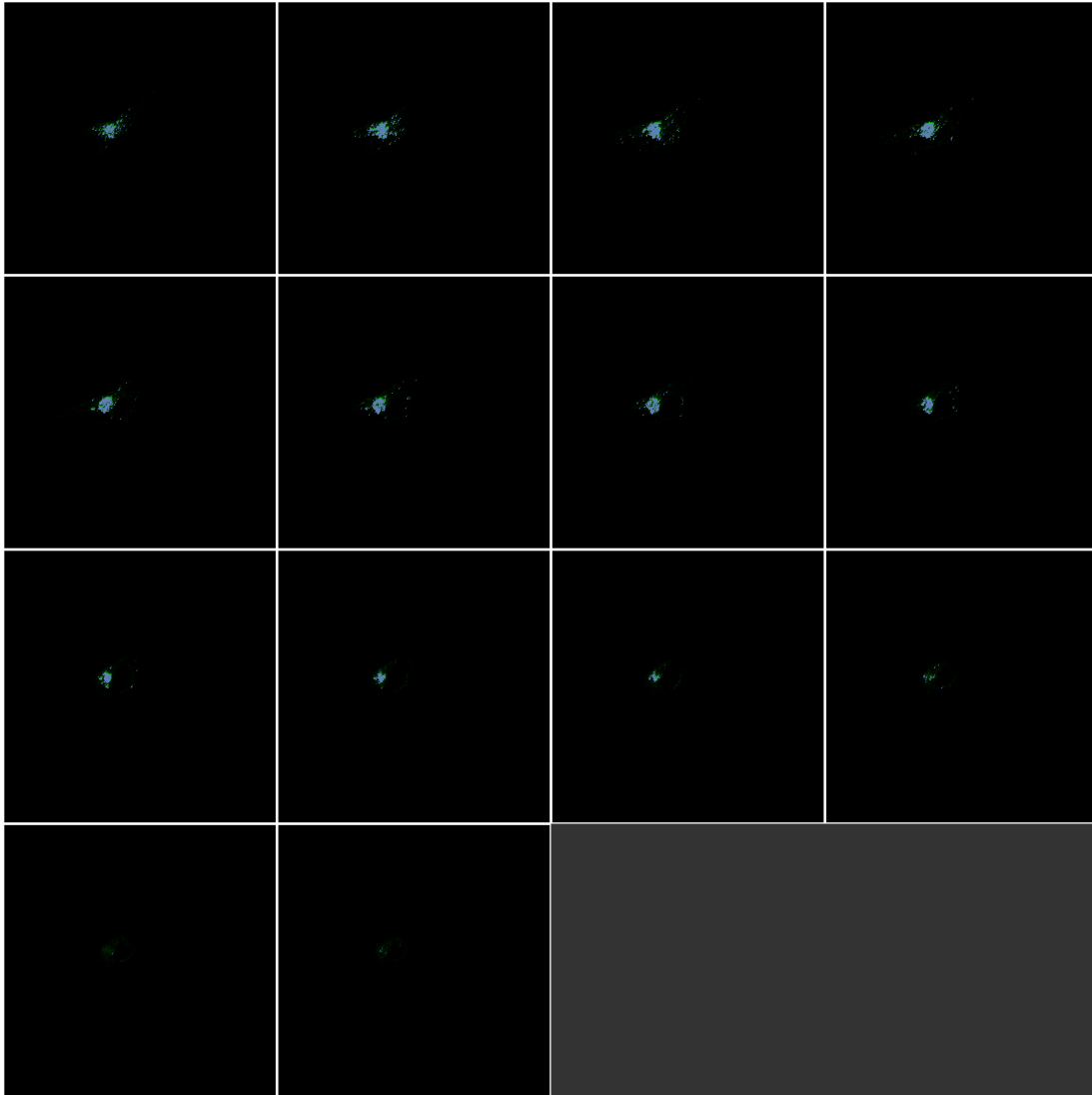
Figure A.18: Supplementary figure which depicts the overlay of accepted pixels and the original image for a pre-insulinic cell. Each image is 750×450 pixels which corresponds to a length of 98 μm and a height of 59 μm. The green pixels represent positive GLUT4-GFP signal while the light blue points represent a subset of these pixels that were subsequently assigned to clusters based on the methods described in Chapter 6.
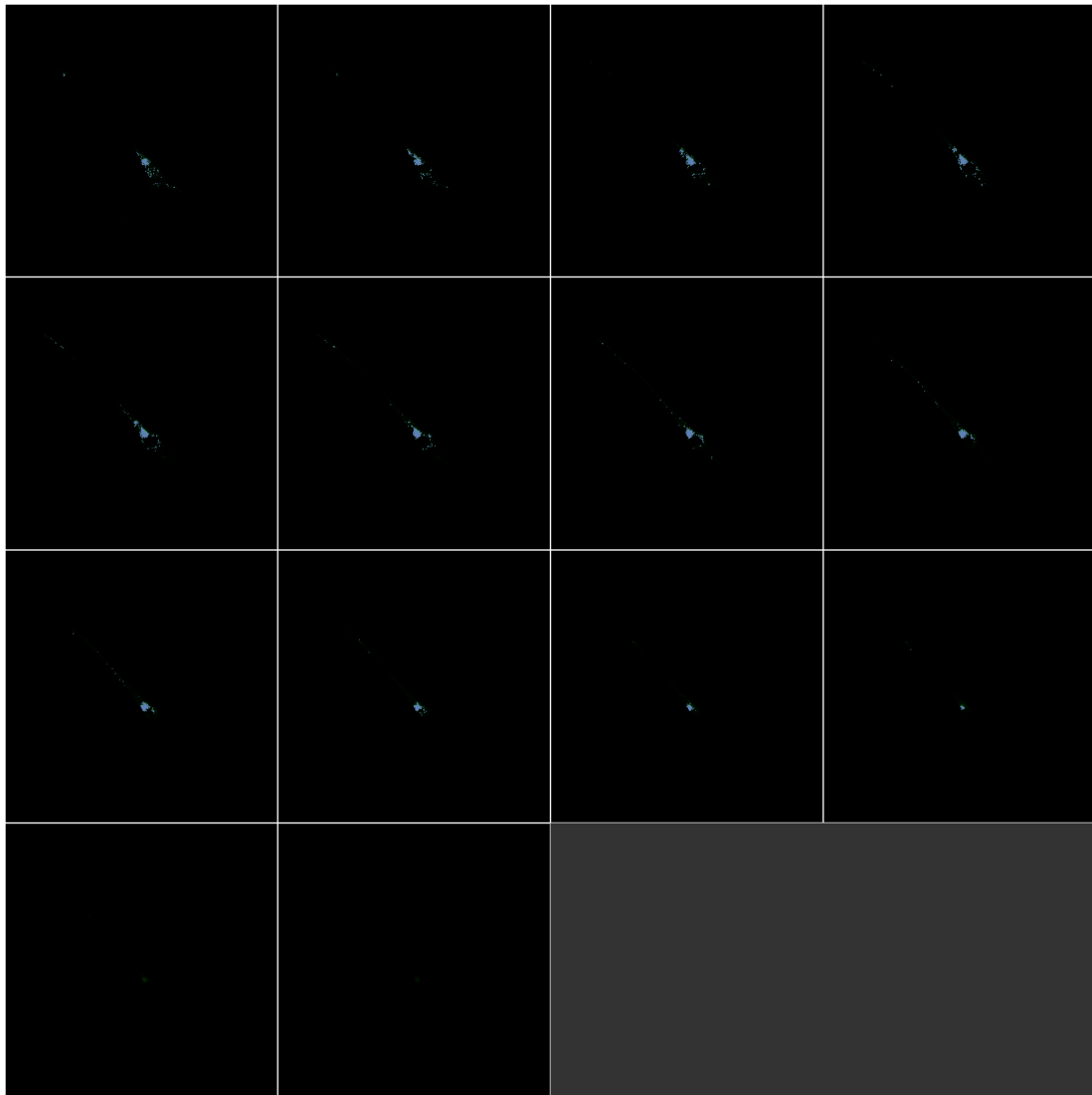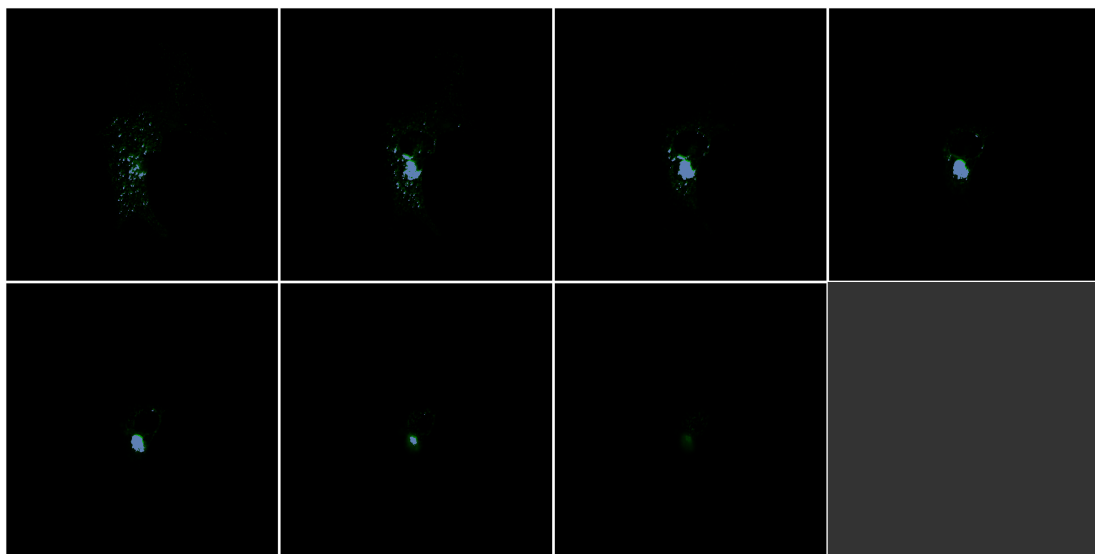
Figure A.19: Supplementary figure which depicts the overlay of accepted pixels and the original image for a pre-insulinic cell. Each image is 600×650 pixels which corresponds to a length of 79 μm and a height of 85 μm. The green pixels represent positive GLUT4-GFP signal while the light blue points represent a subset of these pixels that were subsequently assigned to clusters based on the methods described in Chapter 6.
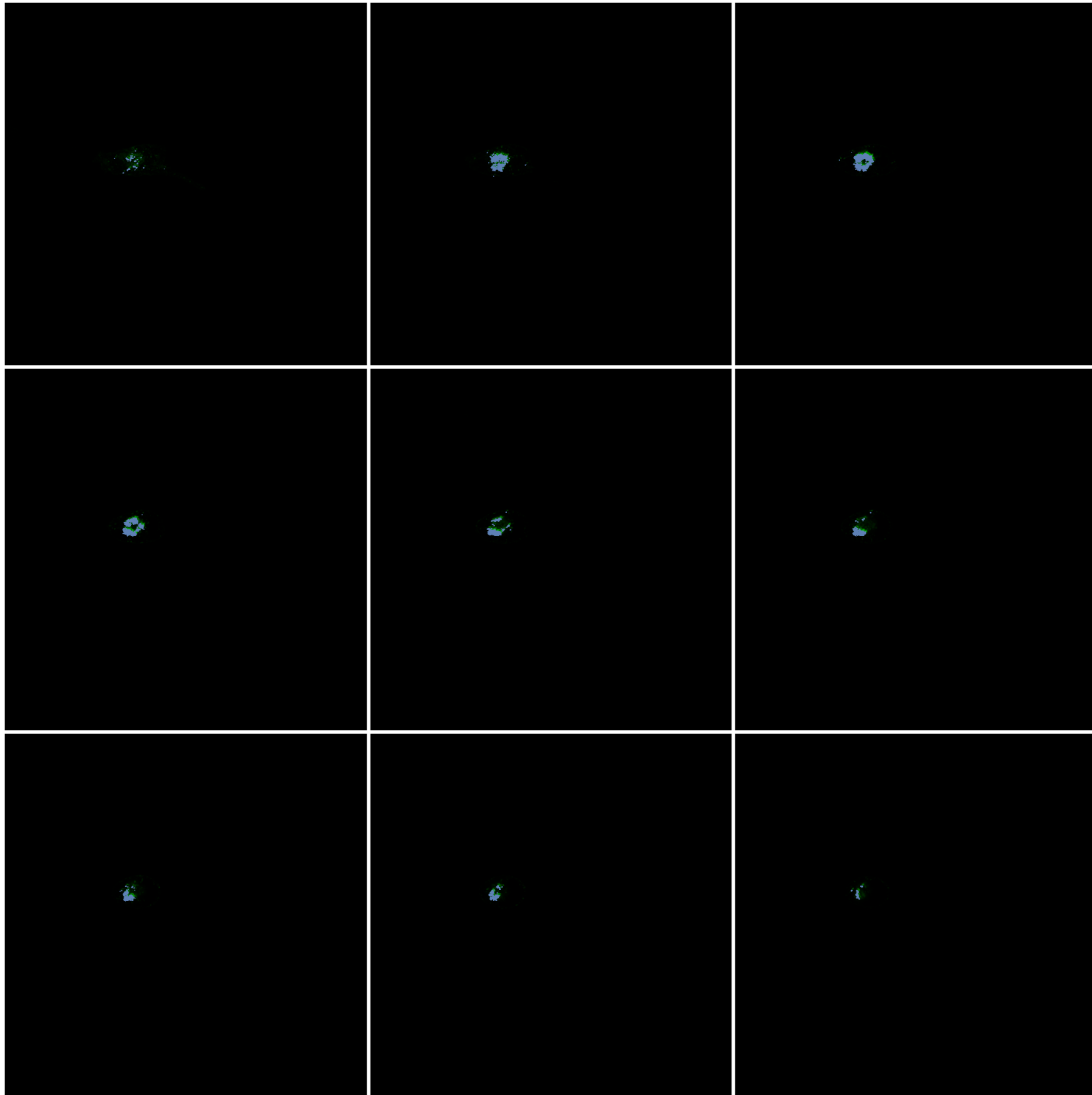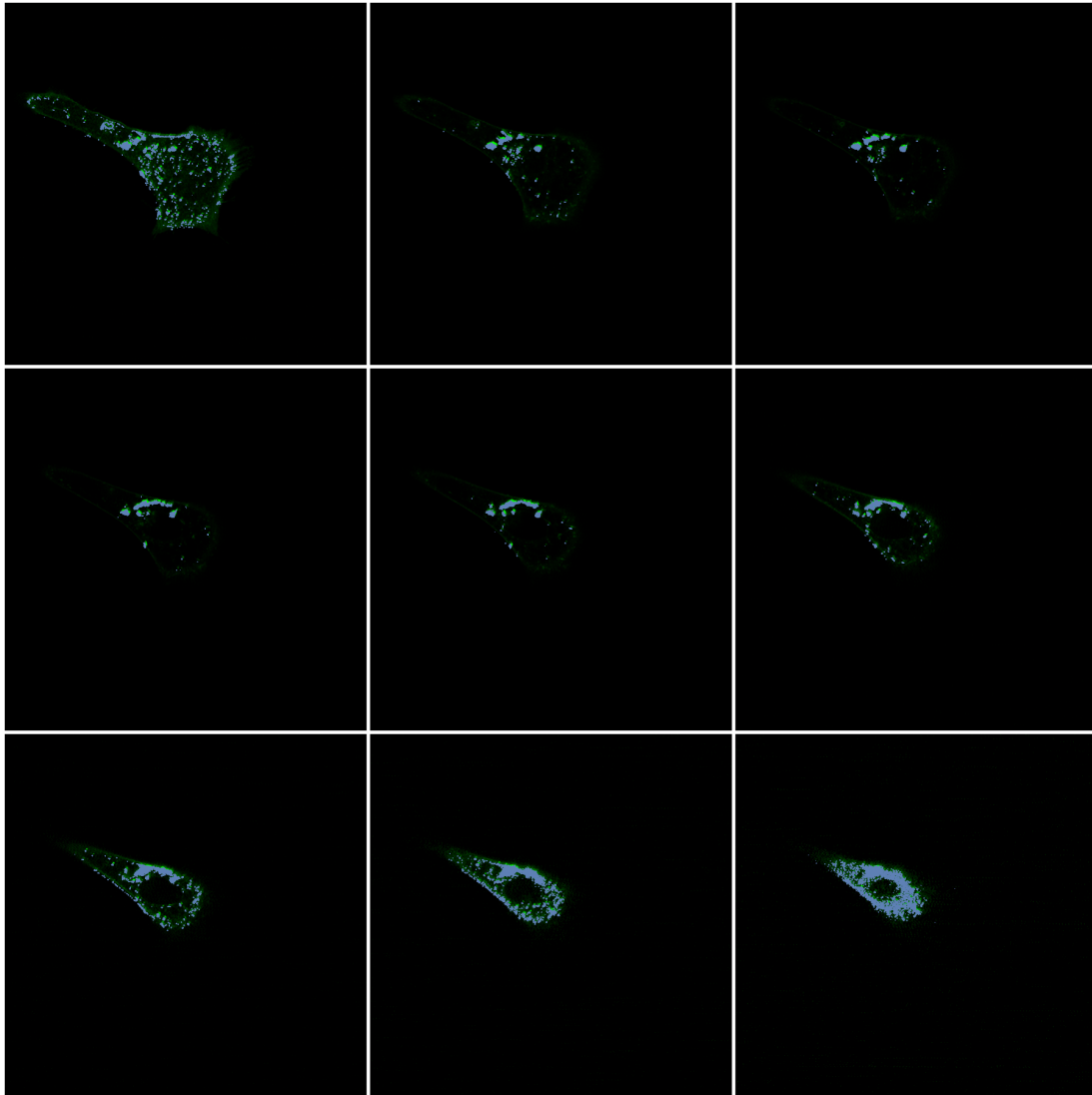
Figure A.20: Supplementary figure which depicts the overlay of accepted pixels and the original image for a pre-insulinic cell. Each image is 700×550 pixels which corresponds to a length of 92 μm and a height of 72 μm. The green pixels represent positive GLUT4-GFP signal while the light blue points represent a subset of these pixels that were subsequently assigned to clusters based on the methods described in Chapter 6.
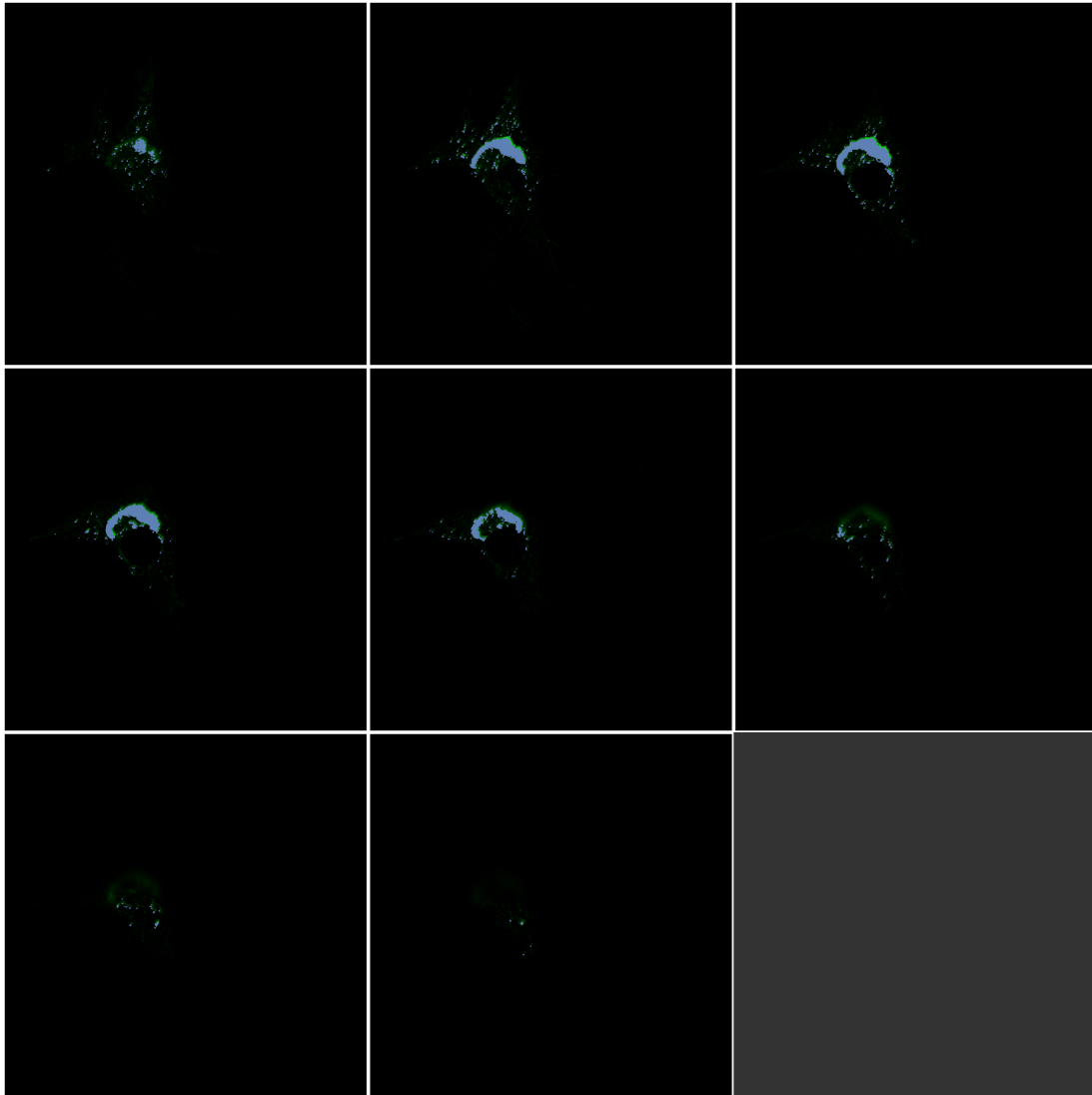
Figure A.21: Supplementary figure which depicts the overlay of accepted pixels and the original image for a pre-insulinic cell. Each image is 500×750 pixels which corresponds to a length of 66 μm and a height of μm. The green pixels represent positive GLUT4-GFP signal while the light blue points represent a subset of these pixels that were subsequently assigned to clusters based on the methods described in Chapter 6.
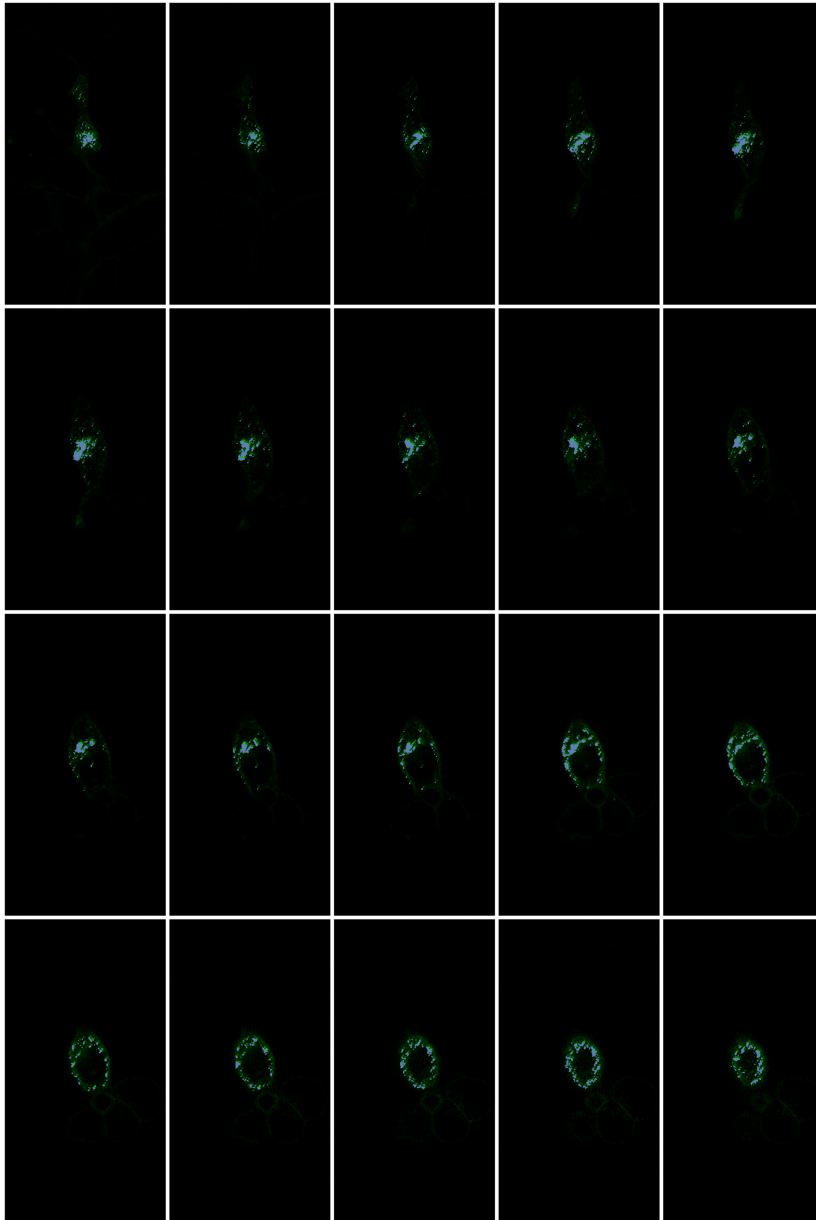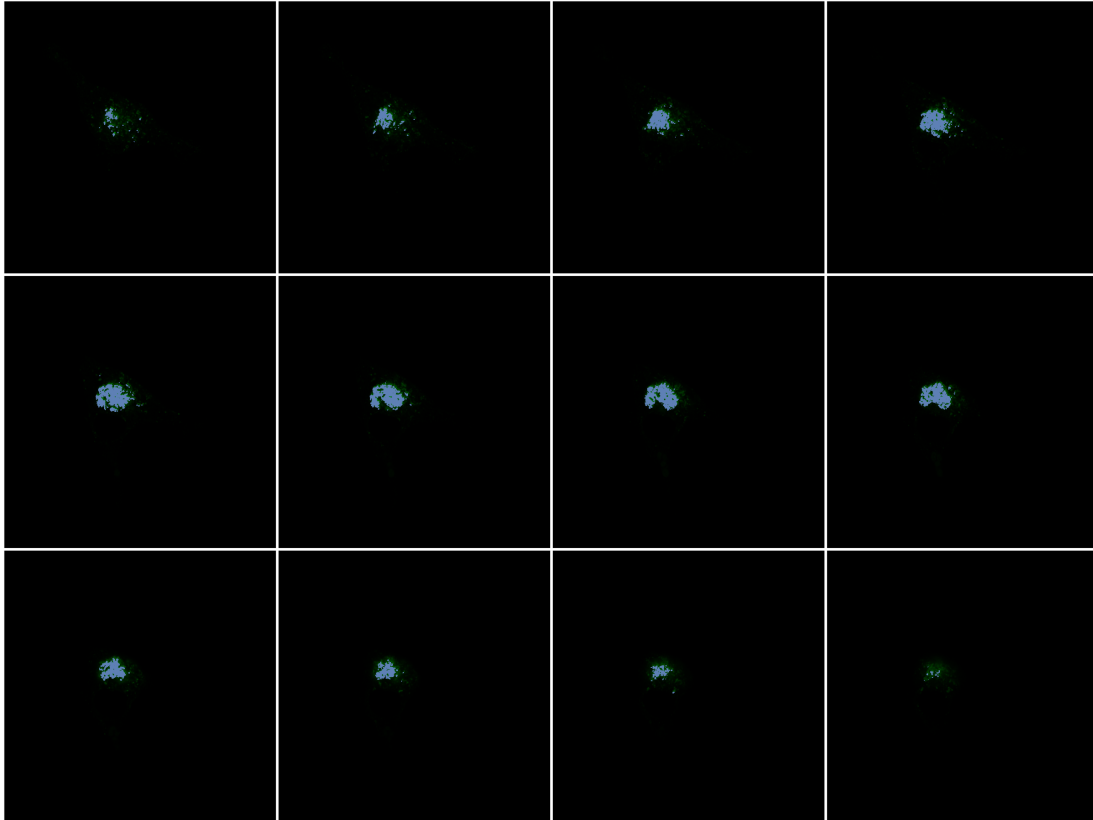
Figure A.22: Supplementary figure which depicts the overlay of accepted pixels and the original image for a pre-insulinic cell. Each image is 650×600 pixels which corresponds to a length of 85 μm and a height of 79 μm. The green pixels represent positive GLUT4-GFP signal while the light blue points represent a subset of these pixels that were subsequently assigned to clusters based on the methods described in Chapter 6.

Bibliography

[1]   Awad M Ahmed.   History of diabetes mellitus.   *Saudi medical journal*, 23(4):373–378, 2002.

[2]   M Notelovitz. Milestones in the history of diabetes-a brief survey. *South African Medical Journal*, 44(40):1158–1161, 1970.

[3]   JJ Meier, A Bhushan, AE Butler, RA Rizza, and PC Butler. Sustained beta cell apoptosis in patients with long-standing type 1 diabetes: indirect evidence for islet regeneration? *Diabetologia*, 48(11):2221–2228, 2005.

[4]   M. H. Shanik, Y. Xu, J. Skrha, R. Dankner, Y. Zick, and J. Roth. Insulin resistance and hyperinsulinemia: Is hyperinsulinemia the cart or the horse? *Diabetes Care*, 31(Supplement 2):S262–S268, jan 2008.

[5]   Wenhong Cao, Hui-Yu Liu, Tao Hong, and Zhenqi Liu. Excess exposure to insulin may be the primary cause of insulin resistance. *American Journal of Physiology-Endocrinology and Metabolism*, 298(2):E372–E372, feb 2010.

[6]   Ignazio Vecchio, Cristina Tornali, Nicola Luigi Bragazzi, and Mariano Martini. The discovery of insulin: an important milestone in the history of medicine. *Frontiers in endocrinology*, 9:613, 2018.

[7]   Louis Rosenfeld. Insulin: discovery and controversy.   *Clinical chemistry*, 48(12):2270–2288, 2002.

[8]   Paul Z Zimmet. Diabetes and its drivers: the largest epidemic in human history? *Clinical diabetes and endocrinology*, 3(1):1, 2017.

[9]   Yan Zheng, Sylvia H Ley, and Frank B Hu. Global aetiology and epidemiology of type 2 diabetes mellitus and its complications. *Nature Reviews Endocrinology*, 14(2):88, 2018.

[10]   Emilie Agardh, Peter Allebeck, Johan Hallqvist, Tahereh Moradi, and Anna Sidorchuk. Type 2 diabetes incidence and socio-economic position: a systematic review and meta-analysis. *International journal of epidemiology*, 40(3):804–818, 2011.

[11]   Lawrence De Koning, Vasanti S Malik, Eric B Rimm, Walter C Willett, and Frank B Hu. Sugar-sweetened and artificially sweetened beverage consumption and risk of type 2 diabetes in men. *The American journal of clinical nutrition*, 93(6):1321–1327, 2011.

[12]   Frank B Hu. Sedentary lifestyle and risk of obesity and type 2 diabetes. *Lipids*, 38(2):103–108, 2003.

[13]   Richard S Surwit, Mark S Schneider, and Mark N Feinglos. Stress and diabetes mellitus. *Diabetes care*, 15(10):1413–1422, 1992.

[14]   Masuma Novak, Lena Björck, Kok Wai Giang, Christina Heden-Ståhl, Lars Wilhelmsen, and Annika Rosengren. Perceived stress and incidence of type 2 diabetes: a 35-year follow-up study of middle-aged swedish men. *Diabetic medicine*, 30(1):e8–e16, 2013.

[15]   Till Seuring, Olga Archangelidi, and Marc Suhrcke. The economic costs of type 2 diabetes: a global systematic review. *Pharmacoeconomics*, 33(8):811–831, 2015.

[16]   Timothy M Dall, Yiduo Zhang, Yaozhu J Chen, William W Quick, Wenya G Yang, and Jeanene Fogli. The economic burden of diabetes. *Health affairs*, 29(2):297–303, 2010.

[17]   Susanne Röckl, Ralph Brinks, Jens Baumert, Rebecca Paprott, Yong Du, Christin Heidemann, and Christa Scheidt-Nave. All-cause mortality in adults

with and without type 2 diabetes: findings from the national health monitoring in germany. *BMJ Open Diabetes Research and Care*, 5(1):e000451, 2017.

[18] Mauro Tancredi, Annika Rosengren, Ann-Marie Svensson, Mikhail Kosiborod, Aldina Pivodic, Soffia Gudbjörnsdottir, Hans Wedel, Mark Clements, Sofia Dahlqvist, and Marcus Lind. Excess mortality among persons with type 2 diabetes. *New England Journal of Medicine*, 373(18):1720–1732, 2015.

[19] R. A. DeFronzo and D. Tripathy. Skeletal muscle insulin resistance is the primary defect in type 2 diabetes. *Diabetes Care*, 32(suppl_2):S157–S163, oct 2009.

[20] Jinzeng Yang. Enhanced skeletal muscle for effective glucose homeostasis. In *Progress in Molecular Biology and Translational Science*, pages 133–163. Elsevier, 2014.

[21] Pierre De Meyts. The insulin receptor and its signal transduction network. In *Endotext [Internet]*. MDText. com, Inc., 2016.

[22] Richard Mackenzie and Bradley Elliott. Akt/PKB activation and insulin signaling: a novel insulin signaling pathway in the treatment of type 2 diabetes. *Diabetes, Metabolic Syndrome and Obesity: Targets and Therapy*, page 55, feb 2014.

[23] Qinghua Wang, Romel Somwar, Philip J. Bilan, Zhi Liu, Jing Jin, James R. Woodgett, and Amira Klip. Protein kinase b/akt participates in GLUT4 translocation by insulin in l6 myoblasts. *Molecular and Cellular Biology*, 19(6):4008–4018, jun 1999.

[24] Ellen M. van Dam, Roland Govers, and David E. James. Akt activation is required at a late stage of insulin-induced GLUT4 translocation to the plasma membrane. *Molecular Endocrinology*, 19(4):1067–1077, apr 2005.

[25] P. Galante, L. Mosthaf, M. Kellerer, L. Berti, S. Tippmer, B. Bossenmaier, T. Fujiwara, A. Okuno, H. Horikoshi, and H. Ulrich Haring. Acute hyperglycemia

provides an insulin-independent inducer for GLUT4 translocation in c2c12 my-
otubes and rat skeletal muscle. *Diabetes*, 44(6):646–651, jun 1995.

[26] Ann Louise Olson. Regulation of GLUT4 and insulin-dependent glucose flux.
ISRN Molecular Biology, 2012:1–12, oct 2012.

[27] Makoto Kanzaki. Insulin receptor signals regulating glut4 translocation and
actin dynamics. *Endocrine journal*, 53(3):267–293, 2006.

[28] Emilie Vander Haar, Seong-il Lee, Sricharan Bandhakavi, Timothy J Griffin,
and Do-Hyung Kim. Insulin signalling to mtor mediated by the akt/pkb substrate
pras40. *Nature cell biology*, 9(3):316, 2007.

[29] Chunaram Choudhary and Matthias Mann. Decoding signalling networks by
mass spectrometry-based proteomics. *Nature reviews Molecular cell biology*,
11(6):427, 2010.

[30] Hiroyuki Sano, Susan Kane, Eiko Sano, Cristinel P Miinea, John M Asara,
William S Lane, Charles W Garner, and Gustav E Lienhard. Insulin-stimulated
phosphorylation of a rab gtpase-activating protein regulates glut4 translocation.
Journal of Biological Chemistry, 278(17):14599–14602, 2003.

[31] Jacqueline Stöckli, Daniel J Fazakerley, and David E James. Glut4 exocytosis.
J Cell Sci, 124(24):4147–4159, 2011.

[32] David B Savage, Kitt Falk Petersen, and Gerald I Shulman. Disordered lipid
metabolism and the pathogenesis of insulin resistance. *Physiological reviews*,
87(2):507–520, 2007.

[33] Chiara Dalla Man, Robert A Rizza, and Claudio Cobelli. Meal simulation model
of the glucose-insulin system. *IEEE Transactions on biomedical engineering*,
54(10):1740–1749, 2007.

[34] J.B. Van Dyk, J.L. Snoep, and D.D. Van Niekerk. Mathematical modelling of
glycolysis in skeletal muscle cells. 2020.

[35] Leona Plum, Bengt F Belgardt, Jens C Brüning, et al. Central insulin action in energy and glucose homeostasis. *The Journal of clinical investigation*, 116(7):1761–1766, 2006.

[36] S. L. Aronoff, K. Berkowitz, B. Shreiner, and L. Want. Glucose metabolism and regulation: Beyond insulin and glucagon. *Diabetes Spectrum*, 17(3):183–190, jul 2004.

[37] Satoshi Fujita, Blake B. Rasmussen, Jerson G. Cadenas, James J. Grady, and Elena Volpi. Effect of insulin on human skeletal muscle protein synthesis is modulated by insulin-induced changes in muscle blood flow and amino acid availability. *American Journal of Physiology-Endocrinology and Metabolism*, 291(4):E745–E754, oct 2006.

[38] Alan R Saltiel and C Ronald Kahn. Insulin signalling and the regulation of glucose and lipid metabolism. *Nature*, 414(6865):799–806, 2001.

[39] JF Wojtaszewski, Bo F Hansen, Bente Kiens, JF Markuns, LJ Goodyear, EA Richter, et al. Insulin signaling and insulin sensitivity after exercise in human skeletal muscle. *Diabetes*, 49(3):325–331, 2000.

[40] Arnold N. Onyango. Cellular stresses and stress responses in the pathogenesis of insulin resistance. *Oxidative Medicine and Cellular Longevity*, 2018:1–27, jul 2018.

[41] H Fukumoto, T Kayano, JB Buse, Y Edwards, PF Pilch, GI Bell, and S Seino. Cloning and characterization of the major insulin-responsive glucose transporter expressed in human skeletal muscle and other insulin-responsive tissues. *Journal of Biological Chemistry*, 264(14):7776–7779, 1989.

[42] Zhuo Fu, Elizabeth R Gilbert, and Dongmin Liu. Regulation of insulin synthesis and secretion and pancreatic beta-cell dysfunction in diabetes. *Current diabetes reviews*, 9(1):25–53, 2013.

[43] Reza Halse, Sylvie M Bonavaud, Jane L Armstrong, James G McCormack, and Stephen J Yeaman. Control of glycogen synthesis by glucose, glycogen, and insulin in cultured human muscle cells. *Diabetes*, 50(4):720–726, 2001.

[44] Jose M Lizcano and Dario R Alessi. The insulin signalling pathway. *Current biology*, 12(7):R236–R238, 2002.

[45] Anton JM Wagenmakers, Arend Bonen, G Lynis Dohm, and Luc JC van Loon. Lipid metabolism, exercise and insulin action. *Essays in biochemistry*, 42:47–59, 2006.

[46] Elaine D. O'Neill, John P. H. Wilding, C. Ronald Kahn, Holly Van Remmen, Anne McArdle, Malcolm J. Jackson, and Graeme L. Close. Absence of insulin signalling in skeletal muscle is associated with reduced muscle mass and function: evidence for decreased protein synthesis and not increased degradation. *AGE*, 32(2):209–222, jan 2010.

[47] Leslie J Saucedo, Xinsheng Gao, Dominic A Chiarelli, Ling Li, Duoija Pan, and Bruce A Edgar. Rheb promotes cell growth as a component of the insulin/tor signalling network. *Nature cell biology*, 5(6):566–571, 2003.

[48] Shidong Jia, Zhenning Liu, Sen Zhang, Pixu Liu, Lei Zhang, Sang Hyun Lee, Jing Zhang, Sabina Signoretti, Massimo Loda, Thomas M Roberts, et al. Essential roles of pi (3) k–p110β in cell growth, metabolism and tumorigenesis. *Nature*, 454(7205):776–779, 2008.

[49] Li Chen, Rui Chen, Hua Wang, and Fengxia Liang. Mechanisms linking inflammation to insulin resistance. *International Journal of Endocrinology*, 2015:1–9, 2015.

[50] Kanwal Rehman and Muhammad Sajid Hamid Akash. Mechanisms of inflammatory responses and development of insulin resistance: how are they interlinked? *Journal of Biomedical Science*, 23(1), dec 2016.

[51] Shu-Ling Chiu, Chih-Ming Chen, and Hollis T Cline. Insulin receptor signaling regulates synapse number, dendritic plasticity, and circuit function in vivo. *Neuron*, 58(5):708–719, 2008.

[52] William E Owen and William L Roberts. Cross-reactivity of three recombinant insulin analogs with five commercial insulin immunoassays. *Clinical chemistry*, 50(1):257–259, 2004.

[53] D L Horwitz, J I Starr, M E Mako, W G Blackard, and A H Rubenstein. Proinsulin, insulin, and c-peptide concentrations in human portal and peripheral blood. *Journal of Clinical Investigation*, 55(6):1278–1283, jun 1975.

[54] R. T. Kennedy, L. M. Kauri, G. M. Dahlgren, and S.-K. Jung. Metabolic oscillations in -cells. *Diabetes*, 51(Supplement 1):S152–S161, feb 2002.

[55] L. E. Fridlyand, N. Tamarina, and L. H. Philipson. Bursting and calcium oscillations in pancreatic β-cells: specific pacemakers for specific mechanisms. *American Journal of Physiology-Endocrinology and Metabolism*, 299(4):E517–E532, oct 2010.

[56] Bernard Thorens. GLUT2, glucose sensing and glucose homeostasis. *Diabetologia*, 58(2):221–232, nov 2014.

[57] Bo Hellman. Pulsatility of insulin release – a clinically important phenomenon. *Upsala Journal of Medical Sciences*, 114(4):193–205, dec 2009.

[58] Judith A. Bryans, Patricia A. Judd, and Peter R. Ellis. The effect of consuming instant black tea on postprandial plasma glucose and insulin concentrations in healthy humans. *Journal of the American College of Nutrition*, 26(5):471–477, oct 2007.

[59] S. Kapur, M. N. Groves, D. T. Zava, and S. Kapur. Postprandial insulin and triglycerides after different breakfast meal challenges: Use of finger stick capillary dried blood spots to study postprandial dysmetabolism. *Journal of Diabetes Science and Technology*, 4(2):236–243, mar 2010.

[60] Philip Felig and Vijay Soman. Insulin receptors in diabetes and other conditions. *The American Journal of Medicine*, 67(6):913–915, 1979.

[61] AP Osterop, RH Medema, JL Bos, GC vd Zon, DE Moller, JS Flier, W Möller, and JA Maassen. Relation between the insulin receptor number in cells, autophosphorylation and insulin-stimulated ras. gtp formation. *Journal of biological chemistry*, 267(21):14647–14653, 1992.

[62] Consuelo Calle, Begoña Maestro, and Moisés García-Arencibia. Genomic actions of 1,25-dihydroxyvitamin d3 on insulin receptor gene expression, insulin receptor number and insulin activity in the kidney, liver and adipose tissue of streptozotocin-induced diabetic rats. *BMC Molecular Biology*, 9(1):65, 2008.

[63] Antonino Belfiore, Roberta Malaguarnera, Veronica Vella, Michael C Lawrence, Laura Sciacca, Francesco Frasca, Andrea Morrione, and Riccardo Vigneri. Insulin receptor isoforms in physiology and disease: an updated view. *Endocrine reviews*, 38(5):379–431, 2017.

[64] J. L. Carpentier. Insulin receptor internalization: molecular mechanisms and physiopathological implications. *Diabetologia*, 37(S2):S117–S124, sep 1994.

[65] Harinda Rajapaksha and Briony E. Forbes. Ligand-binding affinity at the insulin receptor isoform-a and subsequent IR-a tyrosine phosphorylation kinetics are important determinants of mitogenic biological outcomes. *Frontiers in Endocrinology*, 6, jul 2015.

[66] Yang Chen, Lili Huang, Xinzhou Qi, and Chen Chen. Insulin receptor trafficking: Consequences for insulin sensitivity and diabetes. *International Journal of Molecular Sciences*, 20(20):5007, oct 2019.

[67] Alaide Morcavallo, Manuela Stefanello, Renato V. Iozzo, Antonino Belfiore, and Andrea Morrione. Ligand-mediated endocytosis and trafficking of the insulin-like growth factor receptor i and insulin receptor modulate receptor function. *Frontiers in Endocrinology*, 5, dec 2014.

[68] Jongsoon Lee, Masaya Miyasaki, and Steven E Shoelson. Insulin receptor activation with transmembrane domain ligands. *Diabetes*, 48(5):SA328–SA328, 2014.

[69] RA Kohanski. Insulin receptor autophosphorylation. i. autophosphorylation kinetics of the native receptor and its cytoplasmic kinase domain. *Biochemistry*, 32(22):5766–5772, 1993.

[70] Arthur Weiss and Joseph Schlessinger. Switching signals on or off by receptor dimerization. *Cell*, 94(3):277–280, aug 1998.

[71] JF Youngren. Regulation of insulin receptor function. *Cellular and Molecular Life Sciences*, 64(7-8):873, 2007.

[72] G Gorgisen, IM Gulacar, and ON Ozes. The role of insulin receptor substrate (irs) proteins in oncogenic transformation. *Cell Mol Biol (Noisy-le-grand)*, 63(1):1–5, 2017.

[73] G. Sesti, M. Federici, M.L. Hribal, D. Lauro, P. Sbraccia, , and R. Lauro. Defects of the insulin receptor substrate (irs) system in human metabolic disorders. *The FASEB Journal*, 15(12):2099–2111, 2001.

[74] Markus Schubert, Derek P Brazil, Deborah J Burks, Jake A Kushner, Jing Ye, Carrie L Flint, Janet Farhang-Fallah, Pieter Dikkes, Xavier M Warot, Carlos Rio, et al. Insulin receptor substrate-2 deficiency impairs brain growth and promotes tau phosphorylation. *Journal of Neuroscience*, 23(18):7084–7092, 2003.

[75] Susanne R Keller and Gustav E Lienhard. Insulin signalling: the role of insulin receptor substrate 1. *Trends in cell biology*, 4(4):115–119, 1994.

[76] Janet Farhang-Fallah, Varinder K. Randhawa, Anjaruwee Nimnual, Amira Klip, Dafna Bar-Sagi, and Maria Rozakis-Adcock. The pleckstrin homology (PH) domain-interacting protein couples the insulin receptor substrate 1 PH domain to insulin signaling pathways leading to mitogenesis and GLUT4 translocation. *Molecular and Cellular Biology*, 22(20):7325–7336, oct 2002.

[77] Xinxin Gao, Pamela R Lowry, Xin Zhou, Charlene Depry, Zhikui Wei, G William Wong, and Jin Zhang. Pi3k/akt signaling requires spatial compartmentalization in plasma membrane microdomains. *Proceedings of the National Academy of Sciences*, 108(35):14509–14514, 2011.

[78] Klaus Scheffzek and Stefan Welti. Pleckstrin homology (ph) like domains–versatile modules in protein–protein interaction platforms. *FEBS letters*, 586(17):2662–2673, 2012.

[79] Martin G Myers Jr and Morris F White. Insulin signal transduction and the irs proteins. *Annual review of pharmacology and toxicology*, 36(1):615–658, 1996.

[80] Sigalit Boura-Halfon and Yehiel Zick. Phosphorylation of irs proteins, insulin action, and insulin resistance. *American Journal of Physiology-Endocrinology and Metabolism*, 296(4):E581–E591, 2009.

[81] Katerina Mardilovich, Shannon L Pankratz, and Leslie M Shaw. Expression and function of the insulin receptor substrate proteins in cancer. *Cell Communication and Signaling*, 7(1):14, 2009.

[82] KD Copps and MF White. Regulation of insulin sensitivity by serine/threonine phosphorylation of insulin receptor substrate proteins irs1 and irs2. *Diabetologia*, 55(10):2565–2582, 2012.

[83] Moulun Luo, Paul Langlais, Zhengping Yi, Natalie Lefort, Elena A. De Filippis, Hyonson Hwang, Christine Y. Christ-Roberts, and Lawrence J. Mandarino. Phosphorylation of human insulin receptor substrate-1 at serine 629 plays a positive role in insulin signaling. *Endocrinology*, 148(10):4895–4905, oct 2007.

[84] Hagit Eldar-Finkelman and Edwin G Krebs. Phosphorylation of insulin receptor substrate 1 by glycogen synthase kinase 3 impairs insulin action. *Proceedings of the National Academy of Sciences*, 94(18):9660–9664, 1997.

[85] Katsutaro Morino, Kitt Falk Petersen, Sylvie Dufour, Douglas Befroy, Jared Frattini, Nadine Shatzkes, Susanne Neschen, Morris F White, Stefan Bilz, Saki

Sono, et al. Reduced mitochondrial density and increased irs-1 serine phosphorylation in muscle of insulin-resistant offspring of type 2 diabetic parents. *The Journal of clinical investigation*, 115(12):3587–3593, 2005.

[86] Terry M Pederson, Deborah L Kramer, and Cristina M Rondinone. Serine/threonine phosphorylation of irs-1 triggers its degradation: possible regulation by tyrosine phosphorylation. *Diabetes*, 50(1):24–31, 2001.

[87] Steve Jean and Amy A Kiger. Classes of phosphoinositide 3-kinases at a glance, 2014.

[88] S.J. Shuttleworth, F.A. Silva, A.R.L. Cecil, C.D. Tomassi, T.J. Hill, F.I. Raynaud, P.A. Clarke, and P. Workman. Progress in the preclinical discovery and clinical development of class i and dual class i/iv phosphoinositide 3-kinase (pi3k) inhibitors. *Current medicinal chemistry*, 18(18):2686–2714, 2011.

[89] Fiona M Foster, Colin J Traer, Siemon M Abraham, and Michael J Fry. The phosphoinositide (pi) 3-kinase family. *Journal of cell science*, 116(15):3037–3040, 2003.

[90] Pixu Liu, Hailing Cheng, Thomas M Roberts, and Jean J Zhao. Targeting the phosphoinositide 3-kinase pathway in cancer. *Nature reviews Drug discovery*, 8(8):627–644, 2009.

[91] Brendan D Manning and Alex Toker. Akt/pkb signaling: navigating the network. *Cell*, 169(3):381–405, 2017.

[92] Lauren M Thorpe, Haluk Yuzugullu, and Jean J Zhao. Pi3k in cancer: divergent roles of isoforms, modes of activation and therapeutic targeting. *Nature Reviews Cancer*, 15(1):7–24, 2015.

[93] Tania Maffucci, Frank T Cooke, Fiona M Foster, Colin J Traer, Michael J Fry, and Marco Falasca. Class ii phosphoinositide 3-kinase defines a novel signaling pathway in cell migration. *The Journal of cell biology*, 169(5):789–799, 2005.

[94] Kazuaki Yoshioka, Kotaro Yoshida, Hong Cui, Tomohiko Wakayama, Noriko Takuwa, Yasuo Okamoto, Wa Du, Xun Qi, Ken Asanuma, Kazushi Sugihara, et al. Endothelial pi3k-c2α, a class ii pi3k, has an essential role in angiogenesis and vascular barrier function. *Nature medicine*, 18(10):1560, 2012.

[95] Nadia Jaber, Zhixun Dou, Juei-Suei Chen, Joseph Catanzaro, Ya-Ping Jiang, Lisa M Ballou, Elzbieta Selinger, Xiaosen Ouyang, Richard Z Lin, Jianhua Zhang, et al. Class iii pi3k vps34 plays an essential role in autophagy and in heart and liver function. *Proceedings of the National Academy of Sciences*, 109(6):2003–2008, 2012.

[96] Bruce D Cuevas, Yiling Lu, Muling Mao, Jinyi Zhang, Ruth LaPushin, Kathy Siminovitch, and Gordon B Mills. Tyrosine phosphorylation of p85 relieves its inhibitory activity on phosphatidylinositol 3-kinase. *Journal of Biological Chemistry*, 276(29):27455–27461, 2001.

[97] Jonathan M Backer, Martin G Myers Jr, Steven E Shoelson, Debra J Chin, Xiao Jian Sun, Montserrat Miralpeix, Patrick Hu, Benjamin Margolis, Edward Y Skolnik, and Jea Schlessinger. Phosphatidylinositol 3-kinase is activated by association with irs-1 during insulin stimulation. *The EMBO journal*, 11(9):3469–3479, 1992.

[98] Igor Vivanco and Charles L Sawyers. The phosphatidylinositol 3-kinase–akt pathway in human cancer. *Nature Reviews Cancer*, 2(7):489, 2002.

[99] Nobuo Tsuboi, Tadahiko Utsunomiya, Richard L Roberts, Hideyuki Ito, Keiko Takahashi, Masaharu Noda, and Takamune Takahashi. The tyrosine phosphatase cd148 interacts with the p85 regulatory subunit of phosphoinositide 3-kinase. *Biochemical Journal*, 413(1):193–200, 2008.

[100] Sandra B Gabelli, Diana Mandelker, Oleg Schmidt-Kittler, Bert Vogelstein, and L Mario Amzel. Somatic mutations in pi3kα: Structural basis for enzyme activation and drug design. *Biochimica et Biophysica Acta (BBA)-Proteins and Proteomics*, 1804(3):533–540, 2010.

[101] Doreen Ann Cantrell. Phosphoinositide 3-kinase signalling pathways. *Journal of cell science*, 114(8):1439–1445, 2001.

[102] Bart Vanhaasebroeck and Dario R Alessi. The pi3k–pdk1 connection: more than just a road to pkb. *Biochemical Journal*, 346(3):561–576, 2000.

[103] Byung-Chang Suh and Bertil Hille. Pip2 is a necessary cofactor for ion channel function: how and why? *Annu. Rev. Biophys.*, 37:175–195, 2008.

[104] Matthias P Wymann and Luciano Pirola. Structure and function of phosphoinositide 3-kinases. *Biochimica et Biophysica Acta (BBA)-Molecular and Cell Biology of Lipids*, 1436(1-2):127–150, 1998.

[105] Shi-Xiong Tan, Yvonne Ng, James G Burchfield, Georg Ramm, David G Lambright, Jacqueline Stöckli, and David E James. The rab gtpase-activating protein tbc1d4/as160 contains an atypical phosphotyrosine-binding domain that interacts with plasma membrane phospholipids to facilitate glut4 trafficking in adipocytes. *Molecular and cellular biology*, 32(24):4946–4959, 2012.

[106] Tung O Chan, Susan E Rittenhouse, and Philip N Tsichlis. Akt/pkb and other d3 phosphoinositide-regulated kinases: kinase activation by phosphoinositide-dependent phosphorylation. *Annual review of biochemistry*, 68(1):965–1014, 1999.

[107] Louise Chang, Shian-Huey Chiang, and AR Saltlel. Insulin signaling and the regulation of glucose transport. *Molecular medicine*, 10(7-12):65–71, 2004.

[108] Manabu Ishiki, Varinder K Randhawa, Vincent Poon, Lellean JeBailey, and Amira Klip. Insulin regulates the membrane arrival, fusion, and c-terminal unmasking of glucose transporter-4 via distinct phosphoinositides. *Journal of Biological Chemistry*, 280(31):28792–28802, 2005.

[109] Hugo Stocker, Mirjana Andjelkovic, Sean Oldham, Muriel Laffargue, Matthias P Wymann, Brian A Hemmings, and Ernst Hafen. Living with lethal

pip3 levels: viability of flies lacking pten restored by a ph domain mutation in akt/pkb. *Science*, 295(5562):2088–2091, 2002.

[110] Takeshi Ijuin and Tadaomi Takenawa. Regulation of insulin signaling and glucose transporter 4 (glut4) exocytosis by phosphatidylinositol 3, 4, 5-trisphosphate (pip3) phosphatase, skeletal muscle, and kidney enriched inositol polyphosphate phosphatase (skip). *Journal of Biological Chemistry*, 287(10):6991–6999, 2012.

[111] Lewis C Cantley. The phosphoinositide 3-kinase pathway. *Science*, 296(5573):1655–1657, 2002.

[112] Yingke Xu, Di Nan, Jiannan Fan, Jonathan S Bogan, and Derek Toomre. Optogenetic activation reveals distinct roles of pip3 and akt in adipocyte insulin action. *Journal of cell science*, 129(10):2085–2095, 2016.

[113] Peter Storz and Alex Toker. 3â²-phosphoinositide-dependent kinase-1 (pdk-1) in pi 3-kinase signaling. *Front Biosci*, 7:d886–902, 2002.

[114] Michael P Czech. Pip2 and pip3: complex roles at the cell surface. *Cell*, 100(6):603–606, 2000.

[115] Tetsuya Yamada, Hideki Katagiri, Tomoichiro Asano, Masatoshi Tsuru, Kouichi Inukai, Hiraku Ono, Tatsuhiko Kodama, Masatoshi Kikuchi, and Yoshitomo Oka. Role of pdk1 in insulin-signaling pathway for glucose metabolism in 3t3-l1 adipocytes. *American Journal of Physiology-Endocrinology and Metabolism*, 282(6):E1385–E1394, 2002.

[116] Thomas Harris. Pdk1 and pkb/akt: ideal targets for development of new strategies to structure-based drug design. *IUBMB life*, 55(3):117–126, 2003.

[117] Lily Q Dong and Feng Liu. Pdk2: the missing piece in the receptor tyrosine kinase signaling pathway puzzle. *American Journal of Physiology-Endocrinology And Metabolism*, 289(2):E187–E196, 2005.

[118] Michael J Wick, Lily Q Dong, Ramon A Riojas, Fresnida J Ramos, and Feng Liu. Mechanism of phosphorylation of protein kinase b/akt by a constitutively active 3-phosphoinositide-dependent protein kinase-1. *Journal of Biological Chemistry*, 275(51):40400–40406, 2000.

[119] Margaret A Lawlor, Alfonso Mora, Peter R Ashby, Michayla R Williams, Victoria Murray-Tait, Lorraine Malone, Alan R Prescott, John M Lucocq, and Dario R Alessi. Essential role of pdk1 in regulating cell size and development in mice. *The EMBO journal*, 21(14):3728–3738, 2002.

[120] Jose R Bayascas, Stephan Wullschleger, Kei Sakamoto, Juan M Garcia-Martinez, Carol Clacher, David Komander, Daan MF Van Aalten, Krishna M Boini, Florian Lang, Christopher Lipina, et al. Mutation of the pdk1 ph domain inhibits protein kinase b/akt, leading to small size and insulin resistance. *Molecular and cellular biology*, 28(10):3258–3272, 2008.

[121] Kyota Aoyagi, Mica Ohara-Imaizumi, Chiyono Nishiwaki, Yoko Nakamichi, Kohjiro Ueki, Takashi Kadowaki, and Shinya Nagamatsu. Acute inhibition of pi3k-pdk1-akt pathway potentiates insulin secretion through upregulation of newcomer granule fusions in pancreatic β-cells. *PloS one*, 7(10), 2012.

[122] Alfonso Mora, Christopher Lipina, François Tronche, Calum Sutherland, and Dario R Alessi. Deficiency of pdk1 in liver results in glucose intolerance, impairment of insulin-regulated gene expression and liver failure. *Biochemical Journal*, 385(3):639–648, 2005.

[123] Naoko Hashimoto, Yoshiaki Kido, Tohru Uchida, Shun-ichiro Asahara, Yutaka Shigeyama, Tomokazu Matsuda, Akihiko Takeda, Daisuke Tsuchihashi, Akihiko Nishizawa, Wataru Ogawa, et al. Ablation of pdk1 in pancreatic β cells induces diabetes as a result of loss of β cell mass. *Nature genetics*, 38(5):589–593, 2006.

[124] Eric Hajduch, Gary J Litherland, and Harinder S Hundal. Protein kinase b

(pkb/akt)–a key regulator of glucose transport? *FEBS letters*, 492(3):199–203, 2001.

[125] Masahito Hanada, Jianhua Feng, and Brian A Hemmings. Structure, regulation and function of pkb/akt—a major therapeutic target. *Biochimica et Biophysica Acta (BBA)-Proteins and Proteomics*, 1697(1-2):3–16, 2004.

[126] Brendan D Manning. Balancing akt with s6k: implications for both metabolic diseases and tumorigenesis. *J cell biol*, 167(3):399–403, 2004.

[127] Vanessa S Rodrik-Outmezguine, Sarat Chandarlapaty, Nen C Pagano, Poulikos I Poulikakos, Maurizio Scaltriti, Elizabeth Moskatel, José Baselga, Sylvie Guichard, and Neal Rosen. mtor kinase inhibition causes feedback-dependent biphasic regulation of akt signaling. *Cancer discovery*, 1(3):248–259, 2011.

[128] EE Vincent, DJE Elder, EC Thomas, L Phillips, C Morgan, J Pawade, M Sohail, MT May, MR Hetzel, and JM Tavare. Akt phosphorylation on thr308 but not on ser473 correlates with akt protein kinase activity in human non-small cell lung cancer. *British journal of cancer*, 104(11):1755–1761, 2011.

[129] Lakshmipathi Vadlakonda, Abhinandita Dash, Mukesh Pasupuleti, Anil Kumar Kotha, and Pallu Reddanna. The paradox of akt-mtor interactions. *Frontiers in oncology*, 3:165, 2013.

[130] Zhiyong Ding, Jiyong Liang, Jin Li, Yiling Lu, Vathsala Ariyaratna, Zhimin Lu, Michael A Davies, John K Westwick, and Gordon B Mills. Physical association of pdk1 with akt1 is sufficient for pathway activation independent of membrane localization and phosphatidylinositol 3 kinase. *PloS one*, 5(3):e9910, 2010.

[131] Keyong Du and Philip N Tsichlis. Regulation of the akt kinase by interacting proteins. *Oncogene*, 24(50):7401–7409, 2005.

[132] Dario R Alessi, Laura R Pearce, and Juan M Garcia-Martinez. New insights into mtor signaling: mtorc2 and beyond. *Science signaling*, 2(67):pe27–pe27, 2009.

[133] Xian-Guo Chen, Fei Liu, Xing-Fu Song, Zhi-Hua Wang, Zi-Qiang Dong, Zhi-Quan Hu, Ru-Zhu Lan, Wei Guan, Tian-Gui Zhou, Xiao-Ming Xu, et al. Rapamycin regulates akt and erk phosphorylation through mtorc1 and mtorc2 signaling pathways. *Molecular Carcinogenesis: Published in cooperation with the University of Texas MD Anderson Cancer Center*, 49(6):603–610, 2010.

[134] Samantha F Moore, Roger W Hunter, and Ingeborg Hers. mtorc2 protein-mediated protein kinase b (akt) serine 473 phosphorylation is not required for akt1 activity in human platelets. *Journal of Biological Chemistry*, 286(28):24553–24560, 2011.

[135] Itamar Levinger, Kirsten F Howlett, Jonathan Peake, Andrew Garnham, David L Hare, George Jerums, Steve Selig, and Craig Goodman. Akt, as160, metabolic risk factors and aerobic fitness in middle-aged women. *Exercise immunology review*, 16:98–104, 2010.

[136] Henning F Kramer, Carol A Witczak, Nobuharu Fujii, Niels Jessen, Eric B Taylor, David E Arnolds, Kei Sakamoto, Michael F Hirshman, and Laurie J Goodyear. Distinct signals regulate as160 phosphorylation in response to insulin, aicar, and contraction in mouse skeletal muscle. *Diabetes*, 55(7):2067–2076, 2006.

[137] Prashanth T Bhaskar and Nissim Hay. The two torcs and akt. *Developmental cell*, 12(4):487–502, 2007.

[138] Xiaohua Zheng and Gregory D Cartee. Insulin-induced effects on the subcellular localization of akt1, akt2 and as160 in rat skeletal muscle. *Scientific reports*, 6:39230, 2016.

[139] Grantley R Peck, Siying Ye, Vi Pham, Ruani N Fernando, S Lance Macaulay, Siew Yeen Chai, and Anthony L Albiston. Interaction of the akt substrate, as160, with the glucose transporter 4 vesicle marker protein, insulin-regulated aminopeptidase. *Molecular endocrinology*, 20(10):2576–2583, 2006.

[140] Varinder K Randhawa, Shuhei Ishikura, Ilana Talior-Volodarsky, Alex WP Cheng, Nish Patel, John H Hartwig, and Amira Klip. Glut4 vesicle recruitment and fusion are differentially regulated by rac, as160, and rab8a in muscle cells. *Journal of Biological Chemistry*, 283(40):27208–27219, 2008.

[141] Cristinel P Mîinea, Hiroyuki Sano, Susan Kane, Eiko Sano, Mitsunori Fukuda, Johan Peränen, William S Lane, and Gustav E Lienhard. As160, the akt substrate regulating glut4 translocation, has a functional rab gtpase-activating protein domain. *Biochemical Journal*, 391(1):87–93, 2005.

[142] Ingrid Jordens, Marije Marsman, Coen Kuijl, and Jacques Neefjes. Rab proteins, connecting transport and vesicle fusion. *Traffic*, 6(12):1070–1077, 2005.

[143] ALEXANDRA Kessler, E Tomas, D Immler, HE Meyer, A Zorzano, and J Eckel. Rab11 is associated with glut4-containing vesicles and redistributes in response to insulin. *Diabetologia*, 43(12):1518–1527, 2000.

[144] Shuhei Ishikura, Philip J Bilan, and Amira Klip. Rabs 8a and 14 are targets of the insulin-regulated rab-gap as160 regulating glut4 traffic in muscle cells. *Biochemical and biophysical research communications*, 353(4):1074–1079, 2007.

[145] Yu Chen and Jennifer Lippincott-Schwartz. Rab10 delivers glut4 storage vesicles to the plasma membrane. *Communicative & integrative biology*, 6(3):545–60, 2013.

[146] L Amanda Sadacca, Joanne Bruno, Jennifer Wen, Wenyong Xiong, and Timothy E McGraw. Specialized sorting of glut4 and its recruitment to the cell surface are independently regulated by distinct rabs. *Molecular biology of the cell*, 24(16):2544–2557, 2013.

[147] Farah SL Thong, Philip J Bilan, and Amira Klip. The rab gtpase-activating protein as160 integrates akt, protein kinase c, and amp-activated protein kinase signals regulating glut4 traffic. *Diabetes*, 56(2):414–423, 2007.

[148] Grantley R Peck, Jose A Chavez, William G Roach, Bogdan A Budnik, William S Lane, Håkan KR Karlsson, Juleen R Zierath, and Gustav E Lienhard. Insulin-stimulated phosphorylation of the rab gtpase-activating protein tbc1d1 regulates glut4 translocation. *Journal of Biological Chemistry*, 284(44):30016–30023, 2009.

[149] Graham R Smith and Daryl P Shanley. Computational modelling of the regulation of insulin signalling by oxidative stress. *BMC systems biology*, 7(1):41, 2013.

[150] Bo Tang, Fang Tang, Zhenran Wang, Guangying Qi, Xingsi Liang, Bo Li, Shengguang Yuan, Jie Liu, Shuiping Yu, and Songqing He. Upregulation of akt/nf-κb-regulated inflammation and akt/bad-related apoptosis signaling pathway involved in hepatic carcinoma process: suppression by carnosic acid nanoparticle. *International journal of nanomedicine*, 11:6401, 2016.

[151] Li Li, Xiaohua Li, Wenjun Zhou, and Joseph L Messina. Acute psychological stress results in the rapid development of insulin resistance. *The Journal of endocrinology*, 217(2):175, 2013.

[152] Peng Sun, Sheng Wei, Xia Wei, Jieqiong Wang, Yuanyuan Zhang, Mingqi Qiao, and Jibiao Wu. Anger emotional stress influences vegf/vegfr2 and its induced pi3k/akt/mtor signaling pathway. *Neural plasticity*, 2016, 2016.

[153] Alexandros Tzatsos and Konstantin V Kandror. Nutrients suppress phosphatidylinositol 3-kinase/akt signaling via raptor-dependent mtor-mediated insulin receptor substrate 1 phosphorylation. *Molecular and cellular biology*, 26(1):63–76, 2006.

[154] T Yoshihara, H Naito, R Kakigi, N Ichinoseki-Sekine, Y Ogura, T Sugiura, and S Katamoto. Heat stress activates the a kt/m tor signalling pathway in rat skeletal muscle. *Acta Physiologica*, 207(2):416–426, 2013.

[155] Fumin Chang, JT Lee, PM Navolanic, LS Steelman, JG Shelton, WL Blalock, RA Franklin, and JA McCubrey. Involvement of pi3k/akt pathway in cell cy-

cle progression, apoptosis, and neoplastic transformation: a target for cancer chemotherapy. *Leukemia*, 17(3):590–603, 2003.

[156] R Brooks Robey and Nissim Hay. Is akt the "warburg kinase"?—akt-energy metabolism interactions and oncogenesis. In *Seminars in cancer biology*, volume 19, pages 25–31. Elsevier, 2009.

[157] Jesika Faridi, Janet Fawcett, Lihong Wang, and Richard A Roth. Akt promotes increased mammalian cell size by stimulating protein synthesis and inhibiting protein degradation. *American Journal of Physiology-Endocrinology And Metabolism*, 285(5):E964–E972, 2003.

[158] Saori Sato, Naoya Fujita, and Takashi Tsuruo. Modulation of akt kinase activity by binding to hsp90. *Proceedings of the National Academy of Sciences*, 97(20):10832–10837, 2000.

[159] Andrea D Basso, David B Solit, Gabriela Chiosis, Banabihari Giri, Philip Tsichlis, and Neal Rosen. Akt forms an intracellular complex with heat shock protein 90 (hsp90) and cdc37 and is destabilized by inhibitors of hsp90 function. *Journal of Biological Chemistry*, 277(42):39858–39866, 2002.

[160] Rong Zhang, Dianhong Luo, Robert Miao, Lanfang Bai, Qingyuan Ge, William C Sessa, and Wang Min. Hsp90–akt phosphorylates ask1 and inhibits ask1-mediated apoptosis. *Oncogene*, 24(24):3954–3963, 2005.

[161] Han C Dan, Matthew J Cooper, Patricia C Cogswell, Joseph A Duncan, Jenny P-Y Ting, and Albert S Baldwin. Akt-dependent regulation of nf-κb is controlled by mtor and raptor in association with ikk. *Genes & development*, 22(11):1490–1500, 2008.

[162] Antero Salminen and Kai Kaarniranta. Insulin/igf-1 paradox of aging: regulation via akt/ikk/nf-κb signaling. *Cellular signalling*, 22(4):573–577, 2010.

[163] Jun Sunayama, Fuminori Tsuruta, Norihisa Masuyama, and Yukiko Gotoh. Jnk antagonizes akt-mediated survival signals by phosphorylating 14-3-3. *Journal of Cell Biology*, 170(2):295–304, 2005.

[164] Quan-Jiang Zhang, William L Holland, Lloyd Wilson, Jason M Tanner, Devin Kearns, Judd M Cahoon, Dix Pettey, Jason Losee, Bradlee Duncan, Derrick Gale, et al. Ceramide mediates vascular dysfunction in diet-induced obesity by pp2a-mediated dephosphorylation of the enos-akt complex. *Diabetes*, 61(7):1848–1859, 2012.

[165] Alexandra C Newton and Lloyd C Trotman. Turning off akt: Phlpp as a drug target. *Annual review of pharmacology and toxicology*, 54, 2014.

[166] Sun Myung Joung, Zee-Yong Park, Shilpa Rani, Osamu Takeuchi, Shizuo Akira, and Joo Young Lee. Akt contributes to activation of the trif-dependent signaling pathways of tlrs by interacting with tank-binding kinase 1. *The Journal of Immunology*, 186(1):499–507, 2011.

[167] Yi-Hung Ou, Michael Torres, Rosalyn Ram, Etienne Formstecher, Christina Roland, Tzuling Cheng, Rolf Brekken, Ryan Wurz, Andrew Tasker, Tony Polverino, et al. Tbk1 directly engages akt/pkb survival signaling to support oncogenic transformation. *Molecular cell*, 41(4):458–470, 2011.

[168] Taras T Antoniv and Lionel B Ivashkiv. Interleukin-10-induced gene expression and suppressive function are selectively modulated by the pi3k-akt-gsk3 pathway. *Immunology*, 132(4):567–577, 2011.

[169] Effat Emamian. Akt/gsk3 signaling pathway and schizophrenia. *Frontiers in molecular neuroscience*, 5:33, 2012.

[170] Håkan KR Karlsson, Juleen R Zierath, Susan Kane, Anna Krook, Gustav E Lienhard, and Harriet Wallberg-Henriksson. Insulin-stimulated phosphorylation of the akt substrate as160 is impaired in skeletal muscle of type 2 diabetic subjects. *Diabetes*, 54(6):1692–1697, 2005.

[171] Christian C Dibble and Lewis C Cantley. Regulation of mtorc1 by pi3k signaling. *Trends in cell biology*, 25(9):545–555, 2015.

[172] Dos D Sarbassov, Siraj M Ali, Shomit Sengupta, Joon-Ho Sheen, Peggy P Hsu, Alex F Bagley, Andrew L Markhard, and David M Sabatini. Prolonged rapamycin treatment inhibits mtorc2 assembly and akt/pkb. *Molecular cell*, 22(2):159–168, 2006.

[173] Sean J Humphrey, Guang Yang, Pengyi Yang, Daniel J Fazakerley, Jacqueline Stöckli, Jean Y Yang, and David E James. Dynamic adipocyte phosphoproteome reveals that akt directly regulates mtorc2. *Cell metabolism*, 17(6):1009–1020, 2013.

[174] Xinbo Zhang, Naimei Tang, Timothy J Hadden, and Arun K Rishi. Akt, foxo and regulation of apoptosis. *Biochimica et Biophysica Acta (BBA)-Molecular Cell Research*, 1813(11):1978–1986, 2011.

[175] Julian Downward. Mechanisms and consequences of activation of protein kinase b/akt. *Current opinion in cell biology*, 10(2):262–267, 1998.

[176] Jong-Ho Lee, Rui Liu, Jing Li, Chuanbao Zhang, Yugang Wang, Qingsong Cai, Xu Qian, Yan Xia, Yanhua Zheng, Yuji Piao, et al. Stabilization of phosphofructokinase 1 platelet isoform by akt promotes tumorigenesis. *Nature communications*, 8(1):1–14, 2017.

[177] Mike Mueckler and Bernard Thorens. The slc2 (glut) family of membrane transporters. *Molecular aspects of medicine*, 34(2-3):121–138, 2013.

[178] Hans-Georg Joost and Bernard Thorens. The extended glut-family of sugar/polyol transport facilitators: nomenclature, sequence characteristics, and potential function of its novel members. *Molecular membrane biology*, 18(4):247–256, 2001.

[179] Feng-Qi Zhao and Aileen F Keating. Functional properties and genomics of glucose transporters. *Current genomics*, 8(2):113–128, 2007.

[180] Dong Deng, Chao Xu, Pengcheng Sun, Jianping Wu, Chuangye Yan, Mingxu Hu, and Nieng Yan. Crystal structure of the human glucose transporter glut1. *Nature*, 510(7503):121–125, 2014.

[181] Ian A Simpson, Donard Dwyer, Daniela Malide, Kelle H Moley, Alexander Travis, and Susan J Vannucci. The facilitative glucose transporter glut3: 20 years of distinction. *American Journal of Physiology-Endocrinology and Metabolism*, 295(2):E242–E253, 2008.

[182] Shaohui Huang and Michael P Czech. The glut4 glucose transporter. *Cell Metab.*, 5(4):237–252, 2007.

[183] Xiaohua Wu and Hudson H Freeze. Glut14, a duplicon of glut3, is specifically expressed in testis as alternative splice forms. *Genomics*, 80(6):553–557, 2002.

[184] Veronique Douard and Ronaldo P Ferraris. Regulation of the fructose transporter glut5 in health and disease. *American Journal of Physiology-Endocrinology and Metabolism*, 295(2):E227–E237, 2008.

[185] Chris Cheeseman. Glut7: a new intestinal facilitated hexose transporter. *American Journal of Physiology-Endocrinology and Metabolism*, 295(2):E238–E241, 2008.

[186] Stéphanie Bibert, Solange Kharoubi Hess, Dmitri Firsov, Bernard Thorens, Kathi Geering, Jean-Daniel Horisberger, and Olivier Bonny. Mouse glut9: evidences for a urate uniporter. *American Journal of Physiology-Renal Physiology*, 297(3):F612–F619, 2009.

[187] Holger Doege, Andreas Bocianski, Andrea Scheepers, Hubertus Axer, Jürgen Eckel, Hans-Georg Joost, and Annette Schürmann. Characterization of human glucose transporter (glut) 11 (encoded by slc2a11), a novel sugar-transport facilitator specifically expressed in heart and skeletal muscle. *Biochemical Journal*, 359(2):443–449, 2001.

[188] Shotaro Maedera, Tadahaya Mizuno, Hiromu Ishiguro, Takuya Ito, Tomoyoshi Soga, and Hiroyuki Kusuhara. Glut6 is a lysosomal transporter that is regulated by inflammatory stimuli and modulates glycolysis in macrophages. *FEBS letters*, 593(2):195–208, 2019.

[189] Stefan Schmidt, Hans-Georg Joost, and Annette Schurmann. Glut8, the enigmatic intracellular hexose transporter. *American Journal of Physiology-Endocrinology and Metabolism*, 296(4):E614–E618, 2009.

[190] Amanda P Waller, Michael George, Anuradha Kalyanasundaram, Chen Kang, Muthu Periasamy, Keli Hu, and Véronique A Lacombe. Glut12 functions as a basal and insulin-independent glucose transporter in the heart. *Biochimica et Biophysica Acta (BBA)-Molecular Basis of Disease*, 1832(1):121–127, 2013.

[191] Marc Uldry and Bernard Thorens. The slc2 family of facilitated hexose and polyol transporters. *Pflügers Archiv*, 447(5):480–489, 2004.

[192] Vladimir A Lizunov, Hideko Matsumoto, Joshua Zimmerberg, Samuel W Cushman, and Vadim A Frolov. Insulin stimulates the halting, tethering, and fusion of mobile glut4 vesicles in rat adipose cells. *J Cell Biol*, 169(3):481–489, 2005.

[193] Alexandria Brumfield, Natasha Chaudhary, Dorothee Molle, Jennifer Wen, Johannes Graumann, and Timothy E McGraw. Insulin promoted mobilization of glut4 from a perinuclear storage site requires rab10. *bioRxiv*, 2020.

[194] Nia J Bryant, Roland Govers, and David E James. Regulated transport of the glucose transporter glut4. *Nature reviews Molecular cell biology*, 3(4):267, 2002.

[195] Sally Martin, Caroline A Millar, Chris T Lyttle, Timo Meerloo, Brad J Marsh, Gwyn W Gould, and David E James. Effects of insulin on intracellular glut4 vesicles in adipocytes: evidence for a secretory mode of regulation. *Journal of cell science*, 113(19):3427–3438, 2000.

[196] Don T Li, Estifanos N Habtemichael, Omar Julca, Chloe I Sales, Xavier O
Westergaard, Stephen G DeVries, Diana Ruiz, Bhavesh Sayal, and Jonathan S
Bogan. Focus: Organelles: Glut4 storage vesicles: Specialized organelles for
regulated trafficking. *The Yale Journal of Biology and Medicine*, 92(3):453,
2019.

[197] Lin V Li, Kyriaki Bakirtzi, Robert T Watson, Jeffrey E Pessin, and Konstantin V
Kandror. The c-terminus of glut4 targets the transporter to the perinuclear
compartment but not to the insulin-responsive vesicles. *Biochemical Journal*,
419(1):105–113, 2009.

[198] Ann Louise Olson, Alan R Trumbly, and George V Gibson. Insulin-mediated
glut4 translocation is dependent on the microtubule network. *Journal of Biological Chemistry*, 276(14):10706–10714, 2001.

[199] Javier R Jaldin-Fincati, Martin Pavarotti, Scott Frendo-Cumbo, Philip J Bilan,
and Amira Klip. Update on glut4 vesicle traffic: a cornerstone of insulin action.
Trends in Endocrinology & Metabolism, 28(8):597–611, 2017.

[200] J. Huang, T. Imamura, and J. M. Olefsky. Insulin can regulate GLUT4 internalization by signaling to rab5 and the motor protein dynein. *Proceedings of the
National Academy of Sciences*, 98(23):13084–13089, oct 2001.

[201] June Chunqiu Hou and Jeffrey E Pessin. Ins (endocytosis) and outs (exocytosis)
of glut4 trafficking. *Curr. Opin. Cell Biol.*, 19(4):466–473, 2007.

[202] Lan Gao, Junling Chen, Jing Gao, Hongda Wang, and Wenyong Xiong. Super-resolution microscopy reveals the insulin-resistance-regulated reorganization of
glut4 on plasma membranes. *Journal of cell science*, 130(2):396–405, 2017.

[203] Makoto Funaki, Lesley DiFransico, and Paul A Janmey. Pi 4, 5-p2 stimulates
glucose transport activity of glut4 in the plasma membrane of 3t3-l1 adipocytes.
Biochimica et Biophysica Acta (BBA)-Molecular Cell Research, 1763(8):889–
899, 2006.

[204] Nia J. Bryant and Gwyn W. Gould. SNARE proteins underpin insulin-regulated GLUT4 traffic. *Traffic*, 12(6):657–664, feb 2011.

[205] B. Cheatham, A. Volchuk, C. R. Kahn, L. Wang, C. J. Rhodes, and A. Klip. Insulin-stimulated translocation of GLUT4 glucose transporters requires SNARE-complex proteins. *Proceedings of the National Academy of Sciences*, 93(26):15169–15173, dec 1996.

[206] Debbie C. Thurmond, Makoto Kanzaki, Ahmir H. Khan, and Jeffrey E. Pessin. Munc18c function is required for insulin-stimulated plasma membrane fusion of GLUT4 and insulin-responsive amino peptidase storage vesicles. *Molecular and Cellular Biology*, 20(1):379–388, jan 2000.

[207] Jennifer Roccisana, Jessica B. A. Sadler, Nia J. Bryant, and Gwyn W. Gould. Sorting of GLUT4 into its insulin-sensitive store requires the sec1/munc18 protein mVps45. *Molecular Biology of the Cell*, 24(15):2389–2397, aug 2013.

[208] N. Fukuda, M. Emoto, Y. Nakamori, A. Taguchi, S. Miyamoto, S. Uraki, Y. Oka, and Y. Tanizawa. DOC2b: A novel syntaxin-4 binding protein mediating insulin-regulated GLUT4 vesicle fusion in adipocytes. *Diabetes*, 58(2):377–384, nov 2008.

[209] Leonard J. Foster and Amira Klip. Mechanism and regulation of GLUT-4 vesicle fusion in muscle and fat cells. *American Journal of Physiology-Cell Physiology*, 279(4):C877–C890, oct 2000.

[210] Haijia Yu, Shailendra S. Rathore, Eric M. Davis, Yan Ouyang, and Jingshi Shen. Doc2b promotes GLUT4 exocytosis by activating the SNARE-mediated fusion reaction in a calcium- and membrane bending–dependent manner. *Molecular Biology of the Cell*, 24(8):1176–1184, apr 2013.

[211] Peter Tong, Zayna A Khayat, Carol Huang, Nish Patel, Atsunori Ueyama, and Amira Klip. Insulin-induced cortical actin remodeling promotes glut4 insertion at muscle cell membrane ruffles. *The Journal of clinical investigation*, 108(3):371–381, 2001.

[212] B.A.; Brozinick, J.T.; Berkemeier and J.S. Elmendorf. "actin"g on GLUT4 membrane & cytoskeletal components of insulin action. *Current Diabetes Reviews*, 3(2):111–122, 2007.

[213] Barry J. Goldstein, Faiyaz Ahmad, Wendi Ding, Pei-Ming Li, and Wei-Ren Zhang. Regulation of the insulin signalling pathway by cellular protein-tyrosine phosphatases. *Molecular and Cellular Biochemistry*, 182(1/2):91–99, 1998.

[214] R. Michael Sharrard and Norman J. Maitland. Regulation of protein kinase b activity by PTEN and SHIP2 in human prostate-derived cell lines. *Cellular Signalling*, 19(1):129–138, jan 2007.

[215] Christophe Erneux, William's Elong Edimo, Laurence Deneubourg, and Isabelle Pirson. Ship2 multiple functions: a balance between a negative control of ptdins (3, 4, 5) p3 level, a positive control of ptdins (3, 4) p2 production, and intrinsic docking properties. *Journal of cellular biochemistry*, 112(9):2203–2209, 2011.

[216] Nader Chalhoub and Suzanne J. Baker. PTEN and the PI3-kinase pathway in cancer. *Annual Review of Pathology: Mechanisms of Disease*, 4(1):127–150, feb 2009.

[217] A. Kleinridders. Deciphering brain insulin receptor and insulin-like growth factor 1 receptor signalling. *Journal of Neuroendocrinology*, 28(11), nov 2016.

[218] S. M. Gray, R. I. Meijer, and E. J. Barrett. Insulin regulates brain function, but how does it get there? *Diabetes*, 63(12):3992–3997, nov 2014.

[219] Diego F. Calvisi, Chunmei Wang, Coral Ho, Sara Ladu, Susie A. Lee, Sandra Mattu, Giulia Destefanis, Salvatore Delogu, Antje Zimmermann, and Johan Ericsson. Increased lipogenesis, induced by AKT-mTORC1-RPS6 signaling, promotes development of human hepatocellular carcinoma. *Gastroenterology*, 140(3):1071–1083.e5, mar 2011.

[220] CG Proud. Regulation of protein synthesis by insulin, 2006.

[221] Max C. Petersen, Daniel F. Vatner, and Gerald I. Shulman. Regulation of hepatic glucose metabolism in health and disease. *Nature Reviews Endocrinology*, 13(10):572–587, jul 2017.

[222] Maximilian Hatting, Clint D.J. Tavares, Kfir Sharabi, Amy K. Rines, and Pere Puigserver. Insulin regulation of gluconeogenesis. *Annals of the New York Academy of Sciences*, 1411(1):21–35, sep 2017.

[223] Xiaocheng C. Dong, Kyle D. Copps, Shaodong Guo, Yedan Li, Ramya Kollipara, Ronald A. DePinho, and Morris F. White. Inactivation of hepatic foxo1 by insulin signaling is required for adaptive nutrient homeostasis and endocrine growth regulation. *Cell Metabolism*, 8(1):65–76, jul 2008.

[224] A. G. Gomez-Valades, A. Mendez-Lucas, A. Vidal-Alabro, F. X. Blasco, M. Chillon, R. Bartrons, J. Bermudez, and J. C. Perales. Pck1 gene silencing in the liver improves glycemia control, insulin sensitivity, and dyslipidemia in db/db mice. *Diabetes*, 57(8):2199–2210, apr 2008.

[225] Parker L Evans, Shawna L McMillin, Luke A Weyrauch, and Carol A Witczak. Regulation of skeletal muscle glucose transport and glucose metabolism by exercise training. *Nutrients*, 11(10):2432, 2019.

[226] Juleen R Zierath. Invited review: exercise training-induced changes in insulin signaling in skeletal muscle. *Journal of Applied Physiology*, 93(2):773–781, 2002.

[227] Alexander V Chibalin, Mei Yu, Jeffrey W Ryder, Xiao Mei Song, Dana Galuska, Anna Krook, Harriet Wallberg-Henriksson, and Juleen R Zierath. Exercise-induced changes in expression and activity of proteins involved in insulin signal transduction in skeletal muscle: differential effects on insulin-receptor substrates 1 and 2. *Proceedings of the National Academy of Sciences*, 97(1):38–43, 2000.

[228] JF Wojtaszewski, Bo F Hansen, J Gade, Bente Kiens, JF Markuns, LJ Goodyear, and EA Richter. Insulin signaling and insulin sensitivity after exercise in human skeletal muscle. *Diabetes*, 49(3):325–331, 2000.

[229] Yun Chau Long, Zhiyong Cheng, Kyle D Copps, and Morris F White. Insulin receptor substrates irs1 and irs2 coordinate skeletal muscle growth and metabolism via the akt and ampk pathways. *Molecular and cellular biology*, 31(3):430–441, 2011.

[230] Derek LeRoith and Domenico Accili. Mechanisms of disease: using genetically altered mice to study concepts of type 2 diabetes. *Nature clinical practice Endocrinology & metabolism*, 4(3):164–172, 2008.

[231] Jee-Hyun Um, Sung-Jun Park, Hyeog Kang, Shutong Yang, Marc Foretz, Michael W McBurney, Myung K Kim, Benoit Viollet, and Jay H Chung. Amp-activated protein kinase–deficient mice are resistant to the metabolic effects of resveratrol. *Diabetes*, 59(3):554–563, 2010.

[232] A Brunetti, BA Maddux, KY Wong, and ID Goldfine. Muscle cell differentiation is associated with increased insulin receptor biosynthesis and messenger rna levels. *The Journal of clinical investigation*, 83(1):192–198, 1989.

[233] Isabelle Guillet-Deniau, Armelle Leturque, and Jean Girard. Expression and cellular localization of glucose transporters (glut1, glut3, glut4) during differentiation of myogenic cells isolated from rat foetuses. *Journal of cell science*, 107(3):487–496, 1994.

[234] Paola Aguiari, Sara Leo, Barbara Zavan, Vincenzo Vindigni, Alessandro Rimessi, Katiuscia Bianchi, Chiara Franzin, Roberta Cortivo, Marco Rossato, Roberto Vettor, et al. High glucose induces adipogenic differentiation of muscle-derived stem cells. *Proceedings of the National Academy of Sciences*, 105(4):1226–1231, 2008.

[235] S. Kuzmiak-Glancy and W. T. Willis. Skeletal muscle fuel selection occurs at the mitochondrial level. *Journal of Experimental Biology*, 217(11):1993–2003, mar 2014.

[236] Guenther Boden and GI Shulman. Free fatty acids in obesity and type 2 diabetes: defining their role in the development of insulin resistance and β-cell dysfunction. *European journal of clinical investigation*, 32:14–23, 2002.

[237] David S Ludwig, Joseph A Majzoub, Ahmad Al-Zahrani, Gerard E Dallal, Isaac Blanco, and Susan B Roberts. High glycemic index foods, overeating, and obesity. *Pediatrics*, 103(3):e26–e26, 1999.

[238] Steven E Shoelson, Laura Herrero, and Afia Naaz. Obesity, inflammation, and insulin resistance. *Gastroenterology*, 132(6):2169–2180, 2007.

[239] Adam E Locke, Bratati Kahali, Sonja I Berndt, Anne E Justice, Tune H Pers, Felix R Day, Corey Powell, Sailaja Vedantam, Martin L Buchkovich, Jian Yang, et al. Genetic studies of body mass index yield new insights for obesity biology. *Nature*, 518(7538):197–206, 2015.

[240] Youfa Wang and TIM Lobstein. Worldwide trends in childhood overweight and obesity. *International journal of pediatric obesity*, 1(1):11–25, 2006.

[241] Cristiano Capurso and Antonio Capurso. From excess adiposity to insulin resistance: the role of free fatty acids. *Vascular pharmacology*, 57(2-4):91–97, 2012.

[242] Hansongyi Lee, In Seok Lee, and Ryowon Choue. Obesity, inflammation and diet. *Pediatric Gastroenterology, Hepatology & Nutrition*, 16(3):143, 2013.

[243] Mohammed S Ellulu, Ismail Patimah, Huzwah Khaza'ai, Asmah Rahmat, and Yehia Abed. Obesity and inflammation: the linking mechanism and the complications. *Archives of medical science: AMS*, 13(4):851, 2017.

[244] Boudewijn Klop, Jan Willem F Elte, and Manuel Castro Cabezas. Dyslipidemia in obesity: mechanisms and potential targets. *Nutrients*, 5(4):1218–1240, 2013.

[245] Margaret F Gregor and Gökhan S Hotamisligil. Inflammatory mechanisms in obesity. *Annual review of immunology*, 29:415–445, 2011.

[246] Ji-Youn Youn, Kin Lung Siu, Heinrich E Lob, Hana Itani, David G Harrison, and Hua Cai. Role of vascular oxidative stress in obesity and metabolic syndrome. *Diabetes*, 63(7):2344–2355, 2014.

[247] Tadej Debevec, Grégoire P. Millet, and Vincent Pialoux. Hypoxia-induced oxidative stress modulation with physical activity. *Frontiers in Physiology*, 8, feb 2017.

[248] Joe M McCord. The evolution of free radicals and oxidative stress. *The American journal of medicine*, 108(8):652–659, 2000.

[249] Thomas L. Clanton. Hypoxia-induced reactive oxygen species formation in skeletal muscle. *Journal of Applied Physiology*, 102(6):2379–2388, jun 2007.

[250] VR Winrow, PG Winyard, CJ Morris, and DR Blake. Free radicals in inflammation: second messengers and mediators of tissue destruction. *British medical bulletin*, 49(3):506–522, 1993.

[251] Devjit Tripathy, Priya Mohanty, Sandeep Dhindsa, Tufail Syed, Husam Ghanim, Ahmad Aljada, and Paresh Dandona. Elevation of free fatty acids induces inflammation and impairs vascular reactivity in healthy subjects. *Diabetes*, 52(12):2882–2887, 2003.

[252] Liza Makowski and Gökhan S Hotamisligil. Fatty acid binding proteinsâthe evolutionary crossroads of inflammatory and metabolic responses. *The Journal of nutrition*, 134(9):2464S–2468S, 2004.

[253] Caroline Maria Oliveira Volpe, Luana Farnese Machado Abreu, Pollyanna Stephanie Gomes, Raquel Miranda Gonzaga, Clara Araújo Veloso, and José Augusto Nogueira-Machado. The production of nitric oxide, il-6, and tnf-alpha in palmitate-stimulated pbmncs is enhanced through hyperglycemia in diabetes. *Oxidative medicine and cellular longevity*, 2014, 2014.

[254] Patrick Mathieu, Paul Poirier, Philippe Pibarot, Isabelle Lemieux, and Jean-Pierre Despres. Visceral obesity: the link among inflammation, hypertension, and cardiovascular disease. *Hypertension*, 53(4):577–584, 2009.

[255] Charles L Raison, Lucile Capuron, and Andrew H Miller. Cytokines sing the blues: inflammation and the pathogenesis of depression. *Trends in immunology*, 27(1):24–31, 2006.

[256] Anders H Berg and Philipp E Scherer. Adipose tissue, inflammation, and cardiovascular disease. *Circulation research*, 96(9):939–949, 2005.

[257] Ernest HS Choy and Gabriel S Panayi. Cytokine pathways and joint inflammation in rheumatoid arthritis. *New England Journal of Medicine*, 344(12):907–916, 2001.

[258] Francine K Welty. How do elevated triglycerides and low hdl-cholesterol affect inflammation and atherothrombosis? *Current cardiology reports*, 15(400), 2013.

[259] Eric A Schwartz and Peter D Reaven. Lipolysis of triglyceride-rich lipoproteins, vascular inflammation, and atherosclerosis. *Biochimica et Biophysica Acta (BBA)-Molecular and Cell Biology of Lipids*, 1821(5):858–866, 2012.

[260] Maria Ida Malandrino, Raquel Fucho, Minéia Weber, María Calderon-Dominguez, Joan Francesc Mir, Lorea Valcarcel, Xavier Escoté, María Gómez-Serrano, Belén Peral, Laia Salvadó, et al. Enhanced fatty acid oxidation in adipocytes and macrophages reduces lipid-induced triglyceride accumulation and inflammation. *American Journal of Physiology-Endocrinology and Metabolism*, 308(9):E756–E769, 2015.

[261] Pedro A Figueiredo, Scott K Powers, Rita M Ferreira, Francisco Amado, Hans J Appell, and José A Duarte. Impact of lifelong sedentary behavior on mitochondrial function of mice skeletal muscle. *Journals of Gerontology Series A: Biomedical Sciences and Medical Sciences*, 64(9):927–939, 2009.

[262] Adeel Safdar, Mazen J Hamadeh, Jan J Kaczor, Sandeep Raha, Justin Debeer, and Mark A Tarnopolsky. Aberrant mitochondrial homeostasis in the skeletal muscle of sedentary older adults. *PloS one*, 5(5):e10778, 2010.

[263] Jong-Yeon Kim, Robert C Hickner, Ronald L Cortright, G Lynis Dohm, and Joseph A Houmard. Lipid oxidation is reduced in obese human skeletal muscle. *American Journal of Physiology-Endocrinology And Metabolism*, 279(5):E1039–E1044, 2000.

[264] Muhammad Sajid Hamid Akash, Kanwal Rehman, and Aamira Liaqat. Tumor necrosis factor-alpha: role in development of insulin resistance and pathogenesis of type 2 diabetes mellitus. *Journal of cellular biochemistry*, 119(1):105–110, 2018.

[265] Dov B Ballak, Rinke Stienstra, Cees J Tack, Charles A Dinarello, and Janna A van Diepen. Il-1 family members in the pathogenesis and treatment of metabolic disease: focus on adipose tissue inflammation and insulin resistance. *Cytokine*, 75(2):280–290, 2015.

[266] Melek C Arkan, Andrea L Hevener, Florian R Greten, Shin Maeda, Zhi-Wei Li, Jeffrey M Long, Anthony Wynshaw-Boris, Giuseppe Poli, Jerrold Olefsky, and Michael Karin. Ikk-β links inflammation to obesity-induced insulin resistance. *Nature medicine*, 11(2):191–198, 2005.

[267] Takara Tanaka, Noriko Hattori-Aramaki, Ayano Sunohara, Keisuke Okabe, Yoshiaki Sakamoto, Hiroko Ochiai, Ruka Hayashi, and Kazuo Kishi. Alignment of skeletal muscle cells cultured in collagen gel by mechanical and electrical stimulation. *International Journal of Tissue Engineering*, 2014, 2014.

[268] S Burattini, P Ferri, M Battistelli, R Curci, F Luchetti, and E Falcieri. C2c12 murine myoblasts as a model of skeletal muscle development: morpho-functional characterization. *European journal of histochemistry: EJH*, 48(3):223, 2004.

[269] Bo-Geon Yun and Robert L Matts. Hsp90 functions to balance the phosphorylation state of akt during c2c12 myoblast differentiation. *Cellular signalling*, 17(12):1477–1485, 2005.

[270] Christian M Girgis, Roderick J Clifton-Bligh, Nancy Mokbel, Kim Cheng, and Jenny E Gunton. Vitamin d signaling regulates proliferation, differentiation, and myotube size in c2c12 skeletal muscle cells. *Endocrinology*, 155(2):347–357, 2014.

[271] Yasuko Manabe, Shouta Miyatake, Mayumi Takagi, Mio Nakamura, Ai Okeda, Taemi Nakano, Michael F Hirshman, Laurie J Goodyear, and Nobuharu L Fujii. Characterization of an acute muscle contraction model using cultured c2c12 myotubes. *PloS one*, 7(12):e52592, 2012.

[272] Ruben Conejo, Angela M Valverde, Manuel Benito, and Margarita Lorenzo. Insulin produces myogenesis in c2c12 myoblasts by induction of nf-κb and downregulation of ap-1 activities. *Journal of cellular physiology*, 186(1):82–94, 2001.

[273] Ruben Conejo and Margarita Lorenzo. Insulin signaling leading to proliferation, survival, and membrane ruffling in c2c12 myoblasts. *Journal of cellular physiology*, 187(1):96–108, 2001.

[274] Taku Nedachi, Hideaki Fujita, and Makoto Kanzaki. Contractile c2c12 myotube model for studying exercise-inducible responses in skeletal muscle. *American Journal of Physiology-Endocrinology and Metabolism*, 295(5):E1191–E1204, 2008.

[275] Yea-Tzy Deng, Tsai-Wen Chang, Ming-Shyue Lee, and Jen-Kun Lin. Suppression of free fatty acid-induced insulin resistance by phytopolyphenols in c2c12 mouse skeletal muscle cells. *Journal of agricultural and food chemistry*, 60(4):1059–1066, 2012.

[276] Lori L Tortorella and Paul F Pilch. C2c12 myocytes lack an insulin-responsive vesicular compartment despite dexamethasone-induced glut4 expression. *Amer-*

ican Journal of Physiology-Endocrinology and Metabolism, 283(3):E514–E524, 2002.

[277] Taku Nedachi and Makoto Kanzaki. Regulation of glucose transporters by insulin and extracellular glucose in c2c12 myotubes. *American Journal of Physiology-Endocrinology and Metabolism*, 291(4):E817–E828, 2006.

[278] Hee Yun, Jong Hwa Lee, Chang Eun Park, Min-Jung Kim, Byung-Il Min, Hyunsu Bae, Wonchae Choe, Insug Kang, Sung-Soo Kim, and Joohun Ha. Inulin increases glucose transport in c2c12 myotubes and HepG2 cells via activation of AMP-activated protein kinase and phosphatidylinositol 3-kinase pathways. *Journal of Medicinal Food*, 12(5):1023–1028, oct 2009.

[279] Wei Luo, Lei Ai, Bo-fa Wang, and Yue Zhou. High glucose inhibits myogenesis and induces insulin resistance by down-regulating akt signaling. *Biomedicine & Pharmacotherapy*, 120:109498, 2019.

[280] Eunyoung Ha, Sung-Vin Yim, Joo-Ho Chung, Kyung-Sik Yoon, Insug Kang, Yong Ho Cho, and Hyung Hwan Baik. Melatonin stimulates glucose transport via insulin receptor substrate-1/phosphatidylinositol 3-kinase pathway in c2c12 murine skeletal muscle cells. *Journal of pineal research*, 41(1):67–72, 2006.

[281] Ofer Kaplan, Peter C.M. van Zijl, and Jack S. Cohen. Information from combined 1h and 31p NMR studies of cell extracts: Differences in metabolism between drug-sensitive and drug-resistant MCF-7 human breast cancer cells. *Biochemical and Biophysical Research Communications*, 169(2):383–390, jun 1990.

[282] Rebecca L Aft, FW Zhang, and D Gius. Evaluation of 2-deoxy-d-glucose as a chemotherapeutic agent: mechanism of cell death. *British journal of cancer*, 87(7):805–812, 2002.

[283] Yasuhide Mitsumoto, Elena Burdett, Andrew Grant, and Amira Klip. Differential expression of the GLUT1 and GLUT4 glucose transporters during differen-

tiation of l6 muscle cells. *Biochemical and Biophysical Research Communications*, 175(2):652–659, mar 1991.

[284] Farhana R Pinu, David J Beale, Amy M Paten, Konstantinos Kouremenos, Sanjay Swarup, Horst J Schirra, and David Wishart. Systems biology and multi-omics integration: Viewpoints from the metabolomics research community. *Metabolites*, 9(4):76, 2019.

[285] Johann J Eicher, Jacky L Snoep, and Johann M Rohwer. Determining enzyme kinetics for systems biology with nuclear magnetic resonance spectroscopy. *Metabolites*, 2(4):818–843, 2012.

[286] Vladimir A. Likić, Malcolm J. McConville, Trevor Lithgow, and Antony Bacic. Systems biology: The next frontier for bioinformatics. *Advances in Bioinformatics*, 2010:1–10, 2010.

[287] Frank J Bruggeman, Jorrit J Hornberg, Fred C Boogerd, and Hans V Westerhoff. Introduction to systems biology. In *Plant Systems Biology*, pages 1–19. Springer, 2007.

[288] Giovanni Pezzulo and Michael Levin. Top-down models in biology: explanation and control of complex living systems above the molecular level. *Journal of The Royal Society Interface*, 13(124):20160555, 2016.

[289] Jacky L Snoep, Frank Bruggeman, Brett G Olivier, and Hans V Westerhoff. Towards building the silicon cell: a modular approach. *Biosystems*, 83(2-3):207–216, 2006.

[290] Frank J Bruggeman and Hans V Westerhoff. The nature of systems biology. *TRENDS in Microbiology*, 15(1):45–50, 2007.

[291] Andreas Mock, Sara Chiblak, and Christel Herold-Mende. Lessons we learned from high-throughput and top-down systems biology analyses about glioma stem cells. *Current Pharmaceutical Design*, 20(1):66–72, jan 2014.

[292] Ahmad R Sedaghat, Arthur Sherman, and Michael J Quon. A mathematical model of metabolic insulin signaling pathways. *Am. J. Physiol. Endocrinol. Metab.*, 283(5):E1084–E1101, 2002.

[293] Gerald Penkler, Francois du Toit, Waldo Adams, Marina Rautenbach, Daniel C. Palm, David D. van Niekerk, and Jacky L. Snoep. Construction and validation of a detailed kinetic model of glycolysis in Plasmodium falciparum. *FEBS Journal*, 282(8):1481–1511, mar 2015.

[294] Ellen L. Berg. Systems biology in drug discovery and development. *Drug Discovery Today*, 19(2):113–125, feb 2014.

[295] Eric Young and Hal Alper. Synthetic biology: Tools to design, build, and optimize cellular processes. *Journal of Biomedicine and Biotechnology*, 2010:1–12, 2010.

[296] Hans V. Westerhoff and Alexey N. Kolodkin. Advice from a systems-biology model of the corona epidemics. *npj Systems Biology and Applications*, 6(1), jun 2020.

[297] Jeffrey D Orth, Ines Thiele, and Bernhard O Palsson. What is flux balance analysis? *Nature Biotechnology*, 28(3):245–248, mar 2010.

[298] Ewelina Węglarz-Tomczak, Thierry DGA Mondeel, Diewertje GE Piebes, and Hans V Westerhoff. Nature and nurture integrated through an adjustable flux balance analysis: The impact of cell-nutrition changes on the warburg effect in hepatocellular carcinoma. *BioRxiv*, page 674150, 2019.

[299] Jan-Hendrik S Hofmeyr. Metabolic control analysis in a nutshell. In *Proceedings of the 2nd International Conference on systems Biology*, pages 291–300. Omnipress Madison, WI, USA, 2001.

[300] Hans V Westerhoff, Samrina Rehman, Fred C Boogerd, Nilgun Yilmaz, and Malkhey Verma. The control analysis of signal transduction. In *Systems biology of metabolic and signaling networks*, pages 39–62. Springer, 2014.

[301] Malkhey Verma, Maksim Zakhartsev, Matthias Reuss, and Hans V Westerhoff. 'domino'systems biology and the 'a'of atp. *Biochimica et Biophysica Acta (BBA)-Bioenergetics*, 1827(1):19–29, 2013.

[302] J.H.S. Hofmeyr and A. Cornish-Bowden. Regulating the cellular economy of supply and demand. *FEBS Lett.*, 476(1-2):47–51, 2000.

[303] Kazuhiro Maeda, Hans V Westerhoff, Hiroyuki Kurata, and Fred C Boogerd. Ranking network mechanisms by how they fit diverse experiments and deciding on e. coli's ammonium transport and assimilation network. *NPJ systems biology and applications*, 5(1):1–11, 2019.

[304] Robert S Sherwin, Karl J Kramer, Jordan D Tobin, Paul A Insel, John E Liljenquist, Mones Berman, Reubin Andres, et al. A model of the kinetics of insulin in man. *The Journal of clinical investigation*, 53(5):1481–1492, 1974.

[305] Leslie S. Satin, Peter C. Butler, Joon Ha, and Arthur S. Sherman. Pulsatile insulin secretion, impaired glucose tolerance and type 2 diabetes. *Molecular Aspects of Medicine*, 42:61–77, apr 2015.

[306] Rita Basu, Barbara Di Camillo, Gianna Toffolo, Ananda Basu, Pankaj Shah, Adrian Vella, Robert Rizza, and Claudio Cobelli. Use of a novel triple-tracer approach to assess postprandial glucose metabolism. *American Journal of Physiology-Endocrinology and Metabolism*, 284(1):E55–E69, jan 2003.

[307] Athena Makroglou, Jiaxu Li, and Yang Kuang. Mathematical models and software tools for the glucose-insulin regulatory system and diabetes: an overview. *Applied numerical mathematics*, 56(3-4):559–573, 2006.

[308] Cheng-Liang Chen and Hong-Wen Tsai. Modeling the physiological glucose–insulin system on normal and diabetic subjects. *Computer methods and programs in biomedicine*, 97(2):130–140, 2010.

[309] Barbara Di Camillo, Azzurra Carlon, Federica Eduati, and Gianna Maria Toffolo. A rule-based model of insulin signalling pathway. *BMC Systems Biology*, 10(1), jun 2016.

[310] Weijiu Liu, ChingChun Hsin, and Fusheng Tang. A molecular mathematical model of glucose mobilization and uptake. *Math. Biosci.*, 221(2):121–129, 2009.

[311] Yin Hoon Chew, Yoke Lin Shia, Chew Tin Lee, Fadzilah Adibah Abdul Majid, Lee Suan Chua, Mohamad Roji Sarmidi, and Ramlan Abdul Aziz. Modeling of glucose regulation and insulin-signaling pathways. *Mol. Cell. Endocrinol.*, 303(1):13–24, 2009.

[312] Elin Nyman, Gunnar Cedersund, and Peter Strålfors. Insulin signaling–mathematical modeling comes of age. *Trends in Endocrinology & Metabolism*, 23(3):107–115, 2012.

[313] Palakkad Krishnan Unni Vinod and Kareenhalli Viswanath Venkatesh. Quantification of the effect of amino acids on an integrated mtor and insulin signaling pathway. *Molecular BioSystems*, 5(10):1163–1173, 2009.

[314] Elin Nyman, Cecilia Brännmark, Robert Palmér, Jan Brugård, Fredrik H Nyström, Peter Strålfors, and Gunnar Cedersund. A hierarchical whole-body modeling approach elucidates the link between in vitro insulin signaling and in vivo glucose homeostasis. *J. Biol. Chem.*, 286(29):26028–26041, 2011.

[315] Cecilia Brännmark, Elin Nyman, Siri Fagerholm, Linnéa Bergenholm, Eva-Maria Ekstrand, Gunnar Cedersund, and Peter Strålfors. Insulin signaling in type 2 diabetes experimental and modeling analyses reveal mechanisms of insulin resistance in human adipocytes. *Journal of Biological Chemistry*, 288(14):9867–9880, 2013.

[316] Barbara B Kahn. Type 2 diabetes: When insulin secretion fails to compensate for insulin resistance. *Cell*, 92(5):593–596, mar 1998.

[317] Sara Fröjdö, Hubert Vidal, and Luciano Pirola. Alterations of insulin signaling in type 2 diabetes: A review of the current evidence from humans. *Biochimica et Biophysica Acta (BBA) - Molecular Basis of Disease*, 1792(2):83–92, feb 2009.

[318] O. Escribano, N. Beneit, C. Rubio-Longás, A. R. López-Pastor, and A. Gómez-Hernández. The role of insulin receptor isoforms in diabetes and its metabolic and vascular complications. *Journal of Diabetes Research*, 2017:1–12, 2017.

[319] Annika G Sonntag, Piero Dalle Pezze, Daryl P Shanley, and Kathrin Thedieck. A modelling–experimental approach reveals insulin receptor substrate (irs)-dependent regulation of adenosine monosphosphate-dependent kinase (ampk) by insulin. *The FEBS journal*, 279(18):3314–3328, 2012.

[320] Piero Dalle Pezze, Annika G Sonntag, Antje Thien, Mirja T Prentzell, Markus Gödel, Sven Fischer, Elke Neumann-Haefelin, Tobias B Huber, Ralf Baumeister, Daryl P Shanley, et al. A dynamic network model of mtor signaling reveals tsc-independent mtorc2 regulation. *Science signaling*, 5(217):ra25–ra25, 2012.

[321] Hiroyuki Kubota, Rei Noguchi, Yu Toyoshima, Yu-ichi Ozaki, Shinsuke Uda, Kanako Watanabe, Wataru Ogawa, and Shinya Kuroda. Temporal coding of insulin action through multiplexing of the akt pathway. *Molecular cell*, 46(6):820–832, 2012.

[322] Rei Noguchi, Hiroyuki Kubota, Katsuyuki Yugi, Yu Toyoshima, Yasunori Komori, Tomoyoshi Soga, and Shinya Kuroda. The selective control of glycolysis, gluconeogenesis and glycogenesis by temporal insulin patterns. *Molecular systems biology*, 9(1):664, 2013.

[323] Richard N Bergman. Minimal model: perspective from 2005. *Hormone Research in Paediatrics*, 64(Suppl. 3):8–15, 2005.

[324] Tsaffrir Zor and Zvi Selinger. Linearization of the bradford protein assay increases its sensitivity: theoretical and experimental studies. *Analytical biochemistry*, 236(2):302–308, 1996.

[325] Jonathan S. Bogan, Adrienne E. McKee, and Harvey F. Lodish. Insulin-responsive compartments containing GLUT4 in 3t3-l1 and CHO cells: Regulation by amino acid concentrations. *Molecular and Cellular Biology*, 21(14):4785–4806, jul 2001.

[326] Rhys McColl, Mthokozisi Nkosi, Celia Snyman, and Carola Niesler. Analysis and quantification of in vitro myoblast fusion using the ladd multiple stain. *BioTechniques*, 61(6):323–326, 2016.

[327] David Yaffe and ORA Saxel. Serial passaging and differentiation of myogenic cells isolated from dystrophic mouse muscle. *Nature*, 270(5639):725–727, 1977.

[328] Katsuhiko Warita, Nana Oshima, Naoko Takeda-Okuda, Jun-ichi Tamura, and Yoshinao Z Hosaka. Degree of suppression of mouse myoblast cell line c2c12 differentiation varies according to chondroitin sulfate subtype. *Marine drugs*, 14(10):193, 2016.

[329] Eric A Gulve, Jian-Ming Ren, Bess Adkins Marshall, Jiaping Gao, Polly A Hansen, John O Holloszy, and Mike Mueckler. Glucose transport activity in skeletal muscles from transgenic mice overexpressing glut1. increased basal transport is associated with a defective response to diverse stimuli that activate glut4. *Journal of Biological Chemistry*, 269(28):18366–18370, 1994.

[330] Scott A. Summers, Luis A. Garza, Honglin Zhou, and Morris J. Birnbaum. Regulation of insulin-stimulated glucose transporter GLUT4 translocation and akt kinase activity by ceramide. *Molecular and Cellular Biology*, 18(9):5457–5464, sep 1998.

[331] Jonathan S. Fisher, Jiaping Gao, Dong-Ho Han, John O. Holloszy, and Lorraine A. Nolte. Activation of AMP kinase enhances sensitivity of muscle glucose transport to insulin. *American Journal of Physiology-Endocrinology and Metabolism*, 282(1):E18–E23, jan 2002.

[332] L. Bergandi, F. Silvagno, I. Russo, C. Riganti, G. Anfossi, E. Aldieri, D. Ghigo, M. Trovati, and A. Bosia. Insulin stimulates glucose transport via nitric oxide/cyclic GMP pathway in human vascular smooth muscle cells. *Arteriosclerosis, Thrombosis, and Vascular Biology*, 23(12):2215–2221, dec 2003.

[333] Michael P Czech. Insulin action and resistance in obesity and type 2 diabetes. *Nature medicine*, 23(7):804, 2017.

[334] RW Gelling, XQ Du, DS Dichmann, J Rømer, Huan Huang, L Cui, S Obici, B Tang, JJ Holst, C Fledelius, et al. Lower blood glucose, hyperglucagonemia, and pancreatic α cell hyperplasia in glucagon receptor knockout mice. *Proceedings of the National Academy of Sciences*, 100(3):1438–1443, 2003.

[335] Chengxin Sun, Xinzhi Li, Lu Liu, MJ Conet, Yuan Guan, Yuying Fan, and Yifa Zhou. Effect of fasting time on measuring mouse blood glucose level. *Int. J, Clin. Exp, mecl*, 9(2):4186–4189, 2016.

[336] Sung Hee Kim, Sun Hee Hyun, and Se Young Choung. Anti-diabetic effect of cinnamon extract on blood glucose in db/db mice. *Journal of ethnopharmacology*, 104(1-2):119–123, 2006.

[337] Marion Berenguer, Laurène Martinez, Sophie Giorgetti-Peraldi, Yannick Le Marchand-Brustel, and Roland Govers. A serum factor induces insulin-independent translocation of glut4 to the cell surface which is maintained in insulin resistance. *PloS one*, 5(12):e15560, 2010.

[338] Dominique Bonnefont-Rousselot. Glucose and reactive oxygen species. *Current Opinion in Clinical Nutrition and Metabolic Care*, 5(5):561–568, sep 2002.

[339] J. Pi, Y. Bai, Q. Zhang, V. Wong, L. M. Floering, K. Daniel, J. M. Reece, J. T. Deeney, M. E. Andersen, B. E. Corkey, and S. Collins. Reactive oxygen species as a signal in glucose-stimulated insulin secretion. *Diabetes*, 56(7):1783–1791, mar 2007.

[340] Xi Chen, Wei-Bin Shen, Penghua Yang, Daoyin Dong, Winny Sun, and Peixin Yang. High glucose inhibits neural stem cell differentiation through oxidative stress and endoplasmic reticulum stress. *Stem Cells and Development*, 27(11):745–755, jun 2018.

[341] Haruko Nakano, Itsunari Minami, Daniel Braas, Herman Pappoe, Xiuju Wu, Addelynn Sagadevan, Laurent Vergnes, Kai Fu, Marco Morselli, Christopher Dunham, Xueqin Ding, Adam Z Stieg, James K Gimzewski, Matteo Pellegrini, Peter M Clark, Karen Reue, Aldons J Lusis, Bernard Ribalet, Siavash K Kurdistani, Heather Christofk, Norio Nakatsuji, and Atsushi Nakano. Glucose inhibits cardiac muscle maturation through nucleotide biosynthesis. *eLife*, 6, dec 2017.

[342] T.-L. Tsai, P.A. Manner, and W.-J. Li. Regulation of mesenchymal stem cell chondrogenesis by glucose through protein kinase c/transforming growth factor signaling. *Osteoarthritis and Cartilage*, 21(2):368–376, feb 2013.

[343] Jacqueline M Stephens and Paul F Pilch. The metabolic regulation and vesicular transport of glut4, the major insulin-responsive glucose transporter. *Endocrine Reviews*, 16(4):529–546, 1995.

[344] Robert T Watson and Jeffrey E Pessin. Intracellular organization of insulin signaling and glut4 translocation. *Recent progress in hormone research*, 56:175–193, 2001.

[345] Chun Y Wong, Hani Al-Salami, and Crispin R Dass. C2c12 cell model: its role in understanding of insulin resistance at the molecular level and pharmaceutical development at the preclinical stage. *Journal of Pharmacy and Pharmacology*, 72(12):1667–1693, aug 2020.

[346] L Bryan Ray and Thomas W Sturgill. Rapid stimulation by insulin of a serine/threonine kinase in 3t3-l1 adipocytes that phosphorylates microtubule-associated protein 2 in vitro. *Proceedings of the National Academy of Sciences*, 84(6):1502–1506, 1987.

[347] Paul Duffield Brewer, Estifanos N Habtemichael, Irina Romenskaia, Cynthia Corley Mastick, and Adelle CF Coster. Insulin-regulated glut4 translocation: membrane protein trafficking with six distinctive steps. *Journal of Biological Chemistry*, pages jbc–M114, 2014.

[348] Leonard S Kaplow and Charlotte Ladd. Brief report: Simplified myeloperoxidase stain using benzidine dihydrochloride. *Blood*, 26(2):215–219, 1965.

[349] Marina Wright Muelas, Fernando Ortega, Rainer Breitling, Claus Bendtsen, and Hans V Westerhoff. Rational cell culture optimization enhances experimental reproducibility in cancer cells. *Scientific Reports*, 8(1):1–16, 2018.

[350] Frances M Ashcroft, Maria Rohm, Anne Clark, and Melissa F Brereton. Is type 2 diabetes a glycogen storage disease of pancreatic β cells? *Cell metabolism*, 26(1):17–23, 2017.

[351] Ahmed M. Abdelmoez, Laura Sardón Puig, Jonathon A. B. Smith, Brendan M. Gabriel, Mladen Savikj, Lucile Dollet, Alexander V. Chibalin, Anna Krook, Juleen R. Zierath, and Nicolas J. Pillon. Comparative profiling of skeletal muscle models reveals heterogeneity of transcriptome and metabolism. *American Journal of Physiology-Cell Physiology*, 318(3):C615–C626, mar 2020.

[352] Brian W. Parks, Tamer Sallam, Margarete Mehrabian, Nikolas Psychogios, Simon T. Hui, Frode Norheim, Lawrence W. Castellani, Christoph D. Rau, Calvin Pan, Jennifer Phun, Zhenqi Zhou, Wen-Pin Yang, Isaac Neuhaus, Peter S. Gargalovic, Todd G. Kirchgessner, Mark Graham, Richard Lee, Peter Tontonoz, Robert E. Gerszten, Andrea L. Hevener, and Aldons J. Lusis. Genetic architecture of insulin resistance in the mouse. *Cell Metabolism*, 21(2):334–347, feb 2015.

[353] Hans P. M. M. Lauritzen and Jonathan D. Schertzer. Measuring GLUT4 translocation in mature muscle fibers. *American Journal of Physiology-Endocrinology and Metabolism*, 299(2):E169–E179, aug 2010.

[354] W Timothy Garvey, Jerrold M Olefsky, and Stephen Marshall. Insulin induces progressive insulin resistance in cultured rat adipocytes: sequential effects at receptor and multiple postreceptor sites. *Diabetes*, 35(3):258–267, 1986.

[355] K Takeda, K Toda, T Saibara, M Nakagawa, K Saika, T Onishi, T Sugiura, and Y Shizuta. Progressive development of insulin resistance phenotype in male mice with complete aromatase (cyp19) deficiency. *Journal of Endocrinology*, 176(2):237–246, 2003.

[356] Laura Niederstaetter, Benjamin Neuditschko, Julia Brunmair, Lukas Janker, Andrea Bileck, Giorgia Del Favero, and Christopher Gerner. Eicosanoid content in fetal calf serum accounts for reproducibility challenges in cell culture. *Biomolecules*, 11(1):113, 2021.

[357] Krishna Tiwari, Sarubini Kananathan, Matthew G Roberts, Johannes P Meyer, Mohammad Umer Sharif Shohan, Ashley Xavier, Matthieu Maire, Ahmad Zyoud, Jinghao Men, Szeyi Ng, et al. Reproducibility in systems biology modelling. *Molecular Systems Biology*, 17(2):e9982, 2021.

[358] Eva Gonzalez and Timothy E McGraw. Insulin-modulated akt subcellular localization determines akt isoform-specific signaling. *Proceedings of the National Academy of Sciences*, 106(17):7004–7009, 2009.

[359] Jeffrey E Pessin and Alan R Saltiel. Signaling pathways in insulin action: molecular targets of insulin resistance. *The Journal of clinical investigation*, 106(2):165–169, 2000.

[360] Hui-Yu Liu, Tao Hong, Ge-Bo Wen, Jianmin Han, Degen Zuo, Zhenqi Liu, and Wenhong Cao. Increased basal level of akt-dependent insulin signaling may be responsible for the development of insulin resistance. *American Journal of Physiology-Endocrinology and Metabolism*, 297(4):E898–E906, 2009.

[361] Jérémie Boucher, André Kleinridders, and C Ronald Kahn. Insulin receptor signaling in normal and insulin-resistant states. *Cold Spring Harbor perspectives in biology*, 6(1):a009191, 2014.

[362] Juan Guinea Viniegra, Natalia Martínez, Pegah Modirassari, Javier Hernández Losa, Carlos Parada Cobo, Víctor Javier Sánchez-Arévalo Lobo, Clara Isabel Aceves Luquero, Luis Álvarez-Vallina, Santiago Ramón y Cajal, José María Rojas, et al. Full activation of pkb/akt in response to insulin or ionizing radiation is mediated through atm. *Journal of Biological Chemistry*, 280(6):4029–4036, 2005.

[363] Steven B Waters, Keishi Yamauchi, and JE Pessin. Functional expression of insulin receptor substrate-1 is required for insulin-stimulated mitogenic signaling. *Journal of Biological Chemistry*, 268(30):22231–22234, 1993.

[364] Zachary A Knight, Beatriz Gonzalez, Morri E Feldman, Eli R Zunder, David D Goldenberg, Olusegun Williams, Robbie Loewith, David Stokoe, Andras Balla, Balazs Toth, et al. A pharmacological map of the pi3-k family defines a role for p110α in insulin signaling. *Cell*, 125(4):733–747, 2006.

[365] Naoki Yamamoto, Ryo Ishikuro, Mamoru Tanida, Kenji Suzuki, Yuri Ikeda-Matsuo, and Kazuya Sobue. Insulin-signaling pathway regulates the degradation of amyloid β-protein via astrocytes. *Neuroscience*, 385:227–236, 2018.

[366] Anna Danielsson, Fredrik H Nystrom, and Peter Strålfors. Phosphorylation of irs1 at serine 307 and serine 312 in response to insulin in human adipocytes. *Biochemical and biophysical research communications*, 342(4):1183–1187, 2006.

[367] K. Grabiec, M. Gajewska, M. Milewska, M. Błaszczyk, and K. Grzelkowska-Kowalczyk. The influence of high glucose and high insulin on mechanisms controlling cell cycle progression and arrest in mouse c2c12 myoblasts: the comparison with IGF-i effect. *Journal of Endocrinological Investigation*, 37(3):233–245, jan 2014.

[368] Albert Goldbeter and Daniel E Koshland. An amplified sensitivity arising from covalent modification in biological systems. *Proceedings of the National Academy of Sciences*, 78(11):6840–6844, 1981.

[369] Daniel Kahn and Hans V Westerhoff. Control theory of regulatory cascades. *Journal of Theoretical Biology*, 153(2):255–285, 1991.

[370] Jan-Hendrik S Hofmeyr and Athel Cornish-Bowden. Co-response analysis: A new experimental strategy for metabolic control analysis* 1. *J. Theor. Biol.*, 182(3):371–380, 1996.

[371] Eva Tomás, Yen-Shou LIN, Zeina Dagher, Asish Saha, Zhijun Luo, Yasuo Ido, and Neil B Ruderman. Hyperglycemia and insulin resistance: possible mechanisms. *Annals of the New York Academy of Sciences*, 967(1):43–51, 2002.

[372] Michael H Shanik, Yuping Xu, Jan Škrha, Rachel Dankner, Yehiel Zick, and Jesse Roth. Insulin resistance and hyperinsulinemia: is hyperinsulinemia the cart or the horse? *Diabetes care*, 31(Supplement 2):S262–S268, 2008.

[373] Karin G Stenkula, Vladimir A Lizunov, Samuel W Cushman, and Joshua Zimmerberg. Insulin controls the spatial distribution of glut4 on the cell surface through regulation of its postfusion dispersal. *Cell metabolism*, 12(3):250–259, 2010.

[374] Jennine M. Dawicki-McKenna, Yale E. Goldman, and E. Michael Ostap. Sites of glucose transporter-4 vesicle fusion with the plasma membrane correlate spatially with microtubules. *PLoS ONE*, 7(8):e43662, aug 2012.

[375] Aibin He, Xiaojun Liu, Lizhong Liu, Yongsheng Chang, and Fude Fang. How many signals impinge on glut4 activation by insulin? *Cellular signalling*, 19(1):1–7, 2007.

[376] Raffaele Matteoni and Thomas E Kreis. Translocation and clustering of endosomes and lysosomes depends on microtubules. *The Journal of cell biology*, 105(3):1253–1265, 1987.

[377] Georg Ramm, Jan Willem Slot, David E James, and Willem Stoorvogel. Insulin recruits glut4 from specialized vamp2-carrying vesicles as well as from the dy-

namic endosomal/trans-golgi network in rat adipocytes. *Molecular biology of the cell*, 11(12):4079–4091, 2000.

[378] Ola Karylowski, Anja Zeigerer, Alona Cohen, and Timothy E McGraw. Glut4 is retained by an intracellular cycle of vesicle formation and fusion with endosomes. *Molecular biology of the cell*, 15(2):870–882, 2004.

[379] Vincent Blot and Timothy E McGraw. Molecular mechanisms controlling glut4 intracellular retention. *Molecular biology of the cell*, 19(8):3477–3487, 2008.

[380] Amira Klip, Timothy E. McGraw, and David E. James. Thirty sweet years of GLUT4. *Journal of Biological Chemistry*, 294(30):11369–11381, jun 2019.

[381] Dumaine Williams, Stuart W Hicks, Carolyn E Machamer, and Jeffrey E Pessin. Golgin-160 is required for the golgi membrane sorting of the insulin-responsive glucose transporter glut4 in adipocytes. *Molecular biology of the cell*, 17(12):5346–5355, 2006.

[382] C. Wiese and Y. Zheng. Microtubule nucleation: -tubulin and beyond. *Journal of Cell Science*, 119(20):4143–4153, oct 2006.

[383] Dongkuan Xu and Yingjie Tian. A comprehensive survey of clustering algorithms. *Annals of Data Science*, 2(2):165–193, 2015.

[384] Anil K Jain, M Narasimha Murty, and Patrick J Flynn. Data clustering: a review. *ACM computing surveys (CSUR)*, 31(3):264–323, 1999.

[385] Trupti M Kodinariya and Prashant R Makwana. Review on determining number of cluster in k-means clustering. *International Journal*, 1(6):90–95, 2013.

[386] Kamran Khan, Saif Ur Rehman, Kamran Aziz, Simon Fong, and Sababady Sarasvady. Dbscan: Past, present and future. In *The fifth international conference on the applications of digital information and web technologies (ICADIWT 2014)*, pages 232–238. IEEE, 2014.

[387] Rui Xu and Donald C Wunsch. Clustering algorithms in biomedical research: a review. *IEEE Reviews in Biomedical Engineering*, 3:120–154, 2010.

[388] Chandrasagar B Dugani and Amira Klip. Glucose transporter 4: cycling, compartments and controversies. *EMBO reports*, 6(12):1137–1142, dec 2005.

[389] Maria-Florina Balcan, Yingyu Liang, and Pramod Gupta. Robust hierarchical clustering. *The Journal of Machine Learning Research*, 15(1):3831–3871, 2014.

[390] Robert T. Watson, Makoto Kanzaki, and Jeffrey E. Pessin. Regulated membrane trafficking of the insulin-responsive glucose transporter 4 in adipocytes. *Endocrine Reviews*, 25(2):177–204, apr 2004.

[391] Eddy Karnieli and Michal Armoni. Transcriptional regulation of the insulin-responsive glucose transporter GLUT4 gene: from physiology to pathology. *American Journal of Physiology-Endocrinology and Metabolism*, 295(1):E38–E45, jul 2008.

[392] Ruth E. Carmichael, Kevin A. Wilkinson, and Tim J. Craig. Insulin-dependent GLUT4 trafficking is not regulated by protein SUMOylation in l6 myocytes. *Scientific Reports*, 9(1), apr 2019.

[393] Evgenia Platonova, Christian M. Winterflood, Alexander Junemann, David Albrecht, Jan Faix, and Helge Ewers. Single-molecule microscopy of molecules tagged with GFP or RFP derivatives in mammalian cells using nanobody binders. *Methods*, 88:89–97, oct 2015.

[394] Toshio Ando, Satya Prathyusha Bhamidimarri, Niklas Brending, H Colin-York, Lucy Collinson, Niels De Jonge, PJ De Pablo, Elke Debroye, Christian Eggeling, Christian Franck, et al. The 2018 correlative microscopy techniques roadmap. *Journal of physics D: Applied physics*, 51(44):443001, 2018.

[395] Ahsen Chaudhry, Rocky Shi, and Dan S. Luciani. A pipeline for multidimensional confocal analysis of mitochondrial morphology, function, and dynamics in pancreatic -cells. *American Journal of Physiology-Endocrinology and Metabolism*, 318(2):E87–E101, feb 2020.

[396] Erik A Richter, Bo Falck Hansen, and Sven Asp Hansen. Glucose-induced insulin resistance of skeletal-muscle glucose transport and uptake. *Biochemical Journal*, 252(3):733–737, 1988.

[397] Bryce A Nelson, Katherine A Robinson, and Maria G Buse. High glucose and glucosamine induce insulin resistance via different mechanisms in 3t3-l1 adipocytes. *Diabetes*, 49(6):981–991, 2000.

[398] James W Russell, David Golovoy, Andrea M Vincent, PIA Mahendru, James A Olzmann, Alice Mentzer, and Eva L Feldman. High glucose-induced oxidative stress and mitochondrial dysfunction in neurons. *The FASEB Journal*, 16(13):1738–1748, 2002.

[399] N. Porksen, M. Hollingdal, C. Juhl, P. Butler, J. D. Veldhuis, and O. Schmitz. Pulsatile insulin secretion: Detection, regulation, and role in diabetes. *Diabetes*, 51(Supplement 1):S245–S254, feb 2002.